

# **Data Driven Spatio-Temporal Prediction of Landslide Susceptibility for The Himalayan Region**

A Thesis Submitted  
In Partial Fulfilment of the Requirements  
for the Degree of

**DOCTOR OF PHILOSOPHY**

by

**Ankit Tyagi**

(2017CEZ0007)



DEPARTMENT OF CIVIL ENGINEERING  
**INDIAN INSTITUTE OF TECHNOLOGY ROPAR**

**April, 2023**

Ankit Tyagi: Data Driven Spatio-Temporal Prediction of Landslide Susceptibility for The Himalayan Region

Copyright © 2023, Indian Institute of Technology Ropar

All Rights Reserved

DEDICATED  
TO  
FAMILY & FRIENDS



## **Declaration of Originality**

I hereby declare that the work which is being presented in the thesis entitled **Data Driven Spatio-Temporal Prediction of Landslide Susceptibility for The Himalayan Region** has been solely authored by me. It presents the result of my own independent investigation/research conducted during the time period from January 2018 to April 2023 under the supervision of Dr. Naveen James, Assistant Professor, Department of Civil Engineering, IIT Ropar and Dr. Reet Kamal Tiwari, Assistant Professor, Department of Civil Engineering, IIT Ropar. To the best of my knowledge, it is an original work, both in terms of research content and narrative, and has not been submitted or accepted elsewhere, in part or in full, for the award of any degree, diploma, fellowship, associateship, or similar title of any university or institution. Further, due credit has been attributed to the relevant state-of-the-art and collaborations (if any) with appropriate citations and acknowledgments, in line with established ethical norms and practices. I also declare that any idea/data/fact/source stated in my thesis has not been fabricated/ falsified/ misrepresented. All the principles of academic honesty and integrity have been followed. I fully understand that if the thesis is found to be unoriginal, fabricated, or plagiarized, the Institute reserves the right to withdraw the thesis from its archive and revoke the associated Degree conferred. Additionally, the Institute also reserves the right to appraise all concerned sections of society of the matter for their information and necessary action (if any). If accepted, I hereby consent for my thesis to be available online in the Institute's Open Access repository, inter-library loan, and the title & abstract to be made available to outside organizations.



Signature

Name: Ankit Tyagi

Entry Number: 2017CEZ0007

Program: PhD

Department: Civil Engineering

Indian Institute of Technology Ropar

Rupnagar, Punjab 140001

Date: 24/04/2023



## Acknowledgments

The success of this study depended mainly on the encouragement and guidelines of many others. At this juncture, I would like to take this opportunity to thank all those who have directly or indirectly helped me in the completion of my research work.

First and foremost, I would like to give all my gratitude to my supervisors, Dr. Naveen James and Dr. Reet Kamal Tiwari, who kept my confidence and spirit high throughout my research work. Their careful thoughts, valuable comments, and constructive suggestions from time to time made me stay focused in the right direction to achieve the study's objective. I am indebted for their overall guidance and support.

I'm grateful to Prof. Deepak Kashyap and the committee members Dr. Sagar R. Chavan (Head, Department of Civil Engineering), Dr. Putul Haldar, Dr. Muthulingam Subramaniyan and Dr. Arun Kumar for sparing their valuable time in monitoring the work progress and providing helpful tips, critical comments and precious suggestions from time to time. A special thanks to all faculties and lab staff of the Department of Civil Engineering, IIT Ropar, for encouragement and moral support. I would like to express my sincere appreciation and thanks to Dr. Rohan Kumar and Dr. Varinder Saini for sharing their knowledge and experience.

I feel lucky to be blessed by the company of wonderful friends who have shared my failures and triumphs. For help at various stages, special thanks goes to Abhishek Kaushal, Aditya Kapoor, Panna Lal Kurmi, Mrs. Veena U, Shobhit Maheshwari, Manoj Kannan R, Kaipa Kiran Kumar Reddy, Neha Gupta, Gopika Sharma, Supratim Guha, Akshar Triphati, Piyush Pratap Singh, Siddharth Chauhan, Sachchidanand Kushwaha, Onkar Mishra, Shubham Jain, Niraj Janardhan Sahare, Aaditya Bhamidipati, Kavita Mitkari, Amit Kumar Singh, Deepali Gaikwad, Tanisha Ghosh, Aravind K Suresh, and Aarathi Shylu.

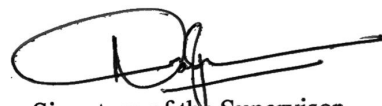
Last but certainly not least, I would like to thank my mother, Mrs. Geeta Tyagi; my father, Mr. D.C. Tyagi; my wife, Mrs. Srishti Tyagi and my younger brother Arjit for their unconditional support throughout this journey. I am deeply thankful to them for their love, support, and sacrifices. Without their help and cooperation, I would never have reached this milestone.



## Certificate

This is to certify that the thesis entitled **Data Driven Spatio-Temporal Prediction of Landslide Susceptibility for The Himalayan Region**, submitted by **Ankit Tyagi (2017CEZ0007)** for the award of the degree of **Doctor of Philosophy** of Indian Institute of Technology Ropar, is a record of bona fide research work carried out under our guidance and supervision. To the best of my knowledge and belief, the work presented in this thesis is original and has not been submitted, either in part or full, for the award of any other degree, diploma, fellowship, associateship or similar title of any university or institution.

In our opinion, the thesis has reached the standard fulfilling the requirements of the regulations relating to the Degree.



Signature of the Supervisor

Dr. Naveen James

Department of Civil Engineering



Signature of the Supervisor

Dr, Reet Kamal Tiwari

Department of Civil Engineering

Indian Institute of Technology Ropar

Rupnagar, Punjab 140001

Date:24/04/2023



## **Lay Summary**

Due to increasing population demand, development in the mountains, such as the construction of buildings, roads, and railways, has led to deforestation, slope cuts, unstable mountains, and global warming. Climate change and associated extreme weather conditions result in a surge of natural hazards such as floods, earthquakes, landslides, and avalanches worldwide. With the present land use scenarios and changing climate, these natural hazards will likely increase in the future. While land-use planning could decrease vulnerability and mitigate risk before a disaster happens, however, these measures are usually implemented after a disaster. Hence, our focus should be sustainable development on mountainous terrain, preservation of the environment, and resistance to natural hazards. The current study focuses on accurate prediction of the future landslide hotspot zones. Here, we have identified the key landslide causing factors and used them for predicting future landslide events. The susceptibility maps generated in this study predict future landslide hotspot zones. The study region of Tehri, Uttarakhand state of India, was chosen for the research. Further, the Himachal Pradesh state of India, along with its two prominent landslide prone sites of Chamba and Bhuntar, were used for validating the results. The results conclude that unplanned rapid urbanization will lead to an increase in landslide susceptibility in the future. The study also concludes that the change climate scenarios will increase the intensity of the dynamic variables like rainfall and temperature, ultimately increasing the very high landslide susceptibility zone by 8%. As the forcing scenarios increase, the climate variables and landslide hotspot zones also increase for the year 2050. These accurate prediction of landslide zones and their future projections can help land use policymakers restrict the urbanization growth in high landslide risk zones and ensure sustainable development.



## Abstract

Worldwide, landslides are the most frequently occurring disaster that are very destructive and unpredictable in nature. Tehri Garhwal in the Uttarakhand State of the Indian Himalayas is one such region where 850 landslide events were detected during 2005-2020. Many researchers have conducted landslide susceptibility mapping (LSM) studies for this region using different static landslide-causing factors. However, these studies lack consistency in selecting landslide causing factors for the susceptibility analysis and mapping. Also, studies considering dynamic factors in predicting future landslide susceptibility scenarios are inadequate. Hence in this study, initially, landslide causing factors were optimized for LSM, and then dynamic factors were utilized for future projection of LSM.

The main objectives of this research include the development of scientific methodology for determining significant landslide causing factors for the Tehri region and validating them on two landslide prone sites of Himachal Pradesh with similar terrain conditions. Further, the LSM was prepared using the derived significant factors, and dynamic factors such as Land Use Land Cover (LULC) and climate variables were incorporated for future projection of the LSM. To achieve these objectives, first, the geospatial database in three temporal categories, 2005-2010, 2010-2015, and 2015-2020, was prepared for the historical landslide events. Second, the landslide-causing factors were optimized using multicollinearity analysis considering Pearson correlation and the Artificial Neural Network (ANN) model's sensitivity analysis. Third, the relevance of these significant factors in predicting landslide susceptibility was checked for the two test sites of the Himalayan region and utilized in LSM for 2010, 2015, and 2020. Fourth, the projected LULC map was generated for the year 2050 using the Artificial Neural Network-Cellular Automata (ANN-CA) model. Fifth, CMIP6 climate projections maps were prepared using the Indian Institute of Tropical Meteorology Earth system model (IITM ESM) under four Shared Socioeconomic Pathway (SSP) scenarios. Finally, the projected maps were used as the driving parameter for the future prediction of LSM. The predicted maps were validated utilizing the Area under the Receiver Operating Characteristic (ROC) curve, and the Kappa coefficient verifies the reliability of the simulated future projected results.

The results reveal that out of 21 parameters considered for the Tehri region, 11 were found to be significant for LSM and achieved the prediction accuracy of 0.93 Area Under Curve (AUC) value. Thus, this study recommends using the derived 11 landslide parameters and their hierarchy for carrying out LSM in the Himalayan region. Also, a high increase in the built-up area (5%) and agriculture land (4%) with a decrease in forest area (10%) in future LULC

projections was observed. This LULC change and change in climate variable under four climate forcing scenarios of SSP 1-2.6, SSP 2-4.5, SSP 3-7.0 and SSP 5-8.5 has resulted in an increase of very high landslide susceptibility class by 2%, 4%, 7%, and 9% respectively. Future Prediction of LSM can help in the proper management and sustainable distribution of environmental resources. The target audiences can be land use policymakers who must decide which direction urbanization takes and which direction to restrict.

**Keywords:** Significant Landslide Causing Factors; Future Landslide susceptibility mapping; Land use land cover projections; Climate projections

## List of Publications from Thesis

### Journal

1. Tyagi, A., Tiwari, R.K. and James, N., 2023. Mapping the landslide susceptibility considering future land-use land-cover scenario. *Landslides*, pp.1-12. [https://doi.org/10.1007/978-981-15-9984-2\\_22](https://doi.org/10.1007/978-981-15-9984-2_22)
2. Tyagi, A., Tiwari, R.K. and James, N., 2022. A Review on Spatial, Temporal and Magnitude prediction of Landslide Hazard. *Journal of Asian Earth Sciences: X*, p.100099. <https://doi.org/10.1016/j.jaesx.2022.100099>
3. Tyagi, A., Tiwari, R.K. and James, N., 2023. Identification of the significant parameters in spatial prediction of landslide hazard. *Bulletin of Engineering Geology and the Environment*, 82(8), pp.1-13. <https://doi.org/10.1007/s10064-023-03334-w>.
4. Tyagi, A., Tiwari, R.K. and James, N., 2023. Prediction of the future landslide susceptibility scenario based on LULC and climate projections. *Landslides*, pp.1-16. <https://doi.org/10.1007/s10346-023-02088-6>.
5. Tyagi, A., Gupta, N., Tiwari, R.K., James, N. and Chavan, S. R., Determining the Impact of Anthropogenic activities and Climate change on Landslide Susceptibility for the Himalayan Region. *Remote Sensing Applications: Society and Environment* (under Review).

### Conference Proceeding

1. Tyagi, A., James, N. and Tiwari, R.K., Spatial Prediction of Landslide Hazard and Risk for Tehri Region. Accepted for publication as book chapter in the Proceedings of Mediterranean Geosciences Union (MedGU) Annual Meeting Istanbul, Turkey 2021. *Advances in Science, Technology & Innovation (ASTI)*. Springer, Germany.

### Book chapter

1. Tyagi, A., Tiwari, R.K. and James, N., 2021. GIS-Based Landslide Hazard Zonation and Risk Studies Using MCDM. In *Local Site Effects and Ground Failures* (pp. 251-266). Springer, Singapore. <https://doi.org/10.1007/s10346-022-01968-7>



## Table of Contents

<b>Declaration of Originality</b>	<b>v</b>
<b>Acknowledgement</b>	<b>vii</b>
<b>Certificate</b>	<b>ix</b>
<b>Lay Summary</b>	<b>xi</b>
<b>Abstract</b>	<b>xiii</b>
<b>List of Publications from Thesis</b>	<b>xv</b>
<b>List of Figures</b>	<b>xxi</b>
<b>List of Tables</b>	<b>xxv</b>
<b>List of Notations and Abbreviations</b>	<b>xxvii</b>

### **1. Introduction**

1.1. Background.....	1
1.2. Motivation .....	2
1.3. Scope of the Research.....	4
1.4. Thesis Outline .....	4

### **2. Literature Review**

2.1. Introduction .....	5
2.2. History of Landslide Susceptibility and Hazard .....	5
2.3. Landslides Causal Factors .....	8
2.3.1. Static Factors .....	8
2.3.2. Dynamic Factors .....	9
2.3.3. Optimization of Factors .....	10
2.4. LSHM Models .....	10
2.4.1. Qualitative Models .....	11
2.4.2. Semi-Quantitative Models.....	13
2.4.3. Quantitative Models.....	17
2.5. Research gaps .....	27
2.6. Research objectives .....	27
2.7. Novelty of the research.....	28
2.8. Summary.....	28

### **3. Study Area and Testing Sites**

3.1. Introduction .....	29
3.2. The Tehri Region.....	30
3.2.1. Location and Geology of Study Area .....	31

3.2.2.	Physiography and Vegetation .....	32
3.2.3.	Climate and Drainage .....	32
3.3.	The Chamba Region .....	32
3.3.1.	Location and Geology of Testing Site 1 .....	33
3.3.2.	Physiography and Vegetation .....	33
3.3.3.	Climate and Drainage .....	34
3.4.	The Bhuntar Region.....	35
3.4.1.	Location and Geology of Testing Site 2 .....	35
3.4.2.	Physiography and Vegetation .....	35
3.4.3.	Climate and Drainage .....	35
3.5.	Summary.....	36
<b>4. Methodology Overview</b>		
4.1.	Introduction .....	37
4.2.	Data Collection .....	37
4.3.	Landslide Inventory Maps .....	38
4.4.	Land Use Land Cover Maps .....	40
4.5.	DEM Derivatives Maps .....	40
4.5.1.	Slope .....	40
4.5.2.	Aspect .....	40
4.5.3.	Relative Relief .....	41
4.5.4.	Curvature .....	42
4.5.5.	Topographic Ruggedness Index .....	42
4.5.6.	Topographic Wetness Index .....	42
4.5.7.	Stream Power Index .....	43
4.5.8.	Sediment Transport Index .....	43
4.6.	Climate Variables Maps .....	44
4.6.1.	Rainfall .....	44
4.6.2.	Surface Temperature .....	44
4.6.3.	Evapotranspiration .....	44
4.6.4.	Soil Moisture.....	45
4.7.	Peak Horizontal Acceleration Map.....	45
4.8.	Distance/Buffer Maps .....	46
4.8.1.	Distance to Road .....	46
4.8.2.	Distance to Waterways .....	47
4.8.3.	Distance to Streams .....	47
4.9.	Ancillary Data .....	48

4.9.1.	Soil Type.....	48
4.9.2.	Geomorphology .....	48
4.9.3.	Lithology .....	49
4.9.4.	Geology .....	49
4.10.	LSM Methods .....	50
4.10.1.	Analytical Hierarchy Process.....	50
4.10.2.	Frequency Ratio .....	51
4.10.3.	Artificial Neural Network .....	51
4.10.4.	Artificial Neural Network Based Cellular Automaton .....	52
4.11.	Accuracy Assessment .....	53
4.12.	Summary.....	54
<b>5. LSM using Significant/Influential Landslide Causative Factors</b>		
5.1.	Introduction .....	55
5.2.	Identification of Significant Landslide Causing Factors .....	55
5.2.1.	Multicollinearity analysis using the Pearson correlation coefficient .....	56
5.2.2.	Sensitivity analysis using ANN model .....	57
5.2.3.	Results and Discussion .....	58
5.3.	LSM using ANN model .....	59
5.3.1.	Mapping and Validating Results .....	59
5.3.2.	Discussion .....	60
5.4.	LSM using FR, AHP and FR-AHP Models .....	60
5.4.1.	Mapping using FR Model and Validating Results.....	60
5.4.2.	Mapping using AHP Model and Validating Results .....	64
5.4.3.	Mapping using FR-AHP Model and Validating Results .....	68
5.4.4.	Discussion .....	69
5.5.	Testing the significant factors at Chamba and Bhuntar test sites .....	69
5.5.1.	Mapping and Validating Results .....	70
5.5.2.	Discussion .....	71
5.6.	Conclusion .....	71
<b>6. Future LSM Considering Future LULC Projections</b>		
6.1.	Introduction .....	73
6.2.	Data preparation.....	73
6.3.	Driving parameters for LULC projection .....	74
6.4.	ANN-CA model.....	74
6.5.	Methodology .....	75
6.6.	Results and Discussion .....	76
6.6.1.	Future Scenario of LULC .....	76

6.6.2.	Change detection of the future scenario of LULC .....	77
6.6.3.	Prediction of Landslide Susceptibility .....	78
6.7.	Validation .....	81
6.7.1.	Cohen's Kappa Coefficient. ....	81
6.7.2.	Area Under Curve Method .....	81
6.8.	Conclusion .....	81
<b>7. Future LSM Incorporating Future Climate Projections</b>		
7.1.	Introduction .....	83
7.2.	Data preparation.....	83
7.2.1.	LULC Projections .....	84
7.2.2.	Climate Projections.....	84
7.3.	Methodology.....	87
7.4.	Results and Discussion .....	87
7.4.1.	Landslide susceptible Maps for Tehri Region .....	87
7.4.2.	Future Projections of LULC, Precipitation and Temperature for Tehri region .....	88
7.4.3.	Future Predicted Landslide Susceptibility Maps for Tehri region .....	89
7.4.4.	Landslide susceptible Maps for Himachal Pradesh State .....	90
7.4.5.	Future Projections of LULC, Precipitation and Temperature for Himachal Pradesh state .....	91
7.4.6.	Future Predicted Landslide Susceptibility Maps .....	92
7.5.	Validation .....	93
7.5.1.	Area Under Curve Method. ....	93
7.5.2.	Cohen's Kappa Coefficient .....	93
7.6.	Conclusion .....	94
<b>8. Summary and Conclusion</b>		
8.1.	Summary.....	97
8.2.	Major Conclusions.....	98
8.3.	Scope of Future Work.....	100
	References.....	101
	Annexure.....	141

## List of Figures

Fig. 1.1 Some landslides were detected along the reservoir embankment in the Tehri region.....	3
Fig. 2.1 Map showing the geographical distribution of LSHM methods for different countries in different colors (Blue- direct method, Red- MCDM, Black- Physically Based, Yellow- Probabilistic, and Green- Statistical). The size of the pie chart is directly proportional to the number of articles for the country.....	7
Fig 2.2 Pie charts showing the percentages of prediction types for landslide hazards.....	7
Fig. 2.3 Landslide susceptibility and hazard zonation methods.....	11
Fig. 3.1 Location of the study area and Testing sites. (A) Tehri region, (B) Chamba region, and (C) Bhuntar region.....	30
Fig. 3.2 Photographs showing landslides in the Tehri region.....	31
Fig. 3.3 Figure on the left shows the map of NH-154A buffering and on the right side shows the LULC class map for the Chamba test site.....	34
Fig. 3.4 The left shows the stream buffer map, and the right side shows the Ravi river buffer map for the Chamba test site.....	34
Fig. 3.5 Figure on the left shows the NH-3 buffer map, and on the right side shows LULC class map for the Bhuntar test site.....	35
Fig. 3.6 Figure on the left shows the stream buffer map and on the right side shows Beas river buffer map for the Bhuntar test site.....	36
Fig. 4.1 Classification of landslides (A) Based on the type of Movement (B) based on the type of Material (C) Based on the type of Land cover. ....	39
Fig. 4.2 Landslide Inventory and LULC Maps for the Tehri region.....	39
Fig. 4.3 Slope and Aspect Maps for the Tehri region.....	41
Fig. 4.4 Relative Relief and Curvature Maps for the Tehri region.....	41

Fig. 4.5 Topographic Ruggedness Index and Topographic Wetness Index Maps for the Tehri region.....	42
Fig. 4.6 Stream Power Index and Sediment Transport Index Maps for the Tehri region.....	43
Fig. 4.7 Rainfall and Soil Temperature Maps for the Tehri region.....	44
Fig. 4.8 Evapotranspiration and Soil Moisture Content Maps for the Tehri region.....	45
Fig. 4.9 Peak Horizontal Acceleration and Distance to Road Maps for the Tehri region.....	46
Fig. 4.10 Distance to Waterway and Distance to Stream Maps for the Tehri region.....	47
Fig. 4.11 Soil Type and Geomorphology Maps for the Tehri region.....	48
Fig. 4.12 Lithology and Geology Maps for the Tehri region.....	49
Fig. 4.13 Neuralnet (nn) plot.....	52
Fig. 4.14 Artificial-neural-network-based cellular automaton (ANN-CA) model structure for simulating future changes.....	53
Fig. 5.1 Significant factors showing percentage agreement with landslide points.....	58
Fig. 5.2 Landslide Susceptibility maps, Area distribution, and area under the ROC curves using ANN Model.....	59
Fig. 5.3 Landslide Susceptibility maps, area under the ROC curves using the FR Model and (A) All 21 factors (B) Significant 11 factors.....	63
Fig. 5.4 Landslide Susceptibility Maps, Area distribution and area under the ROC curves using the AHP Model.....	67
Fig. 5.5 Landslide Susceptibility maps, Area distribution, and ROC curves using FR-AHP Model.....	68

Fig. 5.6 LSMs and area under the ROC curves for (A) Chamba test site, (B) Bhuntar test site, and (C) Tehri region using AHP Technique.....	70
Fig. 6.1 The flow chart showing the proposed methodology for this research...	75
Fig. 6.2 LULC maps for the year 2010, 2015, 2020 and 2030.....	76
Fig. 6.3 LULC change graph for the years 2010, 2015, 2020 and 2030.....	76
Fig. 6.4 Map showing the class shift in LULC classes between the period 2020-2030.....	77
Fig. 6.5 Bar Chart showing the percentage shift in LULC classes between the period.....	78
Fig. 6.6 LSM for the years 2010, 2015, 2020 and 2030.....	79
Fig. 6.7 Change graph of LSM for the years 2010, 2015, 2020 and 2030.....	80
Fig. 6.8 AUC of the Predicted LS Maps for the year 2010 (A) and 2015 (B)....	81
Fig. 7.1 The socioeconomic "Challenge Space" to be spanned by the CMIP6 SSP experiments (O'Neil et al. 2014).....	85
Fig. 7.2 The flow chart showing the proposed methodology for this research....	87
Fig. 7.3 LSM for the Tehri Region of the years 2010, 2015 and 2020.....	88
Fig. 7.4 LULC maps for the Tehri region of the year (A) 2010, (B) 2015, (C) 2020 and (D) 2050.....	88
Fig. 7.5 Projected mean precipitation flux for the Tehri region of the year 2050 under (A) SSP 1-2.6 (B) SSP 2-4.5 (C) SSP 3-7.0 (D)SSP 5-8.5 Scenarios.....	89
Fig. 7.6 Projected surface temperature for the Tehri region of the year 2050 under (A) SSP 1-2.6 (B) SSP 2-4.5 (C) SSP 3-7.0 (D) SSP 5-8.5 Scenarios.....	89
Fig. 7.7 Landslide susceptibility maps for SSP 1-2.6, SSP 2-4.5, SSP 3-7.0 and SSP 5-8.5 Scenarios.....	91
Fig. 7.8 LSM for the Himachal Pradesh State of the years 2010, 2015 and	

2020.....	90
Fig. 7.9 LULC maps for the Himachal Pradesh State of the year (A) 2010, (B) 2015, (C) 2020 and (D) 2050.....	91
Fig. 7.10 Projected mean rainfall for the Himachal Pradesh State of the year 2050 under (A) SSP 1-2.6 (B) SSP 2-4.5 (C) SSP 3-7.0 (D) SSP 5-8.5 Scenarios.....	91
Fig. 7.11 Projected temperature for the Himachal Pradesh State of the year 2050 under (A) SSP 1-2.6 (B) SSP 2-4.5 (C) SSP 3-7.0 (D) SSP 5-8.5 Scenarios.....	92
Fig. 7.12 Landslide susceptibility maps for the Himachal Pradesh State of SSP 1-2.6, SSP 2-4.5, SSP 3-7.0 and SSP 5-8.5 Scenarios.....	92
Fig. 7.13 AUC of the predicted landslide susceptibility maps for the years 2010 (A), 2015 (B) and 2020 (C).....	93

## **List of Tables**

Table 4.1 Various sources utilised for preparing landslide causative factors.....	38
Table 4.2 The priorities scale between two factors defined by Saaty (1977).....	50
Table 4.3. Random consistency index prepared by Saaty.....	50
Table 5.1 Literature review for LSM in the Tehri region.....	56
Table 5.2 Pearson correlations between landslide causative factors.....	57
Table 5.3 Coefficient values for frequency ratio in the case of each factor and their classes.....	61
Table 5.4 Scores of factors and their classes obtained by performing AHP.....	64
Table 6.1 Pearson correlation coefficient between LULC and driving parameters.....	74
Table 6.2 Kappa coefficient values used for validation.....	79
Table 7.1 Details of 6 CMIP6-GCMs used in this study.....	86
Table 7.2 Kappa coefficient values used for validation.....	94



## **List of Notations and Abbreviations**

ABC	Artificial Bee Colony
AHP	Analytic hierarchy process
ANFIS	Adaptive Neuro-Fuzzy Inference System
ANN	Artificial Neural Network
ANP	Analytical Network Process
BBO	Biogeography-Based Optimisation
BRT	Boost Regression Tree
CF	Certainty Factor
CF	Certainty Factor
CNN	Convolutional Neural Networks
CP	Conditional Probability
DA	Discriminant analysis
DE	Differential Evolution
DEM	Digital Elevation Model
DT	Decision Tree
ET	Evapotranspiration
FF	Favourability Function
FL	Fuzzy logic
FLDA	Fisher's Linear Discriminant Analysis
FR	Frequency ratio
GA	Genetic Algorithm
GA	Geomorphic Analysis
GAM	Generalised Additive Model
GIS	Geographic Information Systems

GPM	Global Precipitation Measurement
GVF	Goodness of Variance Fit
GWO	Grey Wolf Optimisation
HHO	Harris Hawks Optimisation
HSU	Homogenous Susceptible Units
IA	Inventory Analysis
ISRO	Indian Space Research Organisation
IV	Information Value
K	Kappa coefficient
LDA	Linear Discriminant Analysis
LEM	Limits Equilibrium Models
LHM	Landslide Hazard Mapping
LR	Logistic Regression
LSHM	Landslide Susceptibility and Hazard Mapping
LSI	Landslide Susceptibility Index
LSM	Landslide Susceptibility Mapping
LULC	Land Use Land Cover
MCDM	Multiple-criteria Decision Making
MLP	Multilayer Perceptron
OWA	Ordered weighted averaging
PBDA	Physically Based Distributed Analysis
PHA	Peak Horizontal Acceleration
PNN	Probabilistic Neural Network
PSO	Particle Swarm Optimisation
QDA	Quadratic Discriminant Analysis

RBFLN	Radial Basis Function Link Net
RBFNN	Radial Basis Function Neural Network
RES	Rock Engineering System
R <sub>JB</sub>	Joyner distance
RMSE	Root Mean Square Error
RNN	Recurrent Neural Networks
ROC	Receiver Operating Characteristic
RR	Relative Relief
SHALSTAB	Shallow Landslide Stability Model
SINMAP	Stability Index Mapping
SLIP	Shallow Landslides Instability Prediction
SM	Soil Moisture
SPI	Stream Power Index
SRC	Success Rate Curve
SSPs	Shared Socioeconomic Pathways
STI	Sediment Transport Index
STI	Sediment Transport Index
SVM	Support Vector Machine
TCU	Terrain Computational Unit
TRI	Topographic Ruggedness Index
TRIGRS	Transient Rainfall Infiltration and Grid-based Regional Slope Stability analysis
TWI	Topographic Wetness Index
USGS	United States Geological Survey
WLC	Weighted Linear Combination
WofE	Weights of Evidence

WOL	Weighted Overlay
$Y_{br}$	spectral acceleration
$\beta$	Slope gradient
$\lambda_{\max}$	Maximum Eigen Value
$\Phi$	activation function

### 1.1 Background

A landslide is the movement of rock, soil, organic matter, and Earth debris down the slope under the influence of gravity. This occurs when the driving forces of gravity go beyond the material frictional resistance on the slope (Varnes, 1978). Many types of mass movements can be triggered by heavy rainfall, earthquakes, typhoons, hurricanes, volcanic eruptions, snowmelt, or anthropogenic activities such as slope cutting for the widening of roads, deforestation, quarrying, tunneling, mining, landfill construction, and unplanned urbanisation.

According to Mousavi et al. (2011), landslides account for about 9% of all-natural disasters globally. Landslide-related fatalities are high in hilly regions with fragile geological environments and intense climatic conditions. According to a report by Froude and Petley (2018), 55 997 people were killed in 4862, distinct by non-seismic landslides from January 2004 to December 2016. Many areas worldwide are susceptible to landslides, which cause loss of life and adversely impact infrastructure, the environment, and communities. According to Lee and Pradhan (2007), approximately 1000 deaths yearly are caused by landslides, with about four billion US dollars in property damages.

Landslides are usually local events compared to other catastrophes such as floods, earthquakes, cyclones, tsunamis, etc. With the increase in population, humans are moving towards hills for the inhabitant to areas of intrinsically fragile land, thereby maintaining a delicate balance in nature. Landslides can be very damaging, especially when failure is significant, long runout, and (or) rapid velocity. In India, about 0.49 million sq. km (15%) of the land surface is landslide-prone, including 16 states and two union territories (NDMA, 2009). Thus, it is necessary to predict landslide hazards accurately.

Shallow landslides are rapidly moving flows of mixed rocks, soil, organic matter, and mud that drive down the hill at 55 km per hour or more, influenced by gravitational force. They are caused primarily by prolonged, heavy rainfall on saturated hill slopes (Baum et al. 2002). Landslides are classified as shallow if not more than 2 m deep (van Asch et al., 1999, Sidle and Ochiai, 2006). Rainfall-induced shallow landslides are global phenomena that result in the loss of human life and destroy homes, roads, bridges, and other property every year. During Extreme rainfall events, landslides are very obvious in the Himalayan portion. Worldwide, landslide research has been in focus for the last four decades, and still, it is challenging to define many

mechanisms dealing with these phenomena. No method has been developed till now which can be standardised at the world level for accurate prediction of landslides. In all methods developed so far, uncertainty for landslide prediction is still present. The approaches used for prediction are generally accompanied by many assumptions. One of the basic assumptions is that what all factors that were responsible for causing landslides in the past will again be responsible for causing landslides in the future. This is not true because the factors causing landslides can also change with time, especially when so many anthropogenic activities are happening worldwide. Another assumption generally observed in (Landslide Susceptibility Mapping) LSM studies is that all the factors are considered static in the analysis. Again, this is false because factors like (Land Use Land Cover) LULC, precipitation, temperature, etc., vary with time. Their influence also changes in due course of time, especially in climate change scenarios, where the extreme rainfall events values and defined rainfall thresholds change drastically.

The probability of determining the location of landslides is called spatial probability. The information on where landslides can possibly take place in the future can be determined using various landslide-causing environmental factors. As all factors do not influence the landslide occurrence equally, therefore these factors are weighted using LSM models. These models determine the relationship between these factors and historical landslide data to derive correlation and define their significance. The significant factors are then further used for preparing the susceptibility map. Some of the dynamic factors that change with time can also be used as triggering factors and can be adopted for future prediction after determining the changing trend of these dynamic factors.

## **1.2 Motivation**

Landslides are among the most common natural hazards in the Himalayas, especially in the monsoons. To some extent, the information on when landslides can take place in the Himalayas can be determined using rainfall data analysis and defining the rainfall thresholds. Similarly, the information on where landslides can occur in the Himalayas can be determined using LSM. However, predicting landslides is challenging due to their high uncertainty. Therefore, accurately predicting when and where landslides will occur is tough.

Alterations of the Earth's land surface for the human settlement, transportation, and communication have made these highlands unstable, causing frequent landslides. Landslides are among the most dangerous, widespread, and destructive natural hazards. They cause serious injuries, loss of life, structural and economic damage, etc. Therefore, landslide study is essential all around the globe. Developments in remote-sensing techniques have considerably improved our capability to map landslides of different sizes with fewer field studies quickly. Petley (2012) has shown that in less developed countries, loss of life is more because of relatively more minor investment in understanding the landslide hazards and risks. Kirschbaum et al. (2010) analysed

and confirmed that emerging nations account for nearly 80% of landslide fatalities.

Landslides studies have drawn world attention primarily because of their socioeconomic influences and urbanisation growth on hilly terrain (Aleotti and Chowdhury, 1999; Champati Ray and Lakhera, 2004). Growing populations and human settlements over hilly regions are increasing the landslide risk worldwide (Rosenfeld, 1994; Alexander, 1995). Due to slope failures, traffic blockage along the road leaves tourists, pilgrims, and locals stuck for hours. Hence, there is a need to identify, divide, and map areas that have or could have the impact of landslides. These maps develop strategies and implement suitable risk mitigation measurements.



Fig. 1.1 Some landslides were detected along the reservoir embankment in the Tehri region.

The Tehri region of Uttarakhand is one such landslide-prone region. Apart from heavy rainfall and high seismic factors, this zone of Uttarakhand has a reservoir effect that adds to developing slope instability in this region. Many landslide activities were observed in the Tehri region of the Himalayas (Fig. 1.1) and predicting these landslides in advance is essential. According to M. Van Den Eeckhaut et al. (2006), LSM is the most important tool for reducing the damage caused by landslides. Identifying the location of future landslides, even if we are unaware of when they will occur, can resist urbanisation and development in the direction of high landslide-risk zones. Developing land use policies considering these future projections of landslide susceptible areas can reduce the landslide risk.

### **1.3 Scope of the research**

This research aims to determine the present and future landslide susceptibility areas incorporating static and dynamic significant landslide causative factors. This work also reviews various landslide susceptibility and hazard mapping methods incorporating various landslide causative factors. Based on this, appropriate procedures were selected, and significant landslide causative factors were derived. The research was conducted for the case study of the Tehri region, India. The significant landslide causative factors were initially derived using multicollinearity and sensitivity analysis. These derived significant factors were correlated with historical landslide data (70%), and weights of factors were derived. The remaining 30% was used to test the model's accuracy using the area under the ROC curve technique. These weighted landslide causative factors were integrated to generate the landslide susceptibility maps for the Tehri region. Further, future projections of Land Use Land Cover (LULC) and climate variables were utilised to derive future scenarios of Landslide Susceptibility Mapping (LSM).

### **1.4 Thesis Outline**

The thesis structure follows the following order to accomplish the study's objectives. Chapter 1 provides an overall introduction to the research background and highlights the existing difficulties in LSM. It also defines the purposes of the study along with the research scope. Chapter 2 discusses the earlier findings and research for landslide susceptibility hazard mapping using various qualitative, semi-quantitative, and quantitative approaches. Further, previous literature emphasising the impact of dynamic factors on landslide activities was also investigated. Chapter 3 describes the study area and test sites in terms of their locations, physiography, vegetation climate, and drainage. Chapter 4 discusses the data used and their derivatives, the fundamental theories of the methods, and the overall methodology adopted for the study. Chapter 5 describes a scientific method of deriving significant landslide causative factors and their application in LSM using different models for deriving their weights. Further, these derived significant factors were tested on two landslide-prone sites. Chapter 6 describes the methodology adopted for deriving future LSM scenarios incorporating LULC projections. Chapter 7 determines the future LSM scenarios using future LULC and climate projections under four Shared Socioeconomic Pathways (SSPs). Chapter 8 summarises and conclude the research work with limitation and recommendations for future work.

#### 2.1 Introduction

Landslides constitute a fragile landscape where habitation or other engineering structures cannot be developed or constructed. The increase in human population and rapid urbanisation has led to the expansion of construction activities in hilly terrains and has resulted in frequent landslide events in recent times. In many developing countries, this problem is remarkable, mainly due to the rapid non-sustainable development of natural resources. The use of landslide susceptibility and hazard maps for land use planning has increased significantly during the last few decades. Landslide Susceptibility Mapping (LSM) and Landslide Hazard Mapping (LHM) are essential steps in mitigation measures for planning and recognising the regions needing protective measurements. Numerous advances have been made in modeling landslide initiation, triggering mechanisms, and probability for slope instability using high-resolution satellite imageries and Geographic Information Systems (GIS). The ultimate aim of all the research is to generate landslide susceptibility maps with reasonable accuracy. This chapter reviews early works and commonly accepted definitions relevant to the landslide hazard. Here, we will discuss various landslide prediction research conducted to produce reliable susceptibility and hazard maps by incorporating various landslide causative factors and models in landslide mapping studies. Also, we will review literature focusing on dynamic factors' impact on future landslide prediction.

#### 2.2 History of Landslide Susceptibility and Hazard Mapping

Many researchers have proposed various Landslide Susceptibility and Hazard Mapping (LSHM) techniques by considering landslide causative and triggering factors. Adopting a unique method and factors responsible for the landslide is difficult due to the heterogeneous terrain of the Earth's surface. Some scientific societies and institutions have proposed guidelines for LSHM, intending to use common terminologies and guide practitioners in their analyses (Wong et al., 2006; Fell et al., 2008). However, the methodologies applied vary from region to region and even within the same area (Corominas, 2010). The methodology to construct the LSHZ map depends on numerous factors divided into intrinsic and triggering factors (Crozier, 1986; Siddle et al., 1991). Intrinsic factors include lithology, structural features, geomorphology, vegetation, hydrogeological conditions, nature of the terrain, etc., and external or triggering factors include seismicity, rainfall, anthropogenic factors, etc.

Varnes (1984) defined landslide hazard as the likelihood of a destructive landslide phenomenon for a specific region at a particular time. This is the most extensively used definition for natural hazard maps representing its scattering over an area (Mitchell, 1988; Einstein, 1988, 1997; Starosolszky and Melder., 1989; Horlick-Jones et al., 1995). The definition includes place, time, and magnitude or intensity. Magnitude refers to landslide destructive power, which is characterised by its intensity (Hung, 1997). The temporal assessment of landslides is usually stated in terms of the return period, frequency, or exceedance probability. Crovelli (2000) formulated the exceedance probability of one or more landslides during a definite time using a continuous-time model (Poisson model) and a discrete-time model (binomial model). LHM uses the LSM and allocates a probable frequency to the landslides of a definite intensity.

Only intrinsic factors are used in LSM, while the recurrence period of the triggering factors is usually used to assess the frequency of events that are subsequently used for LHM (Corominas and Moya, 2008). Frequency and magnitude are two critical components of LHM. The frequency can be expressed either in terms of the number of landslides of a particular character in the study area in a given period or the probability of a specific area experiencing landslides for a given threshold value. Data regarding the number of landslides in the same area requires many years of observation, as Guzzetti et al. (2005) adopted. Hence probability based on a defined threshold is a better alternative for temporal prediction. A threshold can be determined using any landslide-triggering factor like rainfall, earthquake, groundwater level, etc. Most articles on the temporal prediction of landslides have considered rainfall for defining the threshold. The rainfall threshold is the minimum quantity of rainfall required to trigger a landslide (Endo, 1970; Caine, 1980). Some authors have used rainfall thresholds for temporal prediction and permanent intrinsic factors for spatial prediction of landslides (Miller et al., 2009; Segoni et al., 2015; Pham et al., 2017). Guzzetti et al., 1999 recommended using landslide magnitude or size, which represents landslide destructiveness, in the LHM to complete the definition of hazard given by Varnes, 1984. The probability of landslide magnitude or size can be calculated from the study of the frequency–area distribution of landslide inventory prepared (Stark and Hovius, 2001; Guzzetti et al., 2002; Guthrie and Evans, 2004; Malamud et al., 2004).

Landslide hazard in a region is a function of three components, i.e., spatial, temporal, and magnitude probabilities of landslide events. However, because of the severe scarcity of data on landslide dates and magnitudes, many authors have not incorporated the magnitude and time of landslide occurrences in the LHM. LHM is comparatively more challenging than LSM, as susceptibility is one of the three components of landslide hazard. However, in the last four decades, some researchers have repeatedly mistakenly used hazard and susceptibility as synonyms. Many maps in the articles that are susceptible maps were mentioned as hazard maps. Many have shown their concern about mistakenly using these two terms (Guzzetti et al., 1999;

Chacón et al., 2006; Guzzetti et al., 2006a; Cascini, 2008; Hervas and Bobrowsky, 2009; Reichenbach et al., 2018, NDMA, 2019).

Here we present a comprehensive review of different methods available for LSHM. The geographical distribution of LSHM methods for various countries is shown with the size of the pie chart is directly proportional to the number of articles for the country (Fig. 2.1). Further, it was also attempted to classify LSM with LHM based on the information and data these maps can provide (Fig. 2.2). If a map can only provide information on the prediction of where a landslide can take place it is classified as LSM, and if it can provide information of where, when and how big a landslide can take place it will be classified as LHM.

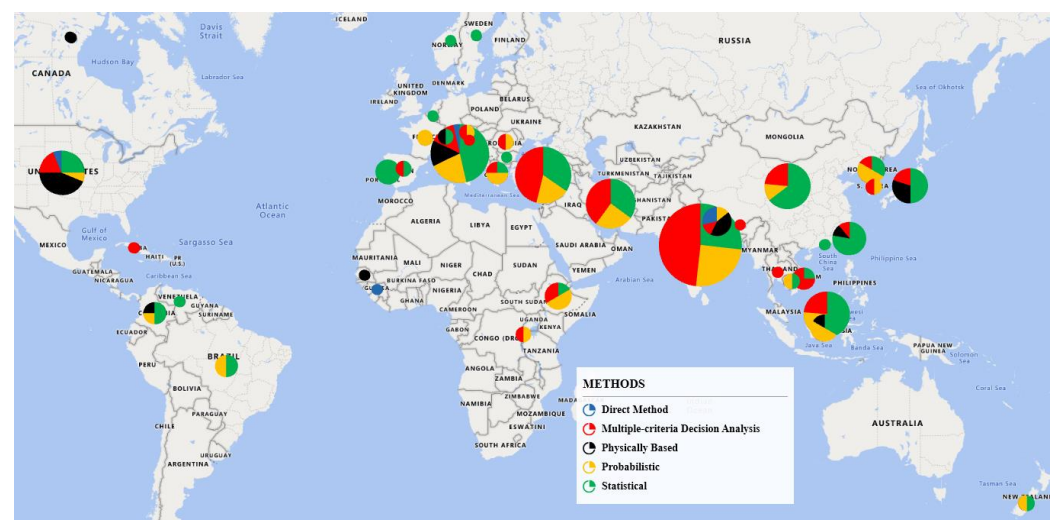


**Fig. 2.1.** Map showing the geographical distribution of LSHM methods for different countries in different colors (Blue- direct method, Red- MCDM, Black- Physically Based, Yellow- Probabilistic, and Green- Statistical). The size of the pie chart is directly proportional to the number of articles for the country.

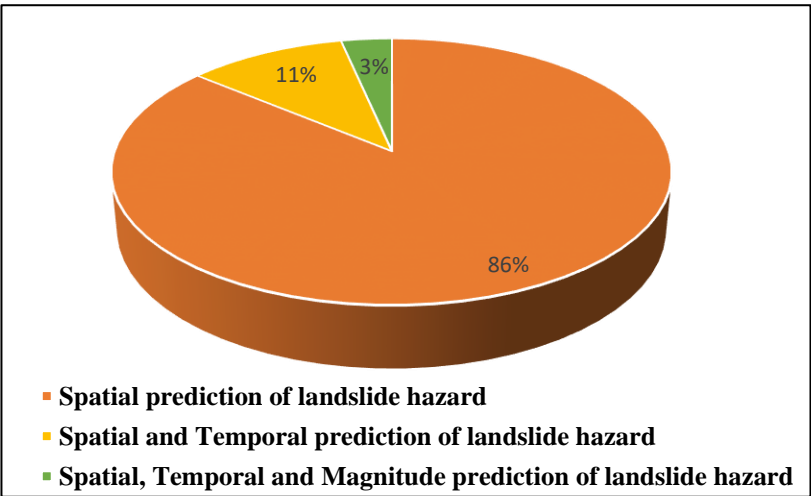


**Fig 2.2** Pie charts showing the percentages of prediction types for landslide hazards.

## **2.3 Landslides Causative Factors**

In landslide studies, factors responsible for landslides are frequently considered based on the analysis of the landslide types and the features of the study region (Ayalew et al. 2005). The occurrence of landslides depends on many factors that can be divided into intrinsic or static factors, which are the areas' inherent properties, causing instability and triggering or dynamic factors that trigger the event. These factors are associated with an area's geology, topography, geotechnical properties, geomorphology, LULC, rainfall, seismicity, anthropogenic activities, etc. (Dai et al., 2002). All factors have different influences in causing landslides depending on the environmental setting of that area. As the terrain conditions vary from place to place, these factors and their combination also change. Hence, no standard methodology is available worldwide for choosing the significant landslide causative factors.

Terzaghi (1950) divided landslide causes into external causes, which increase shearing stress (e.g., Geotechnical changes, unloading the slope toe, loading the slope crest, shocks, vibrations, drawdown, changes in water regime, etc.) and internal causes, which result in a decrease of the shearing resistance (e.g., progressive failure, weathering, seepage erosion, etc.). Varnes (1984) identified landslide causative factors like geology, geomorphology, hydrologic conditions, climate, vegetation, factors that change stress conditions, and the strength of materials. Hutchinson (1995) discussed the various combination of geo-environmental factors leading to landslides. He concluded that bedrock geology, geomorphology, soil properties, LULC, and hydrological condition are essential factors and should be incorporated in LSM. The landslide-inducing factors may be divided into static and dynamic factors (Jia et al., 2008; Tyagi et al., 2023).

### **2.3.1 Static Factors**

The static factors include geological and geographical ones, e.g., the lithology, fault, hydrogeology, topography, etc., that are relatively steady and invariable and provide the necessary prerequisite for forming landslides slopes. Brabb (1972) was the first to analyse the frequency of landslides using geology and slope as the causative factors in San Mateo County, California. He defined susceptibility as the likelihood of a landslide happening in a region based on intrinsic parameters. It provides us with information of "where" landslides are likely to occur. Basic surface-related characteristics related to sliding are called static factors or primary factors (Sidle and Ochiai, 2006). Static factors are the determinants of landslide susceptibility and can be derived from surface characteristics.

### 2.3.2 Dynamic Factors

The dynamic factors include rainfall, earthquake, human activities (LULC), and groundwater that accelerate or decelerate the landslide occurrences. The dynamic factors of landslides can be divided into human and natural factors. Natural factors include meteorological hydrology, hydrogeology, weathering, and new tectonic movements due to earthquakes, river erosion, freezing, and thawing (Capitani et al., 2013). Human factors refer to human engineering activities, indicating that human factors are the most significant factors for developing landslides and are often even the decisive influencing factors. The landslides are often triggered by torrential heavy rainfall, flash floods, seismic activities, or anthropological reasons such as heavy vehicles' movement or, usually, human activities on unstable slopes (Kwan et al. 2014; Li et al. 2014). Many past literature reviews suggest that complex hydrogeological settings and increasing anthropogenic activities are among the key factors that often influence landslide occurrences (Rai et al., 2014; Singh and Sharma, 2021).

Researchers have concluded that human-induced LULC change has a significant impact on the initiation of landslide events (Guillard and Zêzere 2012; Galve et al. 2015; Meneses et al. 2019), particularly in populated areas where landslides are the main threat to human settlements and infrastructures (Pinyol et al. 2012; Abancó and Hürlimann, 2014). Developments such as road and railways construction, building construction due to increasing population, etc., have led to deforestation, slope cuts, construction landfills, and garbage dumps, thereby destabilizing the area and making the region prone to landslides. Though urban development leads to industrialization and commercialization, it has some limitations. It has a significant impact on the regional and global climate (Karl and Trenberth 2003), biogeochemical systems (Oleson et al. 2008), hydrological condition (Chung et al. 2011), and LULC change (Patra et al. 2018).

Deforested areas have a diminished capacity to act as a carbon dioxide sink and are a direct source of greenhouse gases if accompanied by biomass burning. Land conversion from natural vegetation to agriculture or pasturage also alters the terrestrial albedo, contributing to changes in the surface radiative balance (Krishnan et al., 2020). The severe changes in land cover and climate, particularly in developing countries, are mainly due to widespread urban growth and the alteration of natural regions into industrial or agricultural areas (Jat, 2008). About one-third of the Earth's surface is used for irrigation, and over half of the surface has been altered over the past few years (Houghton, 1994). In future decades, this depletion trend in natural land, thick forests, watersheds, and increased urbanization will increase regional precipitation and temperature due to climate change (Schuster 1996; Andersson-Sköld et al. 2013).

The extreme changes in climatic conditions will further cause rivers to dry in summer and heavy runoff during the rainy season (Olsson et al. 2011). These changes will cause soil erosion, water level change, and vegetation changes that will affect slope stability (Parry et al. 2007). The increased erosion will increase the landslide probability, while other climate change impacts on landslide probability are challenging to predict (Suh et al. 2011; Korup et al. 2012). Dynamic factors like climate change and LULC change are the most influencing and can also be used in predicting future LSM. Climate and its variations control or affect landslide activities, chiefly precipitation and temperature (Sidle and Ochiai 2006; Crozier 2010; Huggel et al. 2012).

### **2.3.3 Optimization of factors**

In landslide studies, these parameters are frequently considered based on the analysis of the landslide types and the features of the study region (Ayalew et al. 2005). Selecting landslide causal parameters and their classes should be considered an essential step in LSM analysis (Costanzo et al. 2012; Meinhardt et al. 2015). According to Lee and Talib (2005), selecting significant parameters can increase the model's prediction accuracy. Thus, determining parameter significance for the study area is essential before performing susceptibility analysis. Removing less effective factors can reduce noise and uncertainties and thus improve the predicting ability of the model (Pradhan and Lee 2010; Martínez-Álvarez et al. 2013). Methods like multicollinearity analysis and correlation attribute evaluation can eliminate the least significant parameters (Chen et al. 2017).

## **2.4 LSHM Models**

The spatial probability of landslide occurrence, known as susceptibility, is the probability that any given region will be affected by landslides with influences of a set of environmental variables (Brabb, 1984). The susceptibility map aims to identify areas likely to be affected by landslides in the near future by various natural and artificial causes. LSM aims to differentiate a land surface into homogeneous regions according to the degree of potential hazard caused by a mass movement in specific locations (Varnes, 1978).

According to Brabb (1984), landslide susceptibility is the likelihood of a landslide happening in a region based on intrinsic factors. It provides us with information of "where" landslides are likely to occur. LSM does not consider the size or intensity of the landslides but can be prepared for different landslides (Carrara et al., 1995). LSM uses landslide inventory data to predict future slope failure assuming all the environmental conditions will remain the same. Landslides inventory data is prepared by recognising, categorising, and mapping these landslides through remote sensing and field surveys (Rib and Liang, 1978; Varnes, 1978; Hutchinson, 1988; Dikau et al., 1996). The prediction to identify the place of landslide happening over an area based on intrinsic landslide-causing factors is termed as a spatial prediction of landslide. It can also be defined as partitioning a study area into homogeneous

zones based on geological and geomorphological characteristics and then ranking them based on the degrees of landslide susceptibility.

The LSHM is complex as the terrain and climatic conditions vary from place to place (Brabb, 1991). Factors responsible for causing landslides also change as these conditions change. Several methods have been proposed for ranking slope instability factors (Fig. 2.3). These methods are used for assigning the levels of danger to terrain that can be done in a qualitative, semi-quantitative, or quantitative way. The most effective methods in practice for more than 20 years were investigated and can be grouped into a few main categories: Qualitative, Semi-Quantitative, and Quantitative.

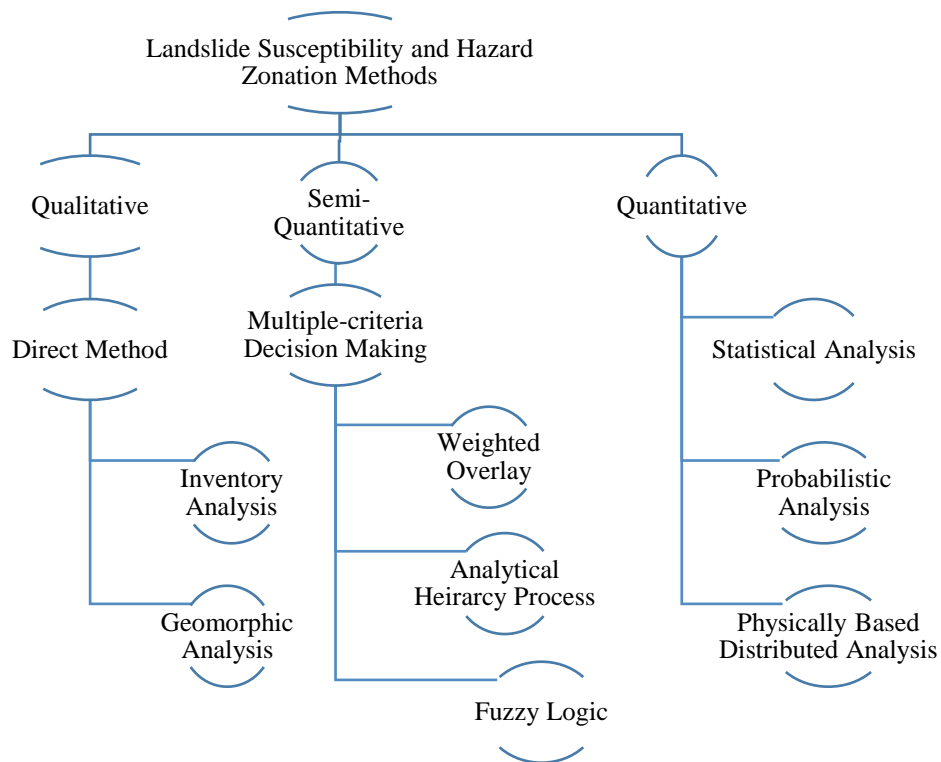


**Fig. 2.3** Landslide susceptibility and hazard zonation methods

#### 2.4.1 Qualitative Models

In qualitative methods, the data used for analysis are generally non-numeric. Also, the high proportion of subjectivity is involved in the generation of numerous thematic data layers responsible for landslide events combined in LSM for the region. Qualitative methods are direct methods that portray zoning in descriptive terms. We obtained two qualitative methods from the database prepared, i.e., Inventory analysis and Geomorphic analysis used by various authors in landslide studies, as discussed below.

### **Inventory Analysis (IA)**

It is one of the most straightforward, direct, and qualitative methods for LSM. Past landslide data are obtained through field study, old records, aerial photographs, and satellite images. In this analysis, inventory maps that depict the spatial arrangement of landslide scattering are prepared. Campbell (1973), Wright and Nilsen (1974), and Wright et al. (1974) generated isopleth maps of landslide data using the areal distribution of landslides. The Isopleth map shows the number or percent of the area covered by landslide deposits over a region. Further, they discussed their uses in different fields of applications. DeGraff (1985) transformed landslide inventory maps into isopleth maps and defined relative landslide susceptibility as the percent of a standard area underlain by landslides. Cruden (1991) explained inventory analysis as the simplest type of landslide data consisting of landslide type, location, and event date. Guzzetti et al. (1994) prepared the inventory of areas historically affected by landslides and floods in Italy to predict future instability patterns from the past and present distribution of landslide deposits. They used mainly three sources of information for inventory preparation, i.e., newspapers, interviews, and the review of technical and scientific documents. According to Dai and Lee (2002) and Galli et al. (2008), IA methods are a mandatory step for all data-driven LSM methods, as they are used to prepare input data for analysis and validation purposes. Guzzetti et al. (2002) used universal area statistics to compare three landslide inventories. The result shows that as the landslide area increases, the number of landslide events rapidly increases to an extreme value and then reduces as a power-law function. Chau et al. (2004) used the IA method and prepared a GIS structure for organised LHM by using past landslide records in the Hong Kong region, combining geological, rainfall, climatic population, and geomorphological data. Colombo et al. (2005) generated landslide inventory maps by orderly inspections using aerial photos and GIS records to process the data. The IA approaches are expensive, cumbersome, and laborious, but maps obtained from this give basic information on areas affected by landslides.

### **Geomorphic Analysis (GA)**

It is a direct, qualitative technique that depends on the researcher's capability to evaluate actual and potential slope failures. The investigator prepares LSM based on his experience by studying the geomorphological properties of the study region. Kienholz et al. (1983, 1984) presented land use maps and geomorphic damages maps, which were further used to prepare a base map. The base map contains information like actual and potential damage by erosion and landslides, an area protected by forests and streams, and supplementary information. Zimmerman et al. (1986) mapped numerous geomorphic hazard processes (avalanches, rockfall, landslide hazards) on a scale of 1: 50,000. Seeley and West (1990) evaluated and zoned geological hazards for land-use planning without describing any rules. They used aerial photographs, field data and consulted with selected geologists and volcanologists for this

purpose. Hansen et al. (1995) reviewed factors like terrain classification, geology type, etc., related to the application of GIS services concerning landslides. In the same year, Hearn (1995) study consisted of a thorough landslide inventory, geomorphological mapping using aerial photographs, and assessment of available geological and geotechnical data. He commented that the LSM is directly prepared from comprehensive geomorphological maps. Cardinali et al. (2002) presented a geomorphological method to produce landslide hazards and risk maps. They used multi-temporal landslide inventory maps to represent the scattering of the current and past landslides and their variation for about 60 years. Reichenbach et al. (2005) used a geomorphological method for LSM and risk assessment in Umbria, Italy. It is built on vigilant recognition of landslides, inspecting the regional geology and morphology, and studying past data on landslides for the selected region. Much evidence used to determine LSM was gathered from the investigation of past landslide data that depicts evidence on the scattering, nature, and shape of landslides and how they vary with time. The multitemporal map was generated by integrating historic landslide data of different periods, which were prepared using aerial photographs and field studies. Calista et al. (2016) used this technique to study the development of new landslides and the likely retreat of the prominent scarp. This was done by performing multitemporal geomorphological investigation using aerial photographs, LiDAR data, and field data interpretation.

#### **2.4.2 Semi-Quantitative Models**

Semi-quantitative methods are a hybrid of both qualitative and quantitative methods. These methods have the ability to make decisions in the calculation of weights and ratings of factors and their classes in LSM. To make a decision, these methods use some criteria like past landslide data or expert knowledge, or a combination of both in analysis. In the database analysis, we obtained three semi-quantitative Multiple-criteria Decision Making (MCDM) methods used extensively over the last three decades. These methods include weighted overlay, analytical hierarchy process, and fuzzy logic, as discussed below.

##### **Weighted Overlay (WOL)**

It is an indirect semi-quantitative method where the investigator uses prior knowledge and information to give weightage subjectively. These weights and rating is given numerically based on the scales defined by different authors. These approaches are based on the a priori information of all the factors responsible for causing landslides in the area. Accuracy depends on how good an investigator is at understanding the terrain geomorphology. Brabb et al. (1972) were the first to analyse the frequency of landslides using the geology and slope as the causative factors in San Mateo County, California. Further, Nilsen and Brabb (1977) mentioned other factors apart from slope and geology responsible for causing slope failure in their study. Hollingsworth and Kovacs (1981) assigned numeric values to three factors responsible for causing southern California soil slumps during heavy rainstorms. Takei (1980) considered

fracturing, vegetation cover, rock types, landslide inventory, slopes, and springs as the contributing factors for susceptibility map preparation in Japan. Roth (1983) constructed a data set to analyse regional landslide-susceptibility with six input variables, i.e., slope angle, Soil, rainfall, rock, vegetation, and landslide inventory. Gupta and Joshi (1990) used the landslide nominal risk factor method with field surveys and aerial photography for LHM. Thereafter, many authors followed this technique in landslide studies.

The WOL method is a simple overlay technique for LHM, considering factors that cause slope instability. These factors are signed by weight subjectively by analysing the relationship between causative factors and landslide frequency (McKean et al., 1991; Pachauri and Pant, 1992; Sarkar et al., 1995; Gökçeoglu and Aksoy, 1996; Turrini and Visintainer, 1998; Abella and Van Westen, 2008; Ruff and Czurda, 2008; Nithya and Prasanna, 2010; Balteanu et al., 2010; Lallianthanga et al., 2013; Ayele et al., 2014). Further, Anbalagan (1992) suggested a rating system called Landslide hazard evaluation factor for LHM. This empirical system used major intrinsic factors of landslide, such as geology, slope, relative relief, groundwater, and LULC. Van Westen (1994) discussed the applications and suitability of GIS in indirect LSM, where all promising landslide-responsible factors were correlated with past landslide data using data-integration methods. A method presented by Mejía-Navarro et al. (1994) uses the GIS technique to evaluate geological hazards in the region of concentrated debris flows and sheet erosion activated by landslides. Further, vulnerability and risk were also assessed for Glenwood Springs, Colorado. For LHM, obtaining various thematic layers of factors responsible for landslides was preferred using aerial photographs and satellite images (Panikkar and Subramaniyan, 1997; Saha et al., 2002; Parise, 2002; Patwary and Parvaiz, 2009; Chandel et al., 2011) and analysing them in GIS environment (Sarkar and Kanungo, 2004; Champati Ray, 2005; Pandey et al., 2008; Deshpande et al., 2009; Gupta et al., 2009; Raghuvanshi et al., 2014; Kumar et al., 2018; Prakasam et al., 2020).

### **Analytic hierarchy process (AHP)**

It is an MCDM approach invented by Satty (1980) to break complex decisions into a hierarchy of simple forms which can be evaluated subjectively. Using a numerical scale, this subjectivity is removed, and each alternative is ranked numerically. It assists decision-makers in determining the relative influence of different factors by comparing them pair-wise (Yoon and Hwang, 1995). Saaty (1990) and Saaty and Vargas (2007) gave a stepwise procedure for applying AHP. The first step is to define the problem. Afterward, goals and alternatives are determined, followed by a pair-wise comparison. Further, weights are obtained based on the results of the comparison. AHP can be used successfully for medium-scale LSM, where various landslide causative factors are considered as alternatives (Soeters and van Westen, 1996). The AHP method was compared with the WOL method (Barredo et al., 2000), Logistic Regression (LR) method (Ayalew et al., 2005), Information Value (IV) method (Yalcin, 2008), and Support

Vector Machine (SVM) method (Kavzoglu et al., 2014). The comparison showed that the AHP method gave a more accurate image of the real distribution of landslide susceptibility than other methods for their respective study areas.

AHP method was applied for LSM using various topographical and geological factors responsible for causing landslides (Yoshimatsu and Abe, 2006; Mondal and Maiti, 2012; Thanh and De Smedt, 2012; Feizizadeh et al., 2013; Kayastha et al., 2013; Ma et al., 2013; Kumar et al., 2018; Bera et al., 2019). The attractive characteristic of the AHP is the ability to calculate the inconsistent weights produced. The eigenvalues obtained in the calculation are used to measure the consistency of the matrix defined by Satty (1980). The inconsistencies obtained while making the decision can find out using AHP and can be corrected. Hence, the performance of the AHP model is often more for LSM than other models. However, in AHP, it is assumed that factors are independent and are not correlated with each other. To overcome this limitation, Saaty developed Analytical Network Process (ANP) technique after twenty-five years of development of the AHP method, which considers inner dependence among factors in a network. Neaupane and Piantanakulchai (2006) used this successor of the AHP for the LHM of a region in the mountainous terrain of Nepal. The main drawback in ANP is the formation and calculation of multiple matrices, which gets complicated as the number of factors increases in landslide analysis. Komac (2006) used multivariate statistical analysis to obtain the relation between landslide distribution and factors. Based on the statistical results, many LSM analysis were performed using the AHP method. Akgun et al. (2008) used the Frequency ratio (FR) method and weighted linear combination (WLC) method to produce LSM for the Findikli district, Rize, Northeast Turkey. The WLC model used expert judgment in decision-making, and analysis was performed using the reliable mathematical AHP method. Wu and Chen (2009) generated an LSM model for Taiwan using the AHP technique. They considered rainfall as the main contributing factor in causing landslides. Akgun and Turk (2010) used the fuzzy set model to prepare a pair-wise matrix by assigning values to the AHP matrix for comparison and obtaining weights. Intarawichian and Dasananda (2010) used AHP to give weights and WLC methods to generate Landslide Susceptibility Index (LSI), which were classified and divided into zones to obtain an LSM of the Mae Chaem Watershed, north Thailand.

GIS-MCDM combines and transforms geographical data and makes decisions by judgments to obtain information (Feizizadeh and Blaschke, 2013). They used the landslide inventory dataset and Dempster-Shafer theory to measure the uncertainty in the LSM. Results indicated that the AHP model accuracy was the best compared to the WLC and Ordered weighted averaging (OWA) models. WLC and OWA are two commonly used MCDM methods in landslide studies. According to Kumar and Anbalagan (2016), a major drawback of AHP is that the relative weightage given to factors causing landslides by an individual is often not understood by others. Although, if weights are provided by considering past landslide records,

they are more evident to others. Van et al. (2016) combined AHP and WLC methods to produce LSM for Vietnam. They used AHP for pair-wise comparison and to build the weights of individual factors. After that, the weights are integrated by the WLC to form a single score for each pixel. Based on this pixel value, they are further classified into zones to generate a susceptible map. Yan et al. (2019) combined AHP with FR methods to generate LSM. They used the AHP method to obtain the weight of individual factors and the FR method to obtain the weight of each class for all factors. Further, they concluded that the AHP method is suitable for solving complex problems in landslide studies. Still, as different experts give different weights to all the factors, it has this limitation of subjectivity. Dikshit et al. (2020) used the Poisson probability model for the temporal assessment of landslides, which was further used as a factor in the AHP method for LSM. Roccati et al. (2021) applied AHP for risk mitigation planning. They added objectivity to the model by using landslide inventory data and obtaining quantitative results. Further, the subjective component that arises from the expert's opinion helped the decision-making process.

### **Fuzzy logic (FL)**

The term fuzzy logic was first introduced by La (1965) using fuzzy set theory. His theory is generally considered an effective tool for dealing with linguistic data. This theory can deliver a method where multiple datasets can be quantitatively processed. Juang et al. (1992) and Davis and Keller (1997) used fuzzy set analysis to develop an inexpensive, qualitative evaluation scheme for mapping slope failure potential. Fuzzy set theory is comparatively more flexible than classical theory (Berkan and Trubatch, 1997). FL method for LSM used bivariate analysis where all factors are represented by 0 and 1 values depending on their influence on landslide occurrence. FL methods help to handle data uncertainty, particularly at small scales of LHM, because data have to classify in sets (Elias and Bandis, 2000). FL method can be used for LHM by using the correlation between landslide inventory and factors responsible for causing landslides (Chi et al., 2002; Champatiray et al., 2007; Rampini et al., 2013; Zhu et al., 2014; Uvaraj and Neelakantan, 2018; Razifard et al., 2019; Baharvand et al., 2020). Ercanoglu and Gokceoglu (2002) extracted factors representing if-then rules and fuzzy sets from landslide inventory. Factors were selected for generating LSM using these rules. Ross (2004), in his book "Fuzzy Logic with Engineering Applications," explained in detail the methods of fuzzy systems, differences in classical and fuzzy relations, and how decisions are made using fuzzy Information. Ercanoglu and Gokceoglu (2004) analysed both factors and landslide data using FULLSA. This computer program generated LSM utilising fuzzy relations.

Further, Kanungo et al. (2006) prepared LSM in a part of the Darjeeling Himalayas using three methods, i.e., ANN, FL, and a combination of both. Among all these methods, the LSM prepared based on the hybrid method was significantly better than others. Lee (2007) and Kumar and Anbalagan (2015a) combined FR and FL to increase the accuracy of LSM. They aimed to

provide subjectivity using FL to a data-driven method like FR to improve the model's flexibility. Pradhan (2011) attempted to produce the LSM of Malaysia using the relationships of FL. Further, he commented that the main advantage of FL over other methods is that it does not depend on the statistical distribution of the data, and there is no requirement for particular statistical variables. Pourghasemi et al. (2012a) produced the LSM of an area in Iran subjected to landslide by using both FL and AHP methods. The comparison results showed that the FL method's accuracy was better than the AHP method. Bui et al. (2012a) used FR to calculate factors contribution, and then the ratio value was normalised from 0.1 to 0.9. These fuzzy membership values were combined using fuzzy operators like fuzzy SUM, fuzzy PRODUCT, and fuzzy GAMMA to calculate landslide susceptibility index (LSI) values. Further, they concluded that fuzzy SUM had the least prediction ability than PRODUCT and GAMMA operators. Akgun et al. (2012) developed a method that uses expert opinion in LSM for the Sinop area in Turkey. This method applied Mamdani fuzzy inference system (Mamdani and Assilian, 1975) developed using the MATLAB program. Ahmed et al. (2014) used semi-qualitative WOL and FL techniques for LSM in the Upper Indus River basin. Also, they highlighted those critical local areas which demand a more comprehensive site-specific investigation. Berenguer et al. (2015) used the FL method for spatial and temporal prediction and combined them to produce dynamic LHM at a regional scale in Spain. Meten et al. (2015) used FL and a Rock Engineering System (RES) for LSM in the Selelkula area in Central Ethiopian Highland. They applied different fuzzy operators using the input fuzzy membership functions for LSM. All different kinds of fuzzy operators used in the analysis produced various quality maps. They generated 12 maps using multiple operators and compared them using the AUC of the Receiver Operating Characteristic (ROC) curve. The result showed that the gamma operator ( $\gamma = 0.8$ ) presented the finest prediction accuracy while the fuzzy OR operator presented the least. The results showed that the accuracy of the technique is appropriate in predicting landslide occurrences.

### **2.4.3 Quantitative Models**

Quantitative methods generate numerical approximations of landslide events in an area using landslide inventory. These methods calculate the probability of landslides based on the assumption that landslide-responsible factors and landslides are uniformly distributed in an area. These methods can estimate the weightage and rating of factors objectively for LSM. Several quantitative methods are used in LSHM, which are summarised below.

#### **Statistical Analysis**

The statistical method uses mathematical equations for the analysis of raw research data. They are built on studying the functional relations between factors responsible for landslides and inventory. Carrara et al. (1977, 1978, 1991) correlated the landslide distribution with factors responsible for landslides using software-automated thematic cartography. He commented that

Multivariate techniques are efficient for objectively measuring different landslide susceptibility zones. Predictions about future landslide occurrences can be made using statistical relationships between landslide inventory and factors responsible for landslides (Chung and Fabbri, 1995; Pan et al., 2008). Both bivariate and multivariate statistical models can be used for the analysis. Multivariate methods are superior to bivariate as they are more sensitive in intermixing the landslide-responsible factors considered for the modeling (Süzen and Doyuran, 2004). Multivariate methods give more reliable results, both in terms of the training and prediction portions of the susceptibility analysis, as these methods simultaneously consider all the factors contributing to landslides (Nandi and Shakoor, 2010). To reduce the subjectivity in giving weight, data-driven methods are used instead of knowledge-driven (Kanungo et al., 2012). Here, we discuss five data-driven statistical methods used in LSHM by the researcher.

### **Discriminant analysis (DA)**

It is one of the oldest statistical methods which uses multiple variables for LSM. It helps to differentiate between the effect of different landslide responsible factors and give weightage to them. Neuland (1976) used principal component analysis to clarify the relationships between the topography of Germany and 250 past landslide records. Further, a prediction is made using a bivariate DA whose efficiency is tested by a procedure of the Euclid distance. Carrara (1983) used DA and regression analysis for LHM in Calabria, Italy. He used geological and geomorphological factors in the investigation responsible for landslides. Neeley and Rice (1990) used the checklist for mass movement and field data to generate a three-variable equation. This equation was used to predict the risk of debris slides in California. Inventory maps accuracy has a significant influence on the accuracy of predicted LHM. Hence, assessing the impact of errors in inventory maps on predictive models of landslide hazards is essential (Ardizzone et al., 2002).

DA method is a very effective multivariate statistical technique for situations involving categorical dependent variables like landslide inventory and quantitative independent variables like geological-geomorphological factors (Santacana et al., 2003; Lee et al., 2008; Eeckhaut et al., 2009; Dong et al., 2009; Chen and Chang, 2016). Guzzetti et al. (2006) used this method for the spatial prediction of landslides. They adopted a Poisson probability model for temporal prediction to determine the exceedance probability of having one or more landslides for all pixels or cells. Further, they obtain the probability of landslide size by analysing frequency–area statistics of landslides. Using these three probabilities and assuming their independence, they performed LHM for the area. Rossi et al. (2010) performed LSM using LR, neural network (nn), Linear Discriminant Analysis (LDA), and Quadratic Discriminant Analysis (QDA). In the training set, nn over-fitted the information of landslides. The result concludes that LR, LDA, and QDA had better prediction capability for the area in Umbria, Italy. Calvello et al. (2013) used a methodology based on the evaluation for each Terrain Computational Unit (TCU) of a

score used to discriminate between two groups of terrain units, i.e., landslide-affected and landslide-free areas.

Ramos-Cañón et al. (2016) used LDA to obtain easy mathematical functions that signify the probability of landslides happening in Bogotá, Colombia. The functions were also used to recognise the most relevant variables, such as normalised rainfall intensity and normalised daily rainfall derived from rainfall records linked to the landslide events. Multivariate statistical methods like LR, DA, and IV do well when calculated over diverse terrain, and the selection of these methods for LSM should depend on the variability of these terrain units (Zêzere et al., 2017). Barella et al. (2019) compared FR, IV, LR, Bayesian model, Weights of Evidence (WofE), and landslide density models for LSM in Minas Gerais state in Brazil. Validation of models showed that all methods produced acceptable results. Wang et al. (2020) used WofE, LDA, Fisher's Linear Discriminant Analysis (FLDA), and QDA to obtain the LSM in China. The results based on the Success Rate Curve (SRC) revealed that FLDA had greater accuracy than the other methods. According to Eiras et al. (2021) latest machine learning methods for LSM are very robust, whereas simple methods like DA also have good predictive abilities for generating LSMs.

#### **Information Value (IV)**

It is a bi-variate statistical technique to find a relationship between unstable slopes and their responsible factors (Yin and Yan, 1988). Jade and Sarkar (1993) and Van Westen (1997) proposed the IV method for LHM, which considers the likelihood of landslide occurrence. It is an indirect statistical method that objectively evaluates LSM (Zezere, 2002). This method was compared with Landslide Nominal Susceptibility Factor (LNSF) techniques by Saha et al. (2005) and AHP by Singh and Kumar (2018). It was found that the LHM prepared using the IV method had a better prediction rate than AHP and LNSF for respective study areas. Wang and Sassa (2005) adopted LR and the IV model to produce susceptibility maps of landslide occurrence and combined them to increase the prediction rate. Sarkar et al. (2006) selected six factors for preparing LSM for Sikkim by preparing thematic data layers and determined the IV for every subdivision of landslide-related factors based on the presence or absence of landslide in a given area. The best combination of factors should be chosen for predicting landslides (Pereira et al., 2012). Both optical Balsubramani and Kumaraswamy (2013), Sarda and Pandey (2019), and InSAR satellite data Mengistu et al. (2019) can be used in LHM by adopting the IV method.

#### **Logistic Regression (LR)**

It is a very suitable method for predicting the existence or nonexistence of a landslide (Atkinson and Massari, 1998). The LR prediction rate is approximately 90% in successfully mapping stable and unstable areas (Rowbotham and Dudycha, 1998). This method is widely

adopted in obtaining the correlation between landslide inventory and landslide causative factors (Dai and Lee, 2001; Gorsevski et al., 2006; Nefeslioglu et al., 2008; Mancini et al., 2010; Kumar and Anbalagan, 2015b; Kavzoglu et al., 2015; Erenner et al., 2016; Zhu et al., 2018; Zhao et al., 2019; Du et al., 2020; Goyes-Peñafiel and Hernandez-Rojas, 2021). LR relates landslide-responsible factors to the presence or absence of landslides within topographic cells and uses the relationship to generate a map showing the likelihood of future landslides (Ohlmacher and Davis, 2003). LR method was compared with the FR method (Lee, 2005), the SVM method (Brenning, 2005), the AHP method (Akgun, 2012), Statistical Index (SI) method (Pourghasemi et al., 2013a). Comparison results showed that the LR method is good at simplifying and produced fewer error rates than other methods for their respective study areas.

According to Ayalew and Yamagishi (2005), LR is flexible compared to other multivariate statistical methods as it can be transformed into a bivariate so that interpretation of results can be simple. Greco et al. (2007) gave a stepwise procedure for adopting the LR method. The first step is to collect samples with factors responsible for landslides. In the second step, variables are transformed from non-parametric to parametric. The third step is to fit the model for calculating coefficients, and the last step is applying the model where the function is best fitted. Standard rainfall-induced landslide models are insufficient for areas with a higher frequency of storm and earthquake events. Hence, Chang et al. (2007) generated typhoon- and earthquake-induced landslide models using LR in Taiwan. Chang and Chiang (2009) used a critical rainfall rate, while Lee et al. (2010) used seismic ground motions and amplification factors as landslide causative factors in LHM. Meusburger and Alewell (2009) obtained the variation in LSM prepared for 1959 and 2000 and generated the deviated map. Further, they commented that changing responsible, dynamic factors would affect the landslide prediction.

Jaiswal et al. (2010) used the available historical records of landslide volume for calculating the probability of magnitude prediction of landslide hazard. Further, they estimated the probabilities for spatial and temporal prediction using LR and Poisson models and combined magnitude probability to obtain the joint probability, assuming all three probabilities to be mutually independent. Erner and Düzgün (2010) stated that the LR method does not consider spatial changeability in the regression factors. Hence to increase the efficiency of the technique, factors were investigated to obtain a spatial correlation between them to produce a susceptibility map. Analysis in the LR method becomes complex as the number of causative factors increases. Hence, Atkinson and Massari (2011) omitted several insignificant factors using auto-covariate. The auto-covariate was estimated by applying a Gibbs sampler to the susceptibilities for neighboring pixels. Das et al. (2011) evaluated the landslide hazard based on Homogenous Susceptible Units (HSU). They derived these units from an LSM generated using the LR method using an automated segmentation procedure. Temporal probabilities are estimated using a Poisson method, and size probabilities are calculated using an inverse-gamma method. A

quantitative analysis of landslide hazards for each unit was done by multiplying spatial, temporal, and size probabilities. According to Das et al. (2012), ordinary LR does not permit the addition of previous information. Hence to solve this purpose, they took the help of Bayesian analysis using iterative simulation methods for LSM. Xing et al. (2021) revised the LR technique to estimate dynamic landslide susceptibility using rainfall data. The revised model can evaluate the possibility of future landslides under critical rainfall events.

### **Support Vector Machine (SVM)**

SVMs are the supervised learning methods used for classification applications in the early 1990s, and their application was afterward extended to regression problems based on statistical learning theory by Vapnik (1995). The SVM accomplishes classification jobs by using classifier functions, which can create hyperplanes in multidimensional space, thus separating dissimilar clusters of training data (Vapnick, 1998). The SVM model can be applied for LSM using remote sensing data and GIS techniques (Ma et al., 2003; Jiang et al., 2005; Marjanović et al., 2011; Lin et al., 2017). SVM transfers the input factors into a large-dimension space which can provide non-linear solutions to regression and classification problems (Yao and Dai, 2006; Yao et al., 2008; Ballabio and Sterlacchini, 2012; Xu et al., 2012)

Pourghasemi et al. (2013b) used six kernel classifiers in the SVM technique to generate the LSM. It was concluded that the prediction capability of the radial basis function (RBF) classifier was superior to linear polynomials of degrees 2,3, 4 and sigmoid classifiers. Similarly, Chen et al. (2016) also compared the prediction rate of four kernel classifiers, i.e., linear, polynomial, RBF and sigmoid. Chen et al. (2017) compared the prediction capabilities of three data mining methods. Generalised Additive Model (GAM), SVM, and combined ANFIS with FR methods were adopted for generating LSM in the China region. They concluded that SVM outperformed the other two methods for predicting landslide-prone areas in the China region.

### **Artificial Neural Network (ANN)**

ANNs are fundamentally huge parallel computational models replicating the human brain's role. It comprises a significant number of easy processors connected by a weighted system. Here, neurons are processing units whose output depends only on the data that is locally available at the node, either stored internally or received via the weighted connections. These input units obtain various information based on the internal weighting system. Further, it tries to learn and generate output based on the information provided. ANN can perform large-scale processing by allocating parallel work. ANN is a computational tool that can obtain, represent, and calculate a plotting from a multivariate information space to another given set representing that mapping (Garrett, 1994). The most regularly used algorithm in the neural network method is back-propagation. It is used to define the rules for assigning weights to factors responsible for landslides and to train the multi-layered neural network, which can further classify the whole

database (Paola and Schowengerdt, 1995; Lee et al., 2001; Lee et al., 2003; Ercanglu, 2005; Melchiorre et al. (2008); Nefeslioglu et al., 2008; Caniani et al., 2008; Pradhan and Lee, 2009; Pradhan and Lee, 2010; Bui et al., 2012; Tsangaratos and Benardos, 2014). ANN is quite similar to statistical methods, and numerous ANNs were established on a statistical basis (Bishop, 1995; Patterson, 1996). It is a non-linear technique capable of performing LSM with high accuracy. It does not need specific variables as it is free of the statistical distribution of the data (Perus and Krajnc, 1996; Lee et al., 2004). ANN method was compared with the WOL method (Arora et al., 2004), LR method (Yesilnacar and Topal, 2005), Decision Tree (DT) method, SVM method (Pradhan, 2012), and FR method (Aditian et al., 2018). They concluded from their comparison result that ANN gives more realistic results than others for their respective areas.

Chang and Liu (2004) and Gomez and Kavzoglu (2005) fused multi-source data to build the feature space for landslide investigation. An nn method called Multilayer Perceptron (MLP), along with landslide features, was used for recognizing landslides. Ermini et al. (2005) used two different ANNs, i.e., MLP and the Probabilistic Neural Network (PNN), in classification problems. Both methods can be grouped in black-box models. The MLPs support the back-propagation algorithm, and PNNs use the Kernel approach for estimating the probability density function. Further, they concluded that MLP had slightly better performance than PNN. Catani et al. (2005) adopted the ANN method for the spatial and temporal assessment of landslide hazards in the Arno River, Italy basin. The temporal assessment was achieved by combining the susceptibility values with data on average recurrence intervals to the susceptibility classes, which gives a return period. Further, vulnerability and risk assessment was carried out for land planning and risk prevention. Oh and Pradhan (2011) and Sezer et al. (2011) used both bits of knowledge of an expert and supervised learning algorithm for LSM. They used the Adaptive Neuro-Fuzzy Inference System (ANFIS) model, where factors responsible for landslides are related to past landslides by if-then fuzzy rules and were further optimised by ANN. Kumar and Anbalagan (2015c) used an ANN system called Radial Basis Function Link Net (RBFLN), which is an extension of the Radial Basis Function Neural Network (RBFNN) for the LSM. Further, they stated that integrating factors responsible for landslides using RBFLN had produced satisfactory results for the Tehri region, India. Chen et al. (2017) used a probabilistic method of Certainty Factor (CF) to find the relationships between landslide-responsible factors and past landslides. Further, data mining techniques like a Genetic Algorithm (GA), Differential Evolution (DE), and Particle Swarm Optimisation (PSO) were combined with the ANFIS method to generate a model for LHM. They concluded that the highest accuracy achieved was in the case of the ANFIS-DE model, and the least was in the ANFIS-PSO model.

Moayedi et al. (2019) used PSO to optimise the ANN technique for predicting areas susceptible to sliding. Further, they concluded that the PSO-ANN model presented greater consistency in predicting the LSM than the ANN. Nguyen et al. (2019) evaluated the capability

of ANN created with PSO and Artificial Bee Colony (ABC) algorithms for LSM. They concluded that PSO-ANN performs better than ABC-ANN. Bui et al. (2019) used the metaheuristic algorithm Harris Hawks Optimisation (HHO) to optimise the performance of ANN in LSM. They concluded that the performance of ANN could be improved effectively using the HHO algorithm in both recognising and predicting the landslide pattern. Moayedi et al. (2019) outlined two novel optimisation algorithms of ANN, i.e., Biogeography-Based Optimisation (BBO) and Grey Wolf Optimisation (GWO) for LSM. They stated that both algorithms could be used to increase the learning ability of the MLP. Shahri et al. (2019) generated LSM of a large area by subdivision approach. Apart from ANN, recent authors have also used two different types of neural networks in deep learning, such as Convolutional Neural Networks (CNN) by Fang et al. (2020) and Recurrent Neural Networks (RNN) by Wang et al. (2020). The performance of CNN is considered more powerful than RNN and ANN and has applications in facial recognition, text digitisation, and natural language processing.

### **Probabilistic Analysis**

Probabilistic methods in LSM bring objectivity in allocating weights. According to Chung and Fabbri (1993), the first step is establishing a Favourability Function (FF) for each layer, which sets up a platform for developing integration methods based on probabilistic operations. Lee and Min (2001) compared the probabilistic model with the statistical model and concluded that both models efficiently estimate the susceptible area of landslide. Further, they commented on the simplicity of using a probabilistic model and the easy understanding of results.

### **Certainty Factor (CF)**

The CF method is one of the promising indirect FF approaches to solve the trouble of having dissimilar data and handling the uncertainty of the input data. Shortliffe and Buchanan (1975) were the first to develop the CF model; later, it was modified by Heckerman (1986). This method can either be data-driven, based on expert knowledge, or a combination of both. Suppose past landslide distribution data is not available. In that case, the expert can input crisp CF values for all factors responsible for landslides, but the expert judgment's irregularity is hard to estimate (Binaghi et al., 1998). The CF approach assesses the quantitative relation between the responsible factors and the past landslide. CF values can be evaluated by merging conditional probability and the prior probability of a landslide-prone zone (Luzi and Pergalani, 1999; Lan et al., 2004; Sujatha et al., 2012). This quantitative value of CF ranges from minus one to one to define the possibility of landslides occurring. A positive number indicates a more chance of happening landslide events, while a negative number indicates a less chance. Kanungo et al. (2011) combined ANN with CF, LR, and FL approaches for LSM, and their relative efficiency was checked using visual interpretation, landslide density analysis, and the success rate curves method. Nahayo et al. (2019) compared the performance of the AHP and CF models

in LSM in the western province of Rwanda. The result showed that the CF model generated high accuracy and prediction rates than the AHP model. Wubalem (2021) applied FR, CF, and IV methods to determine the areas susceptible to landslides. Further, they concluded that all three methods accurately predict critical areas susceptible to sliding for the study region.

### **Conditional Probability (CP)**

It measures the probability of an incident happening, given that another incident has already happened. This method is based on Bayes Theorem. Chung and Fabri (1999) delivered a combined framework for predictive modeling with GIS using probability theories for LHM. According to Clerici et al. (2002), among the multivariate methods, the CP method is mainly straightforward from a conceptual point of view and primarily suitable for a GIS platform. Gorsevski et al. (2003) predicted landslide hazards by integrating FL and CP techniques. This modeling technique was built on calculating CPs from relative frequencies of datasets to be modeled and used FL to classify predictor datasets. Yilmaz (2010) compared four methods such as CP, LR, ANN, and SVM, for preparing LSM. He concluded that CP is an easy method in LSM and exceptionally compatible with the GIS platform. Pourghasemi et al. (2012b) used the CP model to produce LSM in the Safarood basin, Iran where the uncertainty was related to landslide phenomena and their relation with factors responsible for landslides. Saha et al. (2021) used the CP method to increase the accuracy of the Boost Regression Tree (BRT) method in the Rudraprayag district, India. They concluded that the combination of the two methods had resolved the deficiencies of the solo method, increased the performance, and lifted the model's predictive capability.

### **Frequency Ratio**

The FR is the ratio of the probabilities of a landslide incidence to a non-incidence for a given factor. It is a bi-variate statistical method for LSM, built on the detected relations between past landslides and factors responsible for landslides. Mehrotra et al. (1996) performed LHM of East Sikkim Himalaya using this technique by evaluating various terrain factors like lithology, drainage, structure, slope, and land use related to past landslides. Süzen and Doyuran (2004) aim was to improve the earlier defined bivariate statistical LSM techniques in a more data-dependent method. For this, they performed frequency analysis, named the landslide zone by seed cells, and obtained weights as the ratio of the seed cell abundance over the class region. The landslide inventory layer is overlaid on each thematic data layer to determine the impact of different factors on landslide occurrence. Further, the area ratio values of landslide-affected area by non-affected area are calculated for all factors. Ratio values are used as the ratings and weights for the factors and their corresponding classes, which were then integrated for LHM (Lee and Talib, 2005; Lee and Pradhan, 2006, 2007; Vijith and Madhu, 2008; Bourenane et al., (2016); Chimidi et al., (2017); Hamza and Raghuvanshi, 2017; Pirasteh and Li, 2017; Maheshwari, 2019).

FR method was compared with other methods like LR (Lee and Sambath, 2006), ANN (Yilmaz, 2009), FL (Pradhan, 2010), AHP (Demir et al., 2012), IV (Kumar et al., 2019) and WofE (Versain et al., 2019; Ozdemir, 2020; Arifianti et al., 2020). They concluded that the FR method is simple and accurate when sufficient data is available. Mounj-Jin et al. (2014) used FR for LSM and rainfall data for the temporal assessment of LHM for the different time frames. Umar et al. (2014) used FR to measure the effect of classes of all factors responsible for landslide activity. As FR method neglects the intermediate correlation between the factors. Hence they used LR to analyse the relationship among the factors. Meten et al. (2015) determined the independence of different causative factors among each other by applying the correlation matrix of LR. These factors were then used for preparing LSM using the FR method. Anbalagan et al. (2015) used FR and FL for LHM for Lachung Valley, Sikkim. They concluded that factors responsible for landslides integrated using FL had yielded good results.

### **Weight of Evidence (WofE)**

WofE is a Bayesian probability method that uses log-linear relations for performing LSM analysis. For training the model, it uses landslide distribution data and predicts both the favorable and unfavorable probabilities of landslide susceptibility (Lee et al., 2002; Lee and Choi, 2004; Thiery et al., 2004; 2007; Sharma and Kumar, 2008). The WofE method was compared with the BIS method (Ghosh et al., 2009), the physically-based model, the FL method (Cervi et al., 2010), the LR method (Schicker and Moon, 2012), and the CF methods (Pourghasemi et al., 2013c). Results showed that the WofE method presented better prediction rates when compared with the other methods for respective study areas. Maximum accuracy can be achieved by combining WofE with other methods such as ANN - WofE (Vahidnia et al., 2009), FL - WofE (Hong et al., 2017), and SVM - WofE (Saha and Saha, 2020). These hybrid methods showed high predictive power than the conventional WofE method. In the WofE method, likelihood ratios are used to define the possibility of a landslide happening and to calculate positive and negative weights in the case of the existence of the evidence. Contrast (C) is defined as the difference between these positive and negative weights (Ilia et al., 2010; Sterlacchini et al., 2011; Xu et al., 2012; Armas, 2012; Kayastha et al., 2012; Neuhauser et al., 2012; Piacentini et al., 2012). When the contrast value is zero, it designates that the factor is not essential for analysis. If the value is positive, it means a positive spatial relationship, and vice versa for a negative contrast. Blahut et al. (2010) compared LSMs generated with the same WofE method but dissimilar landslide inventories and demonstrated that better LSM could be obtained from an accurate landslide inventory prepared. Martha et al. (2013) used the WofE technique for LSM, where weights were obtained from past landslide data combined with landslide-responsible factors. Ilia and Tsangaratos (2016) performed a sensitivity analysis for the WofE method to recognise how this method is reacting to the change made in the weight values of factors responsible for landslides. This was done to identify those critical factors that significantly influence landslide occurrence in Greece.

### **Physically Based Distributed Analysis (PBDA)**

Physically based are built on physical laws governing slope movement (Dunne, 1991). The factors used in the site-specific methods can be obtained from field data collection and performing laboratory experiments. The distributed analysis is not site-specific and needs the spatial distribution of various data. PBDA models like Shallow Landslide Stability Model (SHALSTAB) and Stability Index Mapping (SINMAP) can be used for LHM considering spatially distributed input data of soil-moisture, slope angle, and factor of safety (Montgomery and Dietrich, 1994; Wu and Sidle, 1995; Terlien et al., 1995; Pack and Tarboton, 1998). Modeling slope failure processes can be applied to shallow landslides that use groundwater fluctuation, rainfall data, or earthquake data as a triggering factor in the study (Hungr, 1995; Stead et al., 2001).

Dietrich et al. (1995) developed a method to predict soil depth, which was used to determine the effects of root cohesion and saturated conductivity variation in the vertical direction. Further, these data were used in slope stability modeling. Jibson et al. (2000) used the landslide inventory, earthquake ground motion records, geologic map, soil properties, and DEM in a dynamic model to obtain LHM for study areas in California. Baum et al. (2002, 2008) used a program in Fortran to generate a model called TRIGRS (Transient Rainfall Infiltration and Grid-based Regional Slope Stability analysis) to compute temporary changes in pore pressure and variations in the safety factors due to infiltration of rainfall. A dynamic model for LHM considers both spatial and temporal prediction (Casadei et al., 2003; Xie et al., 2004; Dhakal and Sidle, 2004; Fall et al., 2006; Rosso et al., 2006; Salciarini et al., 2006; Simoni et al., 2008; Godt, 2008; Baum et al., 2010; Wang and Lin., 2010; Takara et al., 2010; Alvioli and Baum, 2016). GIS-based PB models can be done by merging a soil-moisture and a slope-stability model (Acharya et al., 2006; Sharma and Shakya, 2008; Ray and De Smedt, 2009).

Shallow Landslides Instability Prediction (SLIP) is another physically-based deterministic model used by Montrasio and Valentino (2008); Montrasio et al. (2011) in rainfall-induced landslide modeling. Jia et al. (2012), Rossi et al. (2013), and Anagnostopoulos et al. (2015) used Limits Equilibrium Models (LEM) for PB landslide distributed modeling systems to examine the stability/instability conditions. Ciurleo et al. (2017) produced LSM for a Catanzaro in southern Italy using the statistical IV and the deterministic TRIGRS model. They concluded from the result that if sufficient data is available to perform deterministic analysis, it should be preferred over a statistical model. Dolojan et al. (2021) constructed a model for evaluating shallow slope failures triggered by rainstorms by including infiltration rate with slope stability analysis.

## **2.5 Research gaps**

After carrying out the detailed literature survey, a few essential research gaps were derived, as discussed below:

1. The inconsistency is selecting landslide causative factors. This brings the requirement to develop a scientific methodology for identifying significant factors.
2. The factors selection was random and mainly depended on the availability of the data. Also, the testing of the selected factors was not done on other similar terrain conditions.
3. Researchers have restricted themselves in predicting present landslide susceptibility maps. These susceptibility maps should be constantly updated because of dynamic Earth and ecosystem processes and unstoppable anthropogenic activities.
4. Future predictions of landslide susceptible regions have not been quantified. Updating the susceptibility maps frequently is challenging and demands continuous monitories of one particular area. However, future predations of these susceptibility maps can prevent us from updating these maps regularly.
5. Dynamic factors such as LULC and climate variables were not adopted in predicting future LSM scenarios. Most of the studies have only incorporated static factors in their analysis. Although few studies have adopted dynamic factors, however, they have not used them for determining future LSM scenarios.

## **2.6 Research objectives**

Based on the above research gaps defined, the study aims to predict landslide susceptibility scenarios for present and future conditions by incorporating both static and dynamic landslide causative factors. Based on this key objective, specific objectives are defined as follows:

1. Development of scientific methodology for the determination of significant landslide causative factors.
2. Predicting present LSM incorporating the derived significant landslide causative factors and testing the applicability of significant factors on two landslide-prone sites.
3. Development of an innovative methodology for predicting future LSM scenarios considering derived future LULC projections.
4. Adopting the developed methodology for predicting future LSM scenarios incorporating future projections of LULC and Climate under four SSPs.

## 2.7 Novelty of the Research

The novelty of this study is the adaptation of the innovative methodology for deriving future LSM scenarios by incorporating dynamic factors. The methodology used the past data as the input, and based on the changes identified in the past information, future projections are derived. We have observed these changes in landslide susceptibility maps and LULC maps. This methodology projects these changes to the future and helps us understand future scenarios. Further, we have also used future climate projections under four SSPs for predicting future LSM conditions. Based on the different pathways adopted, different susceptibility conditions will be generated. Hence, we have incorporated both LULC and climate projections in the future prediction of LSM scenarios under four SSPs.

## 2.8 Summary

LSHM is the first step in hazard assessment, but it can also be considered the final land-use planning product. This chapter describes the efforts of researchers attempting to determine LSHM for different regions all around the world since the mid-1970s. Most of the works were focused on spatial prediction with inconsistency in the selection of models and landslide causative factors. About 86% of the literature found to be working on spatial prediction only, 11% used both spatial and temporal prediction, and only 3% of the literature used all three spatial, temporal, and magnitude components in landslide hazard analysis, as shown in Fig. 2.2. If sufficient data is available for temporal and magnitude prediction, it should also be carried out along with spatial prediction to understand landslide hazards better. Further, risk analysis should also be carried out if the data related to the vulnerability of structures and other properties are available.

The chapter also summarises the most commonly used methods for susceptibility assessment are LR, ANN, FL, AHP, WofE, and FR. PBDA should also be preferred for areas with homogeneous geological and geomorphological conditions with a clear understanding of the triggering mechanisms. Even though some approaches have shown higher accuracy, no single approach is still superior in all environmental and field conditions. The knowledge and talent of the researcher in using a particular method are more important than the approach. Also, many studies have shown that hybrid methods are better than single methods in terms of performance, as the deficiency of one method is overcome by another.

The last section of this chapter discusses the research gaps, objectives, and novelty of the research work. Based on the literature survey, few research gaps were defined which are necessary for the current situation. Further, the research objectives were derived from the defined research gaps. Also, the novelty of the research was highlighted in the end.

#### 3.1 Introduction

The Himalayas has a conspicuous landscape consisting of tall ridges, steep slopes, large streams, and deep valleys. The topography of the Himalayas and increasing anthropogenic activities are mainly responsible for the landslide incidences (Gupta and Anbalagan, 1997). One of the leading reasons for land degradation in the Himalayan region is landslides, a recurring phenomenon. Above all, the Himalayas is a young mountain involved in numerous geodynamic activities such as earthquakes, shearing, folding, and faulting. Also, they receive prolonged intensify rainfall in the monsoon season, causing saturation of hill slopes. All these adverse phenomena of the Himalayan topography, along with human interventions, lead to slope instability. The Indian Himalayas, particularly Uttarakhand and Himachal, are home to several religious and recreational places, attracting thousands of tourists annually. To cater to the needs of the surging tourists, unplanned constructions like hotels, shops, and other infrastructures have increased the degree of hazard. Financial prosperity among the population of the hilly region has changed the traditional approach of construction and cultivation pattern, which is increasingly resulting in frequent slope instability problems. After carrying out the literature review, the area where the landslide problem dominated was selected. The site should also have the availability of historical landslide data and good-resolution satellite imagery.

The Tehri region of Uttarakhand, the Chamba and the Bhuntar regions of Himachal Pradesh are some of the landslide-prone sites used in this study. These three study regions have an almost similar types of terrain and climatic conditions. Apart from heavy rainfall and high seismic factors, these study areas also have a high stream network that adds to the hills instability. In this chapter, we will discuss in detail the location, physiographic characteristics, and drainage pattern of the selected study area of the Tehri region. Further, two test sites, Chamba and Bhuntar, were also investigated for testing the derived results of optimised landslide causative factors (Fig. 3.1). The Two test sites from the Himalayas were selected from the state of Himachal Pradesh with similar terrain conditions and data availability of historical landslide events and landslide causative factors. This chapter also discusses the characteristic features of these two chosen test sites in detail.

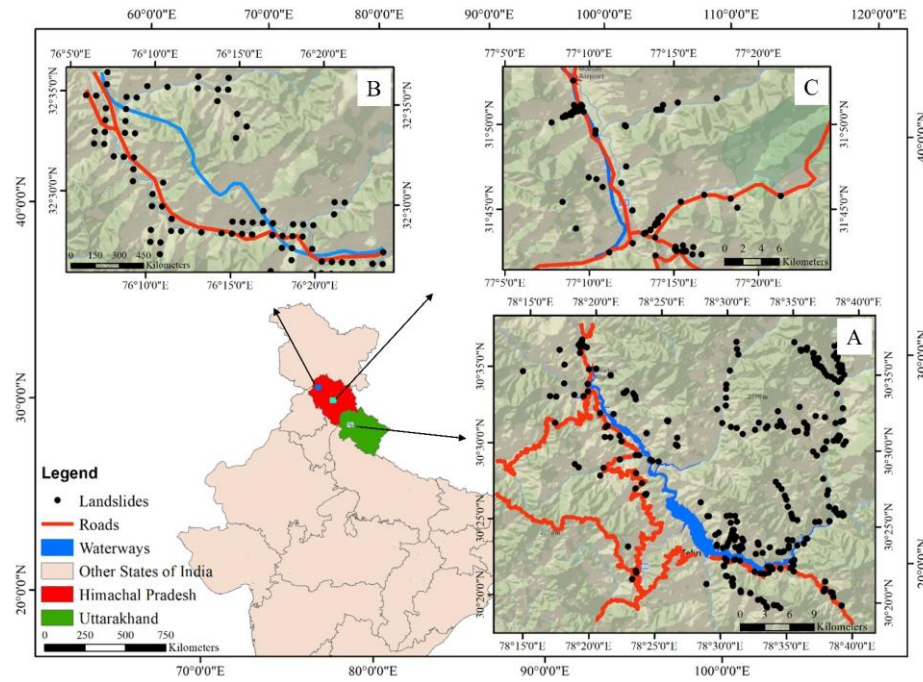


**Fig. 3.1** Location of the study area and Testing sites. (A) Tehri region, (B) Chamba region, and (C) Bhuntar region

### 3.2 The Tehri Region

The Tehri region falls in the state of Uttarakhand, India. The state is undoubtedly a paradise on earth, popularly known as the home of the Himalayas and the land of gods. The state is famous for fresh air, pure water, snow-covered mountains, and small villages with simple people having challenging lifestyles. The state lies along the great Indo-Gangetic plain consisting of the Higher, lesser, and sub-Himalaya parts. The study area falls in the basin of the Bhagirathi and Bhilangna rivers. These two rivers confluence to form a massive reservoir at India's tallest Tehri Dam.

The dam's height is 260.5 m, and its reservoir covers around 45 km<sup>2</sup> of the region, which has submerged 125 villages (Hanumantha Rao Committee Report, 1997 as quoted in Bisht, 2009). Many environmentalists and locals opposed the dam construction as thousands of people were displaced forcefully (Asthana, 2012). The new Tehri town was raised with full civic facilities for the resettlement of villagers. To boost tourism, multiple spots for water sports activities all around the lake were created (Naithani and Saha, 2019). All these activities for economic development and urbanisation are vulnerable to climate change due to the emission of significant quantities of greenhouse gas into the atmosphere (Kumar and Sharma, 2016). Due to this, areas with a lower altitude in the Indian Himalayan region have experienced increased temperatures, rainfall intensity, and decreased number of rainy days. This reduced water availability for farming and overall food production (Pandey et al., 2017).



**Fig. 3.2** Photographs showing landslides in the Tehri region.

### **3.2.1 Location and Geology of Study Area**

The study area ranges between  $30^{\circ} 36' 57.6''$  N to  $30^{\circ} 19' 1.2''$  N latitude and  $78^{\circ} 39' 3.6''$  E to  $78^{\circ} 13' 15''$  E longitude in the Lesser Himalaya of Garhwal hills in Uttarakhand, India (Fig. 3.2). The area covered in this study was about  $1350 \text{ km}^2$ , which falls in the part of Bhagirathi and Bhilangna river basins. These two rivers confluence to form a massive reservoir at India's tallest Tehri Dam with a maximum water level (MWL) of 830 m and dead storage level (DSL) of 740 m (Kumar and Anbalagan, 2015). The Tehri region lies in zone IV of India's seismic zoning map, which comes under high-risk area. Due to the variation of water level in the reservoir, the area has large-scale slope instability and landslide changes along the reservoir's embankment. Hence, many researchers have studied this area for LSM (Gupta and Anbalagan, 1997; Joshi et al., 2003; Ghosh and Bhattacharya, 2010; Kumar and Anbalagan, 2015, 2016; Pandey et al., 2020; Tyagi et al., 2021). In the last three decades, several hydroelectric projects, roads, towers, ropeways, and other public utility works, and indiscriminate mining and quarrying further aggravated the landslide problems.

The geology of the Tehri region can be classified into seven groups, i.e., Garhwal, Baliana, Jaunsar, Tal, Krol, Toli, and basic meta-volcanic. The whole study area is a part of the broader physiographic entity called Lesser Himalaya. Rocks in the central part of the area are low-grade metamorphosed lustrous phyllites and highly weathered quartzites. These rocks are

highly vulnerable to sliding because of the presence of well-developed foliation planes and joints. In the western part of the study area, quartzites with subordinate intercalation of gray and olive green slates with siltstones with white, purple, and green colors were identified. The eastern and northeastern part of the study area consists of fine-grained limestone with minor phyllitic intercalations. These rocks are mainly found at the higher ridges. In the eastern part of the area, the rocks are primarily quartzites. In the western part of the study area, the formation comprises quartzites, slates, and carbonate rocks

### **3.2.2 Physiography and Vegetation**

Physiographically, the study area, falling in the Lesser Himalayas, is highly rugged due to high mountains, steep slopes, and deep valleys. Numerous hazardous incidences were reported from important roads like National Highway 134, commonly referred to as NH-134, a spur road of NH-34. NH-34 crosses the state of Uttarakhand and runs along the left side of the study area. It is a critical road connecting Gangotri in the north and Rishikesh in the south. A spur road connecting old Tehri with Srinagar (NH-707A) running along the Bhilangna river in the southeast direction of the study region has also experienced landslide activities in the few years. The hills of the study area are covered with plants like *Camapanualatum*, *Buras*, *Neem*, *Pinus*, *Pipal*, *Piceasp*, *Deodar*, *Betulautilus*, *Cesrus*, etc. whereas, the moderate to lower altitude regions are generally used in step cultivation. The study area has a good forest cover in many parts. The development processes such as urbanization, road construction, hydroelectric projects, and other civil structures have been primarily responsible for putting additional pressure on vegetation, wildlife, and pastoral lands. In this context, Garhwal Himalaya was greatly subjected to this type of pressure, in addition to intensive cultivation, overgrazing, ruthless felling of trees, new human settlements, and population influx, which resulted in the reduction of forest cover of this region.

### **3.2.3 Climate and Drainage**

Throughout the year, the Tehri area experiences a subtropical temperature climate because of its high altitude location. The maximum elevation of about 2800 m and the minimum of about 600 m were detected with reference to the mean sea level. The study area has received heavy monsoon rainfall for about two months, with more than 2.5 mm daily rainfall (Kumar and Sharma, 2016). The mean minimum temperature for the region is about 4.6°C, obtained in December or January, and the maximum temperature of 35.5°C in June or July. The Bhagirathi river emerges from the Gangotri glacier in Gaumukh of Tethys Himalaya, flowing from the north to south direction of the study area. The river is fed with several small first and second-order streams from both sides. Most of the NH-134 road runs parallel to the Bhagirathi river.

### 3.3 The Chamba Region

Chamba test site falls in the state of Himachal Pradesh, India. It's a state situated in North–West India chiefly covered with mountains with altitudes ranging from 6978m to 350m above mean sea level. It has a very dismembered highland scattered with deep valleys and gorges. The climate of the state varies from semi-tropical to semi-arctic. From the North-East part, it is joined with the China border.

#### 3.3.1 Location and Geology of Testing Site 1

Chamba situated at 32°34'12"N latitude and 76°7'48"E longitude, is a town in the Himachal Pradesh state of India. It lies in the North-West part of Himachal Pradesh. The study area covers about 640 km<sup>2</sup> with the elevation varying from 705m to 4240 m. The town has many temples and hosts two famous fairs, i.e., "Minjar Mela" and "Suhi Mata Mela." These two tourist attraction fairs are organised for many days and include music and dance performance. The geology of the Chamba region (test site 1) includes a wide range of rock formations. The Salkhala Group is surrounded by the Vaikrita Group and Katari Gali formations in the Chamba region. The Bhalai Formation, Chamba Formation, Manjir Formation, Batal Formation, Katarigali Formation, and Mandi granites are present in the area regionally, whereas along the NH-154A, quartzites, slates, and gneiss rocks exist locally (Singh and Kumar, 2021).

#### 3.3.2 Physiography and Vegetation

National Highway 154A, commonly called NH 154A, passes through the study area from North-West to South-East, connecting Chamba town to Bharmour. NH 154A is a spur road of National Highway 54 that runs along with Ravi river in the study area (Fig. 3.3). The area is covered with water body (0.7%), dense forest (48%), agriculture land (0.9%), built-up area (2%), Barren land (2%), snow-covered (0.4%), sparse forest (46%). The sub-Himalayan range of mountains, full of diverse flora and fauna, makes Chamba an exhilarating experience. The hills of the study area are covered with plants like *cedrus deodara*, *Abies pindrow*, *Barain* (*Acorus calamus* L), *Chuang* (*Achillea millefolium* L), *Chharmara* (*Artemisia nilagirica*), *Kosh* (*Alnus nitida*), *Chirndu* (*Sarcococca saligna*), *Bhang* (*Cannabis sativa*), *Kokhua* (*Stellaria media*), *Khaldri* (*Dioscorea deltoidea*), *Cheehun* (*Rhododendron arboreum*), *Kodal* (*Desmodium elegans*), *Chirayta* (*Swertia chirayita*), *Goon* (*Aesculus indica*), *Akhrot* (*Juglans regia* L), *Chirndi* (*Neolitsea pallens*), *Salam-Mishri* (*Polygonatum cirrhifolium*), etc.

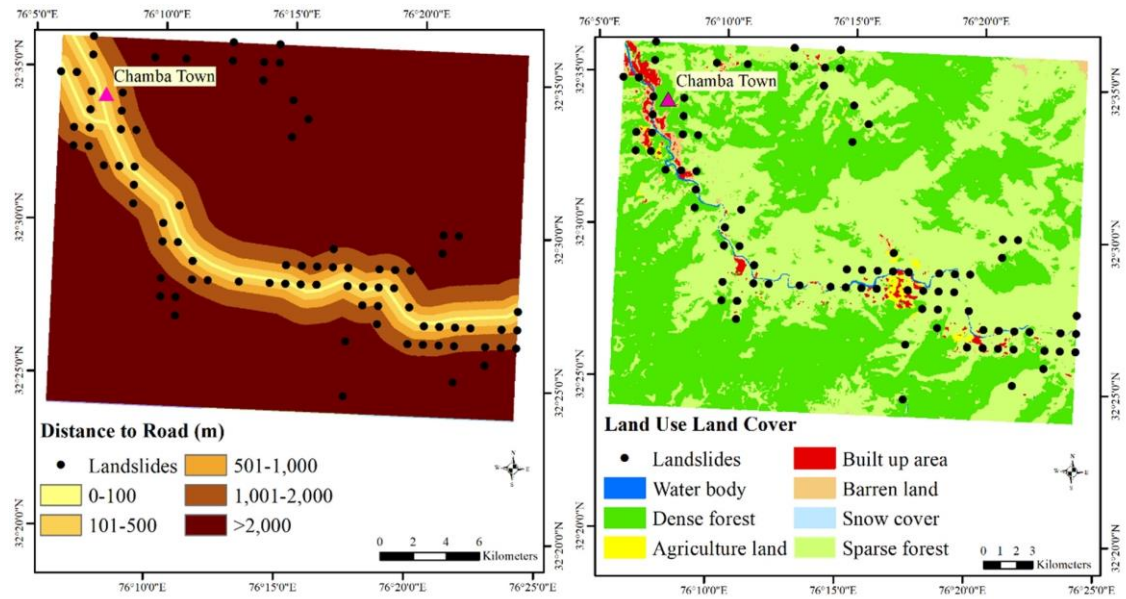


**Fig. 3.3** Figure on the left shows the map of NH-154A buffering and on the right side shows the LULC class map for the Chamba test site.

### 3.3.3 Climate and Drainage

The maximum and minimum temperatures recorded in summer and winter are 42 °C and 0 °C, respectively, with an average annual rainfall of 1190.9 mm (IMD Pune, 2010). The monsoon rainfall occurs in July, August, and mid-September in Chamba. The Ravi river passes through the testing area and flows from the west to the east direction forming canyons (Fig. 3.4). In spring and summer, river water levels increase significantly because of snowmelt.

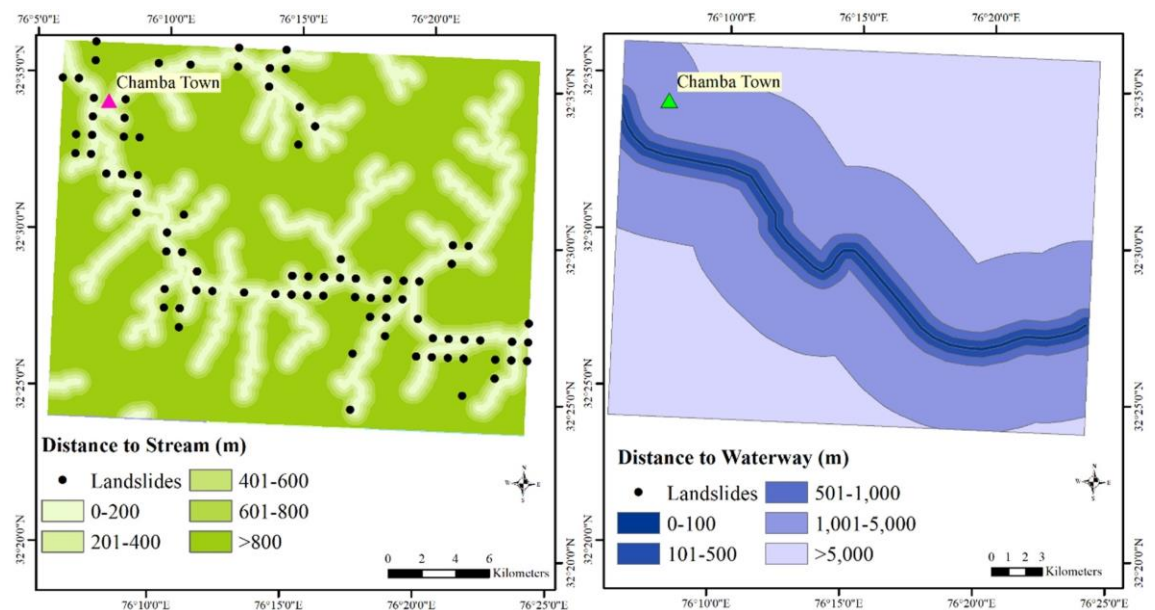


**Fig. 3.4** The left shows the stream buffer map, and the right side shows the Ravi river buffer map for the Chamba test site.

### 3.4 The Bhuntar Region

Bhuntar Town also falls in Himachal Pradesh and is a nagar panchayat in Kullu district, India. Bhuntar has an airport that links prominent cities through the air. Bhuntar is typically a getaway to Kullu, Manali, Kasol, and Manikaran.

#### 3.4.1 Location and Geology of Testing Site 2

Bhuntar situated at 31° 51' 36"N latitude and 77° 9' 0"E longitude, covers about 640 km<sup>2</sup> area with the elevation varying from 888 m to 4230 m. It is just 11 km from Kullu town and lies at the center of Himachal state along National Highway 3. The geology of Bhuntar region (test site 2) mainly comprises metamorphic rocks spread generally along the high slopes and crystalline rocks mainly present in the valleys. Jutogh, Kullu, and Vaikrita thrusts run along the valleys with several local faults/lineaments spread into the southern part of the area.

#### 3.4.2 Physiography and Vegetation

The National Highway-3 passes the study area along the Beas river in the North-South direction. The NH-3 starts from Atari in Amritsar, nearby the India-Pakistan border, and ends at Leh in Ladakh via Bhuntar, Kullu, and Manali in Himachal Pradesh (Fig. 3.5). The area is covered with water body (0.8%), dense forest (47%), agriculture land (1.1%), built-up area (3%), Barren land (6%), snow-covered (0.1%), sparse forest (42%). The site contains Shisham, sal, pine, and broad shiny leaved trees. This region has another range of oaks, blue pines, and fir trees. Sturdy mountain trees with firm tangled roots can be seen if you hike up to the mountains. These are alders and birches. The most prominent and beautiful plant is the Rhodendron. In the summers and autumn, gladiolas, roses, fragrant chrysanthemums, lilies, tulips, gladiolas, and carnations can be seen.

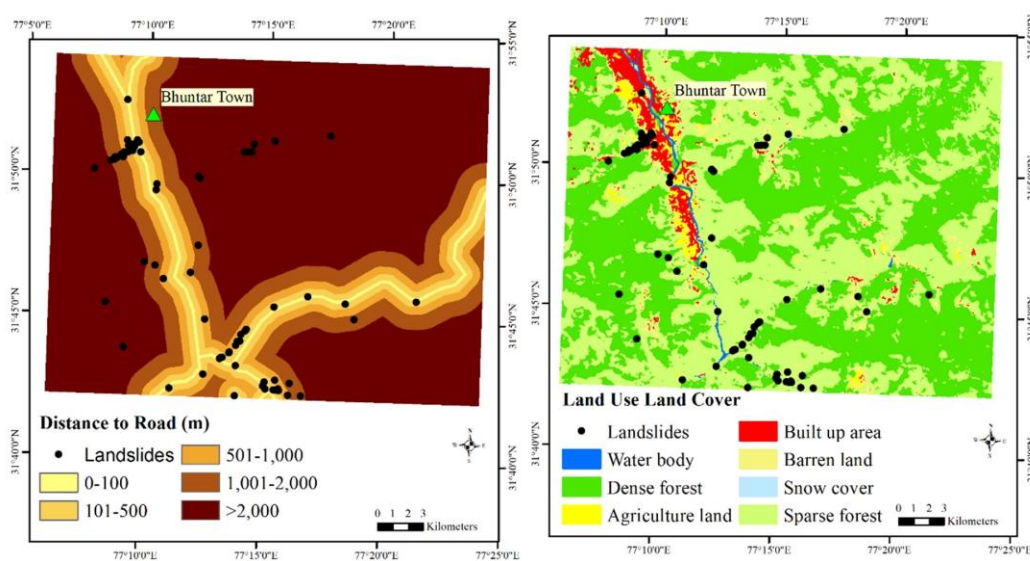


**Fig. 3.5** Figure on the left shows the NH-3 buffer map, and on the right side shows LULC class map for the Bhuntar test site.

### 3.4.3 Climate and Drainage

Bhuntar is situated on the right bank of the Beas River. The Beas river passes through the testing region flowing southward (Fig. 3.6). The maximum and minimum temperatures recorded in summer and winter are 40 °C and -5.2 °C, respectively, with an average annual rainfall of 941.8 mm (IMD 2016).

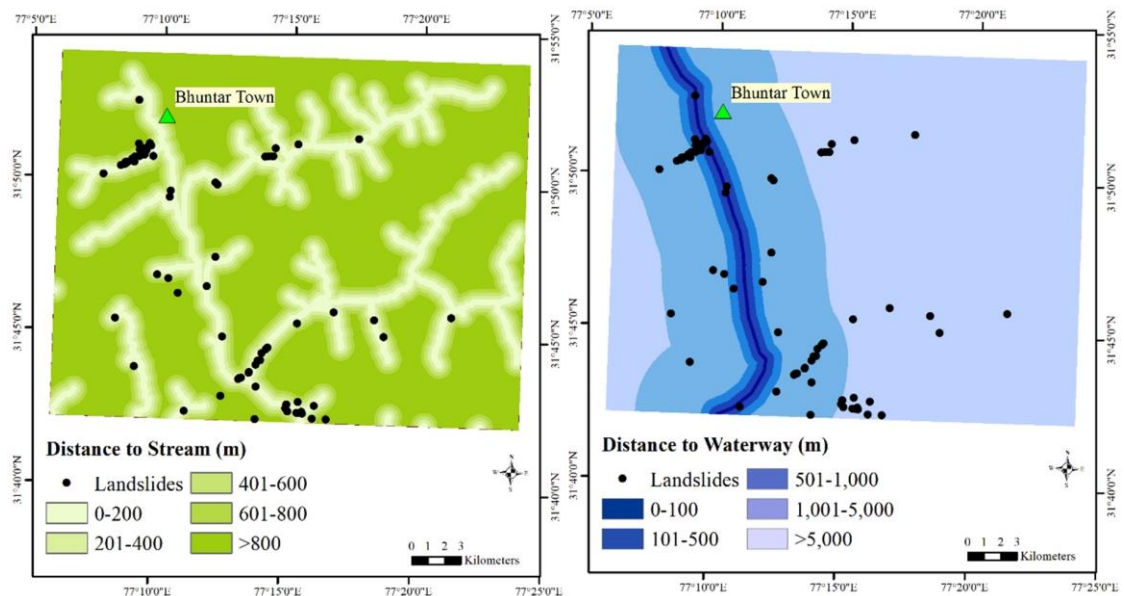


**Fig. 3.6** Figure on the left shows the stream buffer map and on the right side shows Beas river buffer map for the Bhuntar test site.

## 3.5 Summary

This chapter describes in detail the location, physiographic characteristics, vegetation covered, climate, and drainage pattern of the study area of the Tehri region and two test sites of the Chamba and Bhuntar regions of the Indian Himalayas. The study region of Tehri is shown with photographs and was mapped in Uttarakhand, India, with historical landslide data, major roads, and streams network. The two test sites of Chamba and Bhuntar were mapped in Himachal Pradesh, India, with historical landslide data, major roads, and streams network. The unique characteristics and features of these places attract tourists from all over the world, leading to the demand for activities like slope cutting, widening of roads, hotels, construction, etc., which further leads to population growth and urbanisation.

#### 4.1 Introduction

This chapter describes the approach implemented to accomplish the various objectives of this research work. For LSM, it is vital to make a comprehensive landslide inventory of the Tehri region. The spatial prediction of landslides can be achieved using landslide-causing factors, and for deriving weights of these factors, LSM models are required. Factors like slope relative relief, aspect, etc., can be derived from the high-resolution Digital Elevation Model (DEM). Other factors like soil type, geological structure, LULC, etc., require visual and digital interpretation of remotely sensed images to extract the thematic maps for the Tehri region. These thematic maps are classified and weighted using LSM models for spatial prediction of landslide susceptibility. In this chapter, we will discuss various static and dynamic factors used for the analysis of LSM and methods adopted for deriving weights for these factors. The methods used in this study were AHP, FR, and ANN to derive the relation between dependent and independent variables. Also, this chapter discusses the ANN-CA model used to project the current trend to the future. The last section of this chapter describes the two methods namely area under the ROC curve and Kappa coefficient, which were incorporated for validating the results in this study.

#### 4.2 Data Collection

Numerous factors are responsible for causing landslides and should be incorporated into the analysis of LSM. The accuracy of the landslide susceptibility maps depends upon the quality of the input data. Hence, the primary step for LSM is the preparation of the database. Field-based approach for mapping is costly and time-consuming, while both time and cost can be optimised using remote sensing data. Here, remote sensing and GIS technique was adopted to derive all the required input data for LSM analysis. For DEM generation, Cartosat-1 satellite data was utilised. Landslides historical data were taken from the Bhukosh portal and were identified using Google Earth images. Satellite images of Landsat 5 and 8 were taken for mapping the LULC. A brief description of the dataset and respective sources are given below in table 4.1.

**Table 4.1** Various sources utilised for preparing landslide causative factors.

Data Type	Variables	Sources	Derivatives
Dynamic	Landsat 5 and 8 data	Earthexplore.usgs.gov (last accessed on 23/01/2023)	Maps of LULC
	CMIP6 Climate Projections	cds.climate.copernicus.eu	Future projections of temperature and precipitation.
Static	GPM rainfall data	Giovanni.gsfc.nasa.gov	Rainfall map
	NOAH land surface Model		Maps of Soil moisture, Soil Temperature, and Evapotranspiration.
	Earthquake data	Earthquake.usgs.gov	Peak Horizontal Acceleration map
	Cartosat-1 DEM	bhuvan.nrsc.gov.in	Maps of slope, Curvature, Relative relief, Aspect, STI, TRI, TWI, SPI and distance to streams.
	Ancillary data	Bhukosh GSI data	Maps of lithology, geomorphology geology, distance to waterway, and distance to road.
		Kumar and Anbalagan, 2015	Soil map

### 4.3 Landslide Inventory Maps

Some sources of landslide event data are newspapers, governmental documents, and historical travel guides. However, such documents contain overstatements that are still useful for obtaining information about the event. The landslide database of the Tehri region was generated using a field survey, image interpretation from Google Earth, and historical data from the Bhukosh portal ([bhukosh.gsi.gov.in/Bhukosh /MapView.aspx](http://bhukosh.gsi.gov.in/Bhukosh/MapView.aspx) and last accessed on 29/12/2022). In total, 850 landslide events were mapped from 2005 to 2020 for the Tehri region. Also, 166 and 79 landslide points were mapped for Chamba and Bhuntar validation sites. The landslides point data utilised here are centroid points of the landslide polygon prepared by the Geological Survey of India (GSI). The Bhukosh portal of the GSI is a gateway to all geoscientific data used in the scientific domain. The landslide data can further be divided based on the type of land cover, material, and movement, as shown in fig. 4.1. Based on the type of landcover, about 5% of the landslides were observed on barren land, 10% on cultivated land, 18% on extensive cut slope, 13% on moderate vegetation, 1% on settlements, 3% on wasteland, 2% on thick vegetation and remaining 48% on sparse vegetation. Based on the type of material, about 27% of the landslides had debris, and about 73% of them had rocks. Further, based on the type of movement, landslides were divided into slides (98%) and falls (2%). The changes in LULC were observed at every five-year interval (Marquez et al., 2019); hence, these landslide events data were clustered into three major temporal categories, 2005-2010, 2010-2015, and

2015-2020 (Annexure 1). Further, the landslide inventory maps for these periods were prepared using 218, 243, and 387 landslide events, respectively, as shown in fig. 4.2.

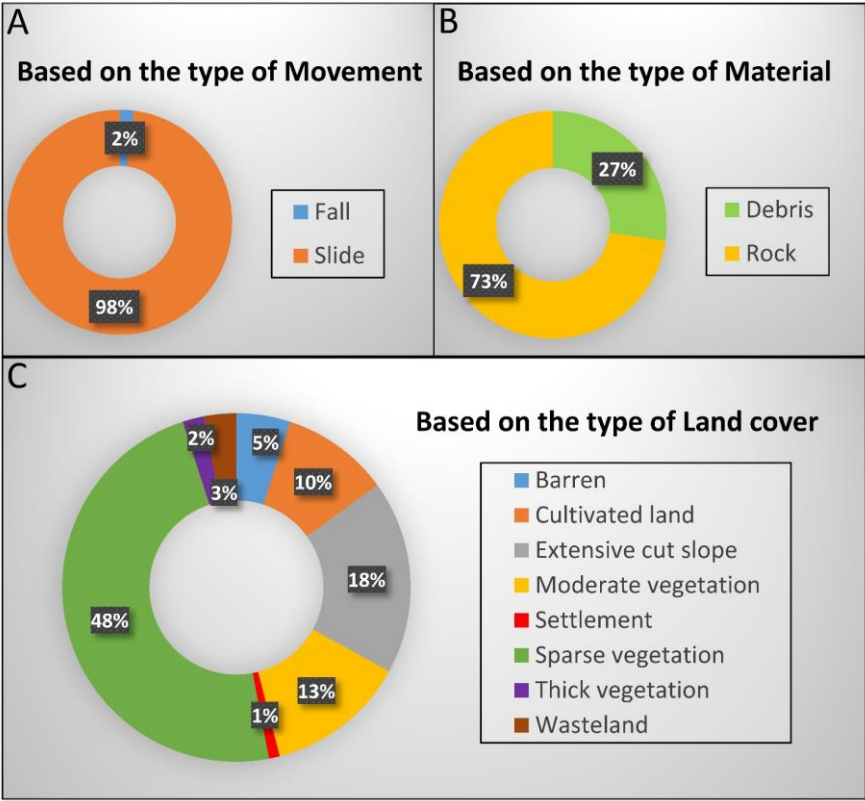


**Fig. 4.1** Classification of landslides (A) Based on the type of Movement (B) based on the type of Material (C) Based on the type of Land cover.

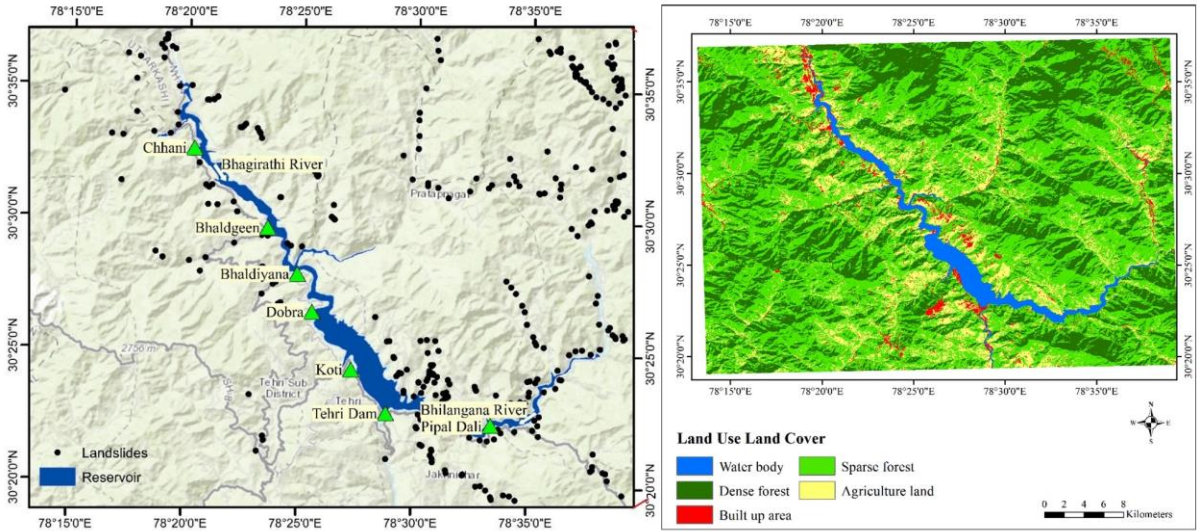


**Fig. 4.2** Landslide Inventory and LULC Maps for the Tehri region.

## 4.4 Land Use Land Cover Maps

Land cover plays an essential part in causing landslides in mountainous areas. Their relationship with landslides can be complicated depending on the type and nature of LULC. Thus, LULC classes were prepared from the satellite Landsat data on 1: 2,50,000 scale using a supervised classification method. The maximum likelihood classification algorithm uses the spectral signature of the training class to classify the whole Tehri region into five categories, i.e., waterbody, dense forest, built-up area, sparse forest, and agriculture land. LULC maps were generated using Landsat 5 and 8 data for 2010, 2015 and 2020. The prepared LULC map is shown in fig. 4.2.

## 4.5 DEM Derivatives Maps

Terrain factors such as slope, aspect, curvature, etc., play a vital part in sharp slopes influencing landslides (Guzzetti et al., 2005). Thus, in the present study, primary topographic attributes such as slope, aspect, relative relief, and curvature were derived with the service of ArcGIS software in a GIS environment using IRS Cartosat-1 DEM data. Acquisition date 01/10/2013, from the PAN Stereo sensor of the Cartosat-1 satellite, was downloaded from [bhuvan.nrsc.gov.in](http://bhuvan.nrsc.gov.in) at the spatial resolution of 30m x30m. (ISRO, Hyderabad, India). Secondary topographic attributes were generated using two or more primary attributes, which include the Sediment Transport Index (STI), Stream Power Index (SPI), Topographic Wetness Index (TWI), and Topographic Ruggedness Index (TRI).

### 4.5.1 Slope

The slope is the main measure for evaluating the slope stability of the hilly terrain. Many researchers have concluded that areas with greater slope gradients are more prone to landslides, while areas with small slope gradients are less prone (Saha et al., 2005; Kayastha et al., 2013; Tyagi et al., 2021). The present study's slope was classified into five classes using the Jenks classification technique (Jenks, 1967; ESRI, 2016). The classified slope map is shown below in fig. 4.3 was found to be varying in the range of 0° to 73°. Five slope categories namely 0°- 15°, 15.1°-23°, 23.1°- 30°, 30.1°- 38° and 38.1°-73° were categorised from the DEM.

### 4.5.2 Aspect

Aspect also significantly impacts the stability of the slope in the mountainous region. This study divided the aspect into nine classes: flat, North, North-East, East, South-East, South, South-West, and North-West. The classified aspect map is shown in fig. 4.3. Landscape aspect often impacts landslide susceptibility. The slope face controls the temperature differences, with slopes facing toward the sun having higher temperatures with respect to faces not receiving

sufficient sunlight. In the Himalayan region, the south-facing surface receives more sunlight; hence, they are warm, moist, and green compared to north-facing surfaces, which are dry, cold, and snow-covered.

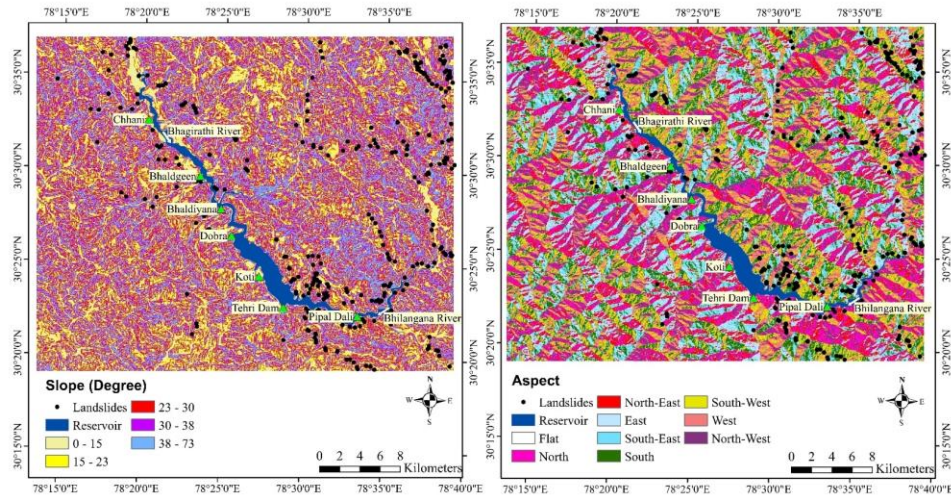


**Fig. 4.3** Slope and Aspect Maps for the Tehri region.

#### 4.5.3 Relative Relief

Relative relief is another essential derivative commonly used in LSM. It measures elevation change in the region (Kumar and Anbalagan, 2015). Here, variation in the relative relief was observed, ranging from 13 to 836 m. Following four classes: 13-200 m, 201-400 m, 401-600 m, and 60-836 m (Fig. 4.4) were used in LSM. Field observations suggest that landscapes with small relative relief are less prone to landslides and vice-versa.

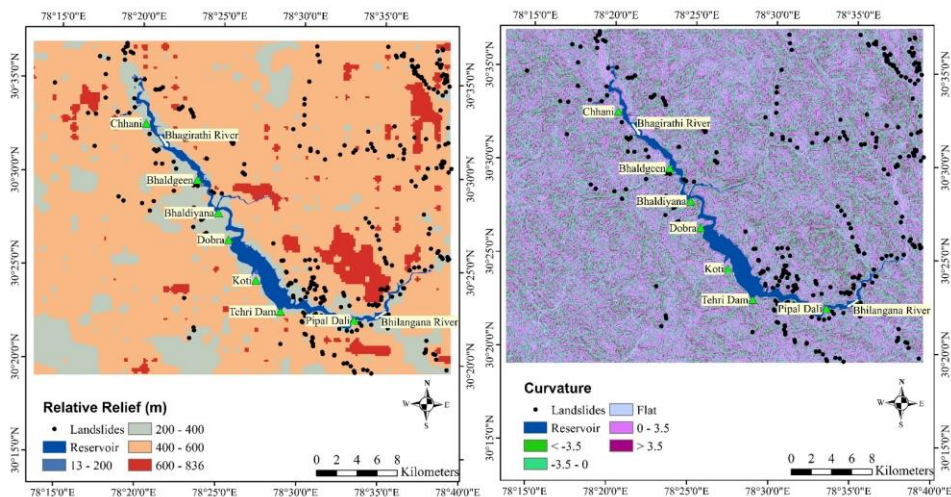


**Fig. 4.4** Relative Relief and Curvature Maps for the Tehri region.

#### 4.5.4 Curvature

Slope curvatures determine the direction of flowing water and hence is very essential to be included in the LSM analysis (Ayalew and Yamagishi, 2005). The curvature is associated with the second derivative of the height. This derivative will give the inflection point of the function (Misagh and Ashouri, 2016). Values greater than the inflection point represent a convex surface (anticline) having a positive value. In contrast, negative values are concave surface (syncline), and zero value indicates a flat surface. The curvature map was generated and classified into five classes, as shown in fig. 4.4.

#### 4.5.5 Topographic Ruggedness Index

TRI is the elevation difference between adjacent cells of a DEM. The roughness of the terrain is computed using the TRI value. It provides an objective quantitative measure of topographic heterogeneity. Topographic roughness for all grid pixels was calculated by taking the mean elevation changes between its neighboring cells (Riley et al., 1999). For the Tehri region, the range of TRI values varies from 0-0.7. The higher the value, the higher the elevation difference between the neighboring cells.

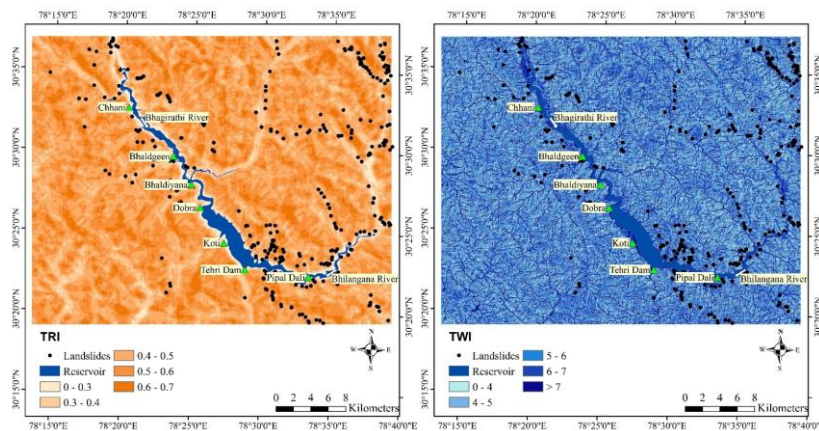


**Fig. 4.5** Topographic Ruggedness Index and Topographic Wetness Index Maps for the Tehri region.

#### 4.5.6 Topographic Wetness Index

TWI is a steady-state wetness index that represents the influence of landscape on the location and size of the saturated source zones for runoff generation under the assumptions of homogeneous soil properties and steady-state conditions. It can be calculated using equation 4.1 by incorporating catchment area (CA) and slope gradient ( $\beta$ ) (Wilson 2011).

$$TWI = \ln \frac{CA}{\tan \beta} \quad (4.1)$$

As the catchment region increases and the slope decreases, TWI increase. It is directly related to flow accumulation and helps to determine the soil moisture condition of the area. For study areas such as the Tehri region, where reservoir fluctuation induces water saturation in side slopes, TWI values can help to understand the water table conditions.

#### 4.5.7 Stream Power Index

SPI measures the erosive power of flowing water. The potential flow erosion at a given point can be described using the SPI, which is directly proportional to the erosion risk. The SPI can be calculated using equation 4.2.

$$SPI = \ln (CA \times \tan \beta) \quad (4.2)$$

Where CA and  $\beta$  are catchment area and surface slope, respectively. High positive SPI represents a high erosive index, associated with more landslides, while negative or low SPI values represent a less erosive index or more deposition index (Kumar and Anbalagan, 2015; Ahmad et al., 2020) (Fig. 4.6).

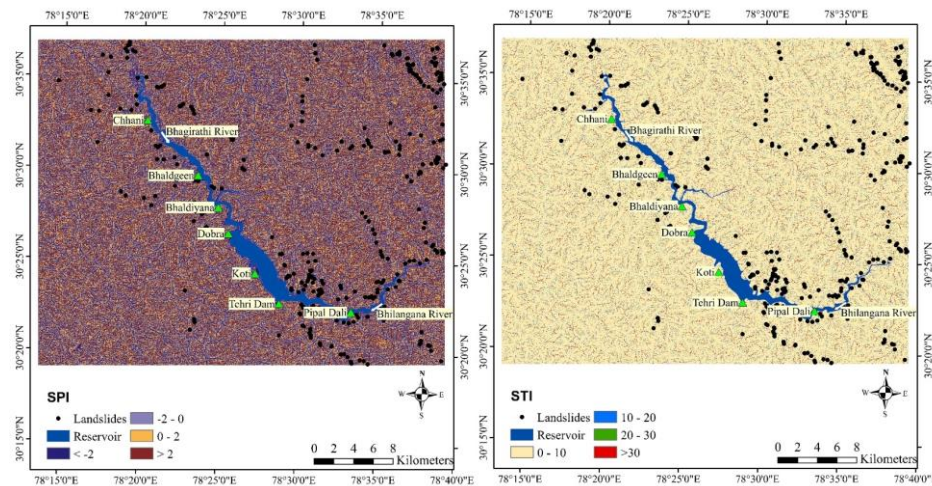


**Fig. 4.6** Stream Power Index and Sediment Transport Index Maps for the Tehri region.

#### 4.5.8 Sediment Transport Index

STI provides vital information on sediment transport potential in the stream network for a given watershed. The index incorporates catchment area under the assumption that the area is directly related to the slope ( $\beta$ ) and discharge. It illustrates the spatial distribution of the sediment transport capacity and accumulation. The index can be defined as:

$$STI = (CA \times \sin \beta) \quad (4.3)$$

## 4.6 Climate Variables Maps

### 4.6.1 Rainfall

The multi-satellite precipitation Global Precipitation Measurement (GPM) product is used to prepare the rainfall intensity map in this study (Huffman et al.2019). The time average rainfall intensity map was generated for the study period between 2005 and 2020 using a web-based application called Giovanni (Giovanni.gsfc.nasa.gov). The average rainfall intensity of the study region is calculated, and the time average map is generated for the GIS domain. The temporal resolution is monthly, and the spatial resolution is 0.1 x 0.1 degrees. The spatial distribution of rainfall intensity varied from 0.16 to 0.22 mm/h (Fig. 4.7).

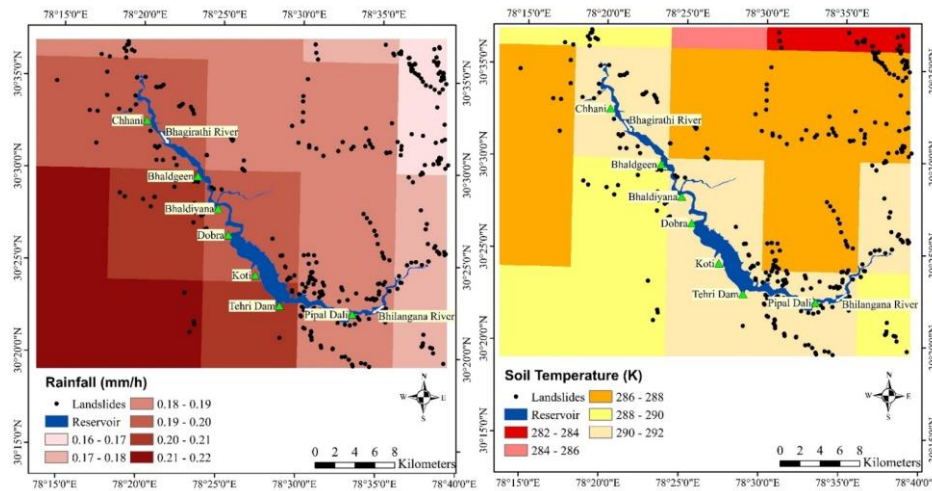


**Fig. 4.7** Rainfall and Soil Temperature Maps for the Tehri region.

### 4.6.2 Soil temperature

The time average soil temperature maps for the study area were prepared using the FLDAS Noah land surface model (McNally 2018). Average layer soil temperature is the depth-averaged temperature beneath the soil surface at a specified layer. These soil temperatures may contribute to the low-frequency variability of energy and water fluxes. For the Tehri region, the variation in soil temperature was observed, varying from 282 to 292 K (Fig. 4.7).

### 4.6.3 Evapotranspiration

The time average map of evapotranspiration for the Tehri region was prepared using the FLDAS Noah land surface model. It is the sum of evaporation and plant transpiration. The evapotranspiration rate expresses the amount of water lost from a unit surface area per unit time. The spatial variation was observed to vary from 0.00003 to 0.000035 kg/m<sup>2</sup>/s (Fig. 4.8).

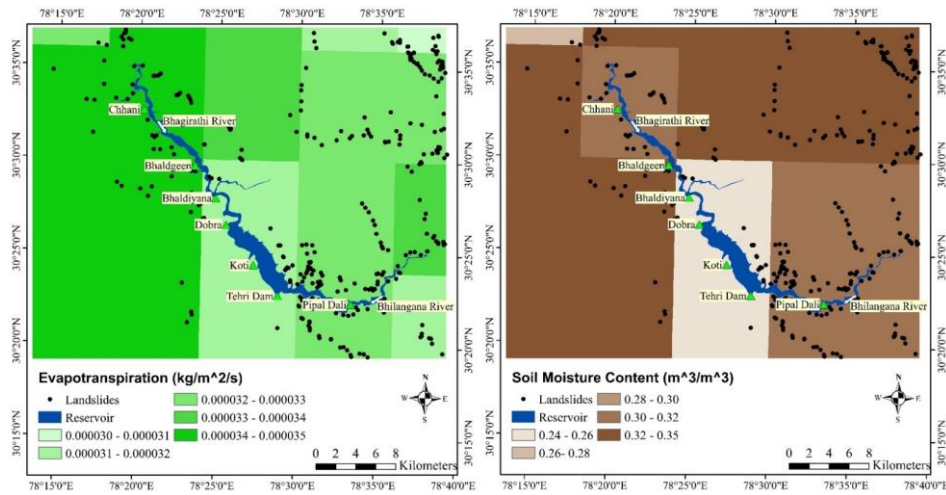


**Fig. 4.8** Evapotranspiration and Soil Moisture Content Maps for the Tehri region.

#### 4.6.4 Soil moisture

The time average maps of soil moisture for the study area was prepared using the FLDAS Noah land surface model. The average layer of soil moisture is the depth-averaged amount of water present beneath the surface in a specific soil layer. Soil moisture can also be expressed as Volumetric Soil Moisture (VSM), which is the volume of water per unit volume of soil. For the Tehri region, the spatial variation in soil moisture was observed from 0.24 to 0.35 (m³/m³).

### 4.7 Peak Horizontal Acceleration Map

Earthquakes have repeatedly shaken Uttarakhand in the past. Uttarkashi suffered one of India's deadliest earthquakes in 1991, which killed nearly 730 people and affected over three lakhs. Another major earthquake hit the Chamoli district of Uttarakhand in 1999, where 103 people died. Hence, it can be stated that Uttarakhand in the Himalayas is situated in a highly seismic zone. In this study, within a 500 km radius of the study area, events of earthquakes were taken from the USGS website. About 950 seismic events were found in the 500 km vicinity of the study area from 1950 to 2019 of magnitude four and above. A deterministic method was used for seismic hazard assessment. A relationship for the Himalayas in India for peak ground accelerations was developed by Sharma (1998) and was used to calculate PHA. The general formula shows the relationship between ground motion and parameters like magnitude, distance, etc.

$$\log(y) = b_1 + b_2M + b_3 \log \left[ \sqrt{R_{JB}^2 + b_4^2} \right] + b_5S + b_6H \quad (4.4)$$

Here,  $y$  is acceleration,  $S$  is kept 1 as the study area is rocky,  $H$  varies from 0-1,  $M$  is the earthquake's magnitude,  $R_{JB}$  is Joyner distance, and  $b_1$ ,  $b_2$ ,  $b_3$ ,  $b_4$ ,  $b_5$ , and  $b_6$  are the regression

coefficients. For the Tehri region, a map of PHA was prepared at the bedrock level (Fig. 4.9). To calculate PHA at the surface level amplification technique was used here (Stewart et al., 2003). The PHA at the surface was calculated having a slope more than or equal to 10 degrees. The surfaces with a slope angle less than 10 degrees were neglected, considering them to be flat (James and Sitharam, 2014). The surfaces with slope angle 10 degrees and above comes under the B-type site class (Wald and Allen, 2007), for which the velocity of shear wave is more than 760 m/s for the top 30 m overburden ( $V_{s30}$ ) (Council, 2003). The following relationship was used to calculate PHA at the surface level.

$$Y_s = Y_{br} + F_s \quad (4.5)$$

Here  $Y_s$  is surface-level PHA,  $F_s$  is the amplification factor, and  $Y_{br}$  is PHA at bedrock. The amplification factor was calculated using the following relationship proposed by Raghu Kanth and Iyengar in 2007.

$$\ln F_s = a_1 Y_{br} + a_2 + \ln(\delta_s) \quad (4.6)$$

Here,  $a_1$  and  $a_2$  are site class regression coefficients,  $Y_{br}$  is the spectral acceleration at the bedrock level, and  $\delta_s$  is the error term.

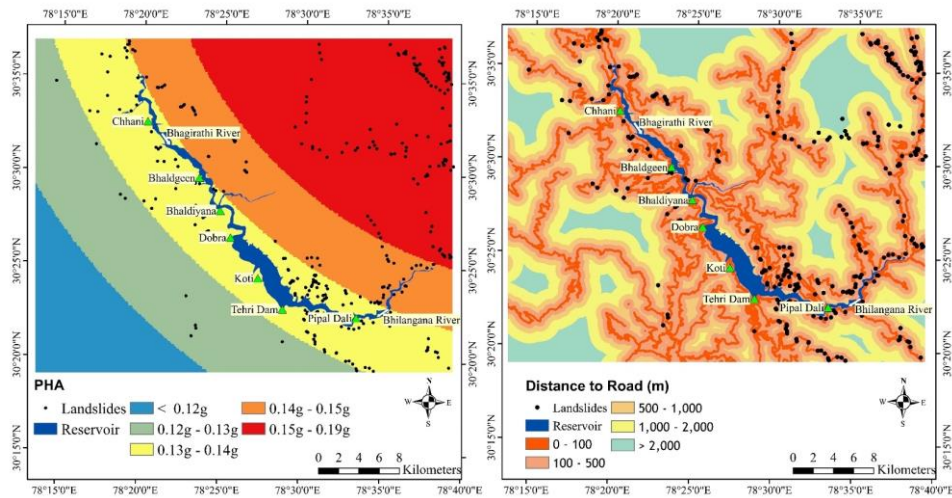


**Fig. 4.9** Peak Horizontal Acceleration and Distance to Road Maps for the Tehri region.

## 4.8 Distance/Buffer Maps

### 4.8.1 Distance to Road

Road construction activities in mountainous regions brutally change the slope stability, creating prone landslide zones. The influence of roads in LSM can be adopted by creating buffer zones along the roads and weighting these zones based on their distance (Ayalew and Yamagishi, 2005). Thus Road buffer map with the multi-buffer (100 m, 500 m, 1000 m, and

2000) layer was prepared, given its proximity to landslides shown in fig. 4.9. The excessive number of landslides were detected along the roads because of unsystematic slope cutting. Most of the cut slopes were found to be untreated. During rainfall, these unstable cuttings fail repeatedly and hamper transportation.

#### 4.8.2 Distance to Waterways

Fluctuation in reservoir water level has led to saturation of embankments, causing instability and landslides. Several landslides were reported from the neighboring regions also. Field observations give an indication of the frequency of landslides along the reservoir region; accordingly, a waterways multi-buffer map (100 m, 500 m, 1000 m, and 5000 m) was prepared (Fig. 4.10)

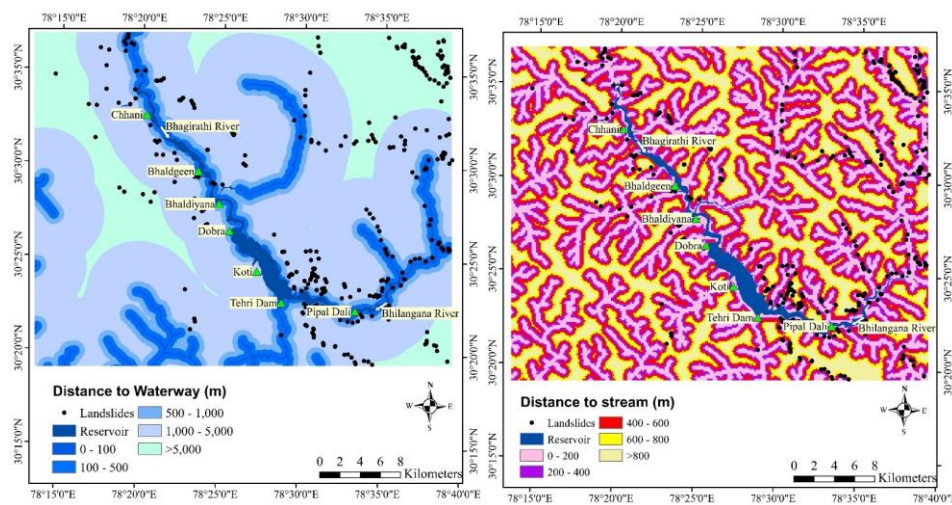


**Fig. 4.10** Distance to Waterway and Distance to Stream Maps for the Tehri region.

#### 4.8.3 Distance to Streams

The Tehri region's extremely undulant topography has supported the drainages network. Earlier researchers have also shown a clear correlation between drainage networks and landslides. The drainage density is directly proportional to the occurrence of landslide events (Kumar and Anbalagan, 2015).

In mountainous areas, streams constantly erode the embankments and craft sharp slopes that are prone to landslides. For the LSM, a drainage buffer map (200 m, 400 m, 600 m, and 800 m) was prepared, complying with field evidence (Fig. 4.10). The streams impact the soil's saturation degree, which directly links to the pore water pressure, a crucial parameter affecting slope stability. Moreover, the erection of drainage structures by the streamside intensively affects stability. The Archydro tool of the ESRI GIS package was used to derive a distance to streams map from the DEM.

## 4.9 Ancillary Data

Ancillary data in polyline and polygon format included maps of soil, geomorphology, lithology, and geology, taken from the online portal of Bhukosh GSI data, and thematic maps were prepared at 1:2,50,000 scale.

### 4.9.1 Soil Type

Soil categories of the Tehri reservoir region consist of alluvial, sandy loam, and black clay soil (Fig. 4.11). Alluvial mixed with boulders were observed at an elevation ranging from 600m to 1000 m. The sandy, loamy soils were identified in the intermediated elevation (1000–1500 m), and black clay soils were observed above 1500 m of elevation (Kumar and Anbalagan, 2015). The soil types with varying properties have a significant influence on landslide occurrence. Due to thick vegetation support, black clay soil is less prone to slope failures. The alluvium and loose boulder deposits are more susceptible to landslides. Sandy loamy soil is also weathering-prone due to less cementation and compaction. Several debris cones formed because older landslides consist of various materials. Soil categories of the reservoir area consist of alluvial soil, sandy soil, and clayey soil. The soil map was digitized from the past literature and mapped at a scale of 1:250000 (Kumar and Anbalagan 2015).

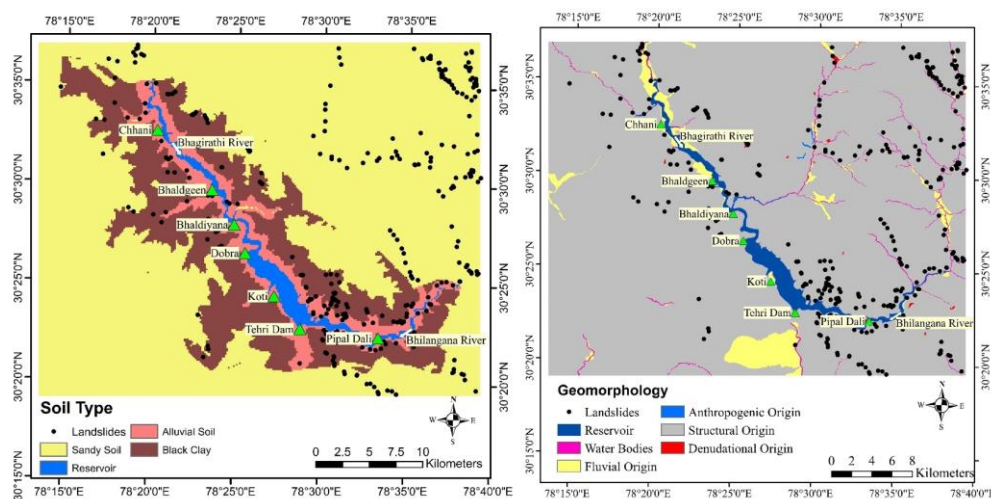


**Fig. 4.11** Soil Type and Geomorphology Maps for the Tehri region.

### 4.9.2 Geomorphology

Geomorphology is the study of landforms, the processes of their formation, and the relations between forms and techniques in their spatial order. The geomorphology of the study area was classified based on its origin into five categories, i.e., water bodies, fluvial origin, anthropogenic origin, structure origin, and denudational origin (Fig. 4.11).

### 4.9.3 Lithology

Different rock types (lithology) behave differently concerning landslide occurrence due to their changing mineral composition that decides their strength. The more substantial rocks provide additional resistance; therefore, they are less susceptible to landslides and vice versa. In the Tehri region, phyllite, quartzite, and shales were found in the center part of the study area. Slate and meta-volcanic in the North-East and Eastern parts and limestone in the South-West part of the region (Fig. 4.12).

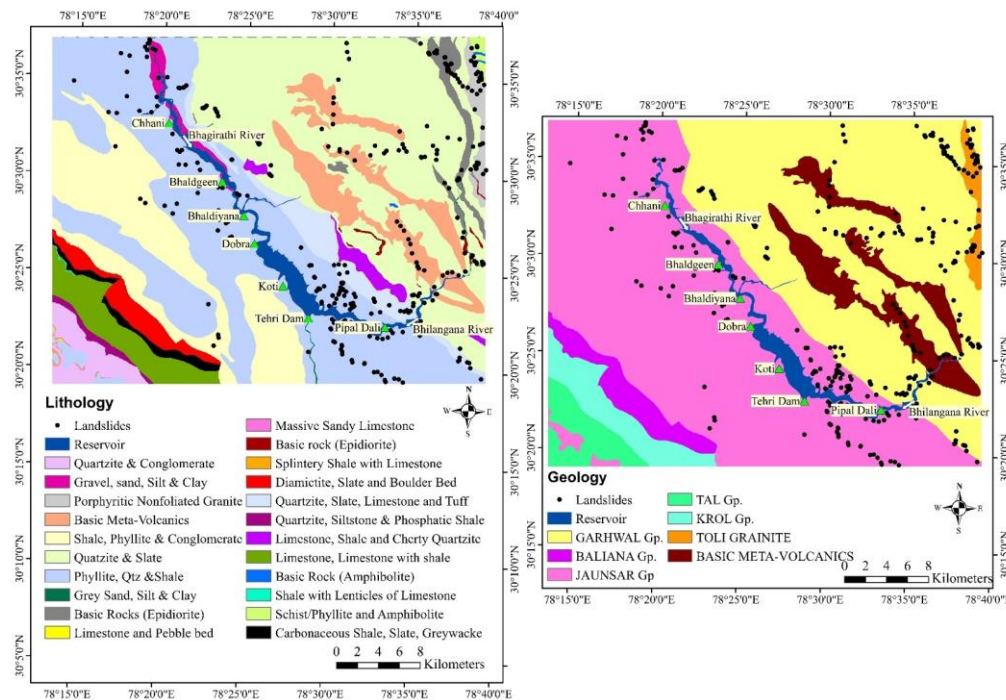


Fig. 4.12 Lithology and Geology Maps for the Tehri region.

### 4.9.4 Geology

The geology map of the area is classified into seven groups, i.e., Garhwal, Baliana, Jaunsar, Tal, Krol, Toli, and Basic Meta-Volcanic (Fig. 4.12). The whole study area is a part of the broader physiographic entity called Lesser Himalaya. Rocks in the central part of the area are low-grade metamorphosed lustrous phyllites and highly weathered quartzites. The well-developed foliation plains and joints make these rocks extremely prone to landslides. In the western part of the study area, quartzites with subordinate intercalation of grey and olive green slates with siltstones with white, purple, and green colors were identified. The Eastern and northeastern part of the study area consists of fine-grained limestone with minor phyllitic intercalations. These rocks are mainly found at the higher ridges. In the eastern part of the area, the rocks are primarily quartzites. In the western part of the study area, the formation comprises quartzites, slates, and carbonate rocks.

## 4.10 LSM Methods

### 4.10.1 Analytical Hierarchy Process

AHP is an MCDM technique invented by Saaty (1988), where both objectives and subjective factors can be considered while making decisions Feizizadeh and Blaschke (2013). AHP breakdowns complex decision-making problems into a pyramid of factors and alternatives. Weights are assigned to factors and alternatives on a nine-point scale (Table 4.2) by pair-wise comparison.

**Table 4.2** The priorities scale between two factors defined by Saaty (1977).

Preference	Degree
1	Equal
3	Moderate
5	Strong
7	Very strong
9	Extreme
2,4,6,8	In-between
Reciprocals	Reverse

As these weights were given subjectively. Therefore, it is essential to check the consistency of the weight provided. To check consistency, Saaty (1977) has defined two terms, i.e., consistency index (CI) and consistency ratio (CR). The following formula is used to calculate the consistency index:

$$CI = \frac{\lambda_{max} - N}{N - 1} \quad (4.7)$$

Here, N is the number of factors, and  $\lambda_{max}$  is the maximum eigenvalue. After calculating the CI, the random index is obtained from the table prepared by Saaty. From the ratio of CI and RI, the consistency ratio is calculated.

**Table 4.3** Random consistency index prepared by Saaty.

N	1	2	3	4	5	6	7	8	9	10	11	12	13	14	15
RI	0	0	0.57	0.90	1.11	1.23	1.31	1.42	1.44	1.48	1.52	1.54	1.55	1.58	1.58

Table 4.3 of the Random index was prepared by Satty in 1977 by random sampling. CR value greater than 0.1 shows inconsistency. While CR value 0 shows that it is perfectly consistent.

#### 4.10.2 Frequency Ratio

The frequency ratio (FR) method deals with the proportion of pixels influenced by the historical landslide events to the proportion of class pixels for the chosen factor. In this study, each class of all landslide-causing factors and their corresponding pixels of landslide and non-landslide information was utilised for LSM (Porghasemi, 2007; Avinash and Ashamanjari, 2010; Karim et al., 2011; Intarawichian and Dasananda, 2011). Equation 4.8 was adopted for calculating the FR values of each class of all the landslide-causing factors selected for LSM analysis.

$$FR = \frac{a/b}{c/d} \quad (4.8)$$

Where a is the number of pixels with landslides for each class, b is the number of landslide pixels in the study region, c is the number of pixels in each category in all factors, and d is the total number of pixels in the Tehri region. FR values of all classes are considered as weights of all categories. Relative frequency (RF) is further calculated to easily understand class influence. For each factor, classes are normalized and shown in percentage.

$$LHI = \sum_{j=1}^N FR_{ij} \quad (4.9)$$

Where  $FR_{ij}$  denotes the weight of an  $i^{th}$  class of causative factor, J. LHI map was then divided into five categories using Jenks natural breaks classification. The Jenks optimization technique, also called the Jenks natural breaks classification method, is one of the data clustering techniques aimed at calculating the finest arrangement of values into various categories. Natural Breaks are the optimum tactic for splitting the ranges, implying that similar categories are grouped together. It is used to minimize the squared deviations of the class means (Jenks, 1967; ESRI, 2016) and is also known as the Goodness of Variance Fit (GVF).

#### 4.10.3 Artificial Neural Network

An ANN is a machine-learning model designed like the human brain. Like the neurons in the human brain, nodes in networking perform a similar function. The neural network structure consists of the input, hidden, and output layers. In this study, n (input layers) × h (hidden layers) × 2 (output layers) structure was selected for the network (Fig. 4.13). A neuron can be defined as declared in equation 4.10 (Jacinth Jennifer and Saravanan 2021):

$$y = \phi\left(\sum_{j=1}^n w_j x_j + b\right) \quad (4.10)$$

Where  $y$  is the output signal of the neuron,  $x_1, \dots, x_n$  are input signals,  $w_1, \dots, w_n$  are synaptic weights,  $b$  is the bias, and  $\phi$  is the activation function. The 'landslide-affected zones' and 'non-landslide affected zones' are the primary attributes of training sites before running the ANN model. Out of this, 70% of the pixels are used as training datasets and the remaining 30% as testing datasets. The landslide inventory data are represented in binary form in the datasets, with '1' denoting landslide pixels and '0' indicating non-landslide pixels. The nominal and interval class group input data were converted to continuous values ranging between 0.1 and 0.9.

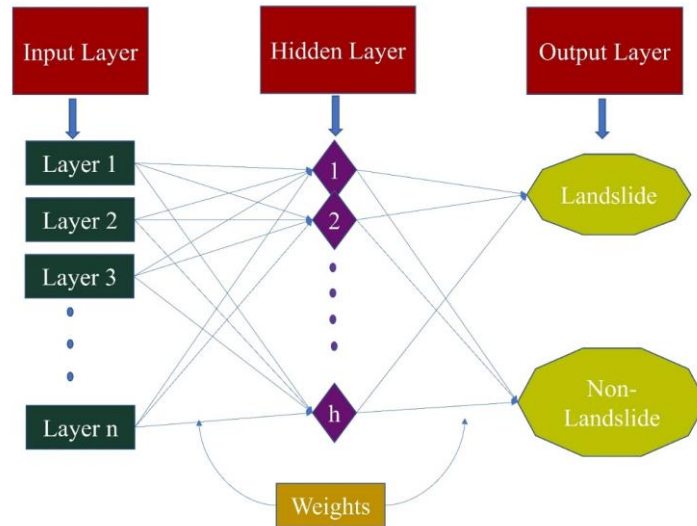


**Fig. 4.13** Neuralnet (nn) plot.

The neural net (nn) package from R software is used in this study. The 'nn' package focuses on multi-layer perceptron (MLP), which is well applicable in modeling functional relationships. The resilient backpropagation with weight backtracking algorithm trains the neural network. The algorithm transferred the error backward and iteratively adjusted the weights. The number of epochs was set to 2,000, and the Root Mean Square Error (RMSE) value was set to 0.01 for terminating the iteration. The primary aim was to fulfill the RMSE stopping condition. If RMSE is not accomplished, the number of epochs can be employed as an ending criterion. According to Saputra and lee (2019),  $2n/3$  hidden neurons can generate results of almost similar accuracy to  $2n+1$  hidden neurons while requiring much less time to train, where  $n$  is the total number of factors.

#### 4.10.4 Artificial-neural-network-based cellular automaton

In an ANN-CA model, the CA provides a spatio-temporal framework for simulation. ANN was used as a data mining tool to calculate the transition probability using multiple output neurons to estimate class changes. Further, the CA algorithm used these transition probabilities to model the changes. A cellular automaton is a collection of cells/pixels on a grid that are synchronously updated through several discrete time steps according to a set of rules based on

the states of neighboring cells. The QGIS and its MOLUSCE module were utilized for the ANN-CA modeling.

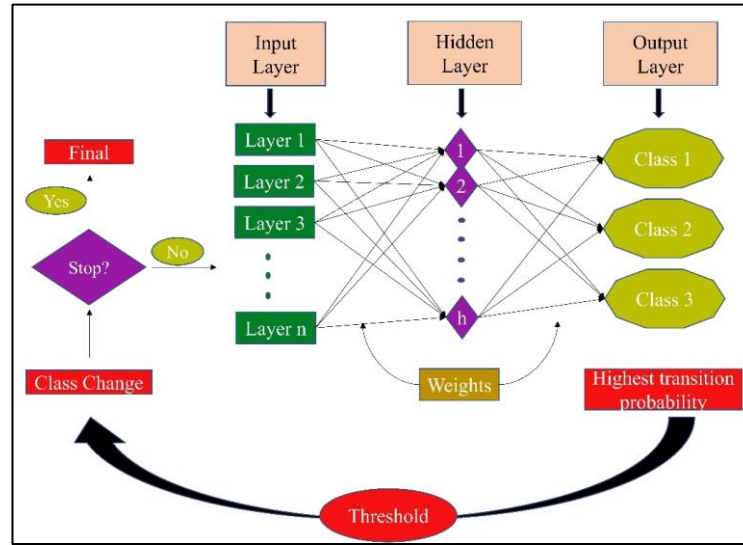


**Fig. 4.14** Artificial-neural-network-based cellular automaton (ANN-CA) model structure for simulating future changes.

The ANN model was used to calculate the transition probability, and further CA simulation uses these transition probabilities to model the changes (Fig 4.14). The transition potential model used in this study was trained with a momentum of 0.050 and a learning rate of 0.01 to stabilize the learning graph. Furthermore, the number of iterations was set to 100 to prevent the issue of overfitting in the model. These inputs were found optimal for training the ANN (Zeshan et al., 2021). The learning algorithm examines the accuracy of training and validation sets of samples and stores the best neural net in memory. The training process finishes when the best accuracy is reached. To control the rate of change in classes, the threshold value of 0.9 was used (Li and Yeh, 2002).

## 4.11 Accuracy Assessment

The scientific importance of the work is incomplete without its validation. Here, we have used two approaches to assess the results accurately. The area under the ROC curve method was used to validate the landslide susceptibility mapping, and Cohen's kappa coefficient was used to validate the LULC classification and future predictions. The area under the ROC curve is used to check the accuracy of the models. The curve delivers a graphical plot that provides the performance of the binary classifier method. Many studies have used this curve to check the accuracy of models in LSM, where the true positive rate is plotted against the false positive rate at several threshold settings. The AUC values between 0.5-1 represent a good fit, and values below 0.5 represent a random fit (Zweig and Campbell 1993). The Kappa coefficient is widely used to measure the true agreement between the observed and chance agreement. The kappa

coefficient has become a standard means of assessment of image classification accuracy (Rwanga and Ndambuki 2017). The Kappa coefficient (K) is calculated using equation 4.11 (Zeshan et al. 2021).

$$K = \frac{N \sum_{i=1}^r x_{ii} - \sum_{i=1}^r (x_{i+} * x_{+i})}{N^2 - \sum_{i=1}^r (x_{i+} * x_{+i})} \quad (4.11)$$

Where r = the number of rows and columns in the error matrix, N = total number of observations (pixels),  $x_{ii}$  = observation in row i and column i,  $x_{i+}$  = marginal total of row i, and  $x_{+i}$  = marginal total of column i. The statistic typically ranges between 0 and 1, with values closest to 1 reflecting the highest agreement (Jenness and Wynne, 2005). Interpretation of the agreement of kappa has been described by Landis and Koch (1977) (Table 4.4).

**Table 4.4** Interpretation of agreement for Kappa coefficient

Value of Kappa coefficient	Nature of agreement
$0.8 \leq K \leq 1$	Almost perfect
$0.61 \leq K \leq 0.80$	Substantial
$0.41 \leq K \leq 0.60$	Moderate
$0.21 \leq K \leq 0.40$	Fair
$0 \leq K \leq 0.20$	Slight
$K < 0.00$	Poor

## 4.12 Summary

The methodology adopted in this study includes the preparation of a landslide inventory map using historical information of landslide events, generation of thematic maps of landslide causative factors, determination of significant landslide causative factors by adopting optimisation techniques, deriving correlation between landslide causative factors and historical landslide events using LSM models and finally based on the derived weights of the factors, LSM was done. Three methods were discussed in this chapter which was adopted for LSM in this study which includes AHP, FR, and ANN. The results of LSM were validated using the area under the ROC curve. Further, the dynamic landslide causative factors were also used for future LSM using the ANN-CA model. The dynamic factors such as LULC, rainfall, and temperature were projected for the future and used as the driving parameter for LSM future prediction. 2010 and 2015 data were used for training, and 2020 data was used for accuracy assessment. The Kappa coefficient values were used to validate the results.

### **LSM using Significant/Influential Landslide Causative Factors**

---

#### **5.1 Introduction**

Landslide causative factors are generally selected based on the mechanism of the landslide process, the scale of analysis, and the features of the study area (Caniani et al., 2008; Sdao et al., 2013). However, standardisation on choosing and selecting these factors is not yet done. The literature review revealed that several studies had employed different landslide causative factors for LSM. The variability in selecting factors for the same region by various researchers has made it difficult to compare the models' prediction accuracies. Thus, the present chapter describes the use of optimising techniques for the determination of significant landslide causative factors for the Tehri region. This chapter discusses two optimising methods of multicollinearity analysis and sensitivity analysis. Also, here we have incorporated four LSM models, i.e., Analytical Hierarchy Process (AHP), Frequency Ratio (FR), FR-AHP, and Artificial Neural Network (ANN), for deriving the weights of these factors. The impact of derived significant factors using ANN sensitivity analysis was also checked using another data-driven FR model. Further, the accuracy of the FR model was enhanced by giving flexibility to it using the AHP model. The later part of the chapter demonstrates the testing of two landslide-prone sites in Himachal Pradesh with similar terrain conditions. The LSM for these two sites was performed using the AHP model adopting derived significant factors.

#### **5.2 Identification of Significant Landslide causing Factors**

Determination of significant landslide causative factors is essential. The literature review revealed that several studies had employed different models and diverse landslide causative factors for LSM. The variability in selecting factors for the same region by various researchers has made it difficult to compare the models' prediction accuracies. Hence, there is a need for the standardization of factors for LSM. Studies related to the identification of significant landslide causative factors are limited. In landslide studies, these factors are frequently considered based on the analysis of the landslide types and the features of the study region (Ayalew et al. 2005). Selecting landslide causal factors and their classes should be considered an essential step in LSM analysis (Meinhardt et al. 2015). According to Lee and Talib (2005), selecting significant factors can increase the model's prediction accuracy. Thus, determining factor significance for the study area is essential before performing susceptibility analysis. Removing less significant factors can reduce noise and uncertainties and thus improve the predicting ability of the model (Pradhan and Lee 2010; Martínez-Álvarez et al. 2013). Methods like multicollinearity analysis

and correlation attribute evaluation can eliminate the least significant factors (Chen et al. 2019). For the Tehri region, many LSM studies (Gupta and Anbalagan 1997; Joshi et al. 2003; Ghosh and Bhattacharya 2010; Kumar and Anbalagan 2015a, b, 2016; Pandey et al. 2020) have been carried out, and factors selection was made based on individual judgment (Table 5.1). This brings the requirement to develop a scientific methodology for identifying significant factors.

**Table 5.1** Literature review for LSM in the Tehri region

<b>Authors</b>	<b>Causative Factors</b>	<b>Models</b>
Gupta and Anbalagan (1997)	Lithology, structural discontinuities, Slope, morphometry, LULC, RR, Hydrogeological conditions	LHEF rating scheme
Joshi et al. (2003)	Lithology, geomorphology, lineament, slope, drainage, land use	Weighted overlay technique
Ghosh and Bhattacharya (2010)	Lithology, Structure, Slope, RR, LULC, Groundwater condition/rainfall	LHEF rating scheme
Kumar and Anbalagan (2015a, b, 2016)	Slope, RR, aspect, curvature, distance to drainage, distance to road, distance to reservoir/waterway, SPI, TWI, LULC class, soil type, lithology, lineament	FR, Fuzzy logic, AHP, and Logistic regression
Pandey et al. (2020)	Altitude, slope, curvature, aspect, geology, soil texture, TWI, NDVI, LULC, distance to rivers, roads, and faults.	Maximum entropy and Support vector machine

### 5.2.1 Multicollinearity analysis using the Pearson correlation coefficient

Multicollinearity happens when independent factors in the regression model are highly correlated. As all 21 factors are closely related to landslides, they may also have a high correlation. Factors with high correlations can be removed to simplify the model interpretation and avoid overfitting problems. This study calculated the linear correlations between two causative factors using Pearson's correlation coefficient (Table 5.2). Pearson correlation coefficient is defined as the covariance of two conditioning factors divided by the product of their standard deviations (Eq. 5.1). The correlation coefficient ranges from  $-1$  to  $1$ . A coefficient value of more than  $0.7$  indicates high collinearity (Al-Najjar et al., 2019).

$$r_{xy} = \frac{\sum_{i=1}^n (x_i - \bar{x})(y_i - \bar{y})}{\sqrt{\sum_{k=1}^n (x_i - \bar{x})^2} \sqrt{\sum_{k=1}^n (y_i - \bar{y})^2}} \quad (5.1)$$

**Table 5.2** Pearson correlations between landslide causative factors

Factors	A	B	C	D	E	F	G	H	I	J	K	L	M	N	O	P	Q	R	S	T	U
A	1	-0.29	0	0	0.12	0.02	0.15	0.01	-0.08	0.08	-0.16	0.18	-0.21	0.14	0.30	0.16	0.09	-0.33	0	0.34	-0.07
B		1	0	0	-0.16	-0.04	-0.08	0.10	0.13	-0.09	0.14	-0.18	0.05	-0.05	-0.63	-0.15	-0.36	0.44	-0.02	-0.55	0.04
C			1	-0.10	-0.04	0	0	0	0.30	-0.06	0.01	-0.03	0.05	-0.09	0.01	0	0.01	0.01	0.22	0	0
D				1	0.01	0	0	0	-0.32	0	0	0.02	-0.05	0.04	0	0	0	0	-0.55	0	0
E					1	0.06	0.06	0	-0.23	0.20	-0.06	0.30	0.03	0.17	0.19	0.19	0.02	0	0.01	0.19	0.10
F						1	0.02	-0.01	-0.11	0.05	0.01	0.14	-0.02	0	0.05	0.07	0.01	0	0.02	0.02	0.05
G							1	0.51	-0.05	0.01	0.13	0.06	0.02	0	0.59	-0.07	-0.43	-0.03	0	-0.07	0.06
H								1	0	-0.04	0.28	0.04	0.04	0.01	0.05	-0.26	-0.66	0.07	-0.01	-0.25	0.23
I									1	-0.41	0.04	-0.38	-0.08	-0.21	-0.13	-0.26	-0.02	0.03	0.52	-0.13	-0.03
J										1	-0.07	0.21	0.02	0.07	0.08	0.33	0.06	-0.01	0.14	0.10	0.04
K											1	-0.05	0.08	-0.09	-0.05	-0.18	-0.32	0.03	0	-0.21	-0.11
L												1	0.09	0.52	0.16	0.32	-0.01	-0.11	0.01	0.22	0.02
M													1	-0.07	-0.03	0.06	-0.05	0.12	0.08	-0.09	0.03
N														1	0.05	0.18	0	-0.15	-0.07	0.12	0.05
O															1	0.13	0.12	-0.36	0.02	0.34	0.01
P																1	0.29	-0.07	0.07	0.22	0.09
Q																	1	-0.17	0.02	0.37	-0.23
R																		1	0	-0.20	0.01
S																			1	0.02	0
T																				1	-0.04
U																					1

A-Distance to road, B-ST, C-STI, D-Curvature, E-Geomorphology, F-Aspect, G-ET, H-Rainfall, I-TWI, J-Slope, K-Geology, L-TRI, M-LULC, N-Distance to stream, O-SM, P-RR, Q-PHA, R-Soil, S-SPI, T-Distance to waterway, U-Lithology.

### 5.2.2 Sensitivity analysis using ANN model

Sensitivity analysis in an ANN identifies the significant factors having more impact on the output. The sensitivity analysis decides the effect of independent factors on dependent factors. Here, both output and input are analysed by changing the input variables. This analysis improves the model's prediction accuracy by selecting the most influencing input factors. The factor hierarchy was built based on the weights of the factors derived using the ANN model. The factor with higher weightage/ percentage agreement with landslide points was considered a more significant factor (Fig. 5.1). Initially, all the factors were considered for LSM, and to identify the significant factors, one by one, the least significant factors were removed, and LS analysis was performed. In total, 21 analyses were performed, and the accuracy of the analysis was checked using the AUC value of the ROC curve.

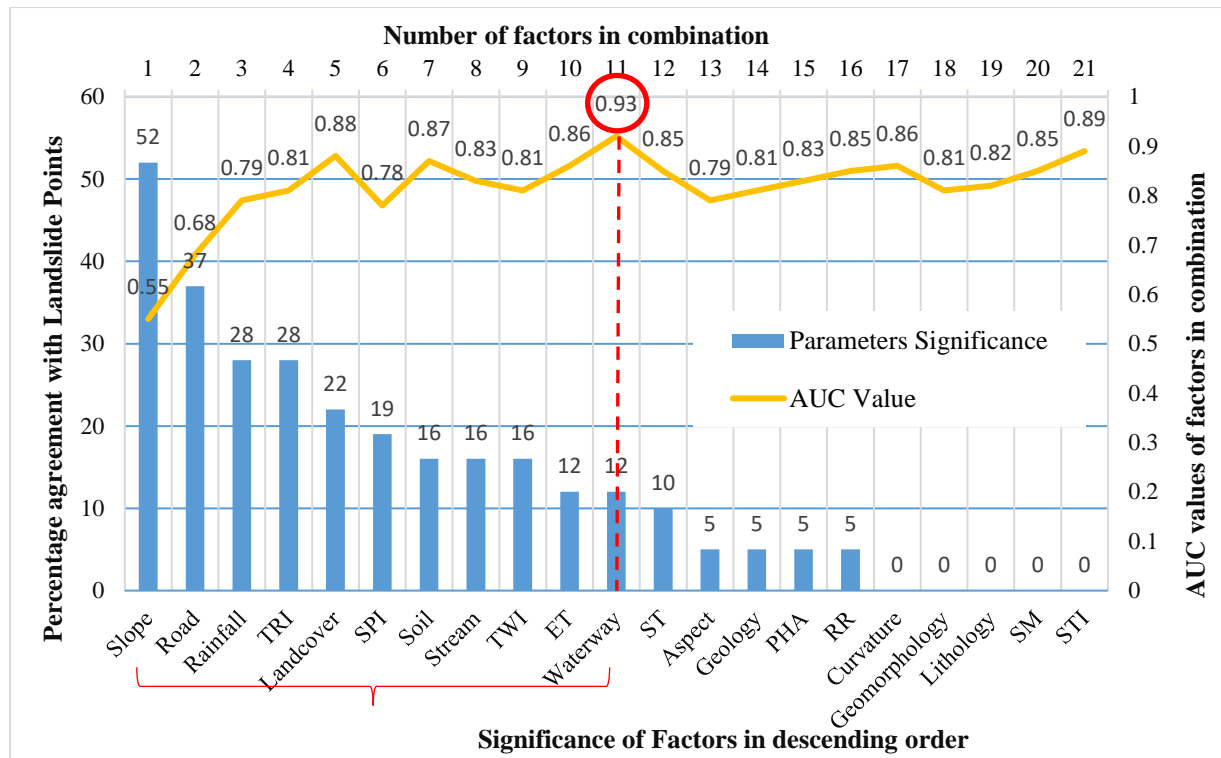


**Fig. 5.1** Significant factors showing percentage agreement with landslide points. (TRI is topographic ruggedness index, SPI is stream power index, TWI is topographic wetness index, ET is evapotranspiration, PHA is peak horizontal acceleration, RR is relative relief, SM is soil moisture, and STI is sediment transport index).

### 5.2.3 Results and Discussion

The significant landslide-causing factors were selected by performing multicollinearity analysis using Pearson's correlation (Table 5.2) and sensitivity analysis using the ANN method (Fig.5.1). As the Pearson's correlation values of all the factors are less than 0.7, they all are taken forward for sensitivity analysis. They are arranged in descending order based on their correlation with historical landslide data, as shown in fig. 5.1. The slope profile factor has shown a maximum agreement of 52% with the landslide points, followed by distance to the road with 37%. The least agreement of zero percent was shown by STI, SM, lithology, geomorphology, and curvature. Initially, all the factors were selected in the analysis, and one by one, factors with least significance were removed. In total, 21 analyses were performed, and accuracy was checked. The top 11 significant factors gave the maximum precision with an AUC value of 0.93. Hence the identified significant landslide causative factors were further used for LSM.

In this research, we have scientifically obtained the most significant landslide-causing factors for the Tehri region. Pearson's correlation test confirmed no multicollinearity among the selected factors. Hence, all 21 factors were taken forward to perform the sensitivity analysis using the ANN model for choosing the most suitable combination of factors. Among 21

analyses, the analysis with the combination of eleven significant factors has shown maximum AUC value and hence was selected for LSM.

### 5.3 LSM using ANN Model

The neural net (nn) package from R software was used here (Jacinth Jennifer and Saravanan, 2022). The 'nn' package focuses on multi-layer perceptron (MLP), which is well applicable in modeling functional relationships. The resilient backpropagation with weight backtracking algorithm trains the neural network. The algorithm transferred the error backward and iteratively adjusted the weights. The number of epochs was set to 2,000, and the root mean square error (RMSE) value was set to 0.01 for terminating the iteration. The primary aim was to fulfill the RMSE stopping condition. If RMSE is not accomplished, the number of epochs can be employed as an ending criterion.

#### 5.3.1 Mapping and Validating Results

The map was divided into five landslide-susceptible zones by applying a natural break classifier. The majority of the areas, about 52%, come under the very low susceptibility zone, with the probability of landslides occurring less than 20%. Whereas about 8% of the area comes under a very high susceptibility zone with more than 80% of landslide occurrence probability. The percentage of the susceptible area with the corresponding percentage of landslide area in each zone is shown in bar chart format (Fig. 5.2). The susceptibility map generated using the ANN model has achieved the prediction accuracy of 0.93 Area Under Curve (AUC) value.

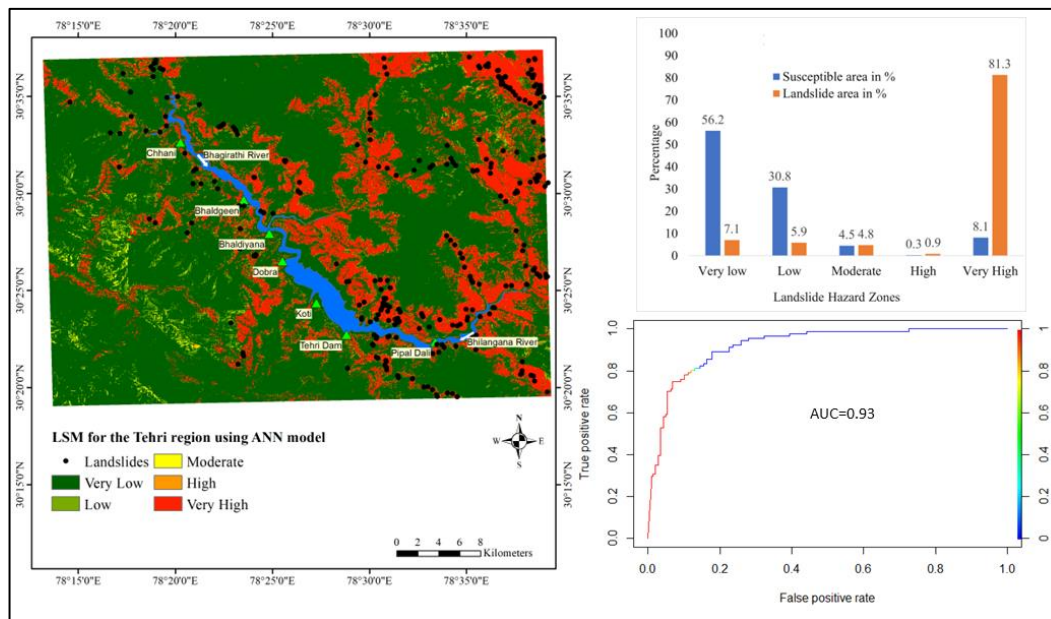


**Fig. 5.2** Landslide Susceptibility maps, Area distribution, and area under the ROC curves using ANN Model.

### 5.3.2 Discussion

The chosen 11 significant factors were used for LSM using the ANN models. The Jenks natural break method was used to determine the threshold values for classifying the landslide causative factor and susceptibility maps (Baeza et al., 2016; Kumar and Anbalagan, 2016). The accuracy achieved using the ANN method using significant factors was considerably high compared to previous results from other researchers working on the Tehri region. Most parts of the high susceptibility zone run along the roads and streams.

## 5.4 LSM using FR, AHP and FR-AHP Models

FR is a data-driven model used to obtain the relationships between the distribution of landslides and each landslide influencing factor and their corresponding classes. The correlation between landslide locations and the factors for the study area is obtained in the form of RF values. The Factors and their classes with higher RF values indicate it has a greater influence on landslide occurrence. AHP is a multi-criteria decision-making technique invented by Saaty, where both objective as well as subjective factors can be considered while taking decisions. Weights are assigned to factors and classes on a nine-point scale by pair-wise comparison between them. AHP has many applications in the selection of in sites and doing LHZ (Ayalew 2005). Further, an attempt was made to increase the prediction accuracy of the data-driven FR model by combining it with the AHP model. The FR method used in this hybrid model gives the class weightage, whereas for obtaining weights of factors, the AHP method was used.

### 5.4.1 Mapping using FR Model and Validating Results

In FR analysis, we obtained that the "0-100 m" class of distance to road, "quartzite, Sandy limestone" class of lithology, and "Toli Granite" class of geology are with higher RF values. Although the lithology factor is not significant factor as per ANN model, however out of 22 classes of lithology one class is showing high agreement with the landslide data. Similarity for geology factor also, single class agreement with landslide data does make factor as the significant factor. Although, in FR analysis these factors have gain more weightage and hence, the influence of these factor classes on the prediction map is strong. Following table 5.3 refer to the factors and their classes with their respective derived FR and RF values. Further, the FR values were integrated for LSM for the Tehri region. Here, we used two sets of data for mapping to determine the impact of derived significant factors. In the first case, all 21 factors FR values were integrated to perform LSM (Fig. 5.3, A), and in the second case, only 11 derived significant factors FR values were integrated for LSM (Fig. 5.3, B). The maps were then classified into five classes using the natural break classifier. The susceptibility maps prepared using the FR method shows the AUC value of 0.83 while incorporating all 21 factors and 0.90 while using only 11 significant factors.

**Table 5.3** Coefficient values for frequency ratio in the case of each factor and their classes

Data Layers of Factors	Class	Landslide Pixels		Class Pixels		FR	RF %
		Count	%	Count	%		
Distance to Roads (m)	0-100	257	77.64	238346	15.00	5.18	86
	100-500	53	16.01	503311	31.67	0.51	8
	500-1000	11	3.32	326750	20.56	0.16	3
	1000-2000	8	2.42	339291	21.35	0.11	2
	2000-5899	2	0.60	181372	11.41	0.05	1
Distance to Waterways (m)	0 - 100	12	3.63	39382	2.48	1.46	23
	100 - 500	47	14.20	143277	9.02	1.57	25
	500 - 1000	39	11.78	164209	10.33	1.14	18
	1000 - 5000	154	46.53	941639	59.26	0.79	13
	5000 - 12816	79	23.87	300563	18.91	1.26	20
Aspect	Flat	0	0.00	2876	0.18	0.00	0
	North	15	4.53	232837	14.66	0.31	4
	North-East	16	4.83	177305	11.17	0.43	5
	East	48	14.50	216728	13.65	1.06	13
	South-East	45	13.60	172203	10.84	1.25	16
	South	74	22.36	214354	13.50	1.66	21
	South-West	64	19.34	206202	12.99	1.49	19
	West	53	16.01	212753	13.40	1.20	15
	North-West	16	4.83	155561	9.80	0.49	6
Curvature	-26.4 - -3.5	25	7.55	113142	7.13	1.06	20
	-3.5 - 0	96	29.00	385739	24.29	1.19	23
	Flat	60	18.13	331932	20.90	0.87	17
	0 - 3.5	121	36.56	642792	40.48	0.90	17
	3.5 - 33.06	29	8.76	114338	7.20	1.22	23
PHA	< 0.12g	0	0.00	161732	10.19	0.00	0
	0.12g - 0.13g	11	3.32	328167	20.68	0.16	4
	0.13g - 0.14g	131	39.58	374788	23.62	1.68	39
	0.14g - 0.15g	66	19.94	275322	17.35	1.15	27
	0.15g - 0.19g	123	37.16	446807	28.16	1.32	31
Lithology	Quartzite, Limestone	0	0.00	33159	2.09	0.00	0
	Gravel, Pebble, Sand, Silt	0	0.00	17280	1.09	0.00	0
	Porphyritic Nonfoliated Granite	5	1.51	18767	1.18	1.28	0
	Basic Meta-Volcanics	32	9.67	105122	6.62	1.46	0
	Quartzite, Shale, Phyllite	24	7.25	213354	13.44	0.54	0
	Quartzite And Slate	6	1.81	464805	29.27	0.06	0
	Phyllite, Qtz, Shale,Dolomite	75	22.66	509412	32.08	0.71	0
	Grey Sand, Silt And Clay	131	39.58	7348	0.46	85.53	8
	Basic Rocks (Epidiorite)	2	0.60	27831	1.75	0.34	0
	Quartzite, Sandy Limestone	27	8.16	138	0.01	938.6	89
	Massive Sandy Limestone	0	0.00	824	0.05	0.00	0
	Basic Rock (Epidiorite)	0	0.00	2915	0.18	0.00	0
	Splintery Shale With Nodular	1	0.30	723	0.05	6.64	1
	Diamictite, Quartzite, Slate	0	0.00	30701	1.93	0.00	0
	Quartzite, Slate, Lensoidal	0	0.00	56385	3.55	0.00	0
	Quartzite, Siltstone, Chert	25	7.55	7064	0.44	16.98	2
	Limestone, Dolomite, Shale	0	0.00	16499	1.04	0.00	0
	Dolomitic Limestone With Shale	0	0.00	55266	3.48	0.00	0
	Basic Rock (Amphibolite)	0	0.00	763	0.05	0.00	0
	Shale	0	0.00	506	0.03	0.00	0

	Quartzite, Schist/Phyllite	0	0.00	3840	0.24	0.00	0
	Carbonaceous Shale, Slate	3	0.91	15241	0.96	0.94	0
Geomorphology	Water Bodies	15	4.53	19640	1.24	3.66	0
	Fluvial Origin	9	2.72	63662	4.01	0.68	0
	Anthropogenic Origin	1	0.30	1486	0.09	3.23	0
	Structural Origin	301	90.94	1501853	94.58	0.96	0
	Denudational Origin	5	1.51	1302	0.08	18.42	2
Geology	Garhwal Group	129	38.97	577496	36.37	1.07	10
	Baliana Group	0	0.00	45227	2.85	0.00	0
	Jaunsar Group	146	44.11	745080	46.92	0.94	9
	Tal Group	0	0.00	42025	2.65	0.00	0
	Krol Group	0	0.00	55770	3.51	0.00	0
	Toli granite	31	9.37	19216	1.21	7.74	71
	Basic Meta-Volcanics	25	7.55	103129	6.49	1.16	11
Rainfall (mm/h)	0.16 - 0.17	32	9.67	78149	4.92	1.96	30
	0.17 - 0.18	39	11.78	145803	9.19	1.28	20
	0.18 - 0.19	145	43.81	529320	33.36	1.31	20
	0.19 - 0.20	55	16.62	345048	21.74	0.76	12
	0.20 - 0.21	15	4.53	220850	13.92	0.33	5
	0.21 - 0.22	45	13.60	267646	16.87	0.81	12
RR(m)	13 - 200	0	0.00	9431	0.59	0.00	0
	200 - 400	54	16.31	269867	16.99	0.96	38
	400 - 600	267	80.66	1217612	76.68	1.05	41
	600 - 836	10	3.02	91033	5.73	0.53	21
Slope	0 - 15	32	9.67	254415	16.02	0.60	12
	15 - 23	72	21.75	347984	21.91	0.99	20
	23 - 30	67	20.24	354372	22.32	0.91	18
	30 - 38	91	27.49	349688	22.02	1.25	25
	38 - 73	69	20.85	281484	17.73	1.18	24
Soil	Sandy Soil	174	52.57	1124264	70.80	0.74	15
	Alluvial Soil	62	18.73	99859	6.29	2.98	58
	Black Clay	95	28.70	329020	20.72	1.39	27
SPI	< -2	100	30.21	545337	34.37	0.88	22
	-2 - 0	59	17.82	279912	17.64	1.01	25
	0 - 2	100	30.21	450516	28.39	1.06	26
	> 2	72	21.75	311051	19.60	1.11	27
STI	0 - 10	297	89.73	1437303	90.58	0.99	23
	10-20	13	3.93	69004	4.35	0.90	21
	20 - 30	6	1.81	29752	1.87	0.97	23
	> 30	15	4.53	50757	3.20	1.42	33
Stream	0 - 200	130	39.27	425212	26.78	1.47	32
	200 - 400	88	26.59	342342	21.56	1.23	27
	400 - 600	58	17.52	334561	21.07	0.83	18
	600 - 800	36	10.88	266996	16.81	0.65	14
	> 800	19	5.74	218832	13.78	0.42	9
TWI	0 - 4	46	13.90	210627	13.27	1.05	21
	4 - 5	123	37.16	556561	35.07	1.06	21
	5 - 6	50	15.11	291908	18.40	0.82	16
	6 - 7	43	12.99	190139	11.98	1.08	22
	< 7	69	20.85	337581	21.27	0.98	20
TRI	0 - 0.3	17	5.14	69790	4.40	1.17	20
	0.3 - 0.4	94	28.40	177622	11.19	2.54	44
	0.4 - 0.5	125	37.76	646857	40.76	0.93	16

	0.5 - 0.6	86	25.98	566730	35.71	0.73	13
	0.6 - 0.7	9	2.72	125817	7.93	0.34	6
ST	282 - 284	21	6.34	41035	2.59	2.45	33
	284-286	12	3.63	24391	1.54	2.36	31
	286-288	123	37.16	627108	39.52	0.94	13
	288-290	35	10.57	387557	24.42	0.43	6
	290-292	140	42.30	506725	31.93	1.32	18
SM	0.24-0.26	21	6.34	221133	13.94	0.46	11
	0.26-0.28	2	0.60	15709	0.99	0.61	15
	0.28-0.30	0	0.00	0	0.00	0.00	0
	0.30-0.32	100	30.21	213583	13.46	2.24	54
	0.32-0.35	208	62.84	1136391	71.61	0.88	21
LULC	Water body	9	2.72	49696	3.13	0.87	8
	Dense Forest	27	8.16	484207	30.49	0.27	3
	Built up area	43	12.99	36204	2.28	5.70	55
	Sparse Forest	132	39.88	811493	51.10	0.78	8
	Agriculture land	120	36.25	206343	12.99	2.79	27
ET	0.000030 - 0.000031	14	4.23	14263	0.90	4.71	55
	0.000031 - 0.000032	36	10.88	299911	18.90	0.58	7
	0.000032 - 0.000033	182	54.98	422313	26.61	2.07	24
	0.000033 - 0.000034	35	10.57	215334	13.57	0.78	9
	0.000034 - 0.000035	64	19.34	634995	40.02	0.48	6

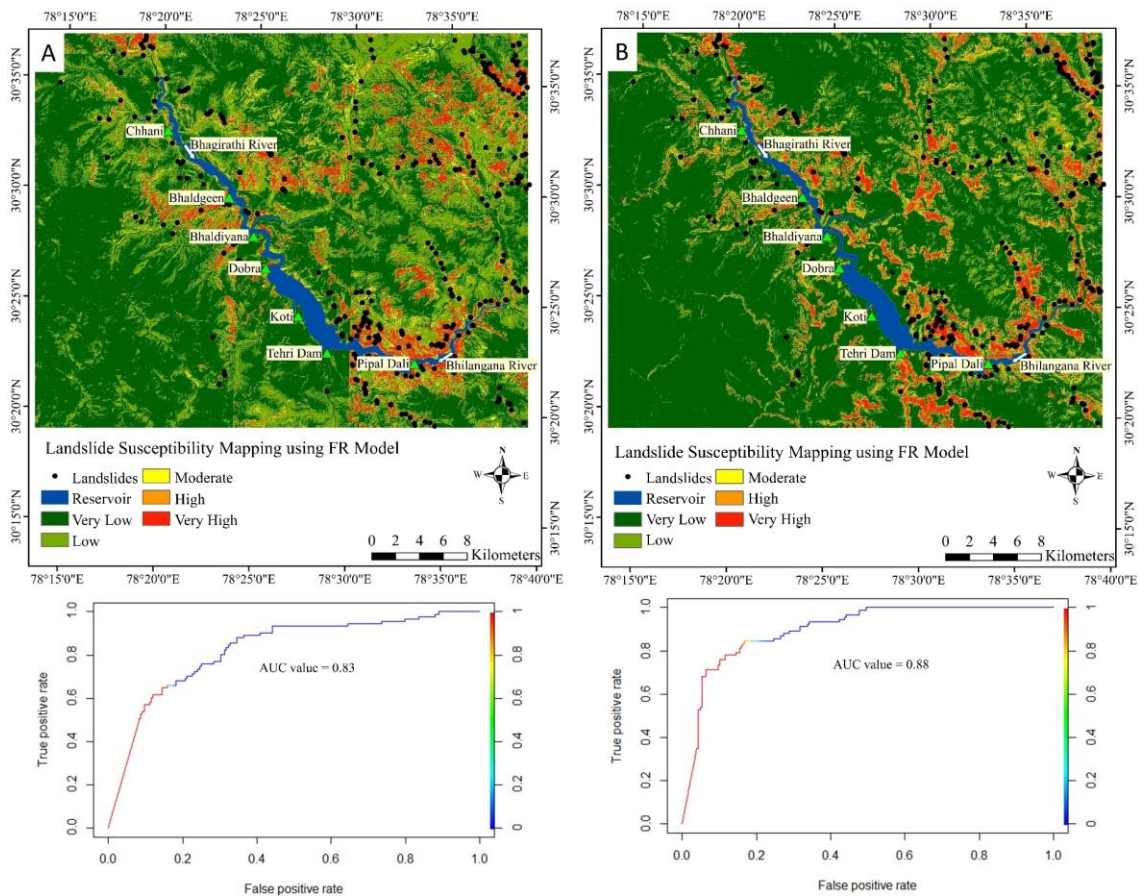


**Fig. 5.3** Landslide Susceptibility maps, area under the ROC curves using the FR Model and (A) All 21 factors (B) Significant 11 factors.

### 5.4.2 Mapping using AHP Model and Validating Results

For synthesizing weights of these causative factors, the AHP method was used. It is a method to derive ratio by paired comparisons. Here, we have compared the eleven factors subjectively by adopting AHP technique. Matrix was formed with different causative factors and their respective classes (Saaty 1977). For comparison, weights are provided which are subjective. In this study, weights are given based on a field visit and past works of literature. From the matrix, Eigen values and Eigen vectors are obtained which represent the influence of that factor or class for causing a landslide. The following are the matrix prepared for all the causative factors and their respective classes (Table 5.4).

**Table 5.4** Scores of factors and their classes obtained by performing AHP

S. No.	Factors	A	B	C	D	E	F	G	H	I	J	K	Weights
1	Distance to road (A)	1	3	5	2	3	5	2	5	5	4	4	0.248
2	Distance to waterways (B)	0.33	1	1.5	0.66	1.25	1.5	0.66	1.5	1.5	1	1	0.077
3	Rainfall (C)	0.2	0.5	1	0.33	0.8	1.25	0.33	1.25	1.25	0.66	0.66	0.049
4	Slope (D)	0.5	1.5	3	1	2	4	1	4	4	1.5	1.5	0.140
5	Soil (E)	0.33	0.8	1.25	0.5	1	1.25	0.5	1.25	1.25	0.8	0.8	0.063
6	SPI (F)	0.2	0.5	0.8	0.25	0.8	1	0.25	1	1	0.66	0.66	0.044
7	Distance to Streams (G)	0.5	1.5	3	1	2	4	1	4	4	1.5	1.5	0.140
8	TWI (H)	0.2	0.5	0.8	0.25	0.8	1	0.25	1	1	0.66	0.66	0.044
9	TRI (I)	0.2	0.5	0.8	0.25	0.8	1	0.25	1	1	0.66	0.66	0.044
10	ET (J)	0.25	1	1.5	0.66	1.25	1.5	0.66	1.5	1.5	1	0.5	0.071
11	LULC (K)	0.25	1	1.5	0.66	1.25	1.5	0.66	1.5	1.5	2	1	0.081
$\lambda_{\max} = 11.0571$ , $CI = 0.00571$ , $CR = 0.003568$													

Distance to Road (A)						
0-100 m	1					0.48637
101 m – 500 m	1/3	1				0.23394
501 m – 1000 m	1/4	1/3	1			0.15493
1001 m – 2000 m	1/5	1/4	1/2	1		0.08045
>2000 m	1/7	1/6	1/4	1/3	1	0.04432
$CR = 0.0781$ , $\lambda_{\max} = 5.347$						

<b>Distance to Waterways (B)</b>						
0-100 m	1					0.48637
101 m – 500 m	1/3	1				0.23394
501 m – 1000 m	1/4	1/3	1			0.15493
1001 m – 5000 m	1/5	1/4	1/2	1		0.08045
>5000 m	1/7	1/6	1/4	1/3	1	0.04432
CR = 0.0781, $\lambda_{\max} = 5.347$						

<b>Rainfall (mm/h) (C)</b>							
0.16 – 0.17	1						0.02964
0.171-0.18	3	1					0.06494
0.181-0.19	4	2	1				0.10303
0.191-0.20	5	3	2	1			0.16406
0.201-0.21	6	4	3	2	1		0.25485
0.211-0.22	9	5	4	3	2	1	0.38348
CR = 0.0923, $\lambda_{\max} = 6.568$							

<b>Slope (D)</b>						
0° – 15°	1					0.04308
15.1° – 23°	2	1				0.06682
23.1° – 30°	4	3	1			0.14245
30.1° – 38°	6	5	3	1		0.29466
38.1° – 73°	8	6	4	2	1	0.45299
CR = 0.051, $\lambda_{\max} = 5.230$						

<b>Soil Cover (E)</b>				
Alluvial Soil	1			0.638
Black clay	1/5	1		0.101
Sandy soil	1/3	3	1	0.262
CR = 0.021, $\lambda_{\max} = 3.030$				

<b>SPI (F)</b>					
0-10	1				0.07173
10-20	3	1			0.15323
20-30	4	2	1		0.24412

>30	5	4	3	1	0.53092
CR = 0.077, $\lambda_{\max} = 4.209$					

Distance to Streams (G)						
0-200 m	1					0.48637
201 m – 400 m	1/3	1				0.23394
401 m – 600 m	1/4	1/3	1			0.15493
601 m – 800 m	1/5	1/4	1/2	1		0.08045
>800 m	1/7	1/6	1/4	1/3	1	0.04432
CR = 0.0781, $\lambda_{\max} = 5.347$						

TWI (H)						
0-4	1					0.06232
4-5	2	1				0.09846
5-6	3	2	1			0.16083
6-7	4	3	2	1		0.26192
>7	5	4	3	2	1	0.41646
CR = 0.0248, $\lambda_{\max} = 5.1103$						

TRI (I)						
0 – 0.3	1					0.06232
0.31 – 0.4	2	1				0.09846
0.41 – 0.5	3	2	1			0.16083
0.51 – 0.6	4	3	2	1		0.26192
0.61 – 0.7	5	4	3	2	1	0.41646
CR = 0.0248, $\lambda_{\max} = 5.1103$						

ET (J)						
0.000030-0.000031	1					0.06232
0.0000311-0.000032	2	1				0.09846
0.0000321-0.000033	3	2	1			0.16083
0.0000331-0.000034	4	3	2	1		0.26192
0.0000341-0.000035	5	4	3	2	1	0.41646
CR = 0.0248, $\lambda_{\max} = 5.1103$						

LULC (K)						
Water body	1					0.04674
Dense forest	2	1				0.07483
Sparse forest	3	2	1			0.11732
Agriculture land	5	4	3	1		0.25099
Built up area	8	6	5	3	1	0.51012
CR = 0.0538, $\lambda_{\max} = 5.239$						

After calculating the weights of all the factors and their class, the next step in AHP analysis was the calculation of LHI. It was computed by multiplying weights with respective classes and then using the following formula:

$$LHI = \sum_{j=1}^N \text{weight of factor } (W_j) \times \text{weight of factor classes } (W_{ij}) \quad (5.1)$$

where  $W_{ij}$  denotes the weight of  $i^{\text{th}}$  class of causative factor  $J$ . LHI map generated was again divided into five classes: very low, low, moderate, high, and very high to achieve a susceptibility map for the Tehri region (Fig. 5.4).

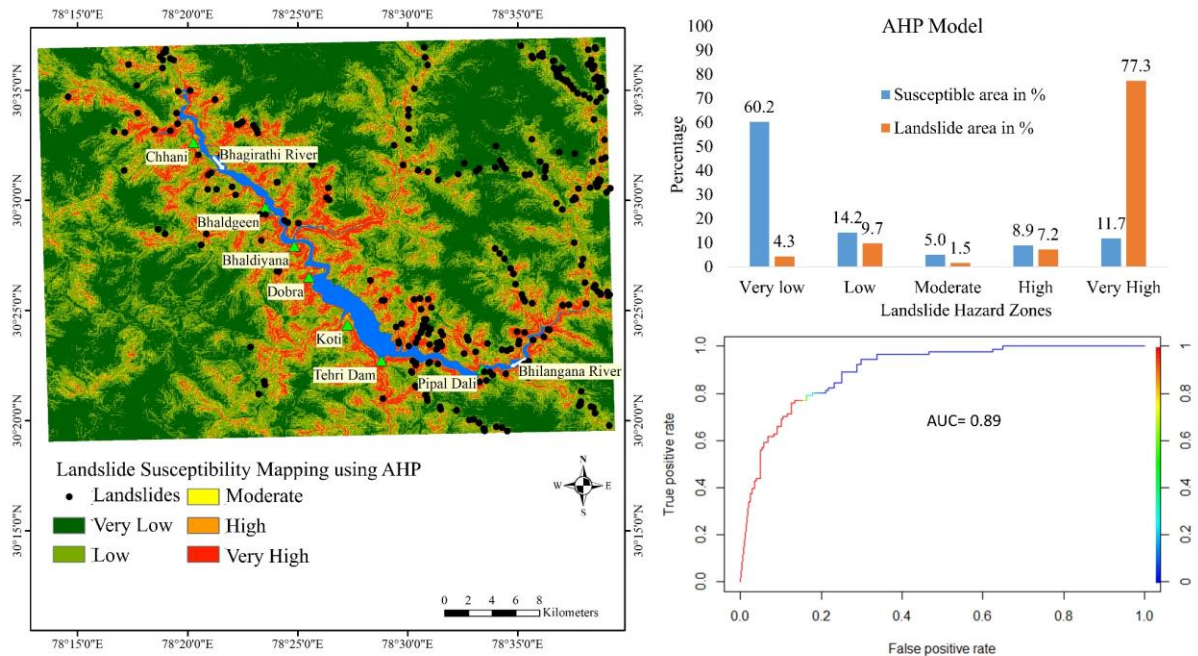


**Fig. 5.4** Landslide Susceptibility Maps, Area distribution and area under the ROC curves using the AHP Model.

### 5.4.3 Mapping using FR-AHP Model and Validating Results

The FR model using significant factors was adopted for LSM, had achieved an accuracy of AUC value of 0.88. An attempt was made to increase the FR model by combining it with AHP model. FR is a rigid data-driven method, which provides output based on the input data, whereas the AHP, on the other hand, is more flexible. Due to its subjective nature, it gives freedom to alter unexpected data-driven outcomes. Distance to road and distance to stream are the two most influencing factors obtained from AHP analysis. The weights of factors derived using AHP analysis were clubbed together with the data-driven FR values of classes. The flexibility was added to the FR-AHP model by giving this subjective preference of weighted factors (Table 5.4) to the rigid FR model having values of weighted classes (Table 5.3).

The weighted factors using the AHP model and their weighted classes using the FR model were integrated to achieve the LSI map. This was further classified into five susceptibility classes using Jenks natural break classifier (Fig. 5.5). About 80% of the landslides were mapped in a very high susceptibility zone covering about 13% of the area. The prediction accuracy of 0.91 AUC value was achieved using the hybrid model. This semi-quantitative hybrid model has shown better result than the individual models.

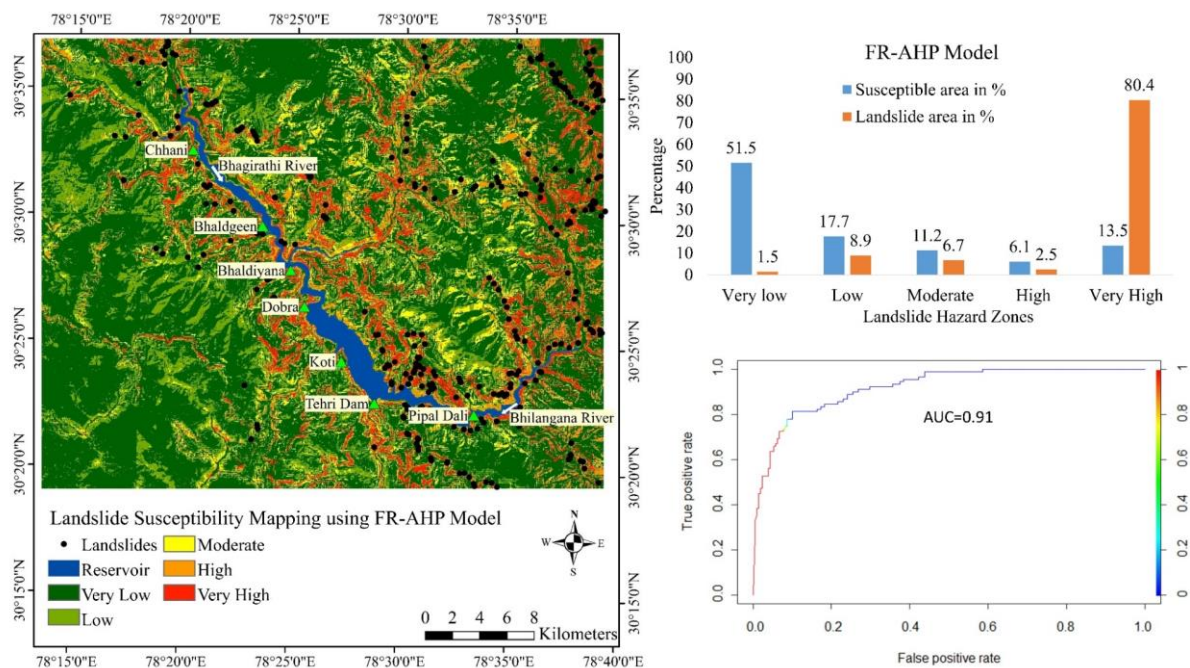


**Fig. 5.5** Landslide Susceptibility maps, Area distribution, and ROC curves using FR-AHP Model.

#### 5.4.4 Discussion

The FR model uses the ratio of classes and landslide pixels to determine their correlation in the form of FR values. A higher FR value indicates a higher significance of factor class with landslides. However, the drawback of this method is its difficulty in determining the factor significance. The factor selection in analysis with less correlation with landslides is expected to lead to less accurate predictions (Martínez-Álvarez et al., 2013). In this study, the accuracy achieved by adopting significant factors was high with an AUC value of 0.88 compared to an AUC value of 0.83 achieved by adopting all the factors. Hence, to achieve higher accuracy, use of significant factors are recommended in LSM analysis.

AHP technique was adopted to obtain the weightage of different causative factors for preparing a susceptibility map for the Tehri area. Each factor in the form of a thematic map was given a weight value. Weighted raster maps were integrated, resulting in an LHI map, where the high value of LHI means that the grid is lying on a more critical landslide zone, and the low value of LHI implies that the grid is lying on a less critical landslide zone. Hence, For LSM, the LHI map was classified into five susceptibility zones using Jenks natural break classifier: very low, low, moderate, high, and very high. (Fig. 5.4). The prediction accuracy of the area under the ROC curve value 0.89 was achieved for LSM using the AHP method. About 77% of the landslides were successfully mapped in the very high susceptibility zone (11.7%). The success of this mapping using the subjective AHP method and its simple procedure and high flexibility make us recommend it with the combination of significant factors as the initial choice for conducting future research in other similar terrains.

The map prepared using the hybrid method has shown considerably better results than individual methods previously applied. The FR method used here is a data-driven method that can produce unreliable results based on input data accuracy. FR method was used to obtain the relationships between the distribution of landslides and each landslide influencing factor and their corresponding classes. The correlation between landslide locations and the factors for the study area can be obtained in the form of RF values. On the other hand, the AHP technique is conventionally based on a rating system provided by expert opinion. Due to its subjective nature, it gives freedom to alter unexpected data-driven outcomes. The unexpected weights of factors were replaced with weights obtained using a pairwise comparison matrix of AHP. However, to some extent, opinions may change for every individual expert and thus may be subjected to reasoning limitations with uncertainty and subjectivity. Combining the two methods reduces these deficiencies of the solo methods, and the hybrid model has the better predictive capability. This result agrees with the past studies that motivate the use of hybrid approaches (Kanungo et al. 2011; Ahmed and Dewan 2017; Hong et al. 2017; Chen et al. 2017; Pradhan et al. 2017; Goyes-Peñafiel and Hernandez-Rojas, 2021).

## 5.5 Validating the significant factors at Chamba and Bhuntar test sites

Two landslide-prone sites were tested to check the applicability of derived significant factors on other similar terrains. This type of analysis can be performed for areas with insufficient historical landslide data, where determining correlations between landslide-causing factors and landslide events is challenging. Hence, significant direct factors can be adopted for LSM using the subjective weightage and ranking system. Here, we have adopted the AHP technique for LSM of the Tehri region, Chamba test site, and Bhuntar test site using the identified significant landslide causative factors. The matrix of 11 rows and 11 columns was prepared, and weights were obtained by pairwise comparison of factors (Table 5.4). The matrix shows weight consistency as the consistency ratio value of 0.0083 was achieved. The weighted raster maps of 11 factors were integrated, resulting in the LSI maps of the three study regions.

### 5.5.1 Mapping and Validating Results

The LSI maps were then classified into five classes using the Jenks natural break classifier. Further, the susceptibility maps for the study area of Tehri and two test sites of the Chamba and Bhuntar areas were generated (Fig 5.6). As AHP is subjective, we have not incorporated historical landslide data of test sites for generating these susceptibility maps. However, the historical landslide data of these regions were used to check the accuracy of the predicted maps. The susceptibility maps of the Chamba, Bhuntar, and Tehri regions have shown high prediction accuracy of 0.86, 0.82, and 0.89 AUC values, respectively.

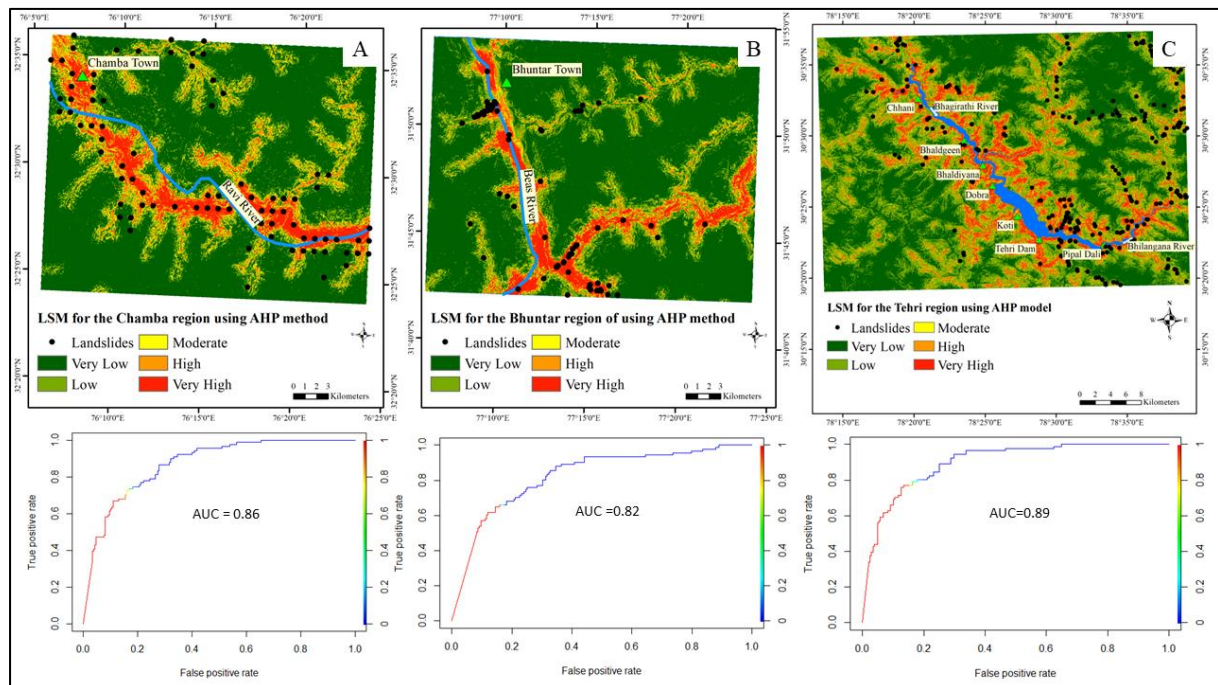


**Fig. 5.6** LSMs and area under the ROC curves for (A) Chamba test site, (B) Bhuntar test site, and (C) Tehri region using AHP Technique.

### 5.5.2 Discussion

The identified significant factors, along with their hierarchy, were imported into the AHP framework for predicting the LSM of the Tehri region as well as two different sites, namely the Chamba and Bhuntar sites of Himachal Pradesh. The AHP technique is based on ranking, where the expert's judgment gives weights. Due to its subjective nature, it offers the freedom to manually weight the factors. We propose this combination of significant factors and the AHP model for LSM in similar terrain conditions as the initial choice to the first-stage researcher having insufficient landslide data or skills to perform robust machine learning methods.

## 5.6 Conclusion

The Himalayan region in India faces severe challenges due to landslide activities. Hence, LSM is an essential step for identifying dangerous areas and a piece of crucial evidence for encouraging people to inhabitant on safe ground. Numerous landslide studies have been conducted in the Tehri region using the different combinations of landside-causing factors. Hence, it was urgent to determine the significant landslide causative factors for the Tehri region and other regions with similar terrain conditions. As the number of factors increases or decreases, the model accuracy changes. To achieve this purpose, two optimising techniques were adopted. Multicollinearity analysis was first applied to remove the high inter-correlations factors. Further, sensitivity analysis was performed to achieve the highest accuracy by identifying the suitable combination of significant factors. The aim was to ensure that the ANN's inputs are those with maximum correlation with the output. The results show that the eleven significant landslide causative factors are the most appropriate combination for LSM. The accuracy achieved using this combination using the ANN model was 0.93 AUC value, the highest accuracy achieved to date for the Tehri region. Earlier research on this study area using multiple models also couldn't achieve this high accuracy. This may be because the selected factors in earlier studies were not all that significant for the LSM analysis. In short, using the significant factors as ANN's inputs in this study generated the best results in all the evaluated cases by the previous researchers. Further, we propose this combination of significant factors as initial choice for conducting future research in similar terrain.

Over the last few decades, several LSM models have been developed. As all these methods used for deriving weights of the causative factors have some pros and cons, hence no one method is standardized at a global scale. By combining the two methods, these deficiencies of the solo methods are reduced, and the hybrid model has better predictive capability. The map generated using this hybrid model shows better accuracy than individual models. The accuracy enhancement could be because of the flexibility provided by the AHP method, which has added subjectivity to the FRM.

The study has also concluded that the identified significant factors and their hierarchy can be applied to other similar regions of the Himalayas. The test performed on the two landslide-prone sites (Chamba and Bhuntar) of the Himalayan region with similar terrain conditions as Tehri gave positive outcomes. High accuracies were achieved by the predicted landslide susceptibility maps using the identified factors in the AHP framework. The identified 11 significant landslide causative factors and their hierarchy derived in this study can also be applied to other regions of the Himalayas with similar terrain conditions.

Conclusively, the present study results may benefit LULC and mitigation strategies planning for the Tehri region and other similar terrain conditions and developing infrastructural facilities in the future. The identified combination of significant factors affecting the landside for the study area is also applicable to other districts of the country. Also, the success of the hybrid FR-AHP model in predicting the landslide susceptibility of the Tehri region permits it to be put into practice in the other parts of the Himalayas. The accuracy of both ANN and hybrid models is excellent in predicting the LSM. However, the computational and data analysis work is comparatively less in the hybrid FR-AHP model. Also, adequate tests and analysis must be performed before applying the model.

### Future LSM Considering Future LULC Projections

---

#### 6.1 Introduction

For mapping the landslide hazard, both static and dynamic factors are required. Several research works presented the significant effect of landslide causative factors considered as constant or quasi-static in times, such as lithology, morphology, hydrology, etc., on the incidence of landslides. However, few research articles have incorporated the impact of Land Use Land Cover, which varies with time due to the influence of human actions in LSM (Bourenane 2021). These dynamic factors can change a lot when continuous and frequent environmental activities occur, such as urbanization, deforestation, and modifications in socioeconomic structures. Change in LULC can be observed using satellite data; however, the minimum time interval to identify those changes depends on the satellite data's spatial resolution. Here we have used the Landsat images of a spatial resolution of 30m where the LULC change can be observed every five years (Marquez et al. 2019). In the Himalayas, the practice of LULC cannot be stopped, but a proper land use policy can lead to these changes more sustainably (Tiwari et al. 2018). Recently, studies have evaluated the effects of LULC change on LSM (Shu et al. 2019; Pham et al. 2021; Hürliemann et al. 2021; Sur et al. 2021). According to Chen et al., 2019, an increase in engineering construction activities causes LULC changes, increasing Landslide susceptible areas. Hence, the LULC change can further be used as the driving parameter to predict LSM for the future. Evaluating landslide hazards in a specific region provides an essential basis and scientific support for governments to prepare the land use policy (Nicu, 2018). LSM is a vital tool for the reduction of landslide hazard losses. This chapter describes the use of future LULC projections to determine the future scenarios of LSM. Initially, LULC changes were simulated to achieve this objective, and this change was projected for the future using the ANN-CA model incorporating LULC change driving parameters. This chapter also describes the process of selecting the significant LULC driving parameters. The later part of this chapter discusses the validation processes adopted to identify the accuracy of the generated projected maps.

#### 6.2 Data Preparation

The LULC describes the physical description of the region and is generated by a supervised classification technique. The maximum likelihood classification algorithm uses the spectral signature of the training class to classify the whole image into five classes, i.e., waterbody, dense forest, built-up area, sparse forest, and agriculture land. LULC maps were prepared using Landsat 5 and 8 data for the years 2010, 2015, and 2020. It is the most preferred

data source as it has an extended temporal coverage (Saini and Tiwari 2020). The initial (2010) and final (2015) data were used as training input data, and the 2020 data was used to validate the result.

### 6.3 Driving parameters for LULC projection

The parameters responsible for driving the LULC change are required for projecting the LULC change for the future. For LULC simulation, the driving parameters were chosen based on the correlation of parameters with LULC using the Pearson correlation coefficient (Table 6.1). The higher value of the coefficient indicates a higher correlation. Slope, distance to road, and distance to stream have shown comparatively good correlation with LULC for the Tehri region. This result agrees with previous studies (Araya and Cabral, 2010; Green and Ahearn, 2016) and is hence considered as driving parameters to obtain future LULC. The correlation coefficient of the two parameters was calculated using the following equation 1. The correlation coefficient ranges from  $-1$  to  $1$ .

**Table 6.1** Pearson correlation coefficient between LULC and driving parameters.

Spatial Variables	Pearson coefficient
<b>Slope</b>	<b>-0.406</b>
<b>Distance to road</b>	<b>-0.335</b>
<b>Distance to stream</b>	<b>0.218</b>
Distance to waterways	0.093
TRI	-0.084
Rainfall	-0.066
SPI	0.063
Soil type	-0.055
TWI	0.049
Evapotranspiration	0.038

### 6.4 ANN-CA model

The ANN-CA model was used twice in this study. At first, it was used to simulate the future scenario of LULC and then for the future prediction of the LSM. The initial (2010), final (2015), and driving parameters maps were used as the input. The area changes for each class between 2010 and 2015 were calculated. These class changes were used to obtain the proportion of pixel change from one class to another in transition matrix form. The ANN model was used to calculate the transition probability, and further CA simulation uses these transition probabilities to model the changes. The transition potential model used in this study was trained with a momentum of 0.050 and a learning rate of 0.01 to stabilize the learning graph. Furthermore, the number of iterations was set to 100 to prevent the issue of overfitting in the model. These inputs were found optimal for training the ANN (Zeshan et al. 2021). The learning algorithm examines the accuracy of training and validation sets of samples and stores the best

neural net in memory. The training process finishes when the best accuracy is reached. To control the rate of change in classes, the threshold value of 0.9 was used (Li and Yeh 2002).

## 6.5 Methodology

Fig. 6.1 presents a flow chart describing the methodology adopted in the present study. The primary prediction methodology adopted in point of projection from past to future includes the prediction of LSM for the years 2010 and 2015 using the ANN model and then projecting it for 2030 using the ANN-CA model. To achieve this objective, significant landslide causative factors were initially identified using the Pearson correlation coefficient and ANN Sensitivity analysis described in detail in Chapter 5. Further, the significant factors and landslide inventories were used in LSM for the years 2010, 2015, and 2020. LULC maps were prepared for the same year by adopting the maximum-likelihood classification technique. The LULC maps were prepared with five major classes: water body, dense forest, built-up area, spare forest, and agriculture land. The ANN-CA model was further used for future projections of LSM and LULC. The future projection of LULC was derived by incorporating slope profile, distance to roads and distance to stream as the LULC change driving parameters. The future projection of LSM was conducted by incorporating future LULC change as the driving parameters.

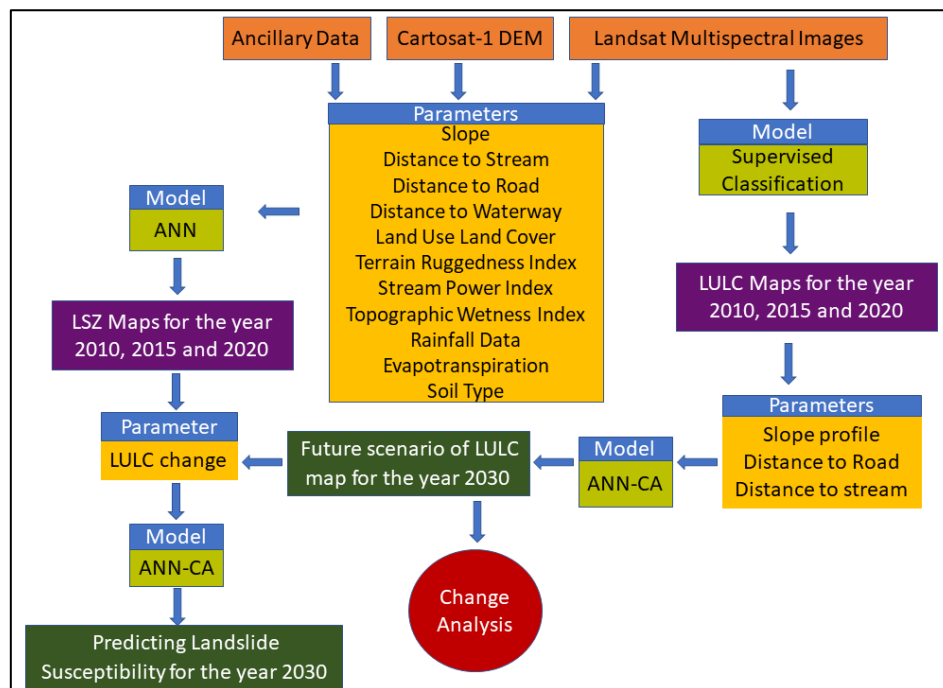


**Fig. 6.1** The flow chart showing the proposed methodology for this research

## 6.6 Results and Discussion

### 6.6.1 Future Scenario of LULC

The LULC of the study area showed built-up area (settlements, industries, and road network), dense forest, spare forest, agriculture land, and water body (reservoir and streams). The future scenario of the LULC was simulated for 2030, and the LULC variations for different years can be observed in fig. 6.2 The future scenario states that the built-up area will increase from 34.3 km<sup>2</sup> to 46 km<sup>2</sup> (34.1%) from the year 2020 to 2030. The areas of the water body and agriculture land will also increase from 46.1 km<sup>2</sup> to 49 km<sup>2</sup> (6.3%) and 195.9 km<sup>2</sup> to 197.8 km<sup>2</sup> (1%), respectively. In contrast, there will be a decrease in the area from 414.3 km<sup>2</sup> to 404.3 km<sup>2</sup> (2.4%) for dense forest and 738.5 km<sup>2</sup> to 732 km<sup>2</sup> (0.9%) for sparse forest (Fig. 6.3).

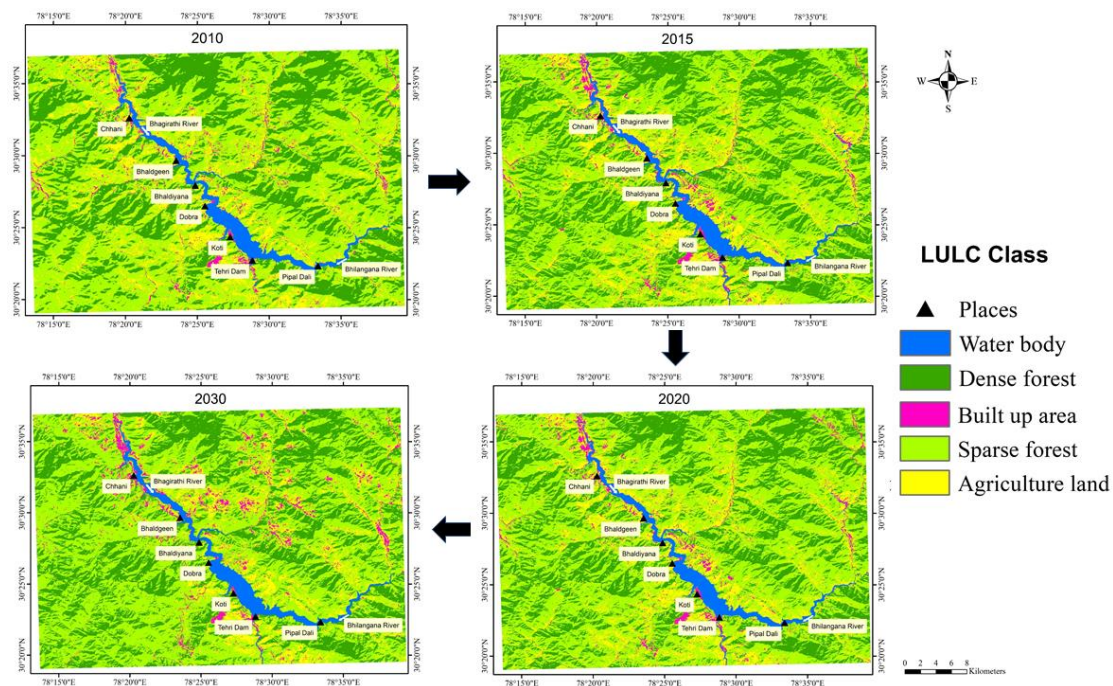


Fig. 6.2 LULC maps for the year 2010, 2015, 2020 and 2030.

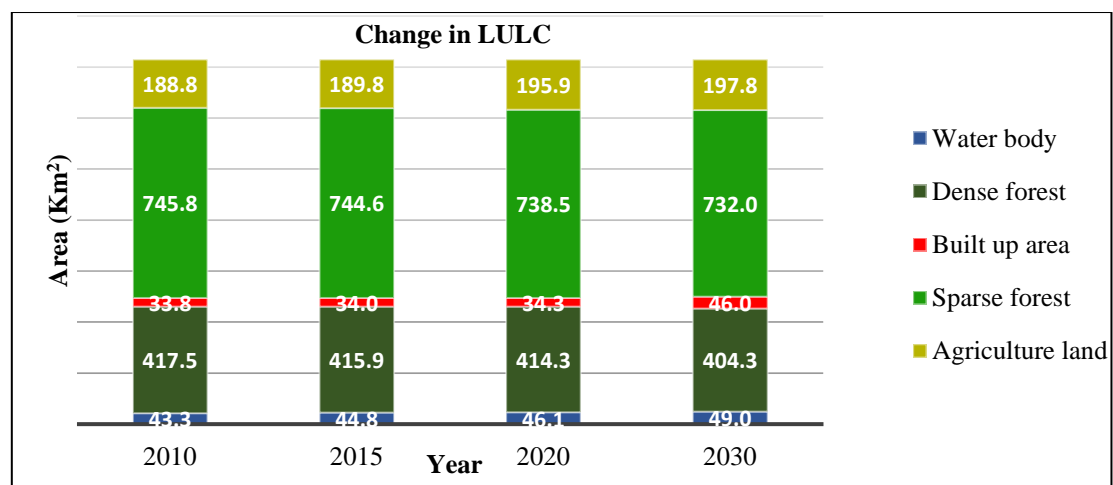
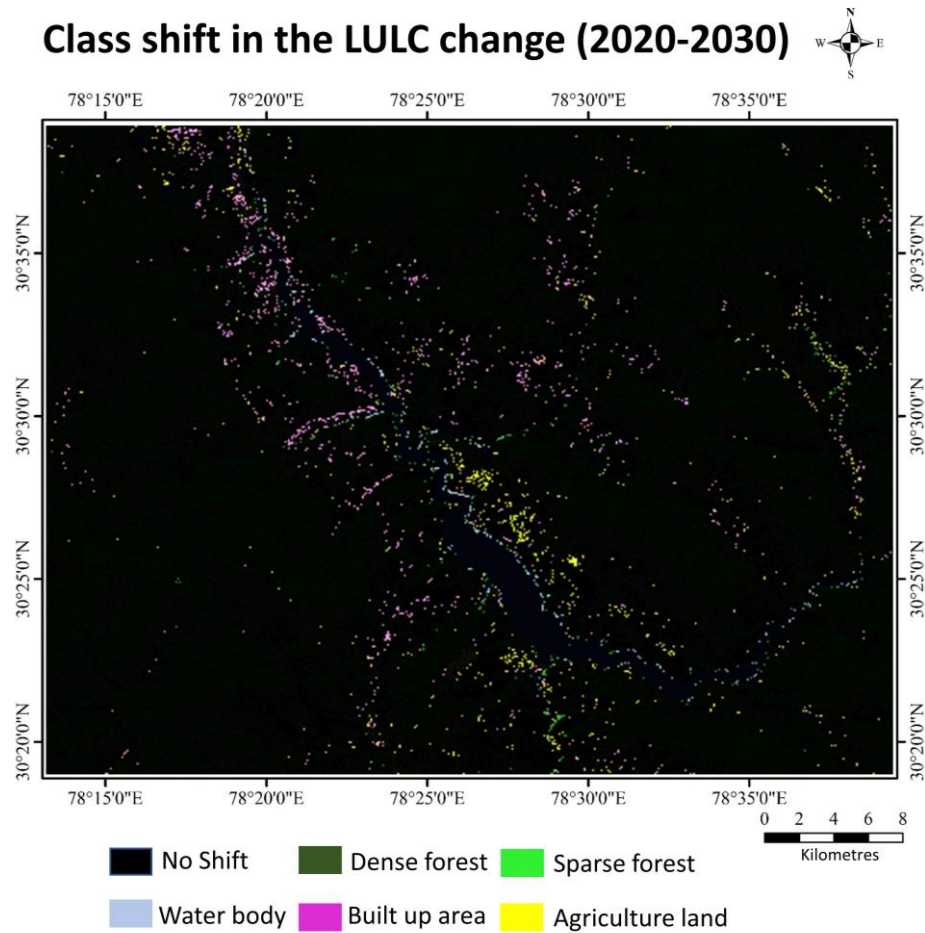


Fig. 6.3 LULC change graph for the years 2010, 2015, 2020 and 2030.

### 6.6.2 Change detection of the future scenario of LULC

Change detection is considered a primary method for recognizing the change in the pattern of different classes in distinct periods. The quantification of shifts or changes in different LULC is essential. The spatial distribution of classes shifts from the 2020 to 2030 time period is shown in fig. 6.4. The shift in LULC from one period to another reveals the future trend. The changes observed in the built-up class were along the road network connecting towns and villages, as shown by the pink color. Mostly the changes in the agriculture area were observed near the reservoir and built-up area. Water body class changes can be observed in light blue color near the river bank. Dense and sparse forest class shifts are shown with dark and light green colors, respectively. The percentage change between LULC class pixels was computed and shown in bar chart form (Fig. 6.5).



**Fig. 6.4** Map showing the class shift in LULC classes between the period 2020-2030.

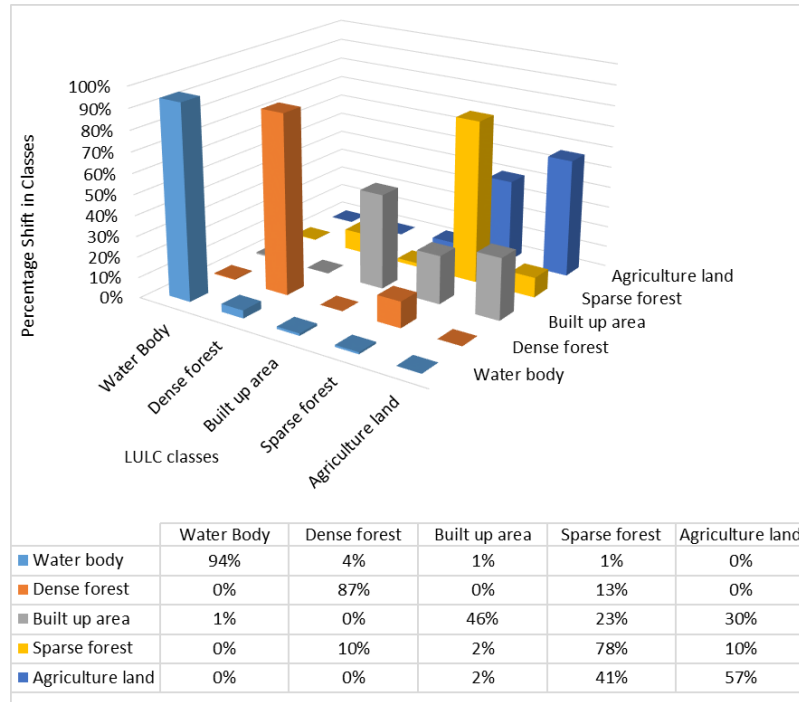


**Fig. 6.5** Bar Chart showing the percentage shift in LULC classes between the period.

### 6.6.3 Prediction of Landslide Susceptibility

The LSM for the year 2030 was predicted using the ANN-CA model and LULC change as the driving parameter. The changes in the susceptibility zones can be observed in Fig 6.6. Significant changes are observed in zones with very low and very high susceptibility classes. The zone with very low landslide susceptibility has shown a reduction from 733.5 to 596.9 km<sup>2</sup> (18.6%), whereas the zone with very high susceptibility has shown an increment from 398.1 km<sup>2</sup> to 529.4 km<sup>2</sup> (33%). Moreover, the high susceptibility zone has also shown an increment in the area from 115.4 km<sup>2</sup> to 131.8 km<sup>2</sup> (14.2%), whereas zones with low and moderate susceptibility have shown a reduction from 92.4 km<sup>2</sup> to 86.3 km<sup>2</sup> (6.6%) and 89.9 km<sup>2</sup> to 84.8 km<sup>2</sup> (5.6%) respectively (Fig. 6.7).

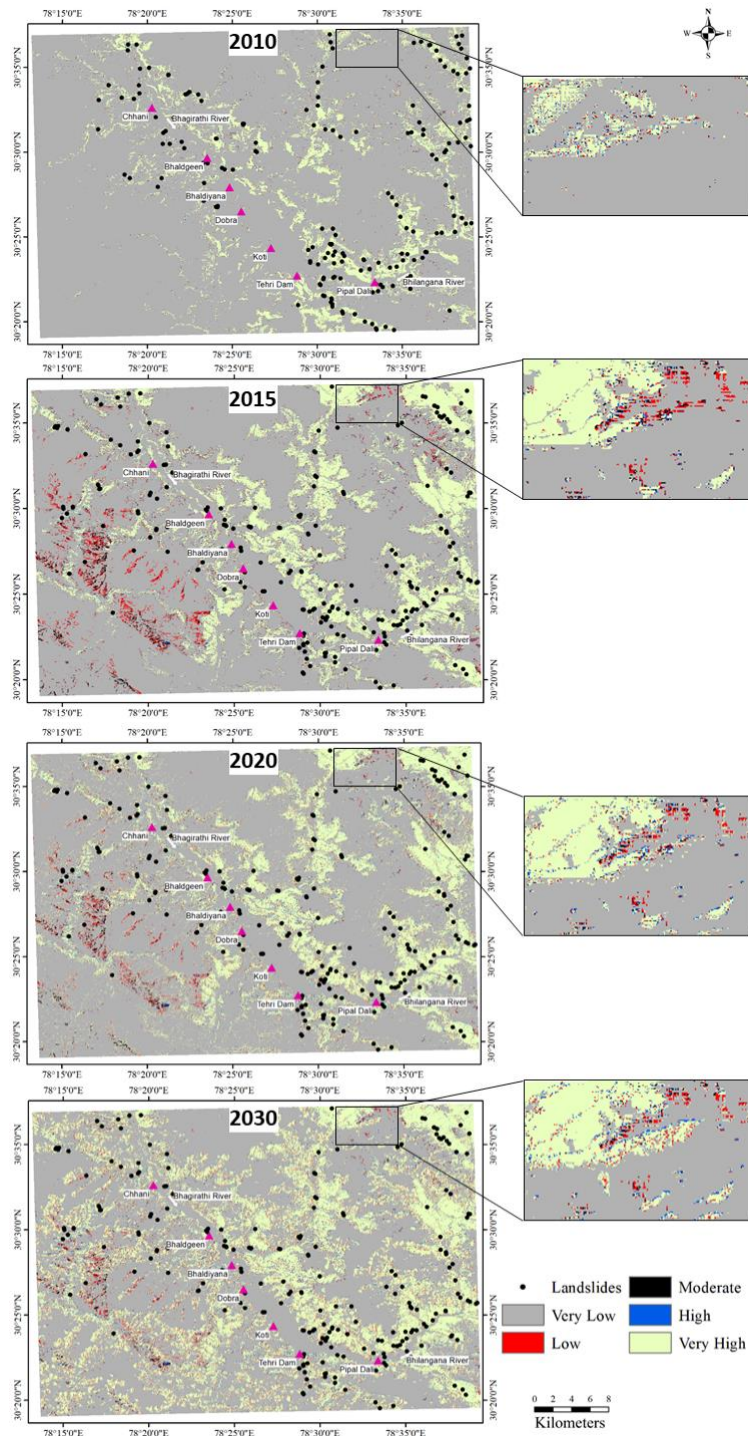


**Fig. 6.6** LSM for the years 2010, 2015, 2020 and 2030.

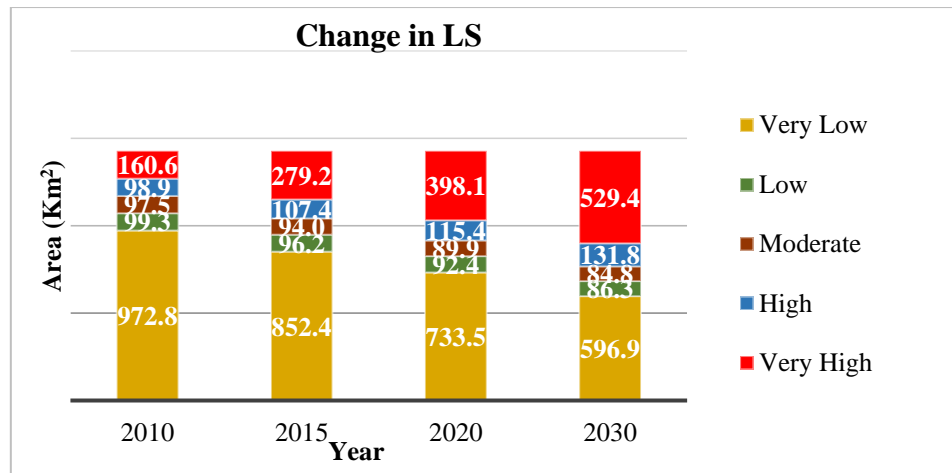


Fig. 6.7 Change graph of LSM for the years 2010, 2015, 2020 and 2030.

## 6.6 Validation

The current LSM, LULC classification and projected results were validated using two approaches. The area under the ROC curve method was used to validate the LSM and Cohen's kappa coefficient was used to validate the LULC classification and future predictions.

### 6.6.1 Cohen's Kappa Coefficient.

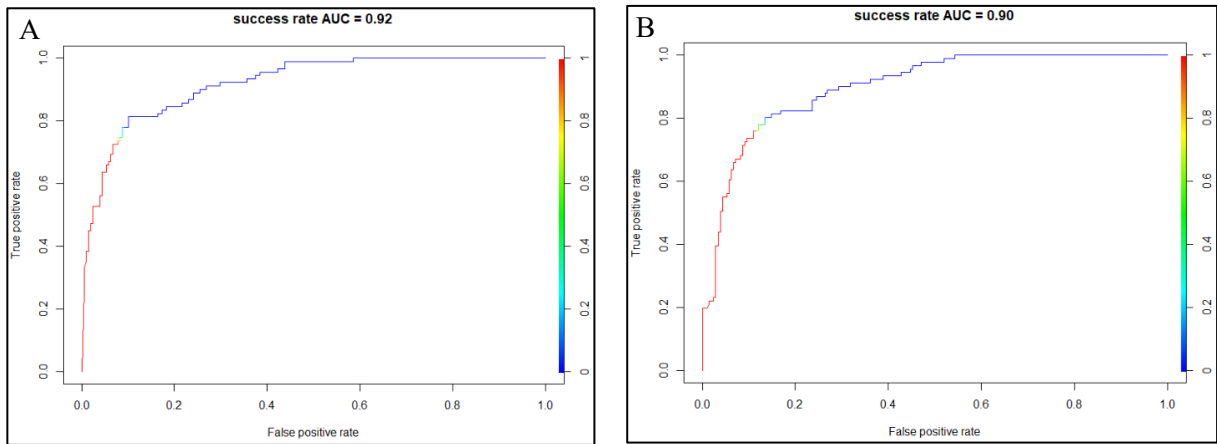
The Kappa coefficient is widely used to measure the true agreement between the observed agreement and chance agreement. The calculated Kappa coefficient showed excellent and reliable results for all the years (Table 6.2). Initially, Then, K- values of LULC maps were determined using google earth data as reference data. Lastly, the K-values were also used to evaluate and compare the real (generated) and predicted (simulated) maps for 2020. The predicted results for the year 2030 have the same accuracies as the predicted 2020 results, as the same simulation was taken forward.

Table 6.2 Kappa coefficient values used for validation

Results	Reference	year	K-Values
LULC classification	Google earth	2010	0.89
		2015	0.87
		2020	0.88
Predicted LULC	Generated LULC	2020	0.82
Predicted LS	Generated LSM	2020	0.85

### 6.6.2 Area Under Curve Method

The area under the ROC curve is used to check the accuracy of the models. In this study, the LS maps of 2010 and 2015 were predicted using the ANN model and have achieved a prediction accuracy of 0.92 and 0.9 AUC values, respectively (Fig. 6.8).



**Fig. 6.8** AUC of the Predicted LS Maps for the year 2010 (A) and 2015 (B).

## 6.7 Conclusion

The past spatiotemporal changes in LSM and LULC can help predict future changes. This beforehand information about future changes due to rapid urban growth in the mountains can help the various government agencies to scientifically plan the various developmental activities. The future prediction for both LULC and LSM was made using the CA-ANN model.

The results conclude that due to rapid urbanization in the Tehri region, 35% of the built-up, 12% of the water body, and 4% of agriculture land classes area will increase by 2030. This will decrease dense and sparse forest class area by 4% and 2%, respectively. These LULC changes will negatively affect natural ecosystems, biodiversity, and climate. The results also conclude that LS increases as the built-up area increases in the hilly region. Such results call for more reasonable land use planning in the urbanization process in the future and suggest a more systematic inclusion of LULC change in hazard assessment so that preventive measures can be implemented from the beginning.

Ultimately, the LULC change on hills could destabilize them, endanger the natural resources and harm the environment. Therefore, predicted future LSM will help policymakers, management professionals and government authorities to develop strategic planning that can reduce the impact of landslides. This can prevent urban growth and development in high LS areas. Moreover, we considered only LULC as the dynamic parameter in predicting future LSM. However, future studies can also consider more spatiotemporal and climatic factors.



### 7.1 Introduction

The landslides are caused by complex interactions among many static and dynamic factors (Dai and Lee 2002). Static factors such as topography, geological structure, pedology, geomorphology, hydrology, and vegetation characteristics are intrinsic to the environmental properties of a specific region and play a significant role in the formation of landslides (Kim et al. 2013; Hess et al., 2017), whereas dynamic factors, such as land use and land cover (LULC) change and climate change are external in nature. These changes are mainly due to anthropogenic activities such as deforestation, slope cuts, construction landfills, and garbage dumps. Consequently, these changes generate instability on hillslopes and induce landslide processes, which sometimes culminate in catastrophic effects (Persichillo et al. 2017; Schmaltz et al. 2017; Mendes et al. 2017; Köning et al. 2019). Researchers have concluded that urbanisation and climate changes will significantly impact landslide frequency (Persichillo et al. 2017). In the Himalayas, the practice of LULC cannot be stopped, but proper land use policy considering future projections can bring about these changes more sustainably (Tiwari et al. 2018). Evaluating landslide hazards in a specific region provides scientific support for governments to prepare land use policies (Nicu, 2018). Landslide Susceptibility Mapping (LSM) and Landslide Hazard Mapping (LHM) are essential steps in mitigation measures for planning and recognizing the regions needing protective measurements and are vital tools for the reduction of landslide hazard losses (Tyagi et al., 2022a). Though, studies have investigated the impact of LULC change (Reichenbach et al. 2014; Pisano et al. 2017; Shu et al. 2019; Pham et al. 2021; Sur et al. 2021) and climate change (Collison et al. 2000; Dixon and Brook 2007; Jakob and Lambert 2009; Comegna et al. 2013; Rianna et al. 2014; Shou and Yang, 2015, Hürlimann et al. 2022) on landslide occurrence. However, the future prediction of the LSM using these dynamic factors has not been quantified. This chapter describes the methodology for predicting future LSM, considering LULC and climate future projections as its prime driving dynamic factors. The LSM future projections were derived under four possible Shared Socioeconomic Pathways Scenarios.

### 7.2 Data preparation

LULC and climate change significantly impact landslide frequency and magnitude (Collison 2000; Moun-Jin et al. 2014). These changes have increased the global average

temperature and altered the rainfall pattern worldwide. The increase in extreme climate events has a dominant effect on LSM. Hence, we have incorporated these two climatic parameters (Temperature and precipitation) along with LULC change for future prediction of LSM.

### **7.2.1 LULC projections**

For predicting the future LSM for the year 2050, one of the driving dynamic factors used in this study was LULC projections. The changing trend in LULC derived using 2010 and 2015 data, was projected to derive the future LULC scenarios. The driving factors for LULC projections were slope, distance to road, and distance to stream. The projected LULC classes for the year 2050 will further be used as the driving factor for LSM. Refer to chapter 6 for more details regarding the derivation of LULC projections.

### **7.2.2 Climate Projections**

Global and regional climate variations on different time scales involve complex interactions among various components of the Earth System, hydrosphere, lithosphere, and biosphere. Earth System Models (ESMs) are essential for understanding these climatic variations resulting from interactions between different Earth system components. The ESMs participated in the sixth Coupled Model Intercomparison Project (CMIP6) allows us to understand and quantify the physical, chemical & biological mechanisms governing the rates of change of elements of the Earth System. The evaluation of CMIP6 simulations over several regions, including South Asia, suggests that their simulated responses exhibit differences from earlier CMIPs studies (Almazroui et al., 2020). The CMIP6 models have typically enhanced versions of the models that participated in earlier phases of CMIP. Most have improved parameterizations of cloud microphysics and better representations of various Earth system processes, such as biogeochemical cycles and ice sheets. The average resolution of CMIP6 GCMs is also finer than that of CMIP5 GCMs (Eyring et al. 2016). The CMIP6 has been improved in several aspects (e.g., higher horizontal resolution, better representation of synoptic processes, and better agreement with the estimation of global energy balance), and more reasonable results can be obtained from climate-extreme studies (e.g., Di Luca et al. 2020; Kim et al. 2020; Nie et al. 2020; Srivastava et al. 2020; Wild 2020). In the Intergovernmental Panel on Climate Change (IPCC) Sixth Assessment Report (IPCC AR6), projections have utilized the new range of scenarios known as Shared Socio-economic Pathways (SSPs) (O'Neill et al. 2017) introduced in the CMIP6.

ESMs are coupled numerical models that incorporate processes within and across the different Earth system components and are expressed as mathematical equations. ESMs are global climate models capable of explicitly representing biogeochemical processes interacting with the physical climate. New simulations of the ESMs from the latest state-of-the-art climate models participating in phase 6 of the CMIP are now available (Eyring et al. 2016). These

simulations provide a new opportunity to evaluate the Earth system's response to radiative forcing change during the twenty-first century. The climate projections in this study includes mean precipitation flux and surface temperature projections, which were obtained from the sixth CMIP6 climate projections.

In this study, the CMIP6 dataset was used to derive future temperature and precipitation projections over the Tehri region of the Indian Himalayas under four different Shared Socioeconomic Pathways (SSPs) with their radiative forcing combinations included in Tier 1 ScenarioMIP simulations. The Scenario Model Intercomparison Project (ScenarioMIP) consists of a set of eight pathways of future emissions, concentrations and land use, with additional ensemble members and long-term extensions, grouped into two tiers of priority (of which only the first constitutes a required set for modeling centers participating in ScenarioMIP). Tier 1 spans a wide range of uncertainty in future forcing pathways important for climate science research, including SSP1-2.6, SSP2-4.5, SSP3-7.0 and SSP5-8.5. (Gidden et al. 2019; O'Neill et al. 2016). The SSP scenario experiments can be understood in terms of two pathways, a SSP and a Representative Concentration Pathway (RCP). The three digits that make up the experiment's name represent the two pathways. The first digit represents the SSP storyline for the socioeconomic mitigation and adaptation challenges that the experiment represents (Fig. 7.1). The second and third digits represent the RCP climate forcing that the experiment follows. For example, experiment SSP1-2.6 follows SSP1, a storyline with intermediate mitigation and adaptation challenges, and RCP2.6, which leads to a radiative forcing of 2.6 Wm<sup>-2</sup> by the year 2100.

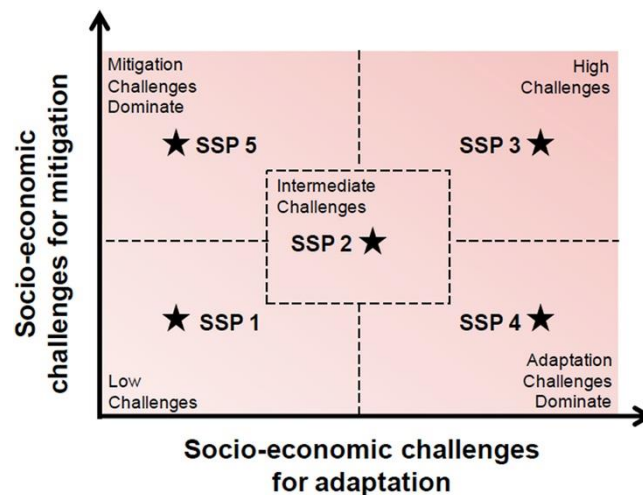


**Fig. 7.1** The socioeconomic "Challenge Space" to be spanned by the CMIP6 SSP experiments (O'Neil et al. 2014).

The GCMs data have considerable biases present due to different spatial resolutions, systematic model error, and inaccurate physical parameterizations (Ghosh and Mujumdar, 2009;

Chen et al., 2013; Turco et al., 2013; Gupta and Chavan, 2021, 2022). Hence, to deal with this issue, the data was downscaled with the help of the multiplicative multiple change factor method for precipitation and additive multiple change factor method for temperature following Semadeni-Davies et al. (2008) and Anandhi et al. (2011), which resolves the issue of bias.

For Tehri region climate projections, we have adopted the Indian Institute of Tropical Meteorology earth system model (IITM ESM) developed recently at the Modelling Centre of CCCR-IITM (Centre for Climate Change Research, Indian Institute of Tropical Meteorology) Pune, India. This is India's first and only climate model contributing to the CMIP6 for the IPCC sixth assessment report (Ar6). The IITM-ESM has shown promising capabilities required for making reliable assessments of the impacts of climate change on the Global and regional monsoon hydro climate and Regional weather and climate extremes (Krishnan et al. 2019). Krishnan et al. (2020a;2020b; 2021) briefly explains the model's salient aspects.

For Himachal Pradesh climate projections, six GCMs models were downscaled and ensembled in MATLAB, a statistical programming package (Table 7.1). According to Aadhar and Mishra (2020), among various CMIP6-GCMs, BCC-CSM2-MR does not capture the coupled variability between monsoon season precipitation and sea surface temperature (SST) over the Indian region. Also, MRI-ESM2-0 exhibited a large bias in the monsoon season precipitation and poor seasonal cycle variability, whereas CESM2-WACCM and IPSL-CM6A-LR showed less bias in precipitation and captured the observed season cycle of precipitation. According to Reddy and Saravanan (2023), EC-Earth3-Veg, MRI-ESM2-0, and GFDL-ESM4 have shown high performance in terms of finding out extreme precipitation indices. Hence, these models exhibit substantial uncertainty, which confirms the necessity of a model ensemble in investigating the climate simulations and projections. The average rainfall and mean average temperature of scenarios showed the trend of projected rainfall and temperature. The trend showed that both the hydro-climatic variables show an increase from SSP1-2.6 to 5-8.5. So, the increased GHGs emission and disrupted socioeconomic conditions will result in a net increase in temperature and precipitation in the future.

**Table 7.1** Details of 6 CMIP6-GCMs used in this study

S. No.	Model Name	Source Institute	Actual resolution (latitude × longitude)
1	BCC-CSM2-MR	Beijing Climate Center, China	1.1121° × 1.125°
2	EC-EARTH3-Veg	EC-Earth-Consortium	0.70° × 0.70°
3	IPSL-CM6A-LR	Institute Pierre Simon Laplace, France	1.2676° × 2.5°
4	MRI-ESM2-0	Meteorological Research Institute, Japan	1.125° × 1.11°
5	CESM2-WACCM	National Center for Atmospheric Research, USA	0.9424° × 1.25°
6	GFDL-ESM4	NOAA/ Geophysical Fluid Dynamics Laboratory, USA	1.3° × 1.0°

## 7.3 Methodology

Fig. 7.2 presents a flow chart describing the methodology adopted in the present study. Initially, both static and dynamic factors were optimized. Chapter 5 describes the optimization technique in detail. Further, the ANN-CA model was adopted in this study for future projection of LSM, considering climate and LULC projections as their derivatives. Chapter 6 explains the ANN-CA model and how it was adopted. The climate projections were obtained using the CMIP6 climate projections with their four different SSPs and lastly, the accuracy assessment methods were adopted for validating the results.

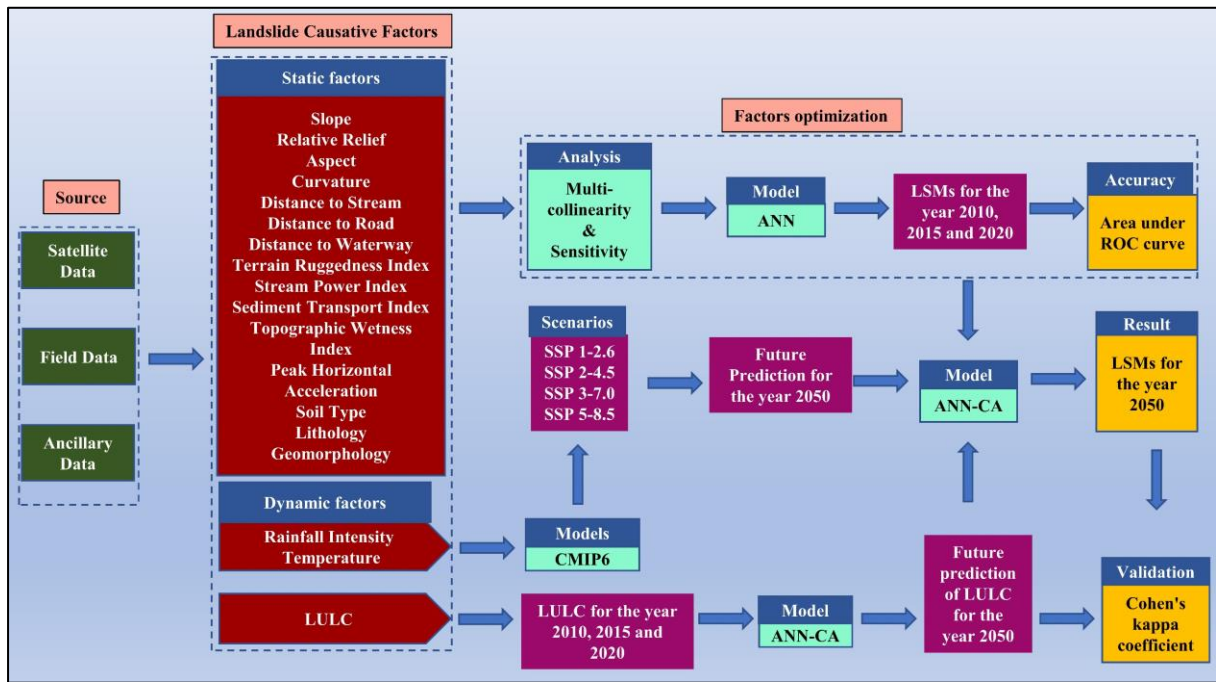
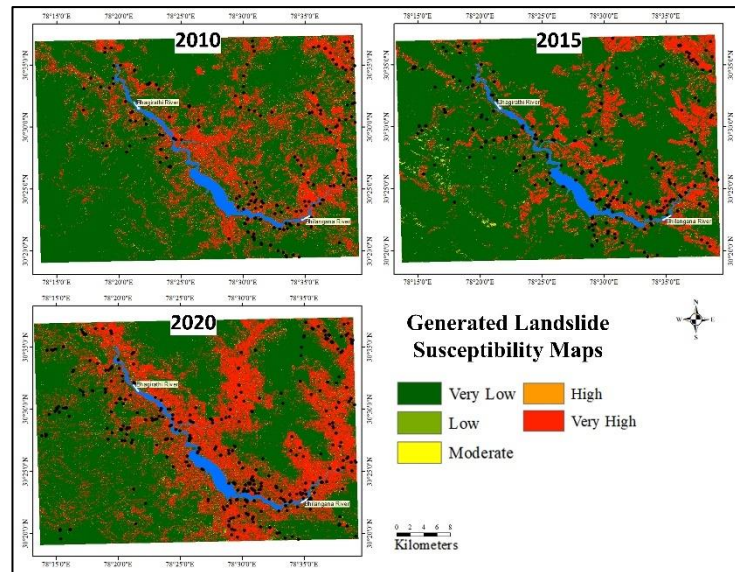


Fig. 7.2 The flow chart showing the proposed methodology for this research.

## 7.4 Results and Discussion

### 7.4.1 Landslide Susceptibility Maps for Tehri Region

The landslide susceptibility maps for 2010, 2015, and 2020 were generated using the ANN model, considering the eleven most significant combinations of factors. The susceptibility map of 2010 has less percentage of the very high landslide susceptibility class, whereas the 2020 landslide susceptibility map has more percentage of it (Fig. 7.3). These maps have shown a trend with an increase in the very high susceptibility class, which indicates the landslide susceptibility for the Tehri region is increasing with time.



**Fig. 7.3** LSM for the Tehri Region of the years 2010, 2015 and 2020.

#### 7.4.2 Future Projections of LULC, Precipitation and Temperature for Tehri Region

The future projections maps of LULC, precipitation and surface temperature were derived for 2050. This projected LULC map has shown an increase in the built-up area, agriculture land and reservoir area. However, the sparse and dense forest classes have decreased. About 5% increment in the built-up class and 4% in agriculture land is expected to take place in 2050, as shown in future projections (Fig. 7.4). This will lead to a decrease of forest (sparse and dense) land by about 10%. The projected precipitation maps and surface temperature maps for the year 2050 for different scenarios, with bar charts showing class percentages for each map, are shown in fig. 7.5 and 7.6. The mean precipitation flux and surface temperature values show an increasing trend as the forcing scenarios change from SSP 1-2.6 to SSP 5-8.5.

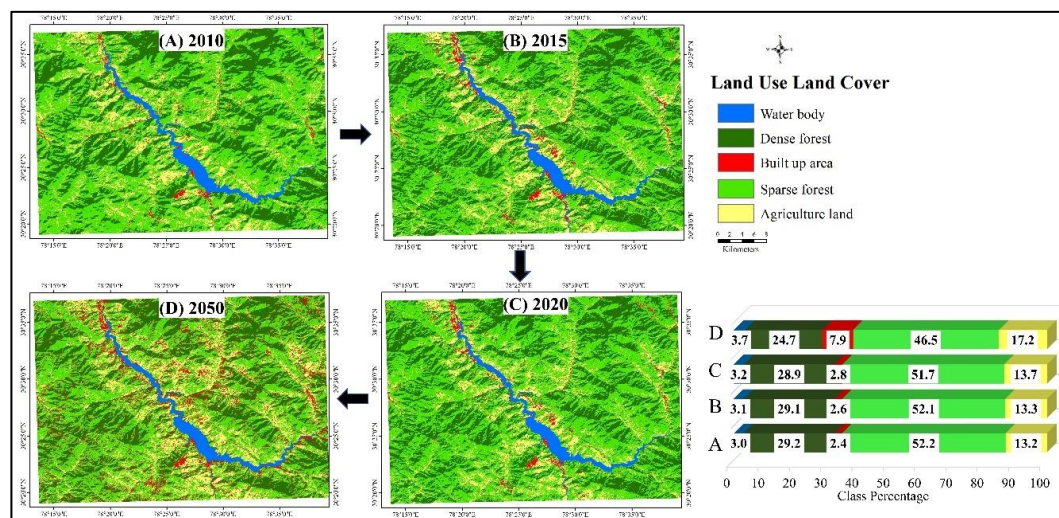


**Fig. 7.4** LULC maps for the Tehri region of the year (A) 2010, (B) 2015, (C) 2020 and (D) 2050.

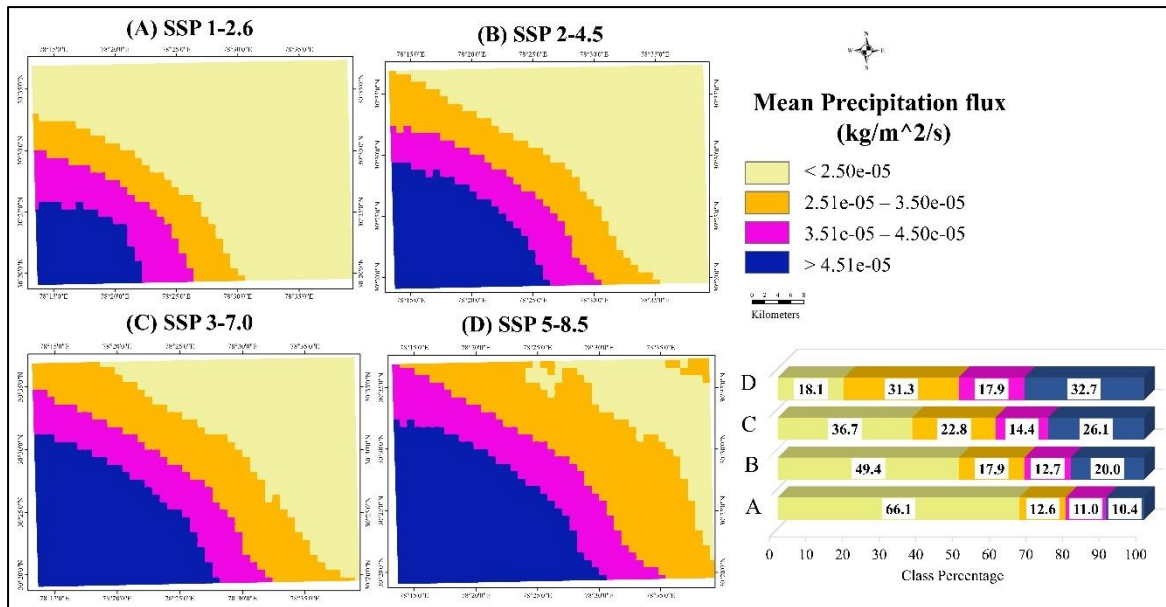


**Fig. 7.5** Projected mean precipitation flux for the Tehri region of the year 2050 under (A) SSP 1-2.6 (B) SSP 2-4.5 (C) SSP 3-7.0 (D) SSP 5-8.5 Scenarios.

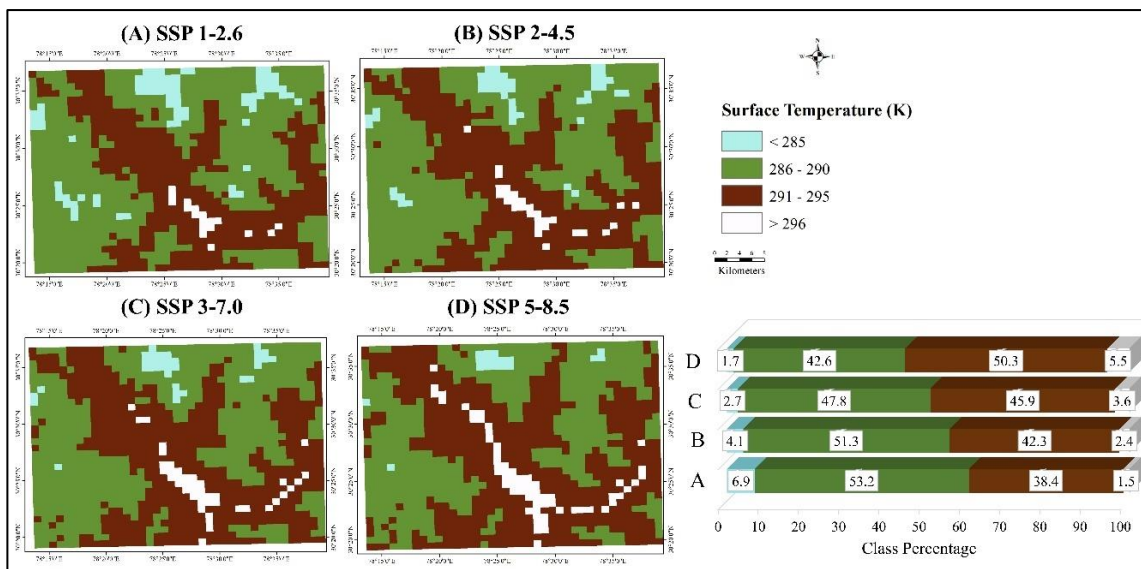


**Fig. 7.6** Projected surface temperature for the Tehri region of the year 2050 under (A) SSP 1-2.6 (B) SSP 2-4.5 (C) SSP 3-7.0 (D) SSP 5-8.5 Scenarios.

### 7.4.3 Future Predicted Landslide Susceptibility Maps for Tehri Region

The Landslide susceptibility maps were predicted for the year 2050 using the ANN-CA model, considering projections of LULC, precipitation and surface temperature. Four susceptibility maps predicted for the Tehri region for different possible future climate change scenarios are shown in Fig.7.7. The bar chart shows the class percentage of maps for different scenarios. Map for SSP 1-2.6 scenario has shown less percentage of very high susceptibility class whereas the SSP 5-8.5 scenario has shown a higher percentage of it. About 8% class

increment in very high landslide susceptibility class was observed between SSP 1-2.6 and SSP 5-8.5 scenarios.

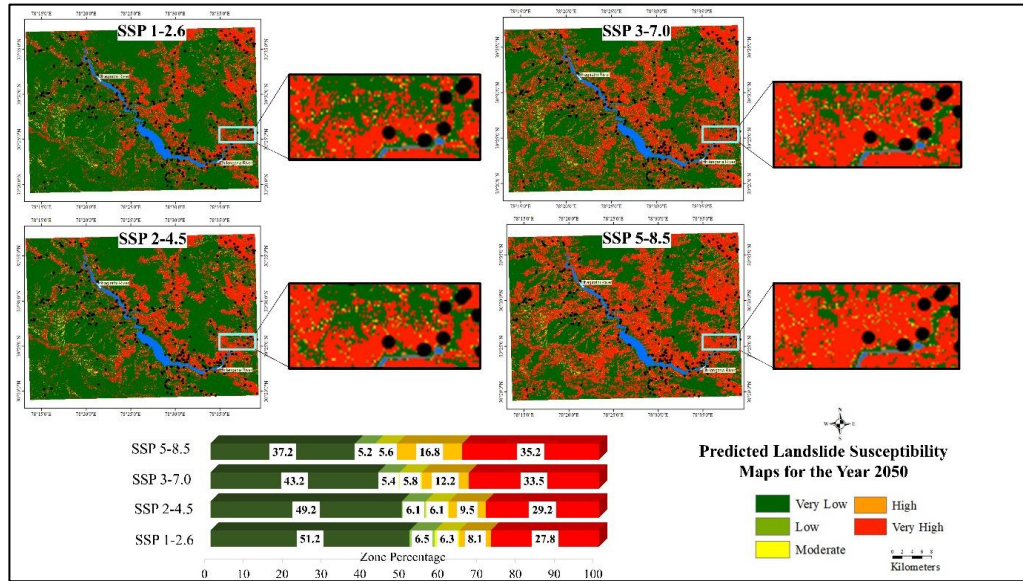


**Fig. 7.7** Landslide susceptibility maps for SSP 1-2.6, SSP 2-4.5, SSP 3-7.0 and SSP 5-8.5 Scenarios.

#### 7.4.4 Landslide susceptible Maps for Himachal Pradesh State.

The landslide susceptibility maps for the years 2010, 2015 and 2020 were prepared for Himachal Pradesh using 11 significant landslide causing factors. These factors were weighted using the ANN model, which were further integrated to generate maps showing LSI. As shown in fig, these maps were classified into five classes using Jenks natural break classifier. 7.8.

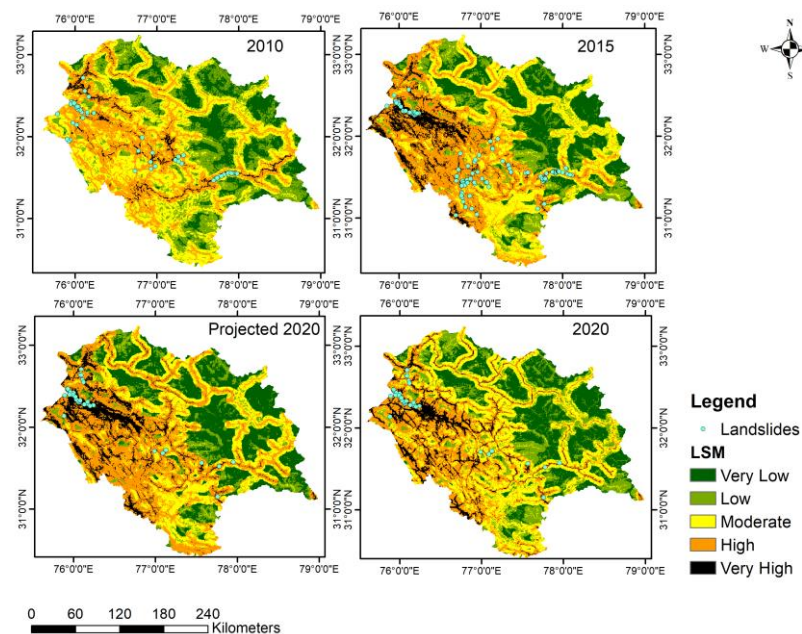


**Fig. 7.8** LSM for the Himachal Pradesh State of the years 2010, 2015 and 2020.

### 7.4.5 Future Projections of LULC, Precipitation and Temperature for Himachal Pradesh State

The projected maps of LULC for the year 2050 have shown a considerable increase in the water body and Built-up and Crop lands classes and a decrease in barren land and permanent snow cover classes, as shown in fig. 7.9. Further, as the forcing scenarios increase from SSP 1-2.6 to SSP 5-8.5, the intensity of rainfall (Fig. 7.10) and temperature (Fig. 7.11) increase for the year 2050.

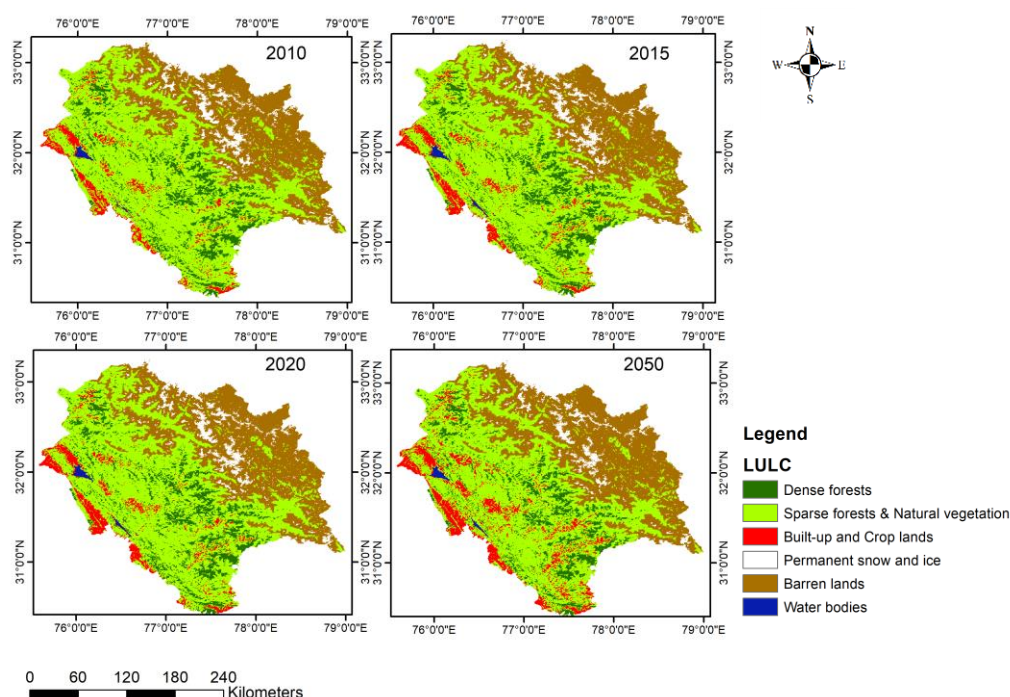


**Fig. 7.9** LULC maps for the Himachal Pradesh State of the year (A) 2010, (B) 2015, (C) 2020 and (D) 2050.

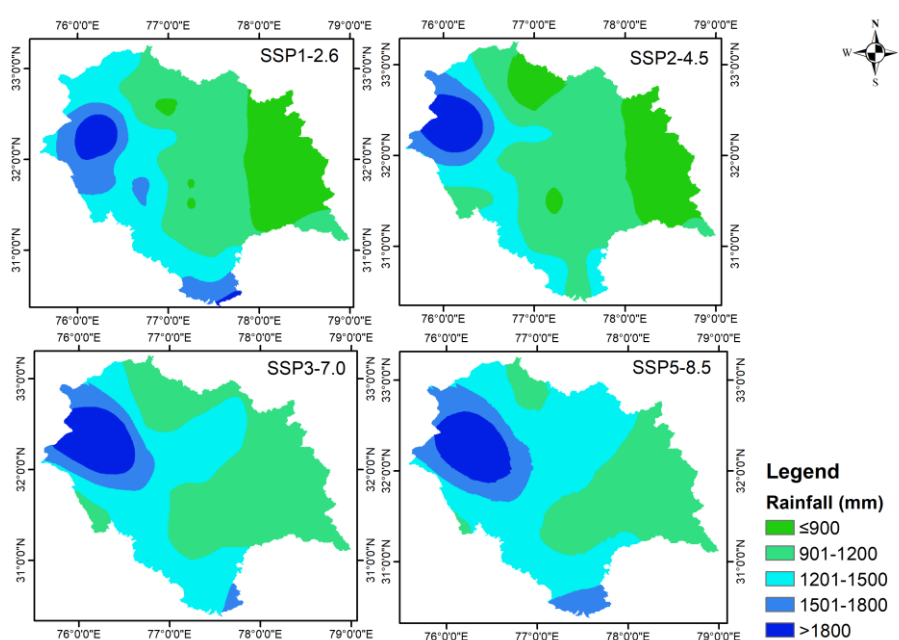


**Fig. 7.10** Projected mean rainfall for the Himachal Pradesh State of the year 2050 under (A) SSP 1-2.6 (B) SSP 2-4.5 (C) SSP 3-7.0 (D) SSP 5-8.5 Scenarios.

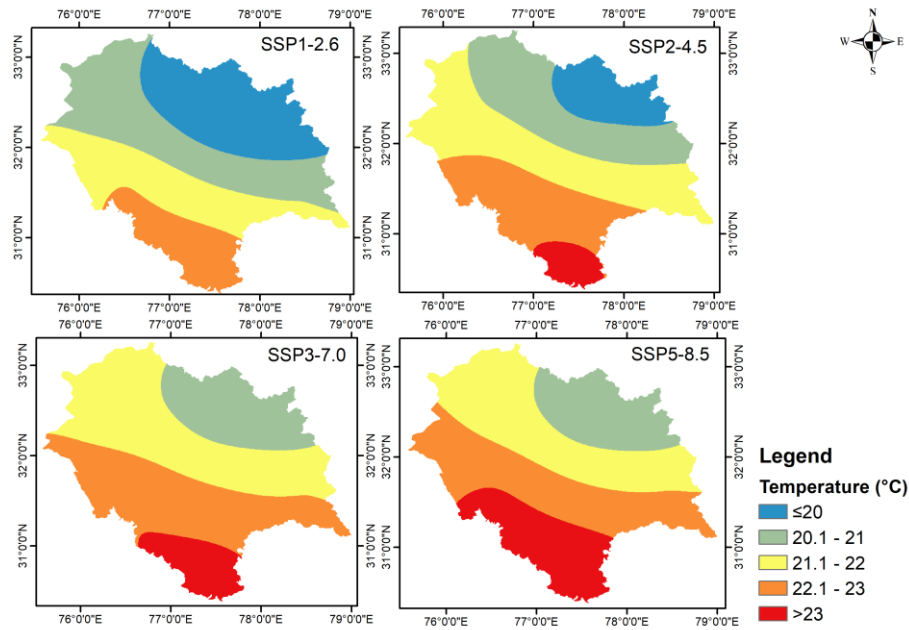


**Fig. 7.11** Projected surface temperature for the Himachal Pradesh State of the year 2050 under (A) SSP 1-2.6 (B) SSP 2-4.5 (C) SSP 3-7.0 (D) SSP 5-8.5 Scenarios.

#### 7.4.6 Future Predicted Landslide Susceptibility Maps

The future landslide susceptibility maps for the year 2050 under four SSPs were prepared, considering projected LULC, rainfall, and temperature as the driving parameters for landslide susceptibility (Fig. 7.12). These maps have shown an increase in the very high landslide susceptibility class as the forcing scenarios increase from SSP 1-2.6 to SSP 5-8.5.

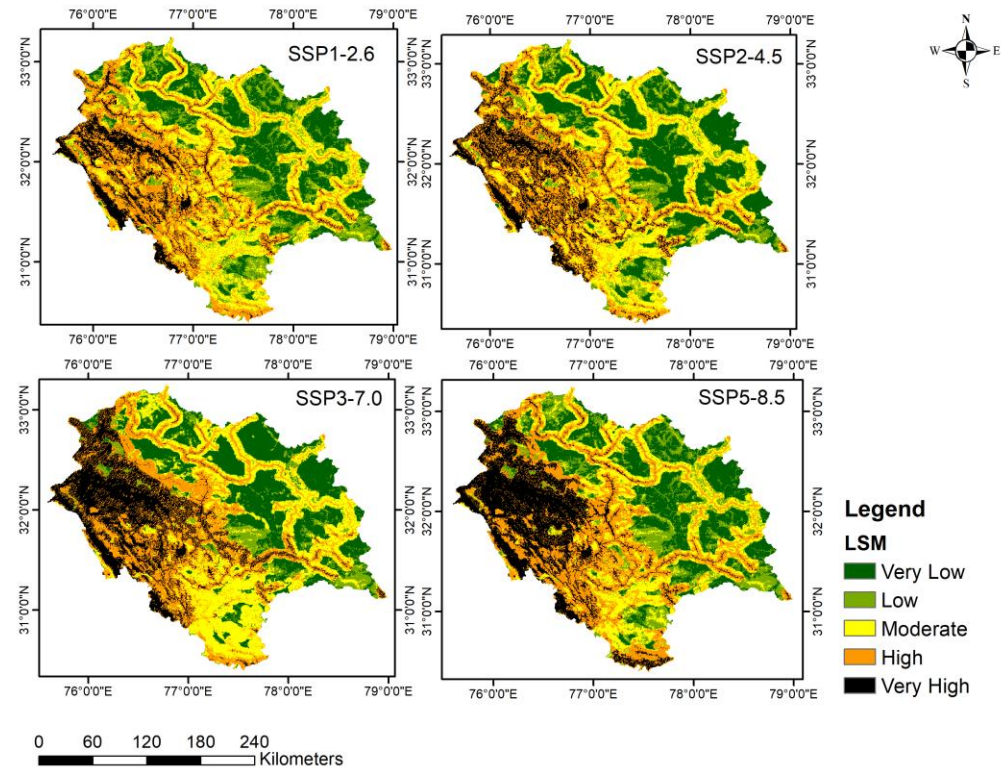


**Fig. 7.12** Landslide susceptibility maps for the Himachal Pradesh State of SSP 1-2.6, SSP 2-4.5, SSP 3-7.0 and SSP 5-8.5 Scenarios.

## 7.5 Validation

### 7.5.1 Area Under Curve Method

The area under the ROC curve was used to check the accuracy of the LSM using the ANN model. In this study, LSM was done for the years 2010, 2015 and 2020 using the ANN model and the derived significant factors. The prediction accuracy achieved by these three maps were 0.93, 0.89 and 0.88, respectively, as shown in fig.7.8.

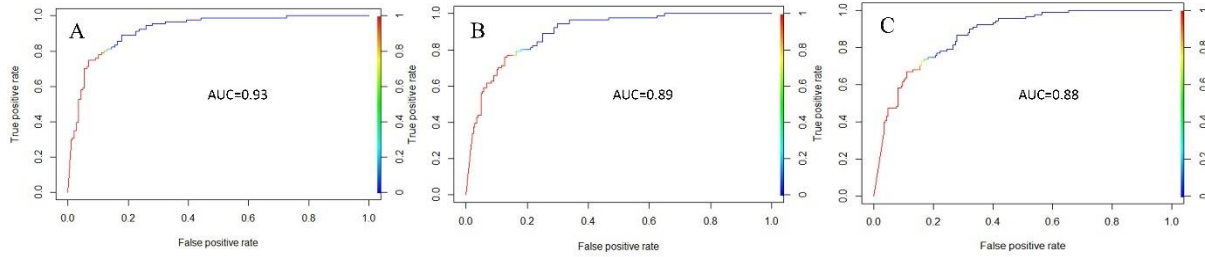


**Fig. 7.13** AUC of the predicted landslide susceptibility maps for the years 2010 (A), 2015 (B) and 2020 (C).

### 7.5.2 Cohen's Kappa Coefficient

The Kappa coefficient (K) is widely used to measure the true agreement between the observed and chance arrangement. The kappa constant coefficient is a perfect pointer of precision in measuring the general agreement between the maps that are thematically classified and referenced data (Adam et al. 2013). The kappa is a multi-separate variables method used to determine the accuracy of map classification. It is calculated from the error matrix and implemented over the classification based on the data reference (Hossen and Negm 2016). More details regarding the calculation of the K-value adopted in this study can be obtained in chapter 4.

This study calculated K-values for all the LULC classifications and projected future maps (Table 7.1). The K- values of LULC classification maps were calculated considering google earth images as their reference data. The K-values for the future projection were derived by comparing the real (generated) and predicted (simulated) maps for 2020. The generated 2020 maps were used as the reference map, while the projected map of 2020 was used as the predicted map of 2020. The predicted results for the year 2050 have the same accuracies as the predicted 2020 results, as the same simulation was taken forward.

**Table 7.2** Kappa coefficient values used for validation

Results	Reference	year	K-Values
LULC classification	Google Earth	2010	0.89
		2015	0.87
		2020	0.88
Predicted LULC	Generated LULC	2020	0.82
Predicted LSM (SSP1-2.6)	Generated LSM		0.86
Predicted LSM (SSP2-4.5)			0.83
Predicted LSM (SSP3-7.0)			0.81
Predicted LSM (SSP5-8.5)			0.79

## 7.6 Conclusion

In this study, future prediction of LSM was performed considering future LULC and climate (precipitation and temperature) projections as their driving parameters. Initially, the LSM for the years 2010, 2015, and 2020 were performed considering significant landslide causative factors. These maps were further used as the input in the ANN-CA model for training the model. The model used projected LULC, precipitation and surface temperature data as their driving parameters in the future prediction of LSM for the year 2050. The precipitation and surface temperature were projected under the four CMIP6 tier-1 future forcing scenarios (SSP1-2.6, SSP2-4.5, SSP3-7.0 and SSP5-8.5). The following summarizes the main conclusions from this study:

The dynamic factors can increase or decrease landslide susceptibility in mountainous areas. Factors such as LULC and climate change can be used for future predictions by examining the trends in change detection. Identification of LULC transitions is a practical approach to addressing the problems regarding unregulated urbanization and environmental degradation. In this study, LULC projections for the year 2050 were obtained using the ANN-CA model. The results of LULC projection for Tehri region of 2050 demonstrate high increases in built-up area of more than 5% and agriculture land of about 4%. Meanwhile, sparse and dense forest areas were projected to decrease by approximately 6% and 4%, respectively, indicating human influences on LULC changes from forest to built-up and agriculture. Hence, developing land management regulations in the Tehri region is required.

ESMs are helpful for enhancing our fundamental understanding of the climate system. Its multi-scale variability, global and regional climatic phenomena and making projections of

future climate change can help in preparing scenario-oriented policies. Climate change is expected to impact the future natural and social systems profoundly. Its influence can be seen in frequent extreme meteorological events such as concentrated precipitation and heat waves. In this study, we have used CMIP6 projections of 2050 from IITM ESM for the Tehri region and six ensembled GCMs models for Himachal Pradesh under four SSP scenarios. The results conclude that the precipitation and surface temperature increase as the forcing scenarios change from SSP 1-2.6 to SSP 5-8.5.

Future Prediction of LSM can help in the proper management and sustainable distribution of environmental resources. In this study, future predictions of LSM for the year 2050 under four different SSP scenarios were carried out. The result concludes that the scale of landslide-susceptible areas is estimated to increase in the future as the forcing scenarios change from SSP 1-2.6 to SSP 5-8.5. Hence, different socioeconomic pathway-based challenges should be considered in developing policies for mitigation and adaptation.

Policymakers, planners, and managers of the Tehri region must therefore consider potential landslide susceptible areas to prevent damages due to landslide hazards. These findings would help decision-makers better understand the interactions between human and natural activities and formulate policies related to landslide mitigation and prevention in the Tehri region, India. In addition, an attempt should be made to minimize urban warming and improve living environments, public health, and community well-being.



#### 8.1 Summary

The entire work of this thesis can be summarised as follows. Landslides inventory data was prepared for the study area of the Tehri region and two test sites of the Chamba and Bhuntar regions. The major portion of historical landslide data was taken from the Bhukosh portal of GSI. These landslide data were identified using 3D imagery in Google Earth. In total, 850, 166, and 79 historical landslides were mapped, and inventory was prepared for the Tehri, Chamba, and Bhuntar regions, respectively. The historical landslide data were correlated with landslide causative factors. In this study, we have adopted 21 landslide causative factors for the analysis. The factor weights were derived by correlating them with historical landslide data using LSM models. Here, we have used four models for determining the weights of these factors, including ANN, FR, AHP, and FR-AHP. The ANN model was initially selected for the analysis, and based on the correlation with the historical data, the hierarchy of factors in decreasing order of their significance was prepared. Significant factors were selected by adopting two optimising techniques of multicollinearity analysis using Pearson correlation and sensitivity analysis using the ANN method. The combination of the first eleven factors from the prepared hierarchy produced the maximum prediction accuracy of 0.93 AUC value. The weights were then integrated to create the landslide susceptible map for the Tehri region.

As the results of one model are insufficient, the FR model was then adopted for deriving weights of the factors by correlating the historical landslide pixels with factors class pixels. The LSM using the FR model was performed by first incorporating all 21 factors and then derived 11 significant ones. The accuracy of the susceptibility map achieved using 21 factors was 0.83 AUC value, and it was 0.88 using 11 significant factors. Further AHP model was adopted for the LSM of the Tehri region. AHP model does not use historical landslide data for deriving weights. Instead, here weights are given subjectively based on the researcher's experience. Hence, the derived significant factors using ANN and confirmed using FR were used in the AHP analysis. The accuracy of 0.89 AUC value was achieved using the AHP model. Also, the LSM was performed using a hybrid model of FR-AHP, and an accuracy of 0.91 was achieved. Lastly, the AHP model was applied to two landslide-prone sites of Chamba and Bhuntar for LSM, and prediction accuracy of 0.86 and 0.82 AUC value was achieved.

In this study, the future prediction of LSM was made with the help of dynamic factors such as LULC and climate variables. These dynamic factors changes with time and their changes are identified and used for future prediction. The ANN-CA model was adopted for determining the future projection of LULC and LSM. The climate projections were directly taken from CMIP6 future projections under four SSPs. These projections of LULC and Climate variables were used as the drivers in the ANN-CA model for future LSM scenarios. Initially, the LSM for the years 2010, 2015, and 2020 were performed considering significant landslide causative factors. These maps were further used as the input in the ANN-CA model for training the model. The model used projected LULC and climate variables data as their driving parameters in the future prediction of LSM for the future. The climate variables were projected under the four CMIP6 tier-1 future forcing scenarios (SSP1-1.9, SSP1-2.6, SSP2-4.5, SSP3-7.0, and SSP5-8.5).

## 8.2 Major Conclusions

The main aim of this research is to develop a scientific methodology to prepare the current and future landslide susceptibility maps incorporating both static and dynamic landslide causative factors. The following summarizes the main conclusions from this study:

The optimization techniques should be adopted in selecting the landslide causative factors. This study adopted multicollinearity and sensitivity analysis to determine significant factors for LSM analysis. The first eleven factors from the prepared hierarchy have shown maximum prediction capability and hence were adopted in LSM for the years 2010, 2015, and 2020. Also, The FR model results confirm the reliability of the derived significant factors. The FR model results conclude that the significant factors in LSM produce higher prediction accuracy. Further, these derived significant factors were also tested on two landslide-prone sites of Chamba and Bhuntar to check the applicability of the significant factors on other similar terrains. The results of LSM from test sites concluded that the identified significant factors and their hierarchy could be applied to other similar regions of the Himalayas. High accuracies were achieved in the predicted landslide susceptibility maps using the identified factors in the AHP framework. The outcome of this research can help the individual make decisions in the selection of factors and in defining the subjective weights. Conclusively, the present study results may be beneficial for developing infrastructural facilities in the future and mitigation strategies planning for the Tehri region or any other regions with similar terrain conditions. Also, the success of the identified significant factors in predicting the landslide susceptibility of the Chamba test site and Bhuntar test site permits them to be put into practice in the other parts of the Himalayas. Thus, the outcome of this research can help the individual make decisions in the selection of factors and in defining the subjective weights.

Over the last few decades, several LSM models have been developed. As all these methods used for deriving weights of the causative factors have some pros and cons, no one method is standardized globally. In this study, we have adopted four such models for LSM. The accuracy achieved using the ANN model was 0.93 AUC value, the highest accuracy achieved till date for the Tehri region. The FR is another data-driven model utilised to confirm the derived significant factors. The AHP technique is conventionally based on a rating system provided by expert opinion. Due to its subjective nature, it gives freedom to alter unexpected data-driven outcomes. We propose the AHP model and the combination of significant factors as the initial choice for conducting research in similar terrain when there is data scarcity. However, to some extent, opinions may change for every individual expert and thus may be subjected to reasoning limitations with uncertainty and subjectivity. Combining the FR and AHP methods reduces these deficiencies of the solo methods, and the hybrid model has the better predictive capability.

The dynamic factors can increase or decrease landslide susceptibility in hilly regions. The spatiotemporal changes in LSM, LULC and climate in the past can help in predicting future changes. Dynamic factors such as LULC and climate variables can be used for future predictions by examining the trends in change detection. Identification of LULC transitions is a practical approach for addressing the problems regarding unregulated urbanization and environmental degradation. In this study, future LULC projections were obtained using the ANN-CA model. The results of LULC projection reveal high increases in the built-up area and agriculture land. Meanwhile, sparse and dense forest areas were projected to decrease, signifying human interference in LULC changes from forest to built-up and agriculture. The results also conclude that landslide susceptible area increases as the built-up area increases in the mountainous area. Fatalities due to landslide hazards are related to human interference in natural processes leading to unsustainable environments. Hence, developing land management regulations in the Tehri region is required.

ESMs help improves our fundamental understanding of the climate system. Its multi-scale changeability, universal and regional climatic phenomena, and projections of future climate change can help prepare scenario-oriented policies. Climate change is expected to impact the future natural and social systems profoundly. Its influence can be seen in frequent extreme meteorological events such as concentrated precipitation and heat waves. In this study, we have used future CMIP6 projections from IITM ESM under four SSP scenarios and carried out future predictions of LSM. The results conclude that as the forcing scenarios change from SSP 1-2.6 to SSP 5-8.5, the surface temperature, precipitation intensity, and the class with very high landslide susceptibility increases. This concludes the importance of considering different socioeconomic pathway-based challenges in developing policies for mitigation and adaptation.

Future Prediction of LSM can help in the proper management and sustainable distribution of environmental resources. Policymakers, planners, and managers of the Tehri region must therefore consider potential landslide susceptible areas to prevent damages due to landslide hazards. These findings would help decision-makers better understand the interactions between human and natural activities and formulate landslide mitigation and prevention policies in the Tehri region, India. In addition, an attempt should be made to minimize urban warming and improve living environments, public health, and community well-being.

### **8.3 Scope of future work**

An outline for future work is recommended as follows.

1. Modification and enhancement of existing landslide Inventory using SAR data.
2. Significant factors for the entire Himalayas can be derived and clustered into different groups.
3. For better prediction accuracy, use a more complex neural network variant, such as Recurrent Neural Network (RNN) or Convolutional Neural Network (CNN).
4. Along with spatial prediction, temporal and magnitude prediction can be carried out.
5. Determining the role of urbanization and climate change in triggering the landslide hazard.
6. Determination of LULC class change having more impact on landslide susceptibility.
7. Impact of change in rainfall pattern on landslide frequency.
8. Assessment of landslide hazard and risk for reducing the impact of landslides.

## Reference

1. Abancó, C., & Hürlimann, M. (2014). Estimate of the debris-flow entrainment using field and topographical data. *Natural hazards*, 71(1), 363-383.
2. Abella, E.A.C., van Westen, C.J., 2008. Qualitative landslide susceptibility assessment by multicriteria analysis: a case study from San Antonio del Sur, Guantánamo, Cuba. *Geomorphology* 94 (3), 453–466. <http://dx.doi.org/10.1016/j.enggeo.2008.03.010>.
3. Acharya, G., De Smedt, F. and Long, N.T., 2006. Assessing landslide hazard in GIS: a case study from Rasuwa, Nepal. *Bulletin of Engineering Geology and the Environment*, 65(1), pp.99-107.
4. Adam, A. H. M., Elhag, A. M. H., & Salih, A. M. (2013). Accuracy assessment of land use & land cover classification (LU/LC), case study of Shomadi area, Renk County, Upper Nile State, South Sudan. *International Journal of Scientific and Research Publications*, 3, 1–6.
5. Aditian, A., Kubota, T. and Shinohara, Y., 2018. Comparison of GIS-based landslide susceptibility models using frequency ratio, logistic regression, and artificial neural network in a tertiary region of Ambon, Indonesia. *Geomorphology*, 318, pp.101-111.
6. Ahmad, I., Dar, M.A. and Andualem, T.G., 2020. Assessment of soil loss rate—Lake Tana basin, Ethiopia. *Arabian Journal of Geosciences*, 13(1), pp.1-7.
7. Ahmed B, Dewan A. 2017. Application of bivariate and multivariate statistical techniques in landslide susceptibility modeling in Chittagong City Corporation, Bangladesh. *Remote Sens* 9(4):304.
8. Ahmed, M.F., Rogers, J.D. and Ismail, E.H., 2014. A regional level preliminary landslide susceptibility study of the upper Indus river basin. *European Journal of Remote Sensing*, 47(1), pp.343-373.
9. Akgun, A. and Türk, N., 2010. Landslide susceptibility mapping for Ayvalik (Western Turkey) and its vicinity by multicriteria decision analysis. *Environmental Earth Sciences*, 61(3), pp.595-611.
10. Akgun, A., 2012. A comparison of landslide susceptibility maps produced by logistic regression, multi-criteria decision, and likelihood ratio methods: a case study at İzmir, Turkey. *Landslides*, 9(1), pp.93-106., doi: 10.1007/s10346-011-0283-7.
11. Akgun, A., Dag, S. and Bulut, F., 2008. Landslide susceptibility mapping for a landslide-prone area (Findikli, NE of Turkey) by likelihood-frequency ratio and weighted linear combination models. *Environmental Geology*, 54(6), pp.1127-1143.
12. Akgun, A., Sezer, E.A., Nefeslioglu, H.A., Gokceoglu, C. and Pradhan, B., 2012. An easy-to-use MATLAB program (MamLand) for the assessment of landslide susceptibility using a Mamdani fuzzy algorithm. *Computers & Geosciences*, 38(1), pp.23-34.
13. Aleotti, P. and Chowdhury, R., 1999. Landslide hazard assessment: summary review and new

perspectives. *Bulletin of Engineering Geology and the environment*, 58(1), pp.21-44.

14. Almazroui M, Saeed S, Islam MN, Ismail M (2020a) Projections of precipitation and temperature over the South Asian Countries in CMIP6. *Earth Syst Environ.* <https://doi.org/10.1007/s41748-020-00157-7>.
15. Al-Najjar, H. A., Kalantar, B., Pradhan, B., & Saeidi, V. (2019, October). Conditioning factor determination for mapping and prediction of landslide susceptibility using machine learning algorithms. In *Earth resources and environmental remote sensing/GIS applications X* (Vol. 11156, p. 111560K). International Society for Optics and Photonics, <https://doi.org/10.1117/12.2532687>.
16. Alvioli, M., Baum, R.L., 2016. Parallelization of the TRIGRS model for rainfall-induced landslides using the message passing interface. *Environ. Model. Softw.* 81, 122–135. <http://dx.doi.org/10.1016/j.envsoft.2016.04.002>.
17. Alexander, E.D., 1995. A survey of the field of natural hazards and disaster studies. In: Carrara, A., Guzzetti, F. (Eds.), *Geographical Information Systems in Assessing Natural Hazards*. Kluwer Academic Publisher, Dordrecht, The Netherlands, pp. 1–19.
18. Anagnostopoulos, G.G., Fatichi, S., Burlando, P., 2015. An advanced process-based distributed model for the investigation of rainfall-induced landslides: the effect of process representation and boundary conditions. *Water Resour. Res.* 51 (9), 7501–7523. <http://dx.doi.org/10.1002/2015WR016909>.
19. Anandhi, A., Frei, A., Pierson, D. C., Schneiderman, E. M., Zion, M. S., Lounsbury, D., & Matonse, A. H. (2011). Examination of change factor methodologies for climate change impact assessment. *Water Resources Research*, 47(3).
20. Anbalagan, R., 1992. Landslide hazard evaluation and zonation mapping in mountainous terrain. *Engineering geology*, 32(4), pp.269-277.
21. Anbalagan, R., Kumar, R., Lakshmanan, K., Parida, S. and Neethu, S., 2015. Landslide hazard zonation mapping using frequency ratio and fuzzy logic approach, a case study of Lachung Valley, Sikkim. *Geoenvironmental Disasters*, 2(1), pp.1-17. <https://doi.org/10.1186/s40677-014-0009-y>.
22. Andersson-Sköld, Y., Bergman, R., Johansson, M., Persson, E., & Nyberg, L. (2013). Landslide risk management—A brief overview and example from Sweden of current situation and climate change. *International Journal of Disaster Risk Reduction*, 3, 44-61.
23. Araya, Y. H., & Cabral, P. (2010). Analysis and modeling of urban land cover change in Setúbal and Sesimbra, Portugal. *Remote Sensing*, 2(6), 1549-1563, <https://doi.org/10.3390/rs2061549>.
24. Ardizzone, F., Cardinali, M., Carrara, A., Guzzetti, F. and Reichenbach, P., 2002. Impact of mapping errors on the reliability of landslide hazard maps. *Natural hazards and earth system sciences*, 2(1/2), pp.3-14.

25. Arifianti, Y., Pamela, P., Agustin, F. and Muslim, D., 2020. Comparative Study among Bivariate Statistical Models in Landslide Susceptibility Map. *Indonesian Journal on Geoscience*, 7(1), pp.51-63.
26. Armaş, I., 2012. Weights of evidence method for landslide susceptibility mapping. Prahova Subcarpathians, Romania. *Natural Hazards*, 60(3), pp.937-950.
27. Arora, M.K., Das Gupta, A.S. and Gupta, R.P., 2004. An artificial neural network approach for landslide hazard zonation in the Bhagirathi (Ganga) Valley, Himalayas. *International Journal of Remote Sensing*, 25(3), pp.559-572.
28. Asthana, V. (2012). Forced displacement: A gendered analysis of the Tehri Dam project. *Economic and Political Weekly*, 96-102. <https://www.jstor.org/stable/41720414>.
29. Atkinson, P.M. and Massari, R., 1998. Generalised linear modelling of susceptibility to landsliding in the central Apennines, Italy. *Computers & Geosciences*, 24(4), pp.373-385.
30. Atkinson, P.M. and Massari, R., 2011. Autologistic modelling of susceptibility to landsliding in the Central Apennines, Italy. *Geomorphology*, 130(1-2), pp.55-64.
31. Avinash, K. G., & Ashamanjari, K. G. (2010). A GIS and frequency ratio based landslide susceptibility mapping: Aghnashini river catchment, Uttara Kannada, India. *International Journal of Geomatics and Geosciences*, 1(3), 343–354.
32. Ayalew, L. and Yamagishi, H., 2005. The application of GIS-based logistic regression for landslide susceptibility mapping in the Kakuda-Yahiko Mountains, Central Japan. *Geomorphology*, 65(1-2), pp.15-31.
33. Ayalew, L., Yamagishi, H., Marui, H. and Kanno, T., 2005. Landslides in Sado Island of Japan: Part II. GIS-based susceptibility mapping with comparisons of results from two methods and verifications. *Engineering geology*, 81(4), pp.432-445. <https://doi.org/10.1016/j.enggeo.2005.08.004>.
34. Ayele, S., Raghuvanshi, T.K. and Kala, P.M., 2014. Application of Remote Sensing and GIS for Landslide Disaster Management: A Case from Abay Gorge, Gohatsion–Dejen Section, Ethiopia. In *Landscape Ecology and Water Management* (pp. 15-32). Springer, Tokyo.
35. Baeza C, Lantada N, Amorim S (2016) Statistical and spatial analysis of landslide susceptibility maps with different classification systems. *Environ Earth Sci* 75:1–17.
36. Baharvand, S., Rahnamarad, J., Soori, S. and Saadatkhah, N., 2020. Landslide susceptibility zoning in a catchment of Zagros Mountains using fuzzy logic and GIS. *Environmental Earth Sciences*, 79, pp.1-10.
37. Balasubramani, K. and Kumaraswamy, K., 2013. Application of geospatial technology and information value technique in landslide hazard zonation mapping: a case study of Giri Valley, Himachal Pradesh. *Disaster advances*, 6(1), pp.38-47.
38. Ballabio, C., Sterlacchini, S., 2012. Support vector machines for landslide susceptibility mapping: the Staffora River Basin case study, Italy. *Math. Geosci.* 44, 47–70.

39. Bălteanu, D., Chendeş, V., Sima, M. and Enciu, P., 2010. A country-wide spatial assessment of landslide susceptibility in Romania. *Geomorphology*, 124(3-4), pp.102-112.
40. Barella, C.F., Sobreira, F.G. and Zêzere, J.L., 2019. A comparative analysis of statistical landslide susceptibility mapping in the southeast region of Minas Gerais state, Brazil. *Bulletin of Engineering Geology and the Environment*, 78(5), pp.3205-3221.
41. Barredo, J., Benavides, A., Hervás, J. and van Westen, C.J., 2000. Comparing heuristic landslide hazard assessment techniques using GIS in the Tirajana basin, Gran Canaria Island, Spain. *International journal of applied earth observation and geoinformation*, 2 (1), pp. 9-23.
42. Baum, R.L., Godt, J.W. and Savage, W.Z., 2010. Estimating the timing and location of shallow rainfall-induced landslides using a model for transient, unsaturated infiltration. *Journal of Geophysical Research: Earth Surface*, 115(F3).
43. Baum, R.L., Savage, W.Z. and Godt, J.W., 2002. TRIGRS—a Fortran program for transient rainfall infiltration and grid-based regional slope-stability analysis. US geological survey open-file report, 424, p.38. Available via <http://pubs.usgs.gov/of/2002/ofr-02-424>.
44. Baum, R.L., Savage, W.Z. and Godt, J.W., 2008. TRIGRS: a Fortran program for transient rainfall infiltration and grid-based regional slope-stability analysis, version 2.0 (pp. 2008-1159). Denver, CO, USA: US Geological Survey.
45. Bera, A., Mukhopadhyay, B.P. and Das, D., 2019. Landslide hazard zonation mapping using multi-criteria analysis with the help of GIS techniques: a case study from Eastern Himalayas, Namchi, South Sikkim. *Natural Hazards*, 96(2), pp.935-959.
46. Berenguer, M., Sempere-Torres, D. and Hürlimann, M., 2015. Debris-flow forecasting at regional scale by combining susceptibility mapping and radar rainfall. *Natural Hazards and Earth System Sciences*, 15(3), pp.587-602.
47. Berkan, R.C. and Trubatch, S., 1997. Fuzzy system design principles. Wiley-IEEE Press.
48. Binaghi, E., Luzi, L., Madella, P., Pergalani, F. and Rampini, A., 1998. Slope instability zonation: a comparison between certainty factor and fuzzy Dempster–Shafer approaches. *Natural hazards*, 17(1), pp.77-97.
49. Bishop, C., 1995. *Neural Networks for Pattern Recognition*. Oxford University Press, Oxford.
50. Bisht, T. C. (2009). Development-induced displacement and women: The case of the Tehri dam, India. *The Asia Pacific Journal of Anthropology*, 10(4), 301–317.
51. Blahut, J., Van Westen, C.J. and Sterlacchini, S., 2010. Analysis of landslide inventories for accurate prediction of debris-flow source areas. *Geomorphology*, 119(1-2), pp.36-51.
52. Bourenane, H. and Bouhadad, Y., 2021. Impact of land use changes on landslides occurrence in urban area: the case of the Constantine City (N.E. Algeria). *Geotechnical and Geological Engineering*, 39(6), pp.1-21.

53. Bourenane, H., Guettouche, M.S., Bouhadad, Y. and Braham, M., 2016. Landslide hazard mapping in the Constantine city, Northeast Algeria using frequency ratio, weighting factor, logistic regression, weights of evidence, and analytical hierarchy process methods. *Arabian Journal of Geosciences*, 9(2), p.154.
54. Brabb, E.E., 1984. Innovative approaches to landslide hazard mapping. In: *Proc. 4th Int. Symp. Landslides*, Toronto. 1. pp. 307–324.
55. Brabb, E.E., 1991. The world landslide problem. *Episodes Journal of International Geoscience*, 14(1), pp.52-61.
56. Brabb, E.E., Pampeyan, E.H. and Bonilla, M.G., 1972. Landslide susceptibility in San Mateo County, California (No. 360). US Geological Survey.
57. Brenning, A., 2005. Spatial prediction models for landslide hazards: review, comparison and evaluation. *Natural Hazards and Earth System Sciences*, 5(6), pp.853-862.
58. Bui, D.T., Moayedi, H., Kalantar, B., Osouli, A., Pradhan, B., Nguyen, H. and Rashid, A.S.A., 2019. A novel swarm intelligence—Harris hawks optimization for spatial assessment of landslide susceptibility. *Sensors*, 19(16), p.3590.
59. Bui, D.T., Pradhan, B., Lofman, O., Revhaug, I. and Dick, O.B., 2012a. Spatial prediction of landslide hazards in Hoa Binh province (Vietnam): a comparative assessment of the efficacy of evidential belief functions and fuzzy logic models. *Catena*, 96, pp.28-40.
60. Bui, D.T., Pradhan, B., Lofman, O., Revhaug, I. and Dick, O.B., 2012. Landslide susceptibility assessment in the Hoa Binh province of Vietnam: a comparison of the Levenberg–Marquardt and Bayesian regularized neural networks. *Geomorphology*, 171, pp.12-29.
61. Caine, N., 1980. The rainfall intensity-duration control of shallow landslides and debris flows. *Geografiska annaler: series A, physical geography*, 62(1-2), pp.23-27.
62. Calista, M., Miccadei, E., Pasculli, A., Piacentini, T., Sciarra, M. and Sciarra, N., 2016. Geomorphological features of the Montebello sul Sangro large landslide (Abruzzo, Central Italy). *Journal of Maps*, 12(5), pp.882-891.
63. Calvello, M., Cascini, L. and Mastroianni, S., 2013. Landslide zoning over large areas from a sample inventory by means of scale-dependent terrain units. *Geomorphology*, 182, pp.33-48.
64. Campbell, R., 1973. Isopleth map of landslide deposits, Point Dume Quadrangle, Los Angeles County, California; an experiment in generalising and quantifying areal distribution of landslides. US Geological Survey Miscellaneous Field Studies Map, MF-535 Scale 1: 24,000.
65. Caniani, D., Pascale, S., Sdao, F. and Sole, A., 2008. Neural networks and landslide susceptibility: a case study of the urban area of Potenza. *Natural Hazards*, 45(1), pp.55-72.
66. Capitani, M., Ribolini, A., Federici, P.R., 2013. Influence of deep-seated gravitational slope

deformations on landslide distributions: a statistical approach. *Geomorphology* 201, 127–134

67. Cardinali, M., Reichenbach, P., Guzzetti, F., Ardizzone, F., Antonini, G., Galli, M., Cacciano, M., Castellani, M. and Salvati, P., 2002. A geomorphological approach to the estimation of landslide hazards and risks in Umbria, Central Italy. *Natural Hazards and Earth System Sciences*, 2(1/2), pp.57-72.
68. Carrara, A., 1983. Multivariate models for landslide hazard evaluation. *Math. Geol.* 15 (3), 403–426. <http://dx.doi.org/10.1007/bf01031290>.
69. Carrara, A., Cardinali, M., Detti, R., Guzzetti, F., Pasqui, V. and Reichenbach, P., 1991. GIS techniques and statistical models in evaluating landslide hazard. *Earth surface processes and landforms*, 16(5), pp.427-445.
70. Carrara, A., Cardinali, M., Guzzetti, F., Reichenbach, P., 1995. GIS technology in mapping landslide hazard. In: Carrara, A., Guzzetti, F. (Eds.), *Geographical Information Systems in Assessing Natural Hazards*. Kluwer Academic Publisher, Dordrecht, The Netherlands, pp. 135–175
71. Carrara, A., Catalano, E., Sorriso-Valvo, M., Reali, C., Osso, I., 1978, Digital terrain analysis for land evaluation. *Geol. Appl. Idrogeol.* 13, 69–127.
72. Carrara, A., Pugliese-Carratelli, E., Merenda, L., 1977. Computer-based data bank and statistical analysis of slope instability phenomena. *Z. Geomorphol. N.F.* 21, 187–222. [http://dx.doi.org/10.1007/978-94-011-2878-0\\_2](http://dx.doi.org/10.1007/978-94-011-2878-0_2).
73. Casadei, M., Dietrich, W.E. and Miller, N.L., 2003. Testing a model for predicting the timing and location of shallow landslide initiation in soil-mantled landscapes. *Earth Surface Processes and Landforms: The Journal of the British Geomorphological Research Group*, 28(9), pp.925-950.
74. Cascini, L., 2008. Applicability of landslide susceptibility and hazard zoning at different scales. *Engineering Geology*, 102(3-4), pp.164-177.
75. Catani, F., Casagli, N., Ermini, L., Righini, G. and Menduni, G., 2005. Landslide hazard and risk mapping at catchment scale in the Arno River basin. *Landslides*, 2(4), pp.329-342.
76. Cervi, F., Berti, M., Borgatti, L., Ronchetti, F., Manenti, F. and Corsini, A., 2010. Comparing predictive capability of statistical and deterministic methods for landslide susceptibility mapping: a case study in the northern Apennines (Reggio Emilia Province, Italy). *Landslides*, 7(4), pp.433-444.
77. Cevik, E., Topal, T., 2003. GIS-based landslide susceptibility mapping for a problematic segment of the natural gas pipeline, Hendek (Turkey). *Environmental Geology* 44, 949–962
78. Chacón, J., Irigaray, C., Fernandez, T. and El Hamdouni, R., 2006. Engineering geology maps: landslides and geographical information systems. *Bulletin of Engineering Geology and the Environment*, 65(4), pp.341-411.

79. Champati Ray, P.K., 2005. Geoinformatics and its application in Geosciences. *Journal of Earth System Science and Environment*, 2(1), pp.4-12.
80. Champati Ray, P.K. and Lakhera, R.C., 2004, September. Landslide Hazards in India. In *Proc. Asian Workshop on Regional Capacity Enhancement for Landslide Mitigation (RECLAIM)*, organized by Asian Disaster Preparedness Centre (ADPC), Bangkok and Norwegian Geo-Technical Institute, Oslo, Bangkok (pp. 13-15).
81. Champatiray P, Dimri, S., Lakhera, R.C. and Sati, S., 2007. Fuzzy based methods for landslide hazard assessment in active seismic zone of Himalaya. *Landslides* 4:101–110
82. Chandel, V.B., Brar, K.K. and Chauhan, Y., 2011. RS & GIS based landslide hazard zonation of mountainous terrains a study from Middle Himalayan Kullu District, Himachal Pradesh, India. *International journal of Geomatics and Geosciences*, 2(1), p.121.
83. Chang, K.T. and Chiang, S.H., 2009. An integrated model for predicting rainfall-induced landslides. *Geomorphology*, 105(3-4), pp.366-373.
84. Chang, K.T. and Liu, J.K., 2004, July. Landslide features interpreted by neural network method using a high-resolution satellite image and digital topographic data. In *Geo-Imagery Bridging Continents; Proc. of 20th ISPRS Congress, Istanbul, 12-23 July 2004*.
85. Chang, K.T., Chiang, S.H. and Hsu, M.L., 2007. Modeling typhoon-and earthquake-induced landslides in a mountainous watershed using logistic regression. *Geomorphology*, 89(3-4), pp.335-347.
86. Chau, K.T., Sze, Y.L., Fung, M.K., Wong, W.Y., Fong, E.L. and Chan, L.C.P., 2004. Landslide hazard analysis for Hong Kong using landslide inventory and GIS. *Computers & Geosciences*, 30(4), pp.429-443.
87. Chen W, Panahi M, Pourghasemi HR. 2017. Performance evaluation of GIS-based new ensemble data mining techniques of adaptive neuro-fuzzy inference system (ANFIS) with genetic algorithm (GA), differential evolution (DE), and particle swarm optimization (PSO) for landslide spatial modelling. *CATENA* 157:310-324.
88. Chen, C.Y. and Chang, J.M., 2016. Landslide dam formation susceptibility analysis based on geomorphic features. *Landslides*, 13(5), pp.1019-1033.
89. Chen, J., Brissette, F.P., Chaumont, D. and Braun, M. (2013) Finding appropriate bias correction methods in downscaling precipitation for hydrologic impact studies over North America. *Water Resources Research*, 49, 4187–4205. <https://doi.org/10.1002/wrcr.20331>.
90. Chen, L., Guo, Z., Yin, K., Shrestha, D. P., & Jin, S. (2019). The influence of land use and land cover change on landslide susceptibility: a case study in Zhushan Town, Xuan'en County (Hubei, China). *Natural hazards and earth system sciences*, 19(10), 2207-2228, <https://doi.org/10.5194/nhess-19-2207-2019>.
91. Chen, W., Chai, H., Zhao, Z., Wang, Q. and Hong, H., 2016. Landslide susceptibility mapping based on GIS and support vector machine models for the Qianyang County, China.

- Environmental Earth Sciences, 75(6), p.474.
92. Chen, W., Panahi, M., & Pourghasemi, H. R. (2017). Performance evaluation of GIS-based new ensemble data mining techniques of adaptive neuro-fuzzy inference system (ANFIS) with genetic algorithm (GA), differential evolution (DE), and particle swarm optimization (PSO) for landslide spatial modelling. *Catena*, 157, 310-324. <https://doi.org/10.1016/j.catena.2017.05.034>.
  93. Chen, W., Pourghasemi, H.R., Panahi, M., Kornejady, A., Wang, J., Xie, X. and Cao, S., 2017. Spatial prediction of landslide susceptibility using an adaptive neuro-fuzzy inference system combined with frequency ratio, generalized additive model, and support vector machine techniques. *Geomorphology*, 297, pp.69-85.
  94. Chi, K.H., Park, N.W. and Chung, C.J., 2002. Fuzzy logic integration for landslide hazard mapping using spatial data from Boeun, Korea. *International archives of photogrammetry remote sensing and spatial information sciences*, 34(4), pp.54-59.
  95. Chimidi, G., Raghuvanshi, T.K. and Suryabhagavan, K.V., 2017. Landslide hazard evaluation and zonation in and around Gimbi town, western Ethiopia—a GIS-based statistical approach. *Applied Geomatics*, 9(4), pp.219-236.
  96. Chung, C.J.F. and Fabbri, A.G., 1993. The representation of geoscience information for data integration. *Nonrenewable Resources*, 2(2), pp.122-139.
  97. Chung, C.J.F. and Fabbri, A.G., 1999. Probabilistic prediction models for landslide hazard mapping. *Photogrammetric engineering and remote sensing*, 65(12), pp.1389-1399.
  98. Chung, Ch.F., Fabbri, A.G., 1995. Multivariate regression analysis for landslide hazard Zonation. In: Carrara, A., Guzzetti, F. Eds., *Geographical Information Systems in Assessing Natural Hazards*. Kluwer Academic Publisher, Dordrecht, The Netherlands, pp. 107–142.
  99. Chung, E. S., Park, K., & Lee, K. S. (2011). The relative impacts of climate change and urbanization on the hydrological response of a Korean urban watershed. *Hydrological processes*, 25(4), 544-560, <https://doi.org/10.1002/hyp.7781>.
  100. Ciurleo, M., Cascini, L. and Calvello, M., 2017. A comparison of statistical and deterministic methods for shallow landslide susceptibility zoning in clayey soils. *Engineering Geology*, 223, pp.71-81.
  101. Clerici, A., Perego, S., Tellini, C. and Vescovi, P., 2002. A procedure for landslide susceptibility zonation by the conditional analysis method. *Geomorphology*, 48(4), pp.349-364.
  102. Collison, A., Wade, S., Griffiths, J., & Dehn, M. (2000). Modelling the impact of predicted climate change on landslide frequency and magnitude in SE England. *Engineering Geology*, 55(3), 205-218.
  103. Colombo, A., Lanteri, L., Ramasco, M. and Troisi, C., 2005. Systematic GIS-based landslide inventory as the first step for effective landslide-hazard management. *Landslides*, 2(4), pp.291-301.

104. Corominas, J. and Mavrouli, O., 2010. Overview of landslide hazards and risk assessment practices. *Living with landslide risk in Europe: Assessment, effects of global change, and risk management strategies*.
105. Comegna, L., Picarelli, L., Bucchignani, E., & Mercogliano, P. (2013). Potential effects of incoming climate changes on the behaviour of slow active landslides in clay. *Landslides*, 10(4), 373-391.
106. Corominas, J. and Moya, J., 2008. A review of assessing landslide frequency for hazard zoning purposes. *Engineering geology*, 102(3-4), pp.193-213.
107. Costanzo, D., Rotigliano, E., Irigaray, C., Jiménez-Perálvarez, J. D., & Chacón, J. (2012). Factors selection in landslide susceptibility modelling on large scale following the gis matrix method: application to the river Beiro basin (Spain). *Natural Hazards and Earth System Sciences*, 12(2), 327-340. <https://doi.org/10.5194/nhess-12-327-2012>, 2012.
108. Council, BSS, 2003. NEHRP recommended provisions for seismic regulations for new buildings and other structures (FEMA 450). Washington, DC.
109. Crovelli, R.A., 2000. Probability models for estimation of number and costs of landslides. *foot (ft)*, 25, pp.0-3048.
110. Crozier, M. J. (2010). Deciphering the effect of climate change on landslide activity: A review. *Geomorphology*, 124(3-4), 260-267.
111. Crozier, M.J., 1986. *Landslides: causes, consequences & environment*. Taylor & Francis.
112. Cruden, D.M., 1991. A simple definition of a landslide. *Bulletin of the International Association of Engineering Geology-Bulletin de l'Association Internationale de Géologie de l'Ingénieur*, 43(1), pp.27-29.
113. Dai, F.C. and Lee, C.F., 2001. Terrain-based mapping of landslide susceptibility using a geographical information system: a case study. *Canadian Geotechnical Journal*, 38(5), pp.911-923.
114. Dai, F.C. and Lee, C.F., 2002. Landslide characteristics and slope instability modeling using GIS, Lantau Island, Hong Kong. *Geomorphology*, 42(3-4), pp.213-228.
115. Dai, F.C., Lee, C.F. and Ngai, Y.Y., 2002. Landslide risk assessment and management: an overview. *Engineering geology*, 64(1), pp.65-87.
116. Das, I., Stein, A., Kerle, N. and Dadhwal, V.K., 2011. Probabilistic landslide hazard assessment using homogeneous susceptible units (HSU) along a national highway corridor in the northern Himalayas, India. *Landslides*, 8(3), pp.293-308.
117. Das, I., Stein, A., Kerle, N. and Dadhwal, V.K., 2012. Landslide susceptibility mapping along road corridors in the Indian Himalayas using Bayesian logistic regression models. *Geomorphology*, 179, pp.116-125.

118. Davis, T.J. and Keller, C.P., 1997. Modelling uncertainty in natural resource analysis using fuzzy sets and Monte Carlo simulation: slope stability prediction. *International Journal of Geographical Information Science*, 11(5), pp.409-434.
119. DeGraff, J.V., 1985. Using isopleth maps of landslides deposits as a tool in timber sale planning. *Bulletin American Association of Engineering Geologists* 22, 445–453
120. Demir, G., Aytekin, M., Akgün, A., Ikizler, S.B. and Tatar, O., 2013. A comparison of landslide susceptibility mapping of the eastern part of the North Anatolian Fault Zone (Turkey) by likelihood-frequency ratio and analytic hierarchy process methods. *Natural hazards*, 65(3), pp.1481-1506.
121. Deshpande, P.K., Patil, J.R., Nainwal, D.C. and Kulkarni, M.B., 2009, December. Landslide hazard Zonation zonation in Gopeshwar, Pipalkoti and Nandprayag areas of Uttarakhand. In *Indian geotechnical conference* (pp. 16-19).
122. Dhakal, A.S. and Sidle, R.C., 2004. Distributed simulations of landslides for different rainfall conditions. *Hydrological Processes*, 18(4), pp.757-776.
123. Dietrich, E.W., Reiss, R., Hsu, M.-L., Montgomery, D.R., 1995. A process-based model for colluvial soil depth and shallow landsliding using digital elevation data. *Hydrological Process* 9, 383–400
124. DIKAU, R.A., Ibsen, M.L. and Ibsen, M.L., 1996. *Landslide recognition: identification, movement and causes* (Vol. 1). Wiley-Blackwell.
125. Dikshit, A., Sarkar, R., Pradhan, B., Jena, R., Drukpa, D. and Alamri, A.M., 2020. Temporal probability assessment and its use in landslide susceptibility mapping for eastern Bhutan. *Water*, 12(1), p.267.
126. Di Luca, A., Pitman, A. J., & de Elía, R. (2020). Decomposing temperature extremes errors in CMIP5 and CMIP6 models. *Geophysical Research Letters*, 47(14), e2020GL088031.
127. Dixon, N. and Brook, E., 2007. Impact of predicted climate change on landslide reactivation: case study of Mam Tor, UK. *Landslides*, 4(2), pp.137-147.
128. Dolojan, N.L.J., Moriguchi, S., Hashimoto, M. and Terada, K., 2021. Mapping method of rainfall-induced landslide hazards by infiltration and slope stability analysis. *Landslides*, pp.1-19.
129. Dong, J.J., Tung, Y.H., Chen, C.C., Liao, J.J. and Pan, Y.W., 2009. Discriminant analysis of the geomorphic characteristics and stability of landslide dams. *Geomorphology*, 110(3-4), pp.162-171
130. Du, J., Glade, T., Woldai, T., Chai, B. and Zeng, B., 2020. Landslide susceptibility assessment based on an incomplete landslide inventory in the Jilong Valley, Tibet, Chinese Himalayas. *Engineering Geology*, 270, p.105572.

131. Dunne, T., 1991. Stochastic aspects of the relations between climate, hydrology and landform evolution. *Transaction Japanese Geomorphological Union* 12, 1–24
132. Eeckhaut, M., Reichenbach, P., Guzzetti, F., Rossi, M. and Poesen, J., 2009. Combined landslide inventory and susceptibility assessment based on different mapping units: an example from the Flemish Ardennes, Belgium. *Natural Hazards and Earth System Sciences*, 9(2), pp.507-521.
133. Einstein, H.H., 1997. Landslide risk-systematic approaches to assessment and management. *Landslide risk assessment*, pp.25-50.
134. EINSTEIN, N., 1988. Special lecture: landslide risk assessment procedure. In *International symposium on landslides*. 5 (pp. 1075-1090).
135. Eiras, C.G.S., de Souza, J.R.G., de Freitas, R.D.A., Barella, C.F. and Pereira, T.M., 2021. Discriminant analysis as an efficient method for landslide susceptibility assessment in cities with the scarcity of predisposition data. *Natural Hazards*, pp.1-16.
136. Elias, P.B. and Bandis, S.C., 2000, July. Neurofuzzy systems in landslide hazard assessment. In *Proceedings of 4th international symposium on spatial accuracy assessment in natural resources and environmental sciences* (pp. 199-202).
137. Endo, T., 1970. Probable distribution of the amount of rainfall causing landslides.
138. Ercanoglu, M. and Gokceoglu, C., 2002. Assessment of landslide susceptibility for a landslide-prone area (north of Yenice, NW Turkey) by fuzzy approach. *Environmental geology*, 41(6), pp.720-730.
139. Ercanoglu, M. and Gokceoglu, C., 2004. Use of fuzzy relations to produce landslide susceptibility map of a landslide prone area (West Black Sea Region, Turkey). *Engineering Geology*, 75(3-4), pp.229-250.
140. Ercanoglu, M.U.R.A.T., 2005. Landslide susceptibility assessment of SE Bartın (West Black Sea region, Turkey) by artificial neural networks. *Natural Hazards and Earth System Sciences*, 5(6), pp.979-992.
141. Erener, A. and Düzgün, H.S.B., 2010. Improvement of statistical landslide susceptibility mapping by using spatial and global regression methods in the case of More and Romsdal (Norway). *Landslides*, 7(1), pp.55-68.
142. Erener, A., Mutlu, A. and Düzgün, H.S., 2016. A comparative study for landslide susceptibility mapping using GIS-based multi-criteria decision analysis (MCDA), logistic regression (LR) and association rule mining (ARM). *Engineering geology*, 203, pp.45-55.
143. Ermini, L., Catani, F. and Casagli, N., 2005. Artificial neural networks applied to landslide susceptibility assessment. *Geomorphology*, 66(1-4), pp.327-343.

144. ESRI FAQ. (2016) What is the Jenks optimization method?  
<https://support.esri.com/en/technical-article/000006743>.
145. Eyring V, Bony S, Meehl GA et al (2016) Overview of the coupled model intercomparison project phase 6 (CMIP6) experimental design and organization. *Geosci Model Dev* 9:1937–1958. <https://doi.org/10.5194/gmd-9-1937-2016>.
146. Fall, M., Azzam, R. and Noubactep, C., 2006. A multi-method approach to study the stability of natural slopes and landslide susceptibility mapping. *Engineering geology*, 82(4), pp.241-263.
147. Fang, Z., Wang, Y., Peng, L. and Hong, H., 2020. Integration of convolutional neural network and conventional machine learning classifiers for landslide susceptibility mapping. *Computers & Geosciences*, 139, p.104470.
148. Feizizadeh, B. and Blaschke, T., 2013. GIS-multicriteria decision analysis for landslide susceptibility mapping: comparing three methods for the Urmia lake basin, Iran. *Natural hazards*, 65(3), pp.2105-2128.
149. Feizizadeh, B., Blaschke, T., Nazmfar, H. and Rezaei Moghaddam, M.H., 2013. Landslide susceptibility mapping for the Urmia Lake basin, Iran: a multi-criteria evaluation approach using GIS. *International Journal of Environmental Research*, 7(2), pp.319-336.
150. Fell, R., Corominas, J., Bonnard, C., Cascini, L., Leroi, E. and Savage, W.Z., 2008. Guidelines for landslide susceptibility, hazard and risk zoning for land-use planning. *Engineering geology*, 102(3-4), pp.99-111.
151. Froude, M.J. and Petley, D.N., 2018. Global fatal landslide occurrence from 2004 to 2016. *Natural Hazards and Earth System Sciences*, 18(8), pp.2161-2181.
152. Galli, M., Ardizzone, F., Cardinali, M., Guzzetti, F., Reichenbach, P., 2008. Comparing landslide inventory maps. *Geomorphology* 94 (3–4), 268–289.  
<http://dx.doi.org/10.1016/j.geomorph.2006.09.023>.
153. Galve, J. P., Cevasco, A., Brandolini, P., & Soldati, M. (2015). Assessment of shallow landslide risk mitigation measures based on land use planning through probabilistic modelling. *Landslides*, 12(1), 101-114.
154. Garrett, J.H., 1994. Where and why artificial neural networks are applicable in civil engineering.
155. Ghosh, J. K., & Bhattacharya, D. (2010). Knowledge-based landslide susceptibility zonation system. *Journal of Computing in civil engineering*, 24(4), 325-334.  
[https://doi.org/10.1061/\(ASCE\)CP.1943-5487.0000034](https://doi.org/10.1061/(ASCE)CP.1943-5487.0000034).
156. Ghosh, S., Van Westen, C.J., Carranza, E.J.M., Ghoshal, T.B., Sarkar, N.K. and Surendranath, M., 2009. A quantitative approach for improving the BIS (Indian) method of medium-scale landslide susceptibility. *Journal of the Geological Society of India*, 74(5), p.625.

157. Ghosh, S. and Mujumdar, P.P. (2009) Climate change impact assessment: uncertainty modeling with imprecise probability. *Journal of Geophysical Research*, 114(D18113), 1–17. <https://doi.org/10.1029/2008JD011648>.
158. Gidden MJ, Riahi K, Smith SJ et al (2019) Global emissions pathways under different socioeconomic scenarios for use in CMIP6: a dataset of harmonized emissions trajectories through the end of the century. *Geosci Mod Dev* 12:1443–1475. <https://doi.org/10.5194/gmd-12-1443-2019>.
159. Godt, J.W., Baum, R.L., Savage, W.Z., Salciarini, D., Schulz, W.H. and Harp, E.L., 2008. Transient deterministic shallow landslide modeling: requirements for susceptibility and hazard assessments in a GIS framework. *Engineering Geology*, 102(3-4), pp.214-226.
160. Gökçeoglu, C. and Aksoy, H.Ü.S.E.Y.İ.N., 1996. Landslide susceptibility mapping of the slopes in the residual soils of the Mengen region (Turkey) by deterministic stability analyses and image processing techniques. *Engineering Geology*, 44(1-4), pp.147-161.
161. Gomez, H. and Kavzoglu, T., 2005. Assessment of shallow landslide susceptibility using artificial neural networks in Jabonosa River Basin, Venezuela. *Engineering Geology*, 78(1-2), pp.11-27.
162. Gorsevski, P.V., Gessler, P.E. and Jankowski, P., 2003. Integrating a fuzzy k-means classification and a Bayesian approach for spatial prediction of landslide hazard. *Journal of geographical systems*, 5(3), pp.223-251.
163. Gorsevski, P.V., Gessler, P.E., Foltz, R.B. and Elliot, W.J., 2006. Spatial prediction of landslide hazard using logistic regression and ROC analysis. *Transactions in GIS*, 10(3), pp.395-415.
164. Goyes-Peñafiel, P. and Hernandez-Rojas, A., 2021. Landslide susceptibility index based on the integration of logistic regression and weights of evidence: A case study in Popayan, Colombia. *Engineering Geology*, 280, p.105958.
165. Greco, R., Sorriso-Valvo, M. and Catalano, E., 2007. Logistic regression analysis in the evaluation of mass movements susceptibility: The Aspromonte case study, Calabria, Italy. *Engineering geology*, 89(1-2), pp.47-66.
166. Green, G. M., & Ahearn, S. C. (2016). Modelling forest canopy trends with on-demand spatial simulation. *International Journal of Geographical Information Science*, 30(1), 61-73, <https://doi.org/10.1080/13658816.2015.1066791>
167. Guillard, C., & Zezere, J. (2012). Landslide susceptibility assessment and validation in the framework of municipal planning in Portugal: the case of Loures Municipality. *Environmental management*, 50(4), 721-735, <https://doi.org/10.1007/s00267-012-9921-7>.
168. Gupta, M., Ghose, M.K. and Sharma, L.P., 2009. Application of remote sensing and GIS for landslides hazard and assessment of their probabilistic occurrence—a case study of NH31A between Rangpo and Singtam. *J Geomatics*, 3(1), pp.13-17.
169. Gupta, N., & Chavan, S. R. (2021). Assessment of temporal change in the tails of probability

distribution of daily precipitation over India due to climatic shift in the 1970s. *Journal of Water and Climate Change*, 12(6), 2753-2773.

170. Gupta, N., & Chavan, S. R. (2022). Characterizing the tail behaviour of daily precipitation probability distributions over India using the obesity index. *International Journal of Climatology*, 42(4), 2543-2565.
171. Gupta, P., & Anbalagan, R. (1997). Slope stability of Tehri Dam Reservoir Area, India, using landslide hazard zonation (LHZ) mapping. *Quarterly Journal of Engineering Geology*, 30(1), 27-36, <https://doi.org/10.1144/GSL.QJEGH.1997.030.P1.03>.
172. Gupta, R. P., Saha, A. K., Arora, M. K. and Kumar, A. (1999) Landslide hazard zonation in a part of Bhagirathy Valley, Garhwal Himalayas, using integrated Remote Sensing & GIS. *J. Him. Geol.*, v.20, pp. 71-85.
173. Gupta, R.P. and Joshi, B.C., 1990. Landslide hazard zoning using the GIS approach—a case study from the Ramganga catchment, Himalayas. *Engineering geology*, 28(1-2), pp.119-131.
174. Guthrie, R.H. and Evans, S.G., 2004. Magnitude and frequency of landslides triggered by a storm event, Loughborough Inlet, British Columbia. *Natural Hazards and Earth System Sciences*, 4(3), pp.475-483.
175. Guzzetti, F., Aleotti, P., Malamud, B. and Turcotte, D.L., 2002, October. Comparison of three landslide event inventories in central and northern Italy. In *Proceedings of the 4th EGS Plinius Conference*, Spain: Universitat de les Illes Balears.
176. Guzzetti, F., Cardinali, M., Reichenbach, P., 1994. The AVI Project: A bibliographical and archive inventory of landslides and floods in Italy. *Environmental Management* 18 4, 623-633
177. Guzzetti, F., Carrara, A., Cardinali, M. and Reichenbach, P., 1999. Landslide hazard evaluation: a review of current techniques and their application in a multi-scale study, Central Italy. *Geomorphology*, 31(1-4), pp.181-216.
178. Guzzetti, F., Galli, M., Reichenbach, P., Ardizzone, F. and Cardinali, M.J.N.H., 2006. Landslide hazard assessment in the Collazzone area, Umbria, Central Italy. *Natural Hazards and Earth System Sciences*, 6(1), pp.115-131.
179. Guzzetti, F., Malamud, B.D., Turcotte, D.L., Reichenbach, P., 2002. Power-law correlations of landslide areas in Central Italy. *Earth and Planetary Science Letters* 195, 169 – 183.
180. Guzzetti, F., Reichenbach, P., Ardizzone, F., Cardinali, M. and Galli, M., 2006a. Estimating the quality of landslide susceptibility models. *Geomorphology*, 81(1-2), pp.166-184.
181. Guzzetti, F., Reichenbach, P., Cardinali, M., Galli, M. and Ardizzone, F., 2005. Probabilistic landslide hazard assessment at the basin scale. *Geomorphology*, 72(1-4), pp.272-299.
182. Hamza, T. and Raghuvanshi, T.K., 2017. GIS based landslide hazard evaluation and zonation—a case from Jeldu District, central Ethiopia. *Journal of King Saud University-Science*, 29(2), pp.151-165.

183. Hansen, A., Franks, C.A.M., Kirk, P.A., Brimicombe, A.J., Tung, F., 1995. Application of GIS to hazard assessment, with particular reference to landslides in Hong Kong. In: Carrara, A., Guzzetti, F. Eds., *Geographical Information Systems. Assessing Natural Hazards*. Kluwer Academic Publisher, Dordrecht, The Netherlands, pp. 135–175
184. Hearn, G.J., 1995. Landslide and erosion hazard mapping at Ok Tedi copper mine, Papua New Guinea. *Quarterly Journal of Engineering Geology and Hydrogeology*, 28(1), pp.47-60.
185. Heckerman, D., 1986. Probabilistic interpretations for MYCIN's certainty factors. In *Machine Intelligence and Pattern Recognition* (Vol. 4, pp. 167-196). North-Holland.
186. Hervás, J. and Bobrowsky, P., 2009. Zonation: inventories, susceptibility, hazard and risk. In *Landslides–Disaster Risk Reduction* (pp. 321-349). Springer, Berlin, Heidelberg.
187. Hess, D. M., Leshchinsky, B. A., Bunn, M., Benjamin Mason, H., & Olsen, M. J. (2017). A simplified three-dimensional shallow landslide susceptibility framework considering topography and seismicity. *Landslides*, 14(5), 1677-1697.
188. Hollingsworth, R., Kovacs, G.S., 1981. Soil slumps and debris flows: prediction and protection. *Bulletin American Association of Engineering Geologists* 18 1, 17–28.
189. Hong, H., Ilia, I., Tsangaratos, P., Chen, W. and Xu, C., 2017. A hybrid fuzzy weight of evidence method in landslide susceptibility analysis on the Wuyuan area, China. *Geomorphology*, 290, pp.1-16.
190. Horlick-Jones, T., Amendola, A. and Casale, R. eds., 1995. *Natural risk and civil protection* (Vol. 16050). CRC Press.
191. Hossen, H., & Negm, A. (2016). Change detection in the water bodies of Burullus Lake, Northern Nile Delta, Egypt, using RS/GIS, 12th International Conference on Hydro informatics, HIC 2016. *Procedia Engineering*, 154, 936–942.
192. Houghton, R. A. (1994). The worldwide extent of land-use change. *BioScience*, 44(5), 305-313.
193. Huffman, G.J., E.F. Stocker, D.T. Bolvin, E.J. Nelkin, Jackson Tan (2019), GPM IMERG Early Precipitation L3 Half Hourly 0.1 degree x 0.1 degree V06, Greenbelt, MD, Goddard Earth Sciences Data and Information Services Center (GES DISC), Accessed: [20/04/2022], 10.5067/GPM/IMERG/3B-HH-E/06.
194. Huggel, C., Clague, J. J., & Korup, O. (2012). Is climate change responsible for changing landslide activity in high mountains? *Earth Surface Processes and Landforms*, 37(1), 77-91.
195. Hungr, O., 1995. A model for the runout analysis of rapid flow slides, debris flows, and avalanches. *Canadian geotechnical journal*, 32(4), pp.610-623.
196. Hungr, O., 1997. Some methods of landslide hazard intensity mapping. *Landslide risk assessment*, pp.215-226.

197. Hürlimann, M., Guo, Z., Puig-Polo, C. and Medina, V., 2022. Impacts of future climate and land cover changes on landslide susceptibility: Regional scale modelling in the Val d'Aran region (Pyrenees, Spain). *Landslides*, 19(1), pp.99-118.
198. Hürlimann, M., Guo, Z., Puig-Polo, C., & Medina, V. (2021). Impacts of future climate and land cover changes on landslide susceptibility: regional scale modelling in the Val d'Aran region (Pyrenees, Spain). *Landslides*, 1-20, <https://doi.org/10.1007/s10346-021-01775-6>.
199. Hutchinson, J.N., 1988. General report: morphological and geotechnical parameters of landslides in relation to geology and hydrogeology. In International symposium on landslides. 5 (pp. 3-35).
200. Hutchinson, J.N., 1995. Keynote paper: Landslide hazard assessment. In International Symposium on Landslides (pp. 1805-1841).
201. Ilia, I. and Tsangaratos, P., 2016. Applying weight of evidence method and sensitivity analysis to produce a landslide susceptibility map. *Landslides*, 13(2), pp.379-397.
202. Ilia, I., Tsangaratos, P., Koumantakis, I. and Rozos, D., 2010. Application of a Bayesian approach in GIS based model for evaluating landslide susceptibility. Case study Kimi area, Euboea, Greece. *Bulletin of the Geological Society of Greece*, 43(3), pp.1590-1600.
203. IMD, 2010. "[Climate of Himachal Pradesh](#)" (PDF). Climatological Summaries of States Series - No. 15. pp. 36–42. [Archived](#) (PDF) from the original on 20 February 2020. Retrieved 8 March 2020.
204. IMD, 2016. "[Extremes of Temperature & Rainfall for Indian Stations \(Up to 2012\)](#)" (PDF). p. M67. Archived from [the original](#) (PDF) on 5 February 2020. Retrieved 15 February 2020.
205. Intarawichian, N. and Dasananda, S., 2010. Analytical Hierarchy Process for Landslide Susceptibility Mapping in Lower Mae Chaem Watershed, Northern Thailand. *Suranaree Journal of Science & Technology*, 17(3).
206. Intarawichian, N., & Dasananda, S. (2011). Frequency Ratio model based landslide susceptibility mapping in lower Mae Chaem watershed, Northern Thailand. *Environment and Earth Science*, 64, 2271–2285.
207. Jacinth Jennifer, J., & Saravanan, S. (2021). Artificial neural network and sensitivity analysis in the landslide susceptibility mapping of Idukki district, India. *Geocarto International*, 1-23, <https://doi.org/10.1080/10106049.2021.1923831>.
208. Jade, S. and Sarkar, S., 1993. Statistical models for slope instability classification. *Engineering geology*, 36(1-2), pp.91-98.
209. Jaiswal, P., van Westen, C.J. and Jetten, V., 2010. Quantitative landslide hazard assessment along a transportation corridor in southern India. *Engineering geology*, 116(3-4), pp.236-250.
210. Jakob, M., & Lambert, S. (2009). Climate change effects on landslides along the southwest coast of British Columbia. *Geomorphology*, 107(3-4), 275-284, 10.1016/j.geomorph.2008.12.009.

211. James, N., & Sitharam, T. G. (2014). Assessment of seismically induced landslide hazard for the State of Karnataka using GIS technique. *Journal of the Indian Society of Remote Sensing*, 42(1), 73-89. <https://doi.org/10.1007/s12524-013-0306-z>.
212. Jat, M. K., Garg, P. K., & Khare, D. (2008). Monitoring and modelling of urban sprawl using remote sensing and GIS techniques. *International journal of Applied earth Observation and Geoinformation*, 10(1), 26-43.
213. Jenks, G.F., 1967. The data model concept in statistical mapping. *International yearbook of cartography*, 7, pp.186-190.
214. Jenness, J., & Wynne, J. J. (2005). Cohen's Kappa and classification table metrics 2.0: An ArcView 3. x extension for accuracy assessment of spatially explicit models. Open-File Report OF 2005-1363. Flagstaff, AZ: US Geological Survey, Southwest Biological Science Center. 86 p.
215. Jia, G., Tian, Y., Liu, Y. and Zhang, Y., 2008. A static and dynamic factors-coupled forecasting model of regional rainfall-induced landslides: A case study of Shenzhen. *Science in China Series E: Technological Sciences*, 51(2), pp.164-175.
216. Jia, N., Mitani, Y., Xie, M. and Djamaluddin, I., 2012. Shallow landslide hazard assessment using a three-dimensional deterministic model in a mountainous area. *Computers and Geotechnics*, 45, pp.1-10.
217. Jiang, Q.W., XU, Q. and HE, Z.W., 2005. Study on landslide hazard zonation based on multi-classification support vector machine. *Journal of Geological Hazards and Environment Preservation*, 3, p.24.
218. Jibson, R.W., Harp, E.L. and Michael, J.A., 2000. A method for producing digital probabilistic seismic landslide hazard maps. *Engineering geology*, 58(3-4), pp.271-289.
219. Joshi, V., Murthy, T. V. R., Arya, A. S., Narayana, A., Naithani, A. K., & Garg, J. K. (2003). Landslide hazard zonation of Dharasu-Tehri-Ghansali area of Garhwal Himalaya, India using remote sensing and GIS techniques. *Journal of Nepal Geological Society*, 28, 85-94, <https://doi.org/10.3126/jngs.v28i0.31727>.
220. Juang, C.H., Lee, D.H. and Sheu, C., 1992. Mapping slope failure potential using fuzzy sets. *Journal of geotechnical engineering*, 118(3), pp.475-494.
221. Kanungo DP, Sarkar S, Sharma S. 2011. Combining neural network with fuzzy, certainty factor and likelihood ratio concepts for spatial prediction of landslides. *Nat Hazards* 59(3):1491-1512.
222. Kanungo, D.P., Arora, M.K., Sarkar, S. and Gupta, R.P., 2006. A comparative study of conventional, ANN black box, fuzzy and combined neural and fuzzy weighting procedures for landslide susceptibility zonation in Darjeeling Himalayas. *Engineering Geology*, 85(3-4), pp.347-366.
223. Kanungo, D.P., Arora, M.K., Sarkar, S. and Gupta, R.P., 2012. Landslide Susceptibility Zonation (LSZ) Mapping—A Review.
224. Kanungo, D.P., Sarkar, S. and Sharma, S., 2011. Combining neural network with fuzzy,

- certainty factor and likelihood ratio concepts for spatial prediction of landslides. *Natural hazards*, 59(3), p.1491.
225. Karim, S., Jalileddin, S., & Ali, M. T. (2011). Zoning landslide by use of frequency ratio method (case study: Deylaman Region). *Middle-East Journal of Scientific Research*, 9(5), 578–583.
  226. Karl, T. R., & Trenberth, K. E. (2003). Modern global climate change. *science*, 302(5651), 1719-1723. [10.1126/science.1090228](https://doi.org/10.1126/science.1090228)
  227. Kavzoglu, T., Sahin, E.K. and Colkesen, I., 2014. Landslide susceptibility mapping using GIS-based multi-criteria decision analysis, support vector machines, and logistic regression. *Landslides*, 11(3), pp.425-439.
  228. Kavzoglu, T., Sahin, E.K. and Colkesen, I., 2015. Selecting optimal conditioning factors in shallow translational landslide susceptibility mapping using genetic algorithm. *Engineering Geology*, 192, pp.101-112.
  229. Kayastha, P., Dhital, M.R. and De Smedt, F., 2012. Landslide susceptibility mapping using the weight of evidence method in the Tinau watershed, Nepal. *Natural hazards*, 63(2), pp.479-498.
  230. Kayastha, P., Dhital, M.R. and De Smedt, F., 2013. Application of the analytical hierarchy process (AHP) for landslide susceptibility mapping: A case study from the Tinau watershed, west Nepal. *Computers & Geosciences*, 52, pp.398-408.
  231. Kienholz, H., Hafner, H., Schneider, G., Tamrakar, R., 1983. Mountain hazards zonation in Nepal's Middle Mountains. *Maps of land use and geomorphic damages Kathmandu-Kakani area. Mountain Research and Development* 33 ,195–220.
  232. Kienholz, H., Schneider, G., Bichsel, M., Grunder, M., Mool, P., 1984. Zonation of mountain hazards and slope stability. *Mountain Research and Development* 4, 247–266.
  233. Kim D, Ima S, Lee C, Wooc C (2013) Modeling the contribution of trees to shallow landslide development in a steep, forested watershed. *Ecol Eng.* <https://doi.org/10.1016/j.ecoleng.2013.05.003>.
  234. Kim, Y. H., Min, S. K., Zhang, X., Sillmann, J., & Sandstad, M. (2020). Evaluation of the CMIP6 multi-model ensemble for climate extreme indices. *Weather and Climate Extremes*, 29, 100269.
  235. Kirschbaum D, Adler R, Hong Y, Hill S, Lerner-Lam A. 2010. A global landslide catalog for hazard applications: method, results, and limitations. *Natural Hazards* 52:561-575
  236. Komac, M., 2006. A landslide susceptibility model using the analytical hierarchy process method and multivariate statistics in perialpine Slovenia. *Geomorphology*, 74(1-4), pp.17-28.
  237. Köning T, Kux HJH, Mendes RM (2019) Shalstab mathematical model and WorldView-2 satellite images to identification of landslide-susceptible areas. *Nat Hazard.* <https://doi.org/10.1007/s11069-019-03691-4>.

238. Korup, O., Görüm, T., & Hayakawa, Y. (2012). Without power? Landslide inventories in the face of climate change. *Earth Surface Processes and Landforms*, 37(1), 92-99.
239. Krishnan, R., Gnanaseelan, C., Sanjay, J., Swapna, P., Dhara, C., Sabin, T.P., Jadhav, J., Sandeep, N., Choudhury, A.D., Singh, M. and Mujumdar, M., 2020b. Introduction to climate change over the Indian region. In *Assessment of climate change over the Indian region* (pp. 1-20). Springer, Singapore.
240. Krishnan, R., Sanjay, J., Gnanaseelan, C., Mujumdar, M., Kulkarni, A. and Chakraborty, S., 2020a. Assessment of climate change over the Indian region: a report of the ministry of earth sciences (MOES), government of India (p. 226). Springer Nature.
241. Krishnan, R., Swapna, P., Choudhury, A.D., Narayansetti, S., Prajeesh, A.G., Singh, M., Modi, A., Mathew, R., Vellore, R., Jyoti, J. and Sabin, T.P., 2021. The IITM Earth System Model (IITM ESM). arXiv preprint arXiv:2101.03410.
242. Krishnan, R., Swapna, P., Vellore, R., Narayanasetti, S., Prajeesh, A.G., Choudhury, A.D., Singh, M., Sabin, T.P. and Sanjay, J., 2019. The IITM earth system model (ESM): development and future roadmap. In *Current trends in the Representation of physical processes in weather and climate models* (pp. 183-195). Springer, Singapore.
243. Kumar, A., & Sharma, M. P. (2016). Assessment of risk of GHG emissions from Tehri hydropower reservoir, India. *Human and Ecological Risk Assessment: An International Journal*, 22(1), 71-85.
244. Kumar, A., Sharma, R.K. and Bansal, V.K., 2018, November. GIS-Based Landslide Hazard Zonation Along NH-3 in Mountainous Terrain of Himachal Pradesh, India Using Weighted Overlay Analysis. In *International Conference on Sustainable Waste Management through Design* (pp. 59-67). Springer, Cham.
245. Kumar, A., Sharma, R.K. and Bansal, V.K., 2018. Landslide hazard zonation using analytical hierarchy process along National Highway-3 in mid Himalayas of Himachal Pradesh, India. *Environmental Earth Sciences*, 77(20), pp.1-19.
246. Kumar, A., Sharma, R.K. and Bansal, V.K., 2019. GIS-based comparative study of information value and frequency ratio method for landslide hazard Zonation in a part of mid-Himalaya in Himachal Pradesh. *Innovative Infrastructure Solutions*, 4(1), p.28.
247. Kumar, R. and Anbalagan, R., 2015a. Landslide susceptibility Zonation in part of Tehri reservoir region using frequency ratio, fuzzy logic and GIS. *Journal of Earth System Science*, 124(2), pp.431-448.
248. Kumar, R. and Anbalagan, R., 2015a. Landslide susceptibility Zonation in part of Tehri reservoir region using frequency ratio, fuzzy logic and GIS. *Journal of Earth System Science*, 124(2), pp.431-448.
249. Kumar, R. and Anbalagan, R., 2015b. Landslide susceptibility Zonation of Tehri reservoir rim

- region using binary logistic regression model. *Current Science*, pp.1662-1672.
250. Kumar, R. and Anbalagan, R., 2015c, July. Remote sensing and GIS based artificial neural network system for landslide susceptibility zonation. In 2015 IEEE International Geoscience and Remote Sensing Symposium (IGARSS) (pp. 4696-4699). IEEE.
  251. Kumar, R. and Anbalagan, R., 2016. Landslide susceptibility zonation using analytical hierarchy process (AHP) in Tehri reservoir rim region, Uttarakhand. *Journal of the Geological Society of India*, 87(3), pp.271-286.
  252. Kwan, J.S., Chan, S.L., Cheuk, J.C. and Koo, R.C.H., 2014. A case study on an open hillside landslide impacting on a flexible rockfall barrier at Jordan Valley, Hong Kong. *Landslides*, 11(6), pp.1037-1050.
  253. La, Z., 1965. Fuzzy sets. *Information and control*, 8(3), pp.338-353.
  254. Lallianthanga, R.K., Lalbiakmawia, F. and Lalramchuana, F., 2013. Landslide hazard Zonation of Mamit town, Mizoram, India using remote sensing and GIS techniques. *Int J Geol Earth Environ Sci*, 3(1), pp.184-194.
  255. Lan H X, Zhou C H, Wang L J, Zhang H Y and Li R H 2004 Landslide hazard spatial analysis and prediction using GIS in the Xiaojiang watershed, Yunnan, China; *Eng. Geol.* 76 109–128.
  256. Landis, J. R., & Koch, G. G. (1977). The measurement of observer agreement for categorical data. *biometrics*, 159-174
  257. Lee S, Talib JA. 2005. Probabilistic landslide susceptibility and factor effect analysis. *Environ Geol.* 47:982990
  258. Lee, C.F., Ye, H., Yeung, M.R., Shan, X. and Chen, G., 2001. AIGIS-based methodology for natural terrain landslide susceptibility mapping in Hong Kong. *Episodes*, 24(3), pp.150-159.
  259. Lee, C.T., Huang, C.C., Lee, J.F., Pan, K.L., Lin, M.L. and Dong, J.J., 2008. Statistical approach to storm event-induced landslides susceptibility. *Natural hazards and earth system sciences*, 8(4), pp.941-960.
  260. Lee, S. and Choi, J., 2004. Landslide susceptibility mapping using GIS and the weight-of-evidence model. *International Journal of Geographical Information Science*, 18(8), pp.789-814.
  261. Lee, S. and Min, K., 2001. Statistical analysis of landslide susceptibility at Yongin, Korea. *Environmental geology*, 40(9), pp.1095-1113.
  262. Lee, S. and Pradhan, B., 2006. Probabilistic landslide hazards and risk mapping on Penang Island, Malaysia. *Journal of Earth System Science*, 115(6), pp.661-672.
  263. Lee, S. and Pradhan, B., 2007. Landslide hazard mapping at Selangor, Malaysia using frequency ratio and logistic regression models. *Landslides*, 4(1), pp.33-41.

264. Lee, S. and Sambath, T., 2006. Landslide susceptibility mapping in the Damrei Romel area, Cambodia using frequency ratio and logistic regression models. *Environmental Geology*, 50(6), pp.847-855.
265. Lee, S. and Talib, J.A., 2005. Probabilistic landslide susceptibility and factor effect analysis. *Environmental Geology*, 47(7), pp.982-990.<https://doi.org/10.1007/s00254-005-1228-z>.
266. Lee, S., 2007. Application and verification of fuzzy algebraic operators to landslide susceptibility mapping. *Environmental Geology*, 52(4), pp.615-623.
267. Lee, S., Choi, J. and Min, K., 2002. Landslide susceptibility analysis and verification using the Bayesian probability model. *Environmental Geology*, 43(1-2), pp.120-131.
268. Lee, S., Ryu, J.H., Lee, M.J. and Won, J.S., 2003. Use of an artificial neural network for analysis of the susceptibility to landslides at Boun, Korea. *Environmental Geology*, 44(7), pp.820-833.
269. Lee, S., Ryu, J.H., Won, J.S. and Park, H.J., 2004. Determination and application of the weights for landslide susceptibility mapping using an artificial neural network. *Engineering Geology*, 71(3-4), pp.289-302.
270. Lee, S.A.R.O., 2005. Application of logistic regression model and its validation for landslide susceptibility mapping using GIS and remote sensing data. *International Journal of remote sensing*, 26(7), pp.1477-1491.
271. Lee, S.T., Yu, T.T., Peng, W.F. and Wang, C.L., 2010. Incorporating the effects of topographic amplification in the analysis of earthquake-induced landslide hazards using logistic regression. *Natural Hazards and Earth System Sciences*, 10(12), pp.2475-2488.
272. Li, X., & Yeh, A. G. O. (2002). Neural-network-based cellular automata for simulating multiple land use changes using GIS. *International Journal of Geographical Information Science*, 16(4), 323-343, <https://doi.org/10.1080/13658810210137004>.
273. Li, Y., Zhou, R., Zhao, G., Li, H., Su, D., Ding, H., Yan, Z., Yan, L., Yun, K. and Ma, C., 2014. Tectonic uplift and landslides triggered by the Wenchuan earthquake and constraints on orogenic growth: a case study from Hongchun Gully, Longmen Mountains, Sichuan, China. *Quaternary International*, 349, pp.142-152.
274. Lin, G.F., Chang, M.J., Huang, Y.C. and Ho, J.Y., 2017. Assessment of susceptibility to rainfall-induced landslides using improved self-organizing linear output map, support vector machine, and logistic regression. *Engineering geology*, 224, pp.62-74.
275. Luzi L and Pergalani F 1999 Slope instability in static and dynamic conditions for urban planning: The 'Oltre Po Pavese' Case History (Regione Lombardia – Italy); *Nat. Hazards* 20 57–82.
276. Ma, F., Wang, J., Yuan, R., Zhao, H. and Guo, J., 2013. Application of analytical hierarchy process and least-squares method for landslide susceptibility assessment along the Zhong-Wu natural gas pipeline, China. *Landslides*, 10(4), pp.481-492.

277. Ma, Z.J., Chen, H.L. and Yang, S.F., 2003. Prediction of landslide hazard based on support vector machine theory. JOURNAL-ZHEJIANG UNIVERSITY-SCIENCES EDITION-, 30(5), pp.592-596.
278. Maheshwari, B.K., 2019. Earthquake-induced landslide hazard assessment of chamoli district, uttarakhand using relative frequency ratio method. Indian Geotechnical Journal, 49(1), pp.108-123.
279. Malamud, B.D., Turcotte, D.L., Guzzetti, F., Reichenbach, P., 2004. Landslide inventories and their statistical properties. Earth Surface Processes and Landforms 29 (6), 687 – 711.
280. Mamdani, E.H. and Assilian, S., 1975. An experiment in linguistic synthesis with a fuzzy logic controller. International journal of man-machine studies, 7(1), pp.1-13.
281. Mancini, F., Ceppi, C. and Ritrovato, G., 2010. GIS and statistical analysis for landslide susceptibility mapping in the Daunia area, Italy. Natural Hazards and Earth System Sciences, 10(9), pp.1851-1864.
282. Marjanović, M., Kovačević, M., Bajat, B. and Voženilek, V., 2011. Landslide susceptibility assessment using SVM machine learning algorithm. Engineering Geology, 123(3), pp.225-234.
283. Márquez, A. M., Guevara, E., & Rey, D. (2019). Hybrid model for forecasting of changes in land use and land cover using satellite techniques. IEEE Journal of Selected Topics in Applied Earth Observations and Remote Sensing, 12(1), 252-273.
284. Martha, T.R., van Westen, C.J., Kerle, N., Jetten, V. and Kumar, K.V., 2013. Landslide hazard and risk assessment using semi-automatically created landslide inventories. Geomorphology, 184, pp.139-150.
285. Martínez-Álvarez, F., Reyes, J., Morales-Esteban, A., & Rubio-Escudero, C. (2013). Determining the best set of seismicity indicators to predict earthquakes. Two case studies: Chile and the Iberian Peninsula. Knowledge-Based Systems, 50, 198-210.<https://doi.org/10.1016/j.knosys.2013.06.011>.
286. McKean, J., Buechel, S. and Gaydos, L., 1991. Remote sensing and landslide hazard assessment. Photogrammetric engineering and remote sensing, 57(9), pp.1185-1193.
287. McNally, A., 2018. FLDAS noah land surface model L4 global monthly 0.1× 0.1 degree (MERRA-2 and CHIRPS). Atmos. Compos. Water Energy Cycles Clim. Var.
288. Mehrotra, G.S., Sarkar, S., Kanungo, D.P. and Mahadevaiah, K., 1996. Terrain analysis and spatial assessment of landslide hazards in parts of Sikkim Himalaya. JOURNAL-GEOLOGICAL SOCIETY OF INDIA, 47, pp.491-498.
289. Meinhardt, M., Fink, M., & Tünschel, H. (2015). Landslide susceptibility analysis in central Vietnam based on an incomplete landslide inventory: Comparison of a new method to calculate weighting factors by means of bivariate statistics. Geomorphology, 234, 80-97. <https://doi.org/10.1016/j.geomorph.2014.12.042>

290. Mejia-Navarro, M., Wohl, E.E., Oaks, S.D., 1994. Geological ' hazards, vulnerability and risk assessment using GIS: model for Glenwood Springs, Colorado. *Geomorphology* 10, 331–354.
291. Melchiorre, C., Matteucci, M., Azzoni, A. and Zanchi, A., 2008. Artificial neural networks and cluster analysis in landslide susceptibility zonation. *Geomorphology*, 94(3-4), pp.379-400.
292. Mendes RM, Andrade MRM, Graminha CA, Prieto CC, Ávila FF, Camarinha PIM (2017) Stability analysis on urban slopes: case study of an anthropogenic-induced landslide in São José dos Campos. *Brazil Geotech Geol Eng.* <https://doi.org/10.1007/s10706-017-0303-z>.
293. Meneses, B. M., Pereira, S., & Reis, E. (2019). Effects of different land use and land cover data on the landslide susceptibility zonation of road networks. *Natural Hazards and Earth System Sciences*, 19(3), 471-487, <https://doi.org/10.5194/nhess-19-471-2019>, 2019.
294. Mengistu, F., Suryabhagavan, K.V., Raghuvanshi, T.K. and Lewi, E., 2019. Landslide Hazard zonation and slope instability assessment using optical and InSAR data: a case study from Gidole town and its surrounding areas, southern Ethiopia. *Remote Sensing of Land*, 3(1), pp.1-14.
295. Meten, M., Bhandary, N.P. and Yatabe, R., 2015. Application of GIS-based fuzzy logic and rock engineering system (RES) approaches for landslide susceptibility mapping in Seleklula area of the Lower Jema River Gorge, Central Ethiopia. *Environmental earth sciences*, 74(4), pp.3395-3416.
296. Meten, M., PrakashBhandary, N. and Yatabe, R., 2015. Effect of landslide factor combinations on the prediction accuracy of landslide susceptibility maps in the Blue Nile Gorge of Central Ethiopia. *Geoenvironmental Disasters*, 2(1), p.9.
297. Meusburger, K. and Alewell, C., 2009. On the influence of temporal change on the validity of landslide susceptibility maps. *Natural Hazards and Earth System Sciences*, 9(4), pp.1495-1507.
298. Miller, S., Brewer, T. and Harris, N., 2009. Rainfall thresholding and susceptibility assessment of rainfall-induced landslides: application to landslide management in St Thomas, Jamaica. *Bulletin of Engineering Geology and the Environment*, 68(4), pp.539-550.
299. Mitchell, J.K., 1988. Confronting natural disasters: An international decade for natural hazard reduction US National Research Council. *Environment: Science and Policy for Sustainable Development*, 30(2), pp.25-29.
300. Moayed, H., Mehrabi, M., Mosallanezhad, M., Rashid, A.S.A. and Pradhan, B., 2019. Modification of landslide susceptibility zonation using optimized PSO-ANN technique. *Engineering with Computers*, 35(3), pp.967-984.
301. Moayed, H., Osouli, A., Tien Bui, D. and Foong, L.K., 2019. Spatial landslide susceptibility assessment based on novel neural-metaheuristic geographic information system based

- ensembles. *Sensors*, 19(21), p.4698.
302. Mondal, S. and Maiti, R., 2012. Landslide susceptibility analysis of Shiv-Khola watershed, Darjiling: a remote sensing & GIS based Analytical Hierarchy Process (AHP). *Journal of the Indian Society of Remote Sensing*, 40(3), pp.483-496.
  303. Montgomery, D.R., Dietrich, W.E., 1994. A physically based model for the topographic control of shallow landsliding. *Water Resources Research* 30 4, 1153–1171.
  304. Montrasio, L. and Valentino, R., 2008. A model for triggering mechanisms of shallow landslides. *Natural Hazards and Earth System Sciences*, 8(5), pp.1149-1159.
  305. Montrasio, L., Valentino, R. and Losi, G.L., 2011. Towards a real-time susceptibility assessment of rainfall-induced shallow landslides on a regional scale. *Natural hazards and earth system sciences*, 11(7), pp.1927-1947.
  306. Moungh-Jin, L., Won-Kyong, S., Joong-Sun, W., Inhye, P. and Saro, L., 2014. Spatial and temporal change in landslide hazard by future climate change scenarios using probabilistic-based frequency ratio model. *Geocarto International*, 29(6), pp.639-662, <https://doi.org/10.1080/10106049.2013.826739>.
  307. Mousavi, S. Z., Kavian, A., Soleimani, K., Mousavi, S. R., & Shirzadi, A. (2011). GIS-based spatial prediction of landslide susceptibility using logistic regression model. *Geomatics Natural Hazards and Risk*, 2, 33–50.
  308. Nahayo, L., Kalisa, E., Maniragaba, A. and Nshimiyimana, F.X., 2019. Comparison of analytical hierarchy process and certain factor models in landslide susceptibility mapping in Rwanda. *Modeling Earth Systems and Environment*, 5(3), pp.885-895.
  309. Naithani, S., & Saha, A. K. (2019). Changing landscape and ecotourism development in a large dam site: a case study of Tehri dam, India. *Asia Pacific Journal of Tourism Research*, 24(3), 193-205, <https://doi.org/10.1080/10941665.2018.1557226>.
  310. Nandi, A. and Shakoor, A., 2010. A GIS-based landslide susceptibility evaluation using bivariate and multivariate statistical analyses. *Engineering Geology*, 110(1-2), pp.11-20.
  311. National Landslide Risk Management Strategy.,2019. A publication of the National Disaster Management Authority, Government of India. New Delhi.
  312. NDMA. (2009). *Management of Landslides and Snow Avalanches*, National Disaster Management Authority (NDMA) Government of India New Delhi, 144.
  313. Neaupane, K.M. and Piantanakulchai, M., 2006. Analytic network process model for landslide hazard zonation. *Engineering Geology*, 85(3-4), pp.281-294.
  314. Neeley, M.K., Rice, R.M., 1990. Estimating risk of debris slides after timber harvest in northwestern California. *Bulletin American Association of Engineering Geologists* 27 3, 281–289.

315. Nefeslioglu, H.A., Duman, T.Y. and Durmaz, S., 2008. Landslide susceptibility mapping for a part of tectonic Kelkit Valley (Eastern Black Sea region of Turkey). *Geomorphology*, 94(3-4), pp.401-418.
316. Nefeslioglu, H.A., Gokceoglu, C. and Sonmez, H., 2008. An assessment on the use of logistic regression and artificial neural networks with different sampling strategies for the preparation of landslide susceptibility maps. *Engineering Geology*, 97(3-4), pp.171-191.
317. Neuhäuser, B., Damm, B. and Terhorst, B., 2012. GIS-based assessment of landslide susceptibility on the base of the weights-of-evidence model. *Landslides*, 9(4), pp.511-528.
318. Neuland, H., 1976. A prediction model of landslips. *Catena* 3, 215–230.
319. Nguyen, H., Mehrabi, M., Kalantar, B., Moayedi, H. and Abdullahi, M.A.M., 2019. Potential of hybrid evolutionary approaches for assessment of geo-hazard landslide susceptibility zonation. *Geomatics, Natural Hazards and Risk*, 10(1), pp.1667-1693.
320. Nicu, I. C. (2018). Application of analytic hierarchy process, frequency ratio, and statistical index to landslide susceptibility: an approach to endangered cultural heritage. *Environmental earth sciences*, 77(3), 1-16. <https://doi.org/10.1007/s12665-018-7261-5>
321. Nie, S., Fu, S., Cao, W., & Jia, X. (2020). Comparison of monthly air and land surface temperature extremes simulated using CMIP5 and CMIP6 versions of the Beijing Climate Center climate model. *Theoretical and Applied Climatology*, 140(1), 487-502.
322. Nilsen, T.H., Brabb, E.E., 1977. Slope stability studies in the San Francisco Bay region, California. Geological Society of America, *Reviews in Engineering Geology* 3, 235–243
323. Nithya, S.E. and Prasanna, P.R., 2010. An integrated approach with GIS and remote sensing technique for landslide hazard Zonation. *International Journal of Geomatics and Geosciences*, 1(1), pp.66-75.
324. O'Neill BC et al (2017) The roads ahead: narratives for shared socioeconomic pathways describing world futures in the 21st century. *Glob Environ Change* 42:169–180. <https://doi.org/10.1016/j.gloenvcha.2015.01.004>.
325. Oh, H.J. and Pradhan, B., 2011. Application of a neuro-fuzzy model to landslide-susceptibility mapping for shallow landslides in a tropical hilly area. *Computers & Geosciences*, 37(9), pp.1264-1276.
326. Ohlmacher, G.C. and Davis, J.C., 2003. Using multiple logistic regression and GIS technology to predict landslide hazard in northeast Kansas, USA. *Engineering geology*, 69(3-4), pp.331-343.
327. Oleson K. W., Bonan G. B., Feddema J., & Vertenstein M. (2008). An urban parameterization for a global climate model. Part I: Formulation and evaluation for two cities. *J. of App. Meteorology and Climatology*. 47, 4, 1038-1060.

328. Olsson, J., Yang, W., Graham, L. P., Rosberg, J. R., & Andr' Easson, J. (2011). Using an ensemble of climate projections for simulating recent and near-future hydrological change to lake V" anern in Sweden. *Tellus A: Dynamic Meteorology and Oceanography*, 63(1), 126-137.
329. Ozdemir, A., 2020. A Comparative Study of the Frequency Ratio, Analytical Hierarchy Process, Artificial Neural Networks and Fuzzy Logic Methods for Landslide Susceptibility Mapping: Taşkent (Konya), Turkey. *Geotechnical and Geological Engineering*, pp.1-29.
330. Pachauri, A.K. and Pant, M., 1992. Landslide hazard mapping based on geological attributes. *Engineering geology*, 32(1-2), pp.81-100.
331. Pack, R.T., Tarboton, D.G. and Goodwin, C.N., 1998. The SINMAP approach to terrain stability mapping.
332. Pan, X., Nakamura, H., Nozaki, T. and Huang, X., 2008. A GIS-based landslide hazard assessment by multivariate analysis. *Journal of the Japan landslide society*, 45(3), pp.187-195.
333. Pandey, A., Dabral, P.P., Chowdary, V.M. and Yadav, N.K., 2008. Landslide hazard Zonation using remote sensing and GIS: a case study of Dikrong river basin, Arunachal Pradesh, India. *Environmental geology*, 54(7), pp.1517-1529.
334. Pandey, R., Aretano, R., Gupta, A. K., Meena, D., Kumar, B., & Alatalo, J. M. (2017). Agroecology as a climate change adaptation strategy for smallholders of Tehri-Garhwal in the Indian Himalayan region. *Small-scale forestry*, 16(1), 53-63.
335. Pandey, V. K., Pourghasemi, H. R., & Sharma, M. C. (2020). Landslide susceptibility mapping using maximum entropy and support vector machine models along the Highway Corridor, Garhwal Himalaya. *Geocarto International*, 35(2), 168-187. <https://doi.org/10.1080/10106049.2018.1510038>.
336. Panikkar, S.V. and Subramanyan, V., 1997. Landslide hazard analysis of the area around Dehra Dun and Mussoorie, Uttar Pradesh. *Current Science*, pp.1117-1123.
337. Paola, J.D. and Schowengerdt, R.A., 1995. A review and analysis of backpropagation neural networks for classification of remotely-sensed multi-spectral imagery. *International Journal of remote sensing*, 16(16), pp.3033-3058.
338. Parise, M., 2002. Landslide hazard zonation of slopes susceptible to rock falls and topples. *Natural Hazards and Earth System Sciences*, 2(1/2), pp.37-49.
339. Parry, M. L., Canziani, O., Palutikof, J., Van der Linden, P., & Hanson, C. (Eds.). (2007). *Climate change 2007-impacts, adaptation and vulnerability: Working group II contribution to the fourth assessment report of the IPCC (Vol. 4)*. Cambridge University Press.
340. Patra, S., Sahoo, S., Mishra, P., & Mahapatra, S. C. (2018). Impacts of urbanization on land use/cover changes and its probable implications on local climate and groundwater level.

341. Patterson, D., 1996. Artificial Neural Networks. Prentice Hall, Singapore
342. Patwary, M.A.A. and Parvaiz, I., 2009. IRS-LISS-III and PAN data analysis for landslide susceptibility zonation using heuristic approach in active tectonic region of Himalaya. Journal of the Indian Society of Remote Sensing, 37(3), pp.493-509.
343. Pereira, S., Zêzere, J.L. and Bateira, C., 2012. Assessing predictive capacity and conditional independence of landslide predisposing factors for shallow landslide susceptibility models. Natural Hazards and Earth System Sciences, 12(4), pp.979-988.
344. Persichillo MG, Bordoni M, Meisina C (2017) The role of land use changes in the distribution of shallow landslides. Total Environ, Sci. <https://doi.org/10.1016/j.scitotenv.2016.09.125>.
345. Perus, I., Krajinc, A., 1996. AiNet: a neural network application for 32bit Windows environment. User's Manual. Version 1.22.
346. Petley, D.N., 2012. Landslides and engineered slopes: protecting society through improved understanding. Landslides and engineered slopes, 1, pp.3-13.
347. Pham, B.T., Bui, D.T., Pham, H.V., Le, H.Q., Prakash, I. and Dholakia, M.B., 2017. Landslide hazard assessment using random subspace fuzzy rules based classifier ensemble and probability analysis of rainfall data: a case study at Mu Cang Chai District, Yen Bai Province (Viet Nam). Journal of the Indian Society of Remote Sensing, 45(4), pp.673-683.
348. Pham, Q. B., Chandra Pal, S., Chakraborty, R., Saha, A., Janizadeh, S., Ahmadi, K., ... & Bannari, A. (2021). Predicting landslide susceptibility based on decision tree machine learning models under climate and land use changes. Geocarto International, 1-27, <https://doi.org/10.1080/10106049.2021.1986579>.
349. Pham, Q. B., Chandra Pal, S., Chakraborty, R., Saha, A., Janizadeh, S., Ahmadi, K., ... & Bannari, A. (2021). Predicting landslide susceptibility based on decision tree machine learning models under climate and land use changes. Geocarto International, 1-27, <https://doi.org/10.1080/10106049.2021.1986579>.
350. Piacentini, D., Troiani, F., Soldati, M., Notarnicola, C., Savelli, D., Schneiderbauer, S. and Strada, C., 2012. Statistical analysis for assessing shallow-landslide susceptibility in South Tyrol (south-eastern Alps, Italy). Geomorphology, 151, pp.196-206.
351. Pinyol, N. M., Alonso, E. E., Corominas, J., & Moya, J. (2012). Canelles landslide: modelling rapid drawdown and fast potential sliding. Landslides, 9(1), 33-51, <https://doi.org/10.1007/s10346-011-0264-x>.
352. Pirasteh, S. and Li, J., 2017. Probabilistic frequency ratio (PFR) model for quality improvement of landslide susceptibility mapping from LiDAR-derived DEMs. Geoenvironmental Disasters, 4(1), pp.1-17.

353. Pisano, L., Zumpano, V., Malek, Ž., Rosskopf, C. M., & Parise, M. (2017). Variations in the susceptibility to landslides, as a consequence of land cover changes: A look to the past, and another towards the future. *Science of The Total Environment*, 601, 1147-1159, <https://doi.org/10.1016/j.scitotenv.2017.05.231>.
354. Porghasemi, H. (2007). Landslide hazard zoning statistical frequency ratio method in the basin Safarood. M.Sc Thesis, TarbiatModarres University, Noor, p. 1386.
355. Pourghasemi HR, Pradhan B, Gokceoglu C. 2012a. Application of fuzzy logic and analytical hierarchy process (AHP) to landslide susceptibility zonation at Haraz watershed, Iran. *Nat Hazards*. 63:965996
356. Pourghasemi, H.R., Jirandeh, A.G., Pradhan, B., Xu, C. and Gokceoglu, C., 2013b. Landslide susceptibility mapping using support vector machine and GIS at the Golestan Province, Iran. *Journal of Earth System Science*, 122(2), pp.349-369.
357. Pourghasemi, H.R., Mohammady, M. and Pradhan, B., 2012b. Landslide susceptibility mapping using index of entropy and conditional probability models in GIS: Safarood Basin, Iran. *Catena*, 97, pp.71-84.
358. Pourghasemi, H.R., Moradi, H.R. and Aghda, S.F., 2013a. Landslide susceptibility mapping by binary logistic regression, analytical hierarchy process, and statistical index models and assessment of their performances. *Natural hazards*, 69(1), pp.749-779.
359. Pourghasemi, H.R., Pradhan, B., Gokceoglu, C., Mohammadi, M. and Moradi, H.R., 2013c. Application of weights-of-evidence and certainty factor models and their comparison in landslide susceptibility mapping at Haraz watershed, Iran. *Arabian Journal of Geosciences*, 6(7), pp.2351-2365.
360. Pradhan B. 2010. Landslide susceptibility zonation of a catchment area using frequency ratio, fuzzy logic and multivariate logistic regression approaches. *J Indian Soc Remote Sens*. 38:301320.
361. Pradhan B. 2011. Use of GIS-based fuzzy logic relations and its cross application to produce landslide susceptibility maps in three test areas in Malaysia. *Environ Earth Sci*. 63:329349
362. Pradhan, B. (2010). Remote sensing and GIS-based landslide hazard analysis and cross validation using multivariate logistic regression model on three test areas in Malaysia. *Advances in Space Research*, 45, 1244–1256.
363. Pradhan, B. and Lee, S., 2009. Landslide risk analysis using artificial neural network model focusing on different training sites. *Int J Phys Sci*, 3(11), pp.1-15.
364. Pradhan, B. and Lee, S., 2010. Regional landslide susceptibility analysis using back-propagation neural network model at Cameron Highland, Malaysia. *Landslides*, 7(1), pp.13-

365. Pradhan, B., & Lee, S. (2009). Delineation of landslide hazard areas using frequency ratio, logistic regression and artificial neural network model at Penang Island, Malaysia. *Environmental Earth Sciences*, 60, 1037–1054.
366. Pradhan, B., & Lee, S. (2010). Landslide susceptibility assessment and factor effect analysis: backpropagation artificial neural networks and their comparison with frequency ratio and bivariate logistic regression modelling. *Environmental Modelling & Software*, 25(6), 747-759. <https://doi.org/10.1016/j.envsoft.2009.10.016>.
367. Pradhan, B., 2012. A comparative study on the predictive ability of the decision tree, support vector machine and neuro-fuzzy models in landslide susceptibility mapping using GIS. *Comput. Geosci.* 51, 350–365
368. Pradhan, B., Seeni, M.I. and Kalantar, B., 2017. Performance evaluation and sensitivity analysis of expert-based, statistical, machine learning, and hybrid models for producing landslide susceptibility maps. In *Laser scanning applications in landslide assessment* (pp. 193-232). Springer, Cham.
369. Prakasam, C., Aravinth, R., Kanwar, V.S. and Nagarajan, B., 2020. Landslide hazard mapping using geo-environmental parameters—a case study on Shimla Tehsil, Himachal Pradesh. In *Applications of Geomatics in Civil Engineering* (pp. 123-139). Springer, Singapore.
370. Raghu Kanth, S.T.G. and Iyengar, R.N., 2007. Estimation of seismic spectral acceleration in peninsular India. *Journal of Earth System Science*, 116(3), pp.199-214.
371. Raghuvanshi, T.K., Ibrahim, J. and Ayalew, D., 2014. Slope stability susceptibility evaluation parameter (SSEP) rating scheme—an approach for landslide hazard zonation. *Journal of African Earth Sciences*, 99, pp.595-612.
372. Rai, P.K., Mohan, K. and Kumra, V.K., 2014. Landslide hazard and its mapping using remote sensing and GIS. *Journal of Scientific Research*, 58, pp.1-13.
373. Ramos-Cañón, A.M., Prada-Sarmiento, L.F., Trujillo-Vela, M.G., Macías, J.P. and Santos-r, A.C., 2016. Linear discriminant analysis to describe the relationship between rainfall and landslides in Bogotá, Colombia. *Landslides*, 13(4), pp.671-681.
374. Rampini A, Bordogna G, Carrara P, Pepe M, Antoninetti M, Mondini A, Reichenbach P. 2013. Modelling landslides' susceptibility by fuzzy emerging patterns. In: C. Margottini, editor. *Landslide science and practice*. Berlin: Springer; p. 363370
375. Ray, R.L. and De Smedt, F., 2009. Slope stability analysis on a regional scale using GIS: a case study from Dhading, Nepal. *Environmental Geology*, 57(7), pp.1603-1611.
376. Razifard, M., Shoaie, G. and Zare, M., 2019. Application of fuzzy logic in the preparation of hazard maps of landslides triggered by the twin Ahar-Varzeghan earthquakes (2012). *Bulletin of Engineering Geology and the Environment*, 78(1), pp.223-245.

377. Reddy, N.M. and Saravanan, S., 2023. Extreme precipitation indices over India using CMIP6: a special emphasis on the SSP585 scenario. *Environmental Science and Pollution Research*, 30(16), pp.47119-47143.
378. Reichenbach, P., Galli, M., Cardinali, M., Guzzetti, F. and Ardizzone, F., 2005. Geomorphologic mapping to assess landslide risk: concepts, methods and applications in the Umbria Region of central Italy. *Landslide Risk Assessment*. John Wiley, Chichester, pp.429-468.
379. Reichenbach, P., Mondini, A. C., & Rossi, M. (2014). The influence of land use change on landslide susceptibility zonation: the Briga catchment test site (Messina, Italy). *Environmental management*, 54(6), 1372-1384.
380. Reichenbach, P., Rossi, M., Malamud, B.D., Mihir, M. and Guzzetti, F., 2018. A review of statistically-based landslide susceptibility models. *Earth-Science Reviews*, 180, pp.60-91.
381. Rianna, G., Zollo, A., Tommasi, P., Paciucci, M., Comegna, L., & Mercogliano, P. (2014). Evaluation of the effects of climate changes on landslide activity of Orvieto clayey slope. *Procedia Earth and Planetary Science*, 9, 54-63, <https://doi.org/10.1016/j.proeps.2014.06.017>.
382. Rib, H.T. and Liang, T., 1978. Recognition and identification. *Transportation Research Board Special Report*, (176).
383. Riley, S.J., DeGloria, S.D. and Elliot, R., 1999. Index that quantifies topographic heterogeneity. *intermountain Journal of sciences*, 5(1-4), pp.23-27.
384. Roccati, A., Paliaga, G., Luino, F., Faccini, F. and Turconi, L., 2021. GIS-Based Landslide Susceptibility Mapping for Land Use Planning and Risk Assessment. *Land*, 10(2), p.162.
385. Rosenfeld, C.L., 1994. The geomorphological dimensions of natural disasters. *Geomorphology* 10, 27–36.
386. Ross, T.J., 2004. *Fuzzy logic with engineering applications* (Vol. 2). New York: Wiley. Available at: <https://doi.org/10.1002/9781119994374>
387. Rossi, G., Catani, F., Leoni, L., Segoni, S. and Tofani, V., 2013. HIRESSS: a physically based slope stability simulator for HPC applications. *Natural Hazards and Earth System Sciences*, 13(1), pp.151-166.
388. Rossi, M., Guzzetti, F., Reichenbach, P., Mondini, A.C. and Peruccacci, S., 2010. Optimal landslide susceptibility zonation based on multiple forecasts. *Geomorphology*, 114(3), pp.129-142.
389. Rosso, R., Rulli, M.C. and Vannucchi, G., 2006. A physically based model for the hydrologic control on shallow landsliding. *Water Resources Research*, 42(6). doi:10.1029/2005WR004369

390. ROTH, R.A., 1983. Factors affecting landslide-susceptibility in San Mateo county, California. *Bulletin of the Association of Engineering Geologists*, 20(4), pp.353-372.
391. Rowbotham, D.N. and Dudycha, D., 1998. GIS modelling of slope stability in Phewa Tal watershed, Nepal. *Geomorphology*, 26(1-3), pp.151-170.
392. Ruff, M., Czurda, K., 2008. Landslide susceptibility analysis with a heuristic approach in the Eastern Alps (Vorarlberg, Austria). *Geomorphology* 94 (3), 314–324. <http://dx.doi.org/10.1016/j.geomorph.2006.10.032>
393. Rwanga, S. S., & Ndambuki, J. M. (2017). Accuracy assessment of land use/land cover classification using remote sensing and GIS. *International Journal of Geosciences*, 8(04), 611, <https://doi.org/10.4236/ijg.2017.84033>.
394. Saaty, T.L., 1977. A scaling method for priorities in hierarchical structures. *Journal of mathematical psychology*, 15(3), pp.234-281. [https://doi.org/10.1016/0022-2496\(77\)90033-5](https://doi.org/10.1016/0022-2496(77)90033-5).
395. Saaty, T.L., 1980. The analytical hierarchy process, planning, priority. Resource allocation. RWS publications, USA.
396. Saaty, T.L., 1988. What is the analytic hierarchy process? In *Mathematical models for decision support* (pp. 109-121). Springer, Berlin, Heidelberg.
397. Saaty, T.L., 1990. *Multicriteria decision making: the analytic hierarchy process: planning, priority setting resource allocation*.
398. Saha, A. and Saha, S., 2020. Comparing the efficiency of weight of evidence, support vector machine and their ensemble approaches in landslide susceptibility modelling: A study on Kurseong region of Darjeeling Himalaya, India. *Remote Sensing Applications: Society and Environment*, 19, p.100323.
399. Saha, A.K., Gupta, R.P. and Arora, M.K., 2002. GIS-based landslide hazard Zonation in the Bhagirathi (Ganga) valley, Himalayas. *International journal of remote sensing*, 23(2), pp.357-369.
400. Saha, A.K., Gupta, R.P., Sarkar, I., Arora, M.K. and Csaplovics, E., 2005. An approach for GIS-based statistical landslide susceptibility zonation—with a case study in the Himalayas. *Landslides*, 2(1), pp.61-69.
401. Saha, S., Arabameri, A., Saha, A., Blaschke, T., Ngo, P.T.T., Nhu, V.H. and Band, S.S., 2021. Prediction of landslide susceptibility in Rudraprayag, India using novel ensemble of conditional probability and boosted regression tree-based on cross-validation method. *Science of the total environment*, 764, p.142928.
402. Saini, V., & Tiwari, R. K. (2020). A systematic review of urban sprawl studies in India: a geospatial data perspective. *Arabian Journal of Geosciences*, 13(17), 1-21, <https://doi.org/10.1007/s12517-020-05843-4>.
403. Salciarini, D., Godt, J.W., Savage, W.Z., Conversini, P., Baum, R.L. and Michael, J.A., 2006. Modeling regional initiation of rainfall-induced shallow landslides in the eastern Umbria Region of central Italy. *Landslides*, 3(3), pp.181-194.

404. Santacana, N., Baeza, B., Corominas, J., De Paz, A. and Marturiá, J., 2003. A GIS-based multivariate statistical analysis for shallow landslide susceptibility mapping in La Poblade Lillet area (Eastern Pyrenees, Spain). *Natural hazards*, 30(3), pp.281-295.
405. Sarda, V.K. and Pandey, D.D., 2019. Landslide susceptibility mapping using information value method. *Jordan journal of civil engineering*, 13(2).
406. Sarkar, S. and Kanungo, D.P., 2004. An integrated approach for landslide susceptibility mapping using remote sensing and GIS. *Photogrammetric Engineering & Remote Sensing*, 70(5), pp.617-625.
407. Sarkar, S., Kanungo, D., Patra, A. and Kumar, P., 2006. Disaster mitigation of debris flows, slope failures and landslides. GIS based landslide susceptibility mapping-a case study in Indian Himalaya.
408. Sarkar, S., Kanungo, D.P. and Mehrotra, G.S., 1995. Landslide hazard zonation: a case study in Garhwal Himalaya, India. *Mountain Research and Development*, pp.301-309.
409. Schicker, R. and Moon, V., 2012. Comparison of bivariate and multivariate statistical approaches in landslide susceptibility mapping at a regional scale. *Geomorphology*, 161, pp.40-57.
410. Schmaltz EM, Steger S, Glade T (2017) The influence of forest cover on landslide occurrence explored with spatio-temporal information. *Geomorphology*. <https://doi.org/10.1016/j.geomorph.2017.04.024>.
411. Schuster, R. L. (1996). Socioeconomic significance of landslides. *Landslides: Investigation and Mitigation*. Washington (DC): National Academy Press. Transportation Research Board Special Report, 247, 12-35.
412. Sdao F, Lioi DS, Pascale S, Caniani D, Mancini IM. 2013. Landslide susceptibility assessment by using a neuro-fuzzy model: A case study in the Rupestrian heritage rich area of Matera. *Nat Hazards Earth Syst Sci*. 13(2):395–407.
413. Seeley, M.W., West, D.O., 1990. Approach to geologic hazard zoning for regional planning, Inyo National Forest, California and Nevada. *Bulletin American Association of Engineering Geologists* 27 1, 23–35
414. Segoni, S., Lagomarsino, D., Fanti, R., Moretti, S. and Casagli, N., 2015. Integration of rainfall thresholds and susceptibility maps in the Emilia Romagna (Italy) regional-scale landslide warning system. *Landslides*, 12(4), pp.773-785.
415. Semadeni-Davies, A., Hernebring, C., Svensson, G., & Gustafsson, L. G. (2008). The impacts of climate change and urbanisation on drainage in Helsingborg, Sweden: Suburban stormwater. *Journal of hydrology*, 350(1-2), 114-125.
416. Sezer, E.A., Pradhan, B. and Gokceoglu, C., 2011. Manifestation of an adaptive neuro-fuzzy model on landslide susceptibility mapping: Klang valley, Malaysia. *Expert Systems with*

Applications, 38(7), pp.8208-8219.

417. Shahri, A.A., Spross, J., Johansson, F. and Larsson, S., 2019. Landslide susceptibility hazard map in southwest Sweden using artificial neural network. *Catena*, 183, p.104225.
418. Sharma ML. 1998. Attenuation relationship for estimation of peak ground horizontal acceleration using data from strong-motion arrays in India. *Bull Seismol Soc Am* 88(4):1063-1069.
419. Sharma, M. and Kumar, R., 2008. GIS-based landslide hazard Zonation: a case study from the Parwanoo area, Lesser and Outer Himalaya, HP, India. *Bulletin of Engineering Geology and the Environment*, 67(1), pp.129-137.
420. Sharma, R.H. and Shakya, N.M., 2008. Rain induced shallow landslide hazard assessment for ungauged catchments. *Hydrogeology Journal*, 16(5), pp.871-877.
421. Shortliffe, E.H. and Buchanan, B.G., 1975. A model of inexact reasoning in medicine. *Mathematical biosciences*, 23(3-4), pp.351-379.
422. Shou, K. J., & Yang, C. M. (2015). Predictive analysis of landslide susceptibility under climate change conditions—A study on the Chingshui River Watershed of Taiwan. *Engineering Geology*, 192, 46-62, <https://doi.org/10.1016/j.enggeo.2015.03.012>.
423. Shu, H., Hürlimann, M., Molowny-Horas, R., González, M., Pinyol, J., Abancó, C., & Ma, J. (2019). Relation between land cover and landslide susceptibility in Val d'Aran, Pyrenees (Spain): Historical aspects, present situation and forward prediction. *Science of the total environment*, 693, 133557, <https://doi.org/10.1016/j.scitotenv.2019.07.363>.
424. Shu, H., Hürlimann, M., Molowny-Horas, R., González, M., Pinyol, J., Abancó, C., & Ma, J. (2019). Relation between land cover and landslide susceptibility in Val d'Aran, Pyrenees (Spain): Historical aspects, present situation and forward prediction. *Science of the total environment*, 693, 133557, <https://doi.org/10.1016/j.scitotenv.2019.07.363>.
425. Siddle, H. J., D. B. Jones, and H. R. Payne. "Development of a methodology for landslip potential mapping in the Rhondda Valley." In *Slope stability engineering developments and applications: Proceedings of the international conference on slope stability organized by the Institution of Civil Engineers and held on the Isle of Wight on 15–18 April 1991*, pp. 137-142. Thomas Telford Publishing, 1991.
426. Sidle, R., & Ochiai, H. (2006). Processes, prediction, and land use. *Water resources monograph*. American Geophysical Union, Washington, 525.
427. Simoni, S., Zanotti, F., Bertoldi, G. and Rigon, R., 2008. Modelling the probability of occurrence of shallow landslides and channelized debris flows using GEOtop-FS. *Hydrological Processes: An International Journal*, 22(4), pp.532-545.
428. Singh, K. and Kumar, V., 2018. Hazard assessment of landslide disaster using information value method and analytical hierarchy process in highly tectonic Chamba region in bosom of

- Himalaya. *Journal of Mountain science*, 15(4), pp.808-824.
429. Singh, P., Sharma, A., Sur, U. and Rai, P.K., 2021. Comparative landslide susceptibility assessment using statistical information value and index of entropy model in Bhanupali-Beri region, Himachal Pradesh, India. *Environment, Development and Sustainability*, 23(4), pp.5233-5250.
  430. Singh, K. and Kumar, V., 2021. Slope stability analysis of landslide zones in the part of Himalaya, Chamba, Himachal Pradesh, India. *Environmental Earth Sciences*, 80(8), p.332.
  431. Soeters, R. and Van Westen, C.J., 1996. Slope instability recognition, analysis and zonation. *Landslides: investigation and mitigation*, 247, pp.129-177.
  432. Srivastava, A., Grotjahn, R., & Ullrich, P. A. (2020). Evaluation of historical CMIP6 model simulations of extreme precipitation over contiguous US regions. *Weather and Climate Extremes*, 29, 100268.
  433. Stark, C.P. and Hovius, N., 2001. The characterization of landslide size distributions. *Geophysical research letters*, 28(6), pp.1091-1094.
  434. Starosolszky, O. and Melder, O.M., 1989. Hydrology of disasters. In *Technical Conference on the Hydrology of Disasters*. World Meteorological Organization.
  435. Stead, D., Eberhardt, E., Coggan, J. and Benko, B., 2001. Advanced numerical techniques in rock slope stability analysis-Applications and limitations. In *International conference on landslides-causes, impacts and countermeasures* (pp. 615-624).
  436. Sterlacchini, S., Ballabio, C., Blahut, J., Masetti, M. and Sorichetta, A., 2011. Spatial agreement of predicted patterns in landslide susceptibility maps. *Geomorphology*, 125(1), pp.51-61.
  437. Suh, J., Choi, Y., Roh, T. D., Lee, H. J., & Park, H. D. (2011). National-scale assessment of landslide susceptibility to rank the vulnerability to failure of rock-cut slopes along expressways in Korea. *Environmental Earth Sciences*, 63(3), 619-632.
  438. Sujatha, E.R., Rajamanickam, G.V. and Kumaravel, P., 2012. Landslide susceptibility analysis using Probabilistic Certainty Factor Approach: A case study on Tevankarai stream watershed, India. *Journal of earth system science*, 121(5), pp.1337-1350.
  439. Sur, U., Singh, P., Rai, P. K., & Thakur, J. K. (2021). Landslide probability mapping by considering fuzzy numerical risk factor (FNRF) and landscape change for road corridor of Uttarakhand, India. *Environment, Development and Sustainability*, 1-29, <https://doi.org/10.1007/s10668-021-01226-1>.
  440. Süzen, M.L. and Doyuran, V., 2004. Data driven bivariate landslide susceptibility assessment using geographical information systems: a method and application to Asarsuyu catchment, Turkey. *Engineering geology*, 71(3-4), pp.303-321.

441. Süzen, M.L., Doyuran, V., 2004. A comparison of the GIS based landslide susceptibility assessment methods: multivariate versus bivariate. *Environmental Geology* 45, 665–679.
442. Takara, K., Yamashiki, Y., Sassa, K., Ibrahim, A.B. and Fukuoka, H., 2010. A distributed hydrological–geotechnical model using satellite-derived rainfall estimates for shallow landslide prediction system at a catchment scale. *Landslides*, 7(3), pp.237-258.
443. Takei, A., 1980. Limitation Methods of Hazard Zones in Japan. Report of Japanese-Austrian Joint Research, Forecast of Disaster Zone in Mountainous Regions, 1981, pp.7-25.
444. Terlien, M.T.J., van Westen, C.J., van Asch, Th.W.J., 1995. Deterministic modelling in GIS-based landslide hazard assessment. In: Carrara, A., Guzzetti, F. Eds., *Geographical Information Systems in Assessing Natural Hazards*. Kluwer Academic Publisher, Dordrecht, The Netherlands, pp. 57–77.
445. Terzaghi, K., 1950. Mechanism of Landslides. *Engineering Geology*, Berkley Volume, The Geological Society of America: 83-123.
446. Thanh, L.N. and De Smedt, F., 2012. Application of an analytical hierarchical process approach for landslide susceptibility mapping in A Luoi district, Thua Thien Hue Province, Vietnam. *Environmental Earth Sciences*, 66(7), pp.1739-1752.
447. Thiery, Y., Malet, J.P., Sterlacchini, S., Puissant, A. and Maquaire, O., 2007. Landslide susceptibility assessment by bivariate methods at large scales: application to a complex mountainous environment. *Geomorphology*, 92(1-2), pp.38-59.
448. Thiery, Y., Sterlacchini, S., Malet, J.P., Puissant, A., Remaître, A. and Maquaire, O., 2004, May. Strategy to reduce subjectivity in landslide susceptibility zonation by GIS in complex mountainous environments. In 7th AGILE Conference on GIScience (pp. 623-634).
449. Tiwari, P. C., Tiwari, A., & Joshi, B. (2018). Urban growth in Himalaya: understanding the process and options for sustainable development. *Journal of Urban and Regional Studies on Contemporary India*, 4(2), 15-27.
450. Tsangaratos, P. and Benardos, A., 2014. Estimating landslide susceptibility through a artificial neural network classifier. *Natural Hazards*, 74(3), pp.1489-1516.
451. Turco, M., Antonella, S., Herrera, G., Sixto, Maria, L. and Gutiérrez, J. (2013) Large biases and inconsistent climate change signals in ENSEMBLES regional projections. *Climatic Change*, 120, 859–869. <https://doi.org/10.1007/s10584-013-0844-y>.
452. Turrini, M.C. and Visintainer, P., 1998. Proposal of a method to define areas of landslide hazard and application to an area of the Dolomites, Italy. *Engineering geology*, 50(3-4), pp.255-265.
453. Tyagi, A., Tiwari, R. K., & James, N. (2021). GIS-Based Landslide Hazard Zonation and Risk Studies Using MCDM. In *Local Site Effects and Ground Failures* (pp. 251-266). Springer, Singapore, [https://doi.org/10.1007/978-981-15-9984-2\\_22](https://doi.org/10.1007/978-981-15-9984-2_22).

454. Tyagi, A., Tiwari, R. K., & James, N. (2022). A Review on Spatial, Temporal and Magnitude prediction of Landslide Hazard. *Journal of Asian Earth Sciences*: X, 100099.
455. Tyagi, A., Tiwari, R.K. and James, N., 2023. Mapping the landslide susceptibility considering future land-use land-cover scenario. *Landslides*, pp.1-12.
456. Umar, Z., Pradhan, B., Ahmad, A., Jebur, M.N. and Tehrany, M.S., 2014. Earthquake induced landslide susceptibility mapping using an integrated ensemble frequency ratio and logistic regression models in West Sumatera Province, Indonesia. *Catena*, 118, pp.124-135.
457. Uvaraj, S. and Neelakantan, R., 2018. Fuzzy logic approach for landslide hazard zonation mapping using GIS: A case study of Nilgiris. *Modeling Earth Systems and Environment*, 4(2), pp.685-698.
458. Uzielli, M., Nadim, F., Lacasse, S. and Kaynia, A.M., 2008. A conceptual framework for quantitative estimation of physical vulnerability to landslides. *Engineering Geology*, 102(3-4), pp.251-256.
459. Vahidnia, M.H., ALE, S.A., ALI, M.A. and Hosseinali, F., 2009. Landslide hazard Zonation using quantitative methods in GIS.
460. Van Den Eeckhaut, M., Vanwalleghe, T., Poesen, J., Govers, G., Verstraeten, G. and Vandekerckhove, L., 2006. Prediction of landslide susceptibility using rare events logistic regression: a case-study in the Flemish Ardennes (Belgium). *Geomorphology*, 76(3-4), pp.392-410.
461. Van Westen, C.J., 1994. GIS in landslide hazard Zonation: a review with examples from the Colombian Andes. In: Price, M.F., Heywood, D.I. Eds., Taylor and Francis, London, pp. 135–165
462. Van Westen, C.J., 1997. Statistical landslide hazard analysis. *Ilwis*, 2, pp.73-84.
463. Van Westen, C.J., Rengers, N., Terlien, M.T.J. and Soeters, R., 1997. Prediction of the occurrence of slope instability phenomenon through GIS-based hazard zonation. *Geologische Rundschau*, 86(2), pp.404-414.
464. Van, N.T.H., Van Son, P., Khanh, N.H. and Binh, L.T., 2016. Landslide susceptibility mapping by combining the analytical hierarchy process and weighted linear combination methods: a case study in the upper Lo River catchment (Vietnam). *Landslides*, 13(5), pp.1285-1301.
465. Vapnik, V.N., 1995. *The Nature of Statistical Learning Theory*. Springer, New York
466. Vapnik, V.N., 1998. *Statistical learning theory* Wiley. New York, 1(624), p.2.
467. Varnes, D.J., 1978. Slope movement types and processes. *Special report*, 176, pp.11-33.
468. Varnes, D.J., 1984. *Landslide hazard zonation: a review of principles and practice* (No. 3).

469. Versain, L.D., Banshtu, R.S. and Pandey, D.D., 2019. Comparative evaluation of GIS based landslide hazard zonation maps using different approaches. *Journal of the Geological Society of India*, 93(6), pp.684-692.
470. Vijith H and Madhu G 2008 Estimating potential landslide sites of an upland sub-watershed in Western Ghat's of Kerala (India) through frequency ratio and GIS; *Environ. Geol.* 55(7) 1397–1405
471. Wang, G., Chen, X. and Chen, W., 2020. Spatial prediction of landslide susceptibility based on gis and discriminant functions. *ISPRS International Journal of Geo-Information*, 9(3), p.144.
472. Wang, H.B. and Sassa, K., 2005. Comparative evaluation of landslide susceptibility in Minamata area, Japan. *Environmental Geology*, 47(7), pp.956-966.
473. Wang, J. and Xing, R., 2007. Decision making with the Analytic Network Process: Economic, political, social and technological applications with benefits, opportunities, costs and risks.
474. Wang, K.L. and Lin, M.L., 2010. Development of shallow seismic landslide potential map based on Newmark's displacement: the case study of Chi-Chi earthquake, Taiwan. *Environmental Earth Sciences*, 60(4), pp.775-785.
475. Wang, Y., Fang, Z., Wang, M., Peng, L. and Hong, H., 2020. Comparative study of landslide susceptibility mapping with different recurrent neural networks. *Computers & Geosciences*, 138, p.104445.
476. Wild, M. (2020). The global energy balance as represented in CMIP6 climate models. *Climate Dynamics*, 55(3), 553-577.
477. Wilson, J. (2011) Digital terrain modelling. *Geomorphology*, v.5, pp. 269–297.
478. Wong, H.N., Ko, F.W.Y. and Hui, T.H.H., 2006. Assessment of landslide risk of natural hillsides in Hong Kong (p. 117). *Geotechnical Engineering Office, Civil Engineering and Development Department*.
479. Wright, R.H., Campbell, R.H., Nilsen, T.H., 1974. Preparation and use of isopleth maps of landslide deposits. *Geological Society of America, Geology* 2, 483–485
480. Wright, R.H., Nilsen, T.H., 1974. Isopleth map of landslide deposits, Southern San Francisco Bay Region, California. *US Geological Survey Miscellaneous Field Studies Map*, MF-550 scale 1:250,00
481. Wu, C.H. and Chen, S.C., 2009. Determining landslide susceptibility in Central Taiwan from rainfall and six site factors using the analytical hierarchy process method. *Geomorphology*, 112(3-4), pp.190-204.
482. Wu, W. and Sidle, R.C., 1995. A distributed slope stability model for steep forested basins. *Water resources research*, 31(8), pp.2097-2110.

483. Wubalem, A., 2021. Landslide susceptibility mapping using statistical methods in Uatzau catchment area, northwestern Ethiopia. *Geoenvironmental Disasters*, 8(1), pp.1-21.
484. Xie, M., Esaki, T. and Cai, M., 2004. A time-space based approach for mapping rainfall-induced shallow landslide hazard. *Environmental Geology*, 46(6-7), pp.840-850.
485. Xing, X., Wu, C., Li, J., Li, X., Zhang, L. and He, R., 2021. Susceptibility assessment for rainfall-induced landslides using a revised logistic regression method. *Natural Hazards*, pp.1-21.
486. Xu, C., Dai, F., Xu, X. and Lee, Y.H., 2012. GIS-based support vector machine modeling of earthquake-triggered landslide susceptibility in the Jianjiang River watershed, China. *Geomorphology*, 145, pp.70-80.
487. Xu, C., Xu, X., Dai, F., Xiao, J., Tan, X. and Yuan, R., 2012. Landslide hazard mapping using GIS and weight of evidence model in Qingshui river watershed of 2008 Wenchuan earthquake struck region. *Journal of Earth Science*, 23(1), pp.97-120.
488. Yalcin, A., 2008. GIS-based landslide susceptibility mapping using analytical hierarchy process and bivariate statistics in Ardesen (Turkey): comparisons of results and confirmations. *Catena*, 72(1), pp.1-12.
489. Yan, F., Zhang, Q., Ye, S. and Ren, B., 2019. A novel hybrid approach for landslide susceptibility mapping integrating analytical hierarchy process and normalized frequency ratio methods with the cloud model. *Geomorphology*, 327, pp.170-187.
490. Yao, X. and Dai, F.C., 2006. Support vector machine modeling of landslide susceptibility using a GIS: A case study. *IAEG2006*, 793, pp.1-12.
491. Yao, X., Tham, L.G. and Dai, F.C., 2008. Landslide susceptibility mapping based on support vector machine: a case study on natural slopes of Hong Kong, China. *Geomorphology*, 101(4), pp.572-582.
492. Yesilnacar, E. and Topal, T.A.M.E.R., 2005. Landslide susceptibility mapping: a comparison of logistic regression and neural networks methods in a medium scale study, Hendek region (Turkey). *Engineering Geology*, 79(3-4), pp.251-266.
493. Yilmaz, I., 2009. Landslide susceptibility mapping using frequency ratio, logistic regression, artificial neural networks and their comparison: a case study from Kat landslides (Tokat—Turkey). *Computers & Geosciences*, 35(6), pp.1125-1138.
494. Yilmaz, I., 2010. Comparison of landslide susceptibility mapping methodologies for Koyulhisar, Turkey: conditional probability, logistic regression, artificial neural networks, and support vector machine. *Environ. Earth Sci.* 61, 821–836.
495. Yin, K.L. and Yan, T.Z., 1988. Statistical prediction models for instability of metamorphosed rocks. In *International symposium on landslides*. 5 (pp. 1269-1272).

496. Yoon, K.P. and Hwang, C.L., 1995. Multiple attribute decision making: an introduction. Sage publications.
497. Yoshimatsu, H. and Abe, S., 2006. A review of landslide hazards in Japan and assessment of their susceptibility using an analytical hierarchic process (AHP) method. *Landslides*, 3(2), pp.149-158.
498. Zeshan, M. T., Mustafa, M. R. U., & Baig, M. F. (2021). Monitoring Land Use Changes and Their Future Prospects Using GIS and ANN-CA for Perak River Basin, Malaysia. *Water*, 13(16), 2286, <https://doi.org/10.3390/w13162286>.
499. Zezere J (2002) Landslide susceptibility assessment considering landslide typology. A case study in the area north of Lisbon (Portugal). *Nat Hazard Earth Syst Sci* 2:73–82
500. Zêzere, J.L., Pereira, S., Melo, R., Oliveira, S.C. and Garcia, R.A., 2017. Mapping landslide susceptibility using data-driven methods. *Science of the total environment*, 589, pp.250-267.
501. Zhao, Y., Wang, R., Jiang, Y., Liu, H. and Wei, Z., 2019. GIS-based logistic regression for rainfall-induced landslide susceptibility mapping under different grid sizes in Yueqing, Southeastern China. *Engineering Geology*, 259, p.105147.
502. Zhu A, Wang R, Qiao J, Qin C-Z, Chen Y, Liu J, Du F, Lin Y, Zhu T. 2014. An expert knowledge-based approach to landslide susceptibility zonation using GIS and fuzzy logic. *Geomorphology*. 214:128138
503. Zhu, A.X., Miao, Y., Wang, R., Zhu, T., Deng, Y., Liu, J., Yang, L., Qin, C.Z. and Hong, H., 2018. A comparative study of an expert knowledge-based model and two data-driven models for landslide susceptibility mapping. *Catena*, 166, pp.317-327.
504. Zimmerman, M., Bichsel, M., Kienholz, H., 1986. Mountain hazards zonation in the Khumbu Himal, Nepal, with prototype map, scale 1: 50,000. *Mountain Research and Development* 6. 1, 29–40.
505. Zweig MH, Campbell G. 1993. Receiver-operating characteristic (ROC) plots: A fundamental evaluation tool in clinical medicine. *Clin Chem* 39(4):561-57.



### Annexure

Landslide Database from 2005-2020 for Tehri Region.

S. No.	Period	LONGITUDE	LATITUDE
1	2005-2010	78.57559	30.32531
2	2005-2010	78.55843	30.32554
3	2005-2010	78.55776	30.32712
4	2005-2010	78.56717	30.32853
5	2005-2010	78.65295	30.32947
6	2005-2010	78.55419	30.33136
7	2005-2010	78.54689	30.33366
8	2005-2010	78.6421	30.33881
9	2005-2010	78.53706	30.34066
10	2005-2010	78.53724	30.34117
11	2005-2010	78.52516	30.34174
12	2005-2010	78.64096	30.34321
13	2005-2010	78.52464	30.34365
14	2005-2010	78.639	30.34377
15	2005-2010	78.62998	30.34454
16	2005-2010	78.63103	30.34536
17	2005-2010	78.63131	30.34764
18	2005-2010	78.51498	30.34851
19	2005-2010	78.51488	30.35061
20	2005-2010	78.51349	30.35275
21	2005-2010	78.51458	30.35564
22	2005-2010	78.51428	30.35644
23	2005-2010	78.50732	30.35872
24	2005-2010	78.506	30.35944
25	2005-2010	78.55457	30.36237
26	2005-2010	78.5494	30.363
27	2005-2010	78.55979	30.36368
28	2005-2010	78.54176	30.36447
29	2005-2010	78.59154	30.36585
30	2005-2010	78.56447	30.36769
31	2005-2010	78.57443	30.3687
32	2005-2010	78.58736	30.36967
33	2005-2010	78.50337	30.36969
34	2005-2010	78.56237	30.36997
35	2005-2010	78.55814	30.37032
36	2005-2010	78.50278	30.3705
37	2005-2010	78.59101	30.37268
38	2005-2010	78.50611	30.37538
39	2005-2010	78.52311	30.37608

40	2005-2010	78.58862	30.37617
41	2005-2010	78.50634	30.37669
42	2005-2010	78.51592	30.37679
43	2005-2010	78.51704	30.37751
44	2005-2010	78.59193	30.3783
45	2005-2010	78.5041	30.37839
46	2005-2010	78.54294	30.38392
47	2005-2010	78.55158	30.38533
48	2005-2010	78.57549	30.38628
49	2005-2010	78.57159	30.38676
50	2005-2010	78.57817	30.38748
51	2005-2010	78.51676	30.39087
52	2005-2010	78.58418	30.3911
53	2005-2010	78.56048	30.39149
54	2005-2010	78.52224	30.39197
55	2005-2010	78.52452	30.39264
56	2005-2010	78.58448	30.39371
57	2005-2010	78.54607	30.39412
58	2005-2010	78.59525	30.39415
59	2005-2010	78.54561	30.39478
60	2005-2010	78.60344	30.39647
61	2005-2010	78.54491	30.3967
62	2005-2010	78.52671	30.398
63	2005-2010	78.51573	30.39881
64	2005-2010	78.5888	30.39987
65	2005-2010	78.58311	30.40044
66	2005-2010	78.52531	30.40058
67	2005-2010	78.51074	30.40113
68	2005-2010	78.60757	30.40186
69	2005-2010	78.6064	30.40209
70	2005-2010	78.51751	30.40235
71	2005-2010	78.51499	30.40361
72	2005-2010	78.5117	30.40364
73	2005-2010	78.51453	30.40431
74	2005-2010	78.51309	30.40487
75	2005-2010	78.51185	30.40591
76	2005-2010	78.51377	30.40926
77	2005-2010	78.51281	30.40978
78	2005-2010	78.51433	30.4099
79	2005-2010	78.51817	30.41881
80	2005-2010	78.61755	30.42045
81	2005-2010	78.62226	30.42091
82	2005-2010	78.63547	30.42171
83	2005-2010	78.63512	30.42177

84	2005-2010	78.59447	30.42208
85	2005-2010	78.58894	30.42364
86	2005-2010	78.51564	30.42508
87	2005-2010	78.58784	30.42541
88	2005-2010	78.65211	30.42782
89	2005-2010	78.65315	30.42858
90	2005-2010	78.6465	30.42875
91	2005-2010	78.58668	30.42876
92	2005-2010	78.64604	30.42973
93	2005-2010	78.65155	30.43052
94	2005-2010	78.64419	30.43098
95	2005-2010	78.64107	30.4341
96	2005-2010	78.64217	30.43565
97	2005-2010	78.58194	30.43655
98	2005-2010	78.63435	30.43761
99	2005-2010	78.58015	30.44439
100	2005-2010	78.57815	30.44845
101	2005-2010	78.63168	30.45079
102	2005-2010	78.63281	30.4556
103	2005-2010	78.5735	30.45582
104	2005-2010	78.5699	30.45979
105	2005-2010	78.56638	30.46352
106	2005-2010	78.62627	30.46788
107	2005-2010	78.6173	30.49313
108	2005-2010	78.61287	30.49755
109	2005-2010	78.62522	30.50003
110	2005-2010	78.44083	30.50028
111	2005-2010	78.62744	30.50103
112	2005-2010	78.43972	30.50111
113	2005-2010	78.43861	30.50194
114	2005-2010	78.62672	30.50194
115	2005-2010	78.65089	30.50594
116	2005-2010	78.34861	30.50833
117	2005-2010	78.62942	30.50892
118	2005-2010	78.44	30.50944
119	2005-2010	78.63847	30.50967
120	2005-2010	78.64367	30.51025
121	2005-2010	78.64416	30.51063
122	2005-2010	78.64258	30.51275
123	2005-2010	78.64583	30.51425
124	2005-2010	78.64456	30.51503
125	2005-2010	78.64614	30.51508
126	2005-2010	78.52314	30.51528
127	2005-2010	78.646	30.51536

128	2005-2010	78.64447	30.51567
129	2005-2010	78.60403	30.51728
130	2005-2010	78.58933	30.51894
131	2005-2010	78.34911	30.51922
132	2005-2010	78.58888	30.51943
133	2005-2010	78.59272	30.51967
134	2005-2010	78.53856	30.51989
135	2005-2010	78.35132	30.52081
136	2005-2010	78.51544	30.52169
137	2005-2010	78.60442	30.52233
138	2005-2010	78.28527	30.5226
139	2005-2010	78.50803	30.52267
140	2005-2010	78.60464	30.52558
141	2005-2010	78.49667	30.52667
142	2005-2010	78.42778	30.52722
143	2005-2010	78.42833	30.52806
144	2005-2010	78.64039	30.52925
145	2005-2010	78.60044	30.52931
146	2005-2010	78.64706	30.53094
147	2005-2010	78.64989	30.53219
148	2005-2010	78.35901	30.53392
149	2005-2010	78.34167	30.53444
150	2005-2010	78.48972	30.54167
151	2005-2010	78.64928	30.54575
152	2005-2010	78.50067	30.546
153	2005-2010	78.59417	30.54611
154	2005-2010	78.32025	30.55268
155	2005-2010	78.30833	30.55361
156	2005-2010	78.50094	30.55419
157	2005-2010	78.64119	30.56128
158	2005-2010	78.2955	30.56591
159	2005-2010	78.325	30.5658
160	2005-2010	78.50078	30.56886
161	2005-2010	78.63811	30.57722
162	2005-2010	78.64639	30.57764
163	2005-2010	78.63383	30.57989
164	2005-2010	78.62883	30.58097
165	2005-2010	78.3263	30.5822
166	2005-2010	78.65003	30.5825
167	2005-2010	78.33528	30.58306
168	2005-2010	78.62558	30.58425
169	2005-2010	78.50517	30.58436
170	2005-2010	78.6445	30.58553
171	2005-2010	78.64742	30.58694

172	2005-2010	78.62361	30.58717
173	2005-2010	78.64725	30.58853
174	2005-2010	78.64542	30.58869
175	2005-2010	78.62089	30.58964
176	2005-2010	78.62028	30.59047
177	2005-2010	78.61947	30.59056
178	2005-2010	78.62097	30.59056
179	2005-2010	78.64678	30.59061
180	2005-2010	78.64683	30.59167
181	2005-2010	78.61706	30.59186
182	2005-2010	78.64689	30.59258
183	2005-2010	78.61353	30.59383
184	2005-2010	78.61417	30.59408
185	2005-2010	78.61383	30.59444
186	2005-2010	78.61458	30.59494
187	2005-2010	78.61319	30.59581
188	2005-2010	78.61417	30.59864
189	2005-2010	78.61178	30.59925
190	2005-2010	78.61708	30.59992
191	2005-2010	78.61131	30.60011
192	2005-2010	78.61683	30.60022
193	2005-2010	78.61094	30.60028
194	2005-2010	78.63939	30.60145
195	2005-2010	78.64139	30.60186
196	2005-2010	78.51528	30.60233
197	2005-2010	78.63663	30.603
198	2005-2010	78.61019	30.60536
199	2005-2010	78.61094	30.60553
200	2005-2010	78.3144	30.6061
201	2005-2010	78.32284	30.60609
202	2005-2010	78.63928	30.60642
203	2005-2010	78.3202	30.6072
204	2005-2010	78.59494	30.60769
205	2005-2010	78.51328	30.60825
206	2005-2010	78.31243	30.60863
207	2005-2010	78.60217	30.60881
208	2005-2010	78.59403	30.60914
209	2005-2010	78.59992	30.60933
210	2005-2010	78.60219	30.61125
211	2005-2010	78.315	30.6116
212	2005-2010	78.31667	30.61222
213	2005-2010	78.63689	30.61386
214	2005-2010	78.3169	30.6144
215	2005-2010	78.64239	30.61483

216	2005-2010	78.64206	30.61575
217	2005-2010	78.5125	30.61583
218	2005-2010	78.58594	30.61692
219	2010-2015	78.2437	30.5803
220	2010-2015	78.2451	30.5786
221	2010-2015	78.2446	30.5799
222	2010-2015	78.2461	30.5804
223	2010-2015	78.2497	30.4909
224	2010-2015	78.2428	30.5791
225	2010-2015	78.3242	30.5564
226	2010-2015	78.4039	30.5004
227	2010-2015	78.3228	30.5552
228	2010-2015	78.3911	30.5013
229	2010-2015	78.4987	30.5759
230	2010-2015	78.2861	30.5191
231	2010-2015	78.3165	30.5527
232	2010-2015	78.2878	30.6013
233	2010-2015	78.3513	30.5209
234	2010-2015	78.4067	30.4844
235	2010-2015	78.3678	30.4841
236	2010-2015	78.257	30.4366
237	2010-2015	78.378	30.4877
238	2010-2015	78.3895	30.4991
239	2010-2015	78.299	30.3986
240	2010-2015	78.4886	30.4758
241	2010-2015	78.2546	30.4951
242	2010-2015	78.4076	30.4891
243	2010-2015	78.4958	30.4835
244	2010-2015	78.4813	30.4941
245	2010-2015	78.2603	30.5016
246	2010-2015	78.2604	30.5011
247	2010-2015	78.2852	30.5227
248	2010-2015	78.3257	30.6121
249	2010-2015	78.3147	30.6118
250	2010-2015	78.3421	30.5098
251	2010-2015	78.4955	30.5547
252	2010-2015	78.4944	30.5557
253	2010-2015	78.2847	30.5234
254	2010-2015	78.287	30.5194
255	2010-2015	78.2552	30.5772
256	2010-2015	78.3063	30.5993
257	2010-2015	78.2971	30.5671
258	2010-2015	78.3062	30.5617
259	2010-2015	78.3512	30.5743

260	2010-2015	78.3527	30.5607
261	2010-2015	78.4369	30.5009
262	2010-2015	78.2513	30.5
263	2010-2015	78.2511	30.5016
264	2010-2015	78.3234	30.5655
265	2010-2015	78.3343	30.5833
266	2010-2015	78.2833	30.6066
267	2010-2015	78.3357	30.5155
268	2010-2015	78.3348	30.513
269	2010-2015	78.3505	30.5428
270	2010-2015	78.3485	30.5427
271	2010-2015	78.4942	30.5218
272	2010-2015	78.4967	30.5309
273	2010-2015	78.4953	30.5321
274	2010-2015	78.3037	30.6082
275	2010-2015	78.2727	30.5532
276	2010-2015	78.3906	30.4979
277	2010-2015	78.4888	30.475
278	2010-2015	78.3569	30.5352
279	2010-2015	78.4086	30.4837
280	2010-2015	78.3414	30.4805
281	2010-2015	78.3679	30.4845
282	2010-2015	78.3784	30.4876
283	2010-2015	78.379	30.4871
284	2010-2015	78.3794	30.4875
285	2010-2015	78.4613	30.4813
286	2010-2015	78.2721	30.4482
287	2010-2015	78.4444	30.4196
288	2010-2015	78.3233	30.4975
289	2010-2015	78.3238	30.4955
290	2010-2015	78.4843	30.4015
291	2010-2015	78.4236	30.459
292	2010-2015	78.4834	30.3406
293	2010-2015	78.4933	30.4015
294	2010-2015	78.4852	30.3608
295	2010-2015	78.3864	30.4478
296	2010-2015	78.3193	30.4593
297	2010-2015	78.4073	30.4214
298	2010-2015	78.4841	30.3395
299	2010-2015	78.3806	30.4868
300	2010-2015	78.3523	30.4579
301	2010-2015	78.3685	30.4861
302	2010-2015	78.4716	30.4394
303	2010-2015	78.4822	30.4383

304	2010-2015	78.4947	30.4027
305	2010-2015	78.4425	30.4476
306	2010-2015	78.3354	30.4722
307	2010-2015	78.382	30.4405
308	2010-2015	78.3813	30.4404
309	2010-2015	78.427	30.438
310	2010-2015	78.2898	30.4831
311	2010-2015	78.4818	30.4393
312	2010-2015	78.4872	30.3539
313	2010-2015	78.4879	30.3696
314	2010-2015	78.4272	30.4237
315	2010-2015	78.4838	30.3681
316	2010-2015	78.3413	30.4793
317	2010-2015	78.3922	30.4568
318	2010-2015	78.3926	30.4587
319	2010-2015	78.3519	30.4821
320	2010-2015	78.405	30.4605
321	2010-2015	78.4623	30.4285
322	2010-2015	78.4601	30.4814
323	2010-2015	78.4327	30.4818
324	2010-2015	78.4161	30.4807
325	2010-2015	78.4793	30.4932
326	2010-2015	78.4844	30.3783
327	2010-2015	78.4838	30.3762
328	2010-2015	78.4461	30.4196
329	2010-2015	78.48	30.3645
330	2010-2015	78.4312	30.4826
331	2010-2015	78.4092	30.4833
332	2010-2015	78.484	30.367
333	2010-2015	78.4905	30.3467
334	2010-2015	78.4057	30.4591
335	2010-2015	78.4331	30.4821
336	2010-2015	78.4999	30.4547
337	2010-2015	78.6279	30.3959
338	2010-2015	78.5306	30.4253
339	2010-2015	78.5351	30.41
340	2010-2015	78.5093	30.4002
341	2010-2015	78.5782	30.3875
342	2010-2015	78.5942	30.4019
343	2010-2015	78.4833	30.4018
344	2010-2015	78.4898	30.4
345	2010-2015	78.4699	30.4373
346	2010-2015	78.4805	30.4922
347	2010-2015	78.4644	30.4496

348	2010-2015	78.5027	30.3942
349	2010-2015	78.5521	30.3796
350	2010-2015	78.5068	30.3943
351	2010-2015	78.507	30.3948
352	2010-2015	78.501	30.3893
353	2010-2015	78.6287	30.3969
354	2010-2015	78.6337	30.3924
355	2010-2015	78.3819	30.4864
356	2010-2015	78.4228	30.4286
357	2010-2015	78.563	30.3756
358	2010-2015	78.5751	30.3863
359	2010-2015	78.4231	30.4621
360	2010-2015	78.512	30.4047
361	2010-2015	78.5059	30.3931
362	2010-2015	78.5049	30.3594
363	2010-2015	78.5713	30.3999
364	2010-2015	78.5755	30.3863
365	2010-2015	78.5056	30.3917
366	2010-2015	78.5111	30.3852
367	2010-2015	78.5647	30.4443
368	2010-2015	78.5804	30.3912
369	2010-2015	78.504	30.4076
370	2010-2015	78.5734	30.4375
371	2010-2015	78.599	30.3869
372	2010-2015	78.6222	30.4206
373	2010-2015	78.6226	30.4781
374	2010-2015	78.6176	30.4807
375	2010-2015	78.6367	30.4337
376	2010-2015	78.6292	30.4665
377	2010-2015	78.5051	30.3563
378	2010-2015	78.589	30.3757
379	2010-2015	78.5893	30.3754
380	2010-2015	78.6229	30.4764
381	2010-2015	78.6261	30.4633
382	2010-2015	78.5005	30.4213
383	2010-2015	78.6013	30.4081
384	2010-2015	78.6097	30.4115
385	2010-2015	78.5156	30.4251
386	2010-2015	78.5028	30.3705
387	2010-2015	78.5175	30.4023
388	2010-2015	78.5847	30.3813
389	2010-2015	78.6036	30.4055
390	2010-2015	78.5845	30.3937
391	2010-2015	78.5888	30.3999

392	2010-2015	78.5801	30.4444
393	2010-2015	78.5874	30.3697
394	2010-2015	78.506	30.3595
395	2010-2015	78.5546	30.3624
396	2010-2015	78.5945	30.4221
397	2010-2015	78.5267	30.398
398	2010-2015	78.5429	30.3839
399	2010-2015	78.5903	30.4022
400	2010-2015	78.5624	30.37
401	2010-2015	78.5171	30.3775
402	2010-2015	78.5246	30.3437
403	2010-2015	78.5714	30.328
404	2010-2015	78.5716	30.3868
405	2010-2015	78.5605	30.3915
406	2010-2015	78.6461	30.4297
407	2010-2015	78.5146	30.3556
408	2010-2015	78.5149	30.3506
409	2010-2015	78.5231	30.3761
410	2010-2015	78.6441	30.431
411	2010-2015	78.5417	30.3645
412	2010-2015	78.5645	30.3677
413	2010-2015	78.5585	30.3256
414	2010-2015	78.6422	30.3388
415	2010-2015	78.6313	30.3476
416	2010-2015	78.639	30.3438
417	2010-2015	78.6223	30.4209
418	2010-2015	78.6317	30.4507
419	2010-2015	78.5831	30.4005
420	2010-2015	78.5117	30.4036
421	2010-2015	78.5621	30.3791
422	2010-2015	78.613	30.418
423	2010-2015	78.5566	30.392
424	2010-2015	78.6343	30.4376
425	2010-2015	78.5891	30.4236
426	2010-2015	78.5881	30.4251
427	2010-2015	78.5869	30.4286
428	2010-2015	78.5699	30.4598
429	2010-2015	78.5735	30.4558
430	2010-2015	78.5543	30.3314
431	2010-2015	78.6521	30.4278
432	2010-2015	78.6532	30.4286
433	2010-2015	78.6173	30.4931
434	2010-2015	78.6369	30.6027
435	2010-2015	78.5234	30.5143

436	2010-2015	78.6181	30.5887
437	2010-2015	78.643	30.5744
438	2010-2015	78.6257	30.5843
439	2010-2015	78.6236	30.5872
440	2010-2015	78.6162	30.5898
441	2010-2015	78.5223	30.5162
442	2010-2015	78.6203	30.5905
443	2010-2015	78.6135	30.5938
444	2010-2015	78.5116	30.6189
445	2010-2015	78.6427	30.6148
446	2010-2015	78.6043	30.5224
447	2010-2015	78.6454	30.5942
448	2010-2015	78.6329	30.5763
449	2010-2015	78.517	30.5788
450	2010-2015	78.6431	30.5121
451	2010-2015	78.6449	30.5151
452	2010-2015	78.6445	30.5156
453	2010-2015	78.6228	30.539
454	2010-2015	78.646	30.5154
455	2010-2015	78.5756	30.5811
456	2010-2015	78.5794	30.5837
457	2010-2015	78.6024	30.6089
458	2010-2015	78.5999	30.6095
459	2010-2015	78.6142	30.5987
460	2010-2015	78.6109	30.6003
461	2010-2015	78.6273	30.5351
462	2015-2020	78.6113	30.6002
463	2015-2020	78.2436	30.5802
464	2015-2020	78.2596	30.5841
465	2015-2020	78.2482	30.581
466	2015-2020	78.2492	30.5812
467	2015-2020	78.2376	30.5793
468	2015-2020	78.2358	30.4662
469	2015-2020	78.2365	30.4654
470	2015-2020	78.2453	30.5795
471	2015-2020	78.2459	30.5801
472	2015-2020	78.2406	30.4932
473	2015-2020	78.2354	30.4641
474	2015-2020	78.248	30.497
475	2015-2020	78.2303	30.4644
476	2015-2020	78.3163	30.5268
477	2015-2020	78.3162	30.5231
478	2015-2020	78.4004	30.5002
479	2015-2020	78.4025	30.5003

480	2015-2020	78.3908	30.501
481	2015-2020	78.3908	30.5013
482	2015-2020	78.323	30.5547
483	2015-2020	78.3911	30.5016
484	2015-2020	78.3907	30.5121
485	2015-2020	78.4983	30.5766
486	2015-2020	78.4987	30.5764
487	2015-2020	78.2861	30.5191
488	2015-2020	78.2984	30.5249
489	2015-2020	78.2992	30.5246
490	2015-2020	78.3203	30.5528
491	2015-2020	78.3165	30.5527
492	2015-2020	78.3251	30.5575
493	2015-2020	78.3224	30.5545
494	2015-2020	78.2877	30.6009
495	2015-2020	78.3429	30.5131
496	2015-2020	78.349	30.5192
497	2015-2020	78.3588	30.5343
498	2015-2020	78.3544	30.5361
499	2015-2020	78.3547	30.5356
500	2015-2020	78.3398	30.5071
501	2015-2020	78.4026	30.4775
502	2015-2020	78.37	30.486
503	2015-2020	78.256	30.3259
504	2015-2020	78.3926	30.4897
505	2015-2020	78.3932	30.4895
506	2015-2020	78.3898	30.4985
507	2015-2020	78.2688	30.3382
508	2015-2020	78.2682	30.3382
509	2015-2020	78.3443	30.4736
510	2015-2020	78.3367	30.4732
511	2015-2020	78.3565	30.346
512	2015-2020	78.2503	30.4995
513	2015-2020	78.4296	30.4925
514	2015-2020	78.4045	30.4786
515	2015-2020	78.4955	30.4835
516	2015-2020	78.4838	30.4997
517	2015-2020	78.3251	30.5567
518	2015-2020	78.3031	30.6082
519	2015-2020	78.2597	30.5012
520	2015-2020	78.2618	30.5017
521	2015-2020	78.262	30.5014
522	2015-2020	78.2636	30.5019
523	2015-2020	78.2822	30.5256

524	2015-2020	78.2857	30.5236
525	2015-2020	78.3127	30.6087
526	2015-2020	78.3304	30.5084
527	2015-2020	78.4946	30.5547
528	2015-2020	78.495	30.5557
529	2015-2020	78.2721	30.551
530	2015-2020	78.2955	30.5659
531	2015-2020	78.3535	30.5764
532	2015-2020	78.3539	30.5761
533	2015-2020	78.3054	30.5613
534	2015-2020	78.3515	30.5747
535	2015-2020	78.3537	30.561
536	2015-2020	78.4375	30.5017
537	2015-2020	78.2896	30.6008
538	2015-2020	78.2857	30.6033
539	2015-2020	78.2506	30.5014
540	2015-2020	78.2509	30.5017
541	2015-2020	78.253	30.5036
542	2015-2020	78.3237	30.5379
543	2015-2020	78.3384	30.5451
544	2015-2020	78.3347	30.5548
545	2015-2020	78.3244	30.6017
546	2015-2020	78.3232	30.6053
547	2015-2020	78.2837	30.6068
548	2015-2020	78.3391	30.5374
549	2015-2020	78.3358	30.5152
550	2015-2020	78.3363	30.5139
551	2015-2020	78.3342	30.5139
552	2015-2020	78.4919	30.516
553	2015-2020	78.4981	30.5231
554	2015-2020	78.2596	30.5016
555	2015-2020	78.4959	30.5321
556	2015-2020	78.4954	30.5327
557	2015-2020	78.273	30.5528
558	2015-2020	78.3826	30.4864
559	2015-2020	78.4148	30.4825
560	2015-2020	78.4309	30.4834
561	2015-2020	78.4298	30.4844
562	2015-2020	78.3704	30.3735
563	2015-2020	78.3833	30.5161
564	2015-2020	78.3333	30.566
565	2015-2020	78.3448	30.4662
566	2015-2020	78.3696	30.486
567	2015-2020	78.3786	30.4874

568	2015-2020	78.4569	30.4872
569	2015-2020	78.4601	30.4819
570	2015-2020	78.4478	30.4185
571	2015-2020	78.3848	30.487
572	2015-2020	78.4854	30.339
573	2015-2020	78.4899	30.3997
574	2015-2020	78.4887	30.4016
575	2015-2020	78.4817	30.445
576	2015-2020	78.4305	30.461
577	2015-2020	78.4299	30.4654
578	2015-2020	78.4069	30.4226
579	2015-2020	78.4931	30.3282
580	2015-2020	78.4897	30.3378
581	2015-2020	78.3193	30.4598
582	2015-2020	78.3987	30.4359
583	2015-2020	78.324	30.4967
584	2015-2020	78.2551	30.338
585	2015-2020	78.388	30.4905
586	2015-2020	78.4823	30.3422
587	2015-2020	78.3591	30.4953
588	2015-2020	78.3788	30.4851
589	2015-2020	78.3525	30.4585
590	2015-2020	78.3511	30.455
591	2015-2020	78.2544	30.4961
592	2015-2020	78.2674	30.4905
593	2015-2020	78.2546	30.337
594	2015-2020	78.3542	30.3925
595	2015-2020	78.4814	30.3441
596	2015-2020	78.482	30.3495
597	2015-2020	78.4843	30.3533
598	2015-2020	78.4879	30.3545
599	2015-2020	78.4904	30.4504
600	2015-2020	78.4891	30.4508
601	2015-2020	78.429	30.4606
602	2015-2020	78.4286	30.4579
603	2015-2020	78.443	30.4469
604	2015-2020	78.3182	30.4745
605	2015-2020	78.3361	30.4726
606	2015-2020	78.3377	30.4721
607	2015-2020	78.3378	30.4728
608	2015-2020	78.3451	30.475
609	2015-2020	78.3969	30.459
610	2015-2020	78.3975	30.4592
611	2015-2020	78.442	30.4481

612	2015-2020	78.4421	30.4484
613	2015-2020	78.4419	30.4477
614	2015-2020	78.4399	30.4412
615	2015-2020	78.342	30.4577
616	2015-2020	78.3383	30.4577
617	2015-2020	78.3247	30.4685
618	2015-2020	78.4956	30.4283
619	2015-2020	78.482	30.4404
620	2015-2020	78.4405	30.4432
621	2015-2020	78.4952	30.3567
622	2015-2020	78.4276	30.4241
623	2015-2020	78.3463	30.4745
624	2015-2020	78.3479	30.4753
625	2015-2020	78.3397	30.4776
626	2015-2020	78.4855	30.3309
627	2015-2020	78.3989	30.4601
628	2015-2020	78.3993	30.4601
629	2015-2020	78.405	30.4605
630	2015-2020	78.3994	30.4605
631	2015-2020	78.4252	30.4296
632	2015-2020	78.416	30.471
633	2015-2020	78.4174	30.4828
634	2015-2020	78.4827	30.4902
635	2015-2020	78.4798	30.3698
636	2015-2020	78.4456	30.4198
637	2015-2020	78.4818	30.4005
638	2015-2020	78.4746	30.3686
639	2015-2020	78.4066	30.487
640	2015-2020	78.4064	30.4924
641	2015-2020	78.4781	30.4886
642	2015-2020	78.4717	30.4865
643	2015-2020	78.4594	30.4854
644	2015-2020	78.484	30.3776
645	2015-2020	78.4843	30.3739
646	2015-2020	78.4744	30.368
647	2015-2020	78.4763	30.3651
648	2015-2020	78.4107	30.4727
649	2015-2020	78.4337	30.4824
650	2015-2020	78.5725	30.4381
651	2015-2020	78.5279	30.4336
652	2015-2020	78.5354	30.41
653	2015-2020	78.5042	30.3987
654	2015-2020	78.5081	30.4007
655	2015-2020	78.5733	30.3857

656	2015-2020	78.5779	30.3877
657	2015-2020	78.579	30.3859
658	2015-2020	78.5953	30.4017
659	2015-2020	78.6139	30.4023
660	2015-2020	78.5253	30.3624
661	2015-2020	78.4879	30.4014
662	2015-2020	78.4896	30.4007
663	2015-2020	78.471	30.4378
664	2015-2020	78.4711	30.4382
665	2015-2020	78.4866	30.4445
666	2015-2020	78.4648	30.4498
667	2015-2020	78.4632	30.4465
668	2015-2020	78.4634	30.4473
669	2015-2020	78.5108	30.4011
670	2015-2020	78.502	30.3897
671	2015-2020	78.552	30.3804
672	2015-2020	78.5093	30.3993
673	2015-2020	78.5098	30.3996
674	2015-2020	78.503	30.3928
675	2015-2020	78.4539	30.3763
676	2015-2020	78.4539	30.3788
677	2015-2020	78.5061	30.3897
678	2015-2020	78.6349	30.3931
679	2015-2020	78.4938	30.3919
680	2015-2020	78.4938	30.3913
681	2015-2020	78.4466	30.4193
682	2015-2020	78.385	30.4522
683	2015-2020	78.3838	30.4868
684	2015-2020	78.4291	30.4242
685	2015-2020	78.4246	30.4291
686	2015-2020	78.5026	30.3906
687	2015-2020	78.5552	30.3787
688	2015-2020	78.5555	30.3783
689	2015-2020	78.5576	30.3758
690	2015-2020	78.5218	30.3872
691	2015-2020	78.5252	30.3966
692	2015-2020	78.4254	30.4371
693	2015-2020	78.5132	30.497
694	2015-2020	78.5126	30.3936
695	2015-2020	78.5151	30.391
696	2015-2020	78.5053	30.3596
697	2015-2020	78.5642	30.3754
698	2015-2020	78.5648	30.3766
699	2015-2020	78.5659	30.3767

700	2015-2020	78.518	30.3868
701	2015-2020	78.5362	30.3794
702	2015-2020	78.6476	30.4176
703	2015-2020	78.545	30.3966
704	2015-2020	78.5083	30.3901
705	2015-2020	78.5253	30.4006
706	2015-2020	78.5135	30.4968
707	2015-2020	78.5636	30.3849
708	2015-2020	78.5653	30.444
709	2015-2020	78.5969	30.3874
710	2015-2020	78.6291	30.4182
711	2015-2020	78.6211	30.4815
712	2015-2020	78.6355	30.4314
713	2015-2020	78.6316	30.45
714	2015-2020	78.5028	30.3369
715	2015-2020	78.5071	30.359
716	2015-2020	78.6227	30.4752
717	2015-2020	78.6218	30.4772
718	2015-2020	78.6173	30.4799
719	2015-2020	78.6219	30.4522
720	2015-2020	78.5006	30.421
721	2015-2020	78.5883	30.3771
722	2015-2020	78.6057	30.44
723	2015-2020	78.5907	30.3793
724	2015-2020	78.5923	30.3804
725	2015-2020	78.5223	30.392
726	2015-2020	78.5167	30.3909
727	2015-2020	78.5131	30.4049
728	2015-2020	78.5146	30.4043
729	2015-2020	78.5138	30.4093
730	2015-2020	78.5143	30.4099
731	2015-2020	78.515	30.4036
732	2015-2020	78.5245	30.3927
733	2015-2020	78.5819	30.3806
734	2015-2020	78.5855	30.3857
735	2015-2020	78.5119	30.406
736	2015-2020	78.5073	30.3587
737	2015-2020	78.4921	30.3785
738	2015-2020	78.5816	30.3868
739	2015-2020	78.5782	30.4485
740	2015-2020	78.5848	30.4009
741	2015-2020	78.5494	30.363
742	2015-2020	78.5819	30.4365
743	2015-2020	78.5915	30.3659

744	2015-2020	78.5582	30.3704
745	2015-2020	78.5063	30.3767
746	2015-2020	78.591	30.3727
747	2015-2020	78.5886	30.3761
748	2015-2020	78.4935	30.3788
749	2015-2020	78.5642	30.3852
750	2015-2020	78.6422	30.4356
751	2015-2020	78.5182	30.4188
752	2015-2020	78.6176	30.4204
753	2015-2020	78.5953	30.3941
754	2015-2020	78.5061	30.3754
755	2015-2020	78.5744	30.3687
756	2015-2020	78.5598	30.3637
757	2015-2020	78.5755	30.3253
758	2015-2020	78.5672	30.3285
759	2015-2020	78.5252	30.3417
760	2015-2020	78.6411	30.4341
761	2015-2020	78.5084	30.3587
762	2015-2020	78.5842	30.3911
763	2015-2020	78.5461	30.3941
764	2015-2020	78.5456	30.3948
765	2015-2020	78.5146	30.3556
766	2015-2020	78.5135	30.3528
767	2015-2020	78.5794	30.3861
768	2015-2020	78.5798	30.3855
769	2015-2020	78.6465	30.4288
770	2015-2020	78.5469	30.3337
771	2015-2020	78.5371	30.3407
772	2015-2020	78.5373	30.3412
773	2015-2020	78.592	30.3783
774	2015-2020	78.6064	30.4021
775	2015-2020	78.653	30.3295
776	2015-2020	78.5159	30.3768
777	2015-2020	78.5034	30.3697
778	2015-2020	78.641	30.3432
779	2015-2020	78.515	30.3485
780	2015-2020	78.6316	30.3554
781	2015-2020	78.63	30.3445
782	2015-2020	78.6311	30.3453
783	2015-2020	78.6351	30.4217
784	2015-2020	78.6354	30.4217
785	2015-2020	78.5157	30.3988
786	2015-2020	78.6076	30.4019
787	2015-2020	78.6262	30.4679

788	2015-2020	78.6048	30.4079
789	2015-2020	78.6286	30.4184
790	2015-2020	78.5521	30.3904
791	2015-2020	78.5041	30.3784
792	2015-2020	78.5664	30.4635
793	2015-2020	78.5578	30.3271
794	2015-2020	78.5503	30.334
795	2015-2020	78.6532	30.4286
796	2015-2020	78.6129	30.4975
797	2015-2020	78.6328	30.4556
798	2015-2020	78.6516	30.4305
799	2015-2020	78.5232	30.5151
800	2015-2020	78.6288	30.5811
801	2015-2020	78.6211	30.5896
802	2015-2020	78.6508	30.5059
803	2015-2020	78.6209	30.5907
804	2015-2020	78.649	30.5933
805	2015-2020	78.6193	30.5907
806	2015-2020	78.6125	30.5951
807	2015-2020	78.6142	30.5941
808	2015-2020	78.6139	30.5944
809	2015-2020	78.5829	30.5973
810	2015-2020	78.6333	30.5975
811	2015-2020	78.5834	30.5987
812	2015-2020	78.6399	30.5998
813	2015-2020	78.6268	30.5354
814	2015-2020	78.6102	30.6055
815	2015-2020	78.578	30.5376
816	2015-2020	78.5857	30.6171
817	2015-2020	78.6424	30.6157
818	2015-2020	78.6371	30.6142
819	2015-2020	78.6454	30.5942
820	2015-2020	78.5793	30.5721
821	2015-2020	78.6329	30.5763
822	2015-2020	78.6345	30.5781
823	2015-2020	78.6046	30.5254
824	2015-2020	78.6294	30.509
825	2015-2020	78.6433	30.5101
826	2015-2020	78.63	30.5436
827	2015-2020	78.6474	30.5915
828	2015-2020	78.6467	30.5904
829	2015-2020	78.6474	30.5884
830	2015-2020	78.5547	30.5078
831	2015-2020	78.5025	30.5111

832	2015-2020	78.6462	30.515
833	2015-2020	78.646	30.514
834	2015-2020	78.518	30.5791
835	2015-2020	78.5181	30.5798
836	2015-2020	78.6406	30.5296
837	2015-2020	78.5794	30.5837
838	2015-2020	78.5521	30.5218
839	2015-2020	78.5927	30.5197
840	2015-2020	78.611	30.6058
841	2015-2020	78.6023	30.6114
842	2015-2020	78.5937	30.6091
843	2015-2020	78.5952	30.6076
844	2015-2020	78.6148	30.5948
845	2015-2020	78.6166	30.6002
846	2015-2020	78.6172	30.5998
847	2015-2020	78.6118	30.5993
848	2015-2020	78.6149	30.5364
849	2015-2020	78.6267	30.5019
850	2015-2020	78.6423	30.6018